Springer Series in Measurement Science and Technology

Pasquale Daponte
Giovanni Battista Rossi
Vincenzo Piscopo *Editors*

Measurement for the Sea

Supporting the Marine Environment and the Blue Economy

Springer

Springer Series in Measurement Science and Technology

The Springer Series in Measurement Science and Technology comprehensively covers the science and technology of measurement, addressing all aspects of the subject from the fundamental principles through to the state-of-the-art in applied and industrial metrology, as well as in the social sciences. Volumes published in the series cover theoretical developments, experimental techniques and measurement best practice, devices and technology, data analysis, uncertainty, and standards, with application to physics, chemistry, materials science, engineering and the life and social sciences.

More information about this series at http://www.springer.com/series/13337

Pasquale Daponte
Giovanni Battista Rossi • Vincenzo Piscopo
Editors

Measurement for the Sea

Supporting the Marine Environment and the Blue Economy

Springer

Editors
Pasquale Daponte
Department of Engineering
University of Sannio
Benevento, Italy

Vincenzo Piscopo
Department of Science and Technology
Parthenope University of Naples
Naples, Italy

Giovanni Battista Rossi
Department of Mechanical, Energy,
Management and Transportation
Engineering
Università degli Studi di Genova
Genoa, Italy

ISSN 2198-7807 ISSN 2198-7815 (electronic)
Springer Series in Measurement Science and Technology
ISBN 978-3-030-82023-7 ISBN 978-3-030-82024-4 (eBook)
https://doi.org/10.1007/978-3-030-82024-4

This Springer imprint is published by the registered company Springer Nature Switzerland AG
The registered company address is: Gewerbestrasse 11, 6330 Cham, Switzerland

Homme libre, toujours tu chériras la mer!
C. Baudelaire, Les Fleurs du Mal, 1857

Preface

In the history of mankind, the sea has always played a key role as a privileged medium for communication, commerce and contact among civilities. It constitutes an essential ecosystem and an invaluable reservoir and source of foods for all living beings. Therefore, its heath is a real challenge for the survival of humanity since it is one the most important environmental components targeted by the global warming. Measuring and monitoring techniques are key tools for supporting the marine environment and the Blue Economy. In this perspective, a series of annual international events, labelled MetroSea (Metrology for the Sea, http://www.metrosea.org/) started in 2017. Their increasing success inspired this book that provides an anthology of tutorials dealing with a representative selection of topics, in this fascinating investigation area, with the aim of reaching a broad readership.

The book deals firstly with hydrography and measurements for meteorology and oceanography. Typical metrological issues, such as calibration and traceability, are also considered for both physical and chemical quantities. Then key techniques, such as underwater acoustic investigation, remote sensing in satellite oceanography, sea-waves and sea-level measurements, and sea-monitoring network, are treated. Marine geology and the monitoring of cetaceans are presented, and finally economical and legal aspects of standardisation with reference to ISO containers are discussed.

Such an unparalleled wide vision of measurement for the sea may be of interest for people involved in sea-related activities as well as for persons that have a cultural interest in the marine natural and human environment and have some scientific or technical background.

Envisaged readership includes:

- students of different University levels, attending courses related to the sea, from different perspectives (science, engineering, economics, etc.), to provide them an overview of the “measurement” issue, of its importance and potentials
- professionals and researchers involved in sea-related activities, interested in having a look at the entire panorama of measurements for the sea, for achieving a better knowledge of the “world” in which they operate

– people generically interested in the sea, including those that practise sea-related sports or leisure activities, those that like to cruise or to spend holidays on the sea, or are interested in the cultural environment related to the sea or in the potentials of the Blue Economy, and just have some mathematical/physical background

To reach such a wide readership, the subjects are presented in a tutorial fashion, featuring a multidisciplinary approach, with a special focus on measurement.

Benevento, Italy — Pasquale Daponte
Genoa, Italy — Giovanni Battista Rossi
Naples, Italy — Vincenzo Piscopo
April 2021

Contents

About the Editors

Pasquale Daponte was born in Minori (SA), Italy, on March 7, 1957. He obtained his bachelor's degree and master's degree "cum laude" in Electrical Engineering in 1981 from the University of Naples, Italy. He is a Full Professor of Electronic Measurements at the University of Sannio—Benevento.

He is Immediate Past Chair of the Italian Association of Electrical and Electronic Measurements, and Past President of IMEKO. He is member of: Working Group of the IEEE Instrumentation and Measurement Technical Committee N°10 Subcommittee of the Waveform Measurements and Analysis Committee, IMEKO Technical Committee TC-4 "Measurements of Electrical Quantities", Editorial Board of Measurement Journal, Acta IMEKO and of Sensors. He is Associate Editor of IET Science Measurement and Technology Journal. He is member of the Board of Armed Forces Communications and Electronics Association (AFCEA) Naples Charter.

He has organised some national or international meetings in the field of Electronic Measurements and European co-operation; he was General Chairman of the IEEE Instrumentation and Measurement Technical Conference for 2006 and Technical Programme Co-Chair for I2MTC 2015.He was a co-founder of the IEEE International Symposium on Medical Measurements and Applications (MeMeA); now, he is the Chair of the MeMeA Steering Committee, memea2018.ieee-ims.org.

He is also the co-founder of the IEEE Workshop on Metrology for the Sea (www.metrosea.org) as well as of several other series of international workshops in various emerging application areas of Metrology.

He is involved in some European projects.

He has published more than 320 scientific papers in journals and at national and international conferences on the following subjects: Measurements and Drones, ADC and DAC Modelling and Testing, Digital Signal Processing, Distributed Measurement Systems.

He receivedin 1987, the award for the researches on the digital signal processing of the ultrasounds in echo-ophthalmology from the Italian Society of Ophthalmologyin 2009, the IEEE Fellowshipin 2009, the Laurea Honoris Causa in Electrical Engineering from Technical University "Gheorghe Asachi" of Iasi

(Romania)the "The Ludwik Finkelstein Medal 2014" from the Institute of Measurement and Control of the United Kingdomin 2015, in the framework of Florence Academic Leader Programme, the "Florence Ambassador Award",in May 2018, the "Career Excellence Award" from the IEEE Instrumentation and Measurement Society "For a lifelong career and outstanding leadership in research and education on instrumentation and measurement, and a passionate and continuous service, international in scope, to the profession",in September 2018, the IMEKO Distinguished Service Awardin 2020, AESS Outstanding Organizational Leadership Award "For contributions to metrology for aerospace applications".

Giovanni Battista Rossi obtained the Diploma in classical humanities in 1974 from Liceo Classico Giuseppe Mazzini, Genoa, and received the Laurea degree (with first-class honours) in mechanical engineering from the University of Genoa, Italy, in 1981.

A certified engineer, he is currently Full Professor of Measurement and Instrumentation, with the University of Genoa. As a teacher, he has lectured for a national televised university teaching programme (Nettuno). He has been coordinator of the M.Sc. course "Mechanical Engineering—Design and Construction" from 2011 to 2020 with the University of Genoa and is a member of the board of lecturers of the Ph.D. School of Mechanical Engineering. He has been a vice-chairman with the Department of Mechanics and Machine Design from 2002 to 2008. He is co-editor of the book *Measurement with Persons* (Taylor and Francis, 2012) and authored the book *Measurement and Probability* (Springer, 2014). He is co-editor of the series *Measurement Science and Technology* of Springer. He is an EU-recognised expert in measurement and testing and has recently chaired an expert group for the evaluation of the European Metrology Research Programme and the European Metrology Programme for Innovation and Research from 2016 to 2017. His current research interests include measurement science, probabilistic models and methods, dynamic measurement and spectral analysis, and measurement for the sea.

He has been chairman of Technical Committee 7 (Measurement Science) of the International Measurement Confederation (IMEKO) from 2012 to 2018 and has co-chaired international scientific events; he was the Italian vice-representative of the General Council of IMEKO from 2011 to 2015. He is currently a member of the Technical and Scientific Board of the Sea Study Centre of the University of Genoa.

Vincenzo Piscopo is Associate Professor of "Ship constructions and marine plants" at the University of Naples "Parthenope", Department of Science and Technology, since 28th December 2020, where he was also Assistant Professor (RTDb) since 28th December 2017 and Research Fellow (RTDa) since 4th January 2016. He also worked at the same University as postdoctoral researcher from 1st October 2012 up to 30th April 2015. At the end of December 2009, he obtained the Ph.D. in Aerospace, Naval and Quality Engineering at the University of Naples "Federico II", where he also earned cum laude the master's and bachelor's degrees in Naval Engineering in July 2006 and July 2004, respectively. He is currently

Editorial Board Member of the “International Journal of Naval Architecture and Ocean Engineering” and Associate Editor of the “IEEE Journal of Oceanic Engineering”.

The main research activities involve ships and marine structures, with particular reference to: (1) non-uniform torsion, buckling and ultimate strength analysis of ships and platings affected by pitting corrosion wastage, (2) mooring design and selection for floating offshore wind turbine, (3) dynamics of offshore structures, (4) design of wave energy converters, and (5) sea spectrum reconstruction based on ship motion analysis.

Chapter 1
Hydrography: From Marine Data to Information

Nicola Marco Pizzeghello and Luigi Sinapi

Contents

Abstract Hydrography is the branch of applied sciences, which deals with the measurement and description of the physical features of oceans, seas, coastal areas, lakes, and rivers. It focuses on measurement itself, and no longer on the use of measurement, as the data-centric approach has become the foundation for the marine knowledge. "Map once and use many times" has become a general rule for all hydrographic surveyors. Collect data using standards and evaluating their quality are not just necessary to safety of navigation products but to all marine applications. The chapter explores why hydrography is useful for the sustainable use of the sea, what are the core hydrographic data, and how they are collected and processed using the international standards, which the International Hydrographic Organization has been updating since 1968. Finally, it focuses on marine knowledge starting from hydrographic data used for creating hydrographic and cartographic products and marine spatial data infrastructures.

N. M. Pizzeghello (✉)
Italian Hydrographic Institute, Genoa, Italy
e-mail: nicolam.pizzeghello@marina.difesa.it

L. Sinapi
International Hydrographic Organization (IHO), CEDEX, Monaco
e-mail: luigi.sinapi@iho.int

P. Daponte et al. (eds.), *Measurement for the Sea*, Springer Series in Measurement Science and Technology,
https://doi.org/10.1007/978-3-030-82024-4_1

1.1 Hydrography: An Applied Science

Defining a certain subject often means having a close view of its connection with other matters. In the case of "Hydrography" the same definition includes its diffusion and use, so that it can be exploited as a common element for different fields of application.

The word hydrography can be divided into two parts: the first, *hydro*, which refers to water, and the suffix *-graphy*, which refers to writing. Hydrography measures and draws the marine environment: today through software, computers, and hydrographers, in the past through pencils, sheets, and always hydrographers. The way of operating has changed over time, but the foundation of the discipline has remained the same, especially for the attention to the hydrographic measurement.

Clarified that hydrography has a quantitative rather than descriptive-qualitative scope, the *International Hydrographic Organization* (IHO)[1] defines it as follows:

"Hydrography is the branch of applied sciences which deals with the measurement and description of the physical features of oceans, seas, coastal areas, lakes, and rivers, as well as with the prediction of their change over time, for the primary purpose of safety of navigation and in support of all other marine activities, including economic development, security and defense, scientific research, and environmental protection".[2]

Wikipedia, the free encyclopedia, reports the same definition: it is an expression of the level of sharing that the IHO definition of hydrography has now reached.

The *International Federation of Hydrographic Societies* (IFHS)[3] defines hydrography as follows:

"Hydrography is the measurement of various physical characteristics of the oceans (or other waters) such as bottom depth, currents, and waves. Although hydrographic surveys were traditionally carried out in order to produce navigation charts, nowadays such surveys are used in many applications from the oil and gas industry, to leisure activities and the fishing industry".[4]

The contents of the IHO and IFHS definitions are similar, and they show the convergence of the use of hydrographic data to a wide range of applications.

Let us analyze step by step the definition given by the IHO.

"Hydrography is a branch of applied sciences….omissis": it is a very elegant way to express the idea that the discipline does not have its own independent and exclusive field, but rather it acts as a bridge between pure sciences (mathematics,

[1] The International Hydrographic Organization is an intergovernmental consultative and technical organization that was established in 1921 to support safety of navigation and the protection of the marine environment (from IHO website, www.iho.int).

[2] From publication S-32 "Hydrographic Dictionary", WIKI Edition.

[3] The International Federation of Hydrographic Societies (IFHS) is a unique partnership of learned national and regional hydrographic societies that, through its worldwide membership, is able to address every specialism within the hydrographic profession and related disciplines, at all levels of experience and expertise (from IFHS website, www.hydrographicsociety.org).

[4] From the IFHS website www.hydrographicsociety.org.

physics, computer science, etc.) and applied sciences (geophysics, oceanography, etc.). In order to understand and deal with the definition of hydrography, we should know other disciplines. Basic knowledge, necessary to work in the hydrographic field, is systematized in the documents that the FIG/IHO/ICA *International Board On Standards Of Competence for Hydrographic Surveyors And Nautical Cartographers* (IBSC) keeps updated.[5]

"omissis… which deals with the measurement and description of the physical features of oceans, seas, coastal areas, lakes, and rivers, as well as with the prediction of their change over time… omissis": hydrography refers to a measured value, the result of a measurement process, understood as the indissoluble union between a number and the physical reference to which it refers, and its description, understood as an analysis linked to the form and nature of the physical conformation of all environments in which water is present: marine water, including the coast above the water surface level, and internal waters, such as lakes and rivers. The focus of the study is oriented to the physics of the marine environment and to its conformation analyzed from a diachronic point of view: maintaining the databases of the measures collected in the past, focusing the present and providing elements for monitoring, included the safety of navigation, and estimating what could happen in the future. It integrates time with the traditional approach of three-dimensional measurement in space, by studying the environment in four dimensions.

The last part of the definition outlines, probably not exhaustively, the areas within which hydrography could operate. Hydrography focuses on measurement and no longer on what it can do with measurement, and there is only an initial emphasis on the safety of navigation, the traditional task within which Hydrographic Offices (HOs) have operated throughout their history. In this latter field, the goal has always been to identify the minimum depth of water and to represent it on nautical charts, rather than the description of the depth of water as best as possible. Today this bias in the working methodology is very weakened, thanks to the diffusion of multibeam echosounders, capable of measuring the depth from multiple directions, continuously soundproofing the seabed at a certain resolution.

Other goals of hydrography have become competitive with safety of navigation, no longer giving to it a priority purpose. In the definition, the list of other marine activities is certainly not exhaustive, especially with regard to what could be linked to hydrographic data in the future.

The definition of hydrography therefore separates the hydrographic domain from the data representation, shifting the focus from products, traditionally charts, to the physical description of the marine environment. We are within the physical geography, today at least academically disjointed but not independent from human geography, descriptions of the environment without and with the presence of humans and their influences.[6]

[5] The syllabi of programs and individual recognition schemes of hydrographic courses are detailed in the IHO publication S-5 "Standard of Competence for Hydrographic Surveyors".

[6] The difference between marine, an adjective linked to all sea-related activities, and maritime, more linked to activities related to human actions, should be here underlined.

For a better understanding of the marine environment, another virtuous trend in progress is to centralize data in the analysis processes, data with geographical connotation, including the position. The consequence of this centralization, which takes place in digital databases, is that all data can be managed through the same computer or many computers able to communicate. Such data sharing makes the study of the environment through different types of data possible (for example, bathymetric, nature of the sea bottom, topography of the coastline, etc.), favoring an integrated approach that produces more solid and coordinated information.

Hydrographers focus on the intrinsic quality of data and on the attempt to collect them in the best possible way, considering the limits of resolution and uncertainty. The extraction of products from the collected data that best represent the dangers to navigation may take place at a later stage.[7] The objective is the creation of a digital database with rules for entering and extracting information, the *Marine Spatial Data Infrastructures* (MSDI).[8] This type of approach makes it easier to exchange data and use the same data for different applications, which is essential, given the scarcity of high quality data at sea and its cost. The data-centric approach, the need to improve technical capabilities of hydrographers, and finally the collaboration with researchers, stakeholders, and other government bodies, appear to be the main future objectives for the hydrographic community.

In conclusion, if we do not know enough about what the marine environment looks like, we cannot really understand how the sea behaves and reacts to disturbing agents. So, hydrography helps to know the environment.

1.2 4D Reference Frame

1.2.1 The Measure

Hydrography aims to measure physical aspects of the marine environment; from the measurements we move on to describe the same environment in an increasingly holistic way, thanks to the diffusion of computer systems and related databases.

So what is a measure? What is it referred to?

The *Bureau International des Poids et Mesures* (BIPM)[9] gives the following definition of quantity:

"property of a phenomenon, body, or substance, where the property has a magnitude that can be expressed as a number and a reference".[10]

[7] On this subject, see the Data-Information-Knowledge triangle from IHO C-17 "Spatial Data Infrastructures: The Marine Dimension—Guidance for Hydrographic Offices", 2017 Edition.

[8] The IHO Marine Spatial Data Infrastructures Working Group is active in this field.

[9] From the BIPM website, you can read: "BIPM is the intergovernmental organization through which Member States act together on matters related to measurement science and measurement standards".

[10] From the BIPM publication "International Vocabulary of Metrology" (VIM), 2008 Edition.

Quantity is therefore a property which can be expressed through a number, and this is quite common and not new in the scientific field, while the reference is more intriguing.

Quantity is also something that is described by numbers and references but it exists before its expression and is somehow disjointed. Without getting as far as philosophy, it is useful to think about how describing reality through measures can sometimes be reductive.

Returning to the definition of quantity, it is useful and opportune to link it to the definition of quantity value, also contained in the International Vocabulary of Metrology (VIM). The definition is as follows:

"number and reference together expressing magnitude of a quantity".

As can be inferred from the definition given by BIPM, quantity value is an entity more linked to what we are used to dealing with and it does not directly refer to the intrinsic property of the studied phenomenon.

Once we defined quantity and quantity value, the measurement operation is what links them. In particular, the definition contained in the VIM about measurement is as follows:

"process of experimentally obtaining one or more quantity values that can reasonably be attributed to a quantity".

In the notes and annotations of the VIM to this last definition, it is made explicit what is meant by the word experimentally; underlining that the measurement is not only the number, but it is also the way in which it is detected. From this point of view, what we mentioned in the first chapter about hydrographers' skills seems more relevant than ever.

Finally, the following annotation 3 to the definition of measurement reported in the VIM is of extreme interest:

"This Note is intended to explain what is needed in order to carry out a measurement. It is first necessary to choose a target measurement uncertainty, and then choose an appropriate procedure and measuring system for performing the measurement in order not to exceed the target uncertainty".

The uncertainty is linked to the measurement and, as mentioned above, it results in two indissoluble elements: number and reference. Uncertainty on the one hand precedes the measurement operation because it determines how in practice it is appropriate to measure. On the other hand, it follows the measurement because once the measurement has been completed, it is necessary to provide an estimation of the quality of the measurement through the uncertainty.

A certain measured value, representative of a quantity, is ultimately made up of a number, its reference, and an estimation of the uncertainty that accompanies it from the choice of the measurement system to the conclusion of the measurement process.

1.2.2 The Reference

The note three to the definition of measurement reported on the VIM contains the most essential operational aspects to establish the reference. It is as follows:

"Measurement presupposes a description of the quantity commensurate with the intended use of a measurement result, a measurement procedure, and a calibrated measuring system operating according to the specified measurement procedure, including the measurement conditions".

Each measuring instrument goes back to the original definition of the unit of measure through a more or less long chain of measurement samples, to which the individual instruments refer to. Obviously, every single measurement, always affected by uncertainty, has different metrics and leads to a different number. This is why a measurement without the relative metric (i.e., the reference) is not representative.

In particular, hydrographic measurements face the four-dimensional space (three spatial dimensions and one temporal dimension) and it always has a direct or indirect physical connection to the territory. The materialization of the reference can only occur through physically determined points.

These points are chosen through a set of theoretical rules that determine the geometry of the system, but without defining its physical realization. As for example, the set of rules of the position reference system established by the International Earth Rotation and Reference Systems Service (IERS) and named International Terrestrial Reference System (ITRS), within which the dimensions of the ellipsoid to which latitude and longitude are measured and its theoretical positioning respect to the Earth are fixed. Another example is the theoretical center of the transducer of an echosounder, usually explained in the operating manual, to which the depth measurements are referred.

The theoretical set of rules (the reference system) is then physically materialized creating a reference frame.

For the same example given above, the physical implementation of ITRS is a set of physically defined points in the Earth that create the physical frame of the rule set. These points form the International Terrestrial Reference Frame.[11] As the points are in motion for the tectonics of the plates, not only the coordinates are reported but also the estimation of their change over time. Since the measurements and estimations of their variations are also affected by uncertainties, the points can be updated (and recalculated) periodically through a new frame construction. In the case of the transducer, measurements will refer to a physical point on the transducer, which may be different from the theoretical point reported on the manual, because it can change over time.

The frame is therefore necessary for each measurement, and may change over time. In the case of hydrographic measurements, the frame has a spatial connotation, and must be physically defined for each individual measure. A frame drift,

[11] See http://itrf.ensg.ign.fr/.

which usually has slow displacements, can cause systematic errors in the measurement.

All hydrographic measurements also have a temporal reference. It has a material realization in the world through a set of atomic clocks that maintain the Coordinated Universal Time (UTC), to which the measurements should refer. The UTC time is directly measurable by modern Global Navigation Satellite Systems (GNSS) satellite receivers and available at the output of the instrument as well as the position.

1.2.3 4D Reference Frame

The hydrographic measures move in a four-dimensional space, where the time coordinate is added to the spatial ones. Therefore, data are collected in four dimensions (4D) through instruments that have their own reference frame. The raw data packages are combined and transformed into processed data which can be shared for different applications through databases.

Each reference frame is, in practice, a trio of Cartesian axes or polar coordinates in space, accompanied by the knowledge of time.

Every spatial reference is not only a set of rules; however, it is also its physical realization. It presupposes measures to realize it, which are therefore uncertain. As a consequence, a reference frame is not made by perfectly orthogonal axes and points without dimensions, but by axes that can be distorted and points that in reality are small portions of space. The same metric of the reference system (the unit of measurement) can be distorted leading to scale variations between different reference systems. The materialization of the unit of measurement in the instruments that measure length does not physically have the length of a meter, a statement that before introducing the previous concepts might have seemed paradoxical but now appears normal, indeed one would have been surprised at the opposite, maybe.

To pass from one reference frame to another, a six-parameter model is necessary,[12] where the two reference systems have different origins (three different coordinates of the origin that determine three translations) and different orientation of the axes (three angles in space that determine three rotations).

1.2.3.1 The Instrumental Reference Frame

Each instrument needs its own reference frame. It is therefore mandatory to know how the frame is positioned in order to understand the correct information content of the data collected.

[12] A scale variation in the metrics, the seventh parameter, is not considered here.

For a very basic analysis, but strongly founded on the previous rules, we now analyze the main instruments used for hydrographic measures, such as position, depth, attitude, state of the water (speed of sound), and vertical level.

As the measure is four-dimensional, it must contain the necessary temporal reference. Depending on the measurement uncertainties required, the instrument can have its own clock to be manually aligned with the standard, or an automatic interface with a more accurate system – GNSS – that determines the time.

Positioning instruments are today mainly GNSS receivers, capable of measuring codes and multifrequency phases of available satellite constellations. The reference frame of the instrument is represented by the phase center of the receiving antenna. GNSS also measures time, while hydrographic GNSS makes available also the synchronization signal at the output, ready to be sent to other instruments (it is usually the combination of a serial string signal and an electrical impulse called Pulse Per Second, PPS).

Alignment instruments are combinations of several GNSS antennas and inertial platforms consisting of gyroscopes and accelerators. Usually the inertial platforms are calibrated by manufacturers and the reference frame is a physical point marked on the measuring platform associated with a trio of Cartesian axes in space. Sometimes a certain direction (e.g., the bow of the vessel) is measured through two GNSS receivers; the direction is identified by the vector joining the phase centers of the respective antennas.

To measure the depth, hydrography uses transducers to convert electrical energy into acoustic one. The phase center of the transducer and the respective axes (identified on the transducer itself) materialize the reference frame of the instrument.

The auxiliary instruments also have a reference frame. For those that determine the physical characteristics of the medium (for example, the temperature of the water used to determine the speed of sound in water), the temperature sensor must be associated with its position in space, i.e., latitude, longitude, and the height with respect to the free surface of the water.

For the measurement of the water level, the problem is substantially similar, remembering that the distance between the free surface of the water and a certain physical vertical reference needs to be measured.

1.2.3.2 Among the Instruments and the Results: The Body Frame

Each instrument registers the data with respect to its own frame; the final objective is to transform data into a standard frame in order to make data interchangeable and representative for everyone. To convert data into this latest frame, hydrographic measures are converted into an intermediate frame, which is directly linked neither to the measurement nor to the results, but it acts as a bridge to combine the measurements.

This frame is attached to the medium on which instruments are installed and it is called the body frame. In the case of a hydrographic vessel, it is attached to the hull and is usually called vessel reference frame.

The axes of the system are fixed with the vessel and oriented along its longitudinal, transverse, and vertical axes.

1.2.3.3 The Position Reference Frame

The position is expressed with respect to an ellipsoidal reference frame, on which the latitude and longitude coordinates are defined.

Geodetic reference systems and frames with a global orientation were created by measurements and points scattered around the globe. This approach has now evolved from WGS 84, the Global Positioning System (GPS)[13] reference system, to ITRS-ITRF, a reference independent of the systems that can use it.

1.2.3.4 The Vertical Reference Frame

Once the planimetric coordinates of the measurement have been defined, the most of hydrographic measurements need of a vertical reference too.

Measures at sea have traditionally been linked to the physical position of the free surface of the water. As this profile is in continuous movement (for example, for tides and waves), a fixed position must be decided in order to use it as a reference level. The most direct reference is the mean sea level (MSL). This reference is established by measuring the sea level at a given location and averaging it over a period long enough to filter out the oscillations of short term. At the same time, as the mean level tends to increase in the long term, the interval should not be too long. The IHO, through resolution 3/1919 and subsequent amendments,[14] has identified, at least for ocean tides, 1 year as the balance between the opposite requirements.

The physical position of the MSL in a given position determines the equipotential surface of the gravity field used as reference. The main advantage of using this surface is that it is strongly linked to the position of the water in that period, being representative for all human activities that depend on the position of the water (for example, navigation or port management). It has the disadvantage of varying over time and therefore it needs to be continuously monitored.

From the position of the MSL, all other tide datums are derived, i.e., the levels that instead of referring to the average water position, refer to an astronomical high or low tide. It should be remembered that these tidal datums, which are traditionally used in nautical charts, refer only to the astronomical tide, ignoring the effects that particular weather conditions may have on sea level.

These physical references are nowadays connected to the ellipsoidal datum. As explained in the previous paragraph, the ellipsoidal datum is the reference frame for

[13] It is the American GNSS.

[14] For resolutions of IHO, see publication M-3 “Resolutions of the International Hydrographic Organization”.

positions, including height. It should be considered that the ellipsoid has a geometric nature, while the MSL has a physical nature. Therefore, the connection between the two can be made only by double and simultaneous measurements. This connection, measured by a vertical difference, changes around the world, because the different definition of the levels does not allow a constant and global difference between them. The advantage of using the ellipsoidal datum is linked to the fact that GNSS can materialize the ellipsoid through the measurement and thus it refers the depth measurement directly to the datum. Known the local difference between ellipsoid and MSL, it is possible to refer the measurements to a more practical physical reference.

The physical reference used for land operations, the geoid, is seldom useful at sea. In practice, as mentioned above, hydrography creates its geoid locally through the MSL, and it is not everywhere on the same equipotential surface of the gravity field.

1.2.3.5 The Time Reference Frame

The time used in hydrography is linked to atomic transitions, very stable and measurable through atomic clocks. A network of clocks scattered around the world, managed by the BIPM, materialize the international atomic time (TAI, temps atomique international). TAI is periodically corrected by a number of integer seconds in order to align it to the real movements of the Earth around its axis. This corrected time is called UTC, and it is the time reference frame more used for hydrographic.[15]

UTC is measured and available as output from GNSS designed for hydrographic purposes; the clock signal (called Pulse per Second, PPS) synchronizes the clocks of the various instruments to UTC. As for the positioning, a degradation of uncertainty of the position is also extended to time measurement, making it more uncertain.

1.3 The Hydrographic Measures

A basic hydrographic system is mainly made up of a positioning system, an attitude system, and a system for the detection of the seabed as well as auxiliary measurements. This basic instrumental analysis will be analyzed in the following paragraphs.

[15] Resolution number 7/2009 contained in the IHO publication M-3 prescribes its use in all nautical publications.

1.3.1 The Positioning

Today almost all positioning operations use GNSS systems. Even in the absence of a signal (for example, inside tunnels), GNSS is used to determine position at the beginning and end of the route.

Hydrographic GNSS can measure codes or phases of each individual satellite frequency that they are able to receive. This general definition indicates the top quality of the receivers (they receive all satellites and process all frequencies). Actually, depending on the quality of the receiver, tracking can be limited to some constellations of satellites. It is the case of a GNSS that receives only the constellation of the American GPS system or some frequencies, or then just code measurements and not the carrier phase of the signal coming from the satellite.

With reference to the performance of the receiver, there is a long-term trend in the hydrographic world which is moving the real-time positioning to the post processed one. Being linked to the safety of navigation, hydrography has a history linked to real-time positioning. This need, however, has not always been linked to the real usefulness of having position data immediately available for hydrographic surveys.

Today, the possibility of recording the measurements of the receiver - which represent the observable measurements previously mentioned - allows to increase, at the same cost, the quality of the positioning. The constraint is obviously to keep the GNSS measurement synchronized with the instruments that will be analyzed in the following paragraphs. This is also easily achievable by the timing signal available through the pulse per second (PPS).

The position is thus calculated in post processing, making the appropriate calculations on the observations and taking advantage of the possibility of correcting some errors that in real time would not have been possible to manage (amongst others, the recalculation of the ephemeris of the satellites or ionospheric modeling).

GNSS measurements are always time-referenced because the position calculation is always correlated with the time of the UTC frame. The measurements are spatial referred to the phase center of the antenna. In relation to the speed of the vessel, the hydrographer adjusts the recording rate. This rate does not usually fall below one position per second.

1.3.2 The Attitude

The vehicle (vessels in water and/or planes/satellites in air) on which the hydrographic sensor is installed directs rays, acoustic or electromagnetic, toward the seabed. In order to position these rays in space, it is necessary to know not only the position of the sensor but also its attitude.

The attitude is measured using inertial platforms whose operating principle is based on the laws of dynamics, or on combined measurements of several GNSS

antennas using relative positioning and extraction of the vector, rigidly oriented in space, which connects the phase centers of the antennas.

The final objective is to obtain the position and attitude of the transducer of the hydrographic sensor. The transducer can be shaped as a rigid body in space with six degrees of freedom, three linear and three angular. Inertial platforms possibly combined with GNSS receivers determine the three angular measurements. The two linear horizontal measurements are determined by positioning. Vertical measurements, including heave (measured by the attitude sensor) and tide (measured by GNSS or a tide gauge), are the most critical, given the importance of depth.

The attitude system measures the three angles with respect to its coordinated axes and the vertical movement with faster rates. The angles are called roll, pitch, and heading (or gyro). Roll is the angle that the transverse axis of the instrument forms with the horizontal plane. Pitch is the angle that the longitudinal axis of the instrument forms with the horizontal plane. Heading (called also gyro), is the angle that the longitudinal axis of the instrument forms with the North direction. Heave is the fast vertical movement that is combined with the tide to determine – at the time of the observation – the exact position on the vertical axis of the hydrographic sensor.

These three angles and one distance enter into the calculation of the positioning of the measurements; they are also dynamic, because the vehicle (vessels in water and/or planes/satellites in air) from which the measurements are taken, are in motion.

1.3.3 The Depth

At the center of the hydrographic acquisition, there is always an instrument for determining depth, which uses acoustic or electromagnetic waves oriented toward the seabed. The main instruments used for this purpose are described in the following paragraphs.

1.3.3.1 The Singlebeam Echosounder (SBES)

It is the traditional instrument used to measure the depth below a transducer, transforming electrical energy into acoustics in transmission and vice versa in reception. This transducer has a directional acoustic lobe, with certain angular amplitude[16]; the direction of maximum irradiation is perpendicular to its surface and it is referred to a point on the transducer, fundamental for the definition of the offsets among instruments.

An acoustic impulse at a certain frequency is emitted at a known time, and the return signal time is measured. Known the profile of the speed of sound in the water,

[16] The beam width is defined as the angle between the direction of maximum power of the wave beam and the direction in which the power is half of the maximum. It depends on the size of the transducer in relation to the wavelength of the signal.

the distance from the transducer to the seabed is calculated by measuring the travel time. The result is a precise measurement of the depth over time, taking advantage of the fact that the vehicle on which the instrument is installed is moving along programmed lines. In order to intercept the depth variation profile on each acquisition line, the lines are generally conducted perpendicularly to the average bathymetric trend of the surveyed area.

The depth measure is representative of an area on the seabed, called footprint[17]: the smaller the lobe, the smaller will be the footprint. Higher acoustic frequencies need smaller transducers to realize the same beam width. Moreover, lower frequencies have longer wavelengths. As the precision of the measure is a function of wavelength, low-frequency systems have worse precision. Conversely, lower frequencies need bigger transducers.[18] Unfortunately, the absorption of the high frequencies is higher, and for deep waters low frequencies are needed.

The other quantity that influences the measurement is the amount of energy radiated in the water, linked to the amplitude of the emitted signal and its duration. Increasing amplitude and duration of the impulse certainly means increasing the range of the system up to a certain physical limit related to the used acoustic frequency. But, it increases also the noise. The best rule to follow during a singlebeam survey for bathymetric applications is to use the highest possible frequency (if more than one is available), coupled with a minimum amplitude and pulse duration that still allows continuous bottom detection. These parameters should then be changed during the survey to better adapt them to the conditions of the surveyed area.

The measurement of the singlebeam echosounder is time-referenced by the instrument, through the alignment of its internal clock with the signal coming from GNSS.

Modern singlebeam, in addition to recording the digital data of the bottom detection, are able to digitize and record the signal intensity over time. This is very useful to analyze the state of the water column, the nature of the bottom, and in case of penetration below the bottom, the stratigraphy.

1.3.3.2 The Multibeam Echosounder (MBES)

The multibeam echosounder is the main hydrographic system, capable of acquire data not only on the vertical angle but also from lateral direction. Its swath, the lateral opening angle of the fan-shaped lobe, is composed by several beams oriented across track, perpendicular to the direction of the ship (Fig. 1.1).

It can be modeled into a physical level, where the electromagnetic signals are transformed into acoustic ones and transmitted and vice versa, and an analytical

[17] It is the area explored by the system calculated by the geometrical spreading of the beam width.

[18] With the same wavelength, a longer transducer in a certain direction generates a narrower beam to the perpendicular direction. With the same transducer size, longer wavelengths, and therefore lower frequencies, generate larger lobes. With the same beam width, longer wavelengths need larger transducers.

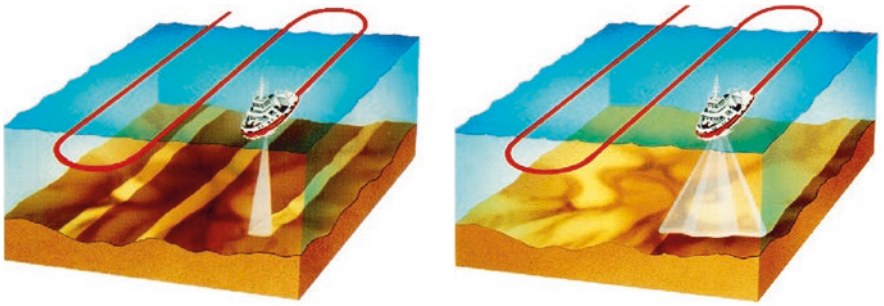

Fig. 1.1 Difference between singlebeam and multibeam survey (courtesy of Kongsberg Maritime AS)

Fig. 1.2 Tx and Rx multibeam transducer (courtesy of Kongsberg Maritime AS)

level, where the received signals are recombined and processed on the basis of algorithms, which represent the real core of the system.

At physical level, a signal transmission projector and an array of receivers are integrated into the multibeam transducer (Fig. 1.2).

The projector, oriented with its major axe per keel, transmits the signal. The transmission acoustic lobe has a width of a few degrees along-track and an across-track width ranging from 120 to 180 degrees, depending on the multibeam model. The lobe has the shape of a crosswise-oriented fan.

To fix the spatial resolution to a certain transverse direction, the system can use two different methods. The first method, called beamforming, is to set a certain number of transverse directions where they are received. From each direction, the travel time is measured. The second method, called interferometry, is set to scan the

received signal discreetly over time, determining for each of the following times t = t0, t1, t2 etc., the angle from which the signal comes from.

Beamforming uses a certain number of receiving elements, usually at least 40, that form an array, aligned across-track. At physical level, each element of the array receives independently the same signal radiated by the projector. The signal arrival times, different for each acoustic element of the array and updated with each new ping, are recorded.

The set of measurements then pass to the analytical level, usually consisting of a computer card that performs the beamforming. For each ping the signals of the individual elements that form the array are recombined several times in different ways according to the beamforming algorithm. Each different recombination changes the transverse direction of measurement. Within the beamformer, the signals are differently delayed before being recombined, and these delays are a function of the transverse angle. At the end of the processing, an artificial lobe is formed and it is no longer a fan but a series of pencil beams whose envelope is a fan. This result is a combination of the projector and receiver array directivity.

The interferometric approach is opposite. Making the same considerations as beamforming for the transmission chain, reception takes place by an array that is composed of at most three to four acoustic elements. On a physical level, for each ping, the array samples and records the phase of the received signal over time.

At an analytical level, the difference between the phases of the array's channels over time is calculated and from these differences, for each instant of sampling, signals angles are calculated. The result is similar to the one of beamforming, but the way to calculate the angle-travel time pairs is the opposite. Beamforming fixes angles and measures travel time, interferometry fixes times and measures angles.

In general, the beamforming systems are more complex, physically larger and more expensive. Interferometric systems are more compact, simple, and economical.

The swath angle, which envelopes the individual pencil beams, reaches greater angles in interferometric systems, although data quality at the more lateral areas greatly degrades.

Beamforming systems generally guarantee top data quality. They calculate for each ping from 300 to 1000 high-quality measurements. Interferometric systems can calculate up to 8000 measures per ping, but the vast majority of them are anomalous. A prefiltering of the interferometric data is required, while beamforming systems normally import data directly into the post processing software.

The multibeam is coupled to a positioning system, which also provides the timing signal, and attitude data.

The frequency of the echosounder is very important for different aspects. It fixes the size, performance, and scope of the system. Multibeams usually acquire data using a single frequency. In some models, this frequency can be modulated and changed within a predefined range. Usually, these modes are used for high frequency multibeams (higher than 200 kHz). Systems that can simultaneously manage and measure data on two frequencies are now entering the market.

In addition to traditional depth measurements, through time measurement and applying acoustics' rules, the multibeam records backscattering from the seabed. This measurement is used to study the nature of the seabed.

To complete the package of measurements available, multibeam beamformers are able to sample the signal strength also along the water column. This data package is called water column data (WCD). It is used for many applications, from wreck surveys to gaseous emission studies, from the study of fishes to the detection of water masses at different physical states. The main problems with these data, partially still unresolved, lie in the processing of WCD, which is not automated, due to data dimension, which is about ten times larger than of the one from the bottom.

1.3.3.3 The Airborne Lidar Bathymetry (ALB)

Electromagnetic measures now accompany traditional acoustic ones. Electromagnetic wave sensors are installed on aircrafts (whether manned or unmanned, guided or autonomous) or satellites.

Only the most developed technology, ALB, is analyzed hereinafter. It is based on LIDAR (Light Detection And Ranging) techniques and it collects data compliance with international standards. The other consolidated application from a technological point of view, but not yet from a hydrographic one, is the satellite derived bathymetry, and it is left to other treatments.

The electromagnetic (EM) energy allows the sensor to be used in the air. The EM propagation in water, in fact, is worse than the acoustic one and remains acceptable in the visible field around the blue-green frequencies; moreover, it is strongly influenced by the transparency of the water. For bottom detection, lasers are used on blue-green frequencies in areas where water transparency is high. For the measurement of transparency, even approximate measurements are sufficient, but they should be extended to the entire area of the survey (the depth of the Secchi disc is used). The maximum depth achievable from the ALB is a multiple of the Secchi depth, from 1–2 times for the higher frequency sensors to 3–4 times for the lower frequency sensors. In the best conditions, the system reaches depths up to 40–50 meters, in the worst a few centimeters. Unlike the multibeam, the laser operates beam steering partly mechanically, using a rotating or mobile mirror.

The ALB sensor is totally out of the water. This has the advantage of increasing the area explored per hour, also considering that the aircraft is less dependent on weather conditions than the vessel, and it is faster. It is possible to acquire data in the water and out of the water, integrating the coastal conformation and realizing an integrated approach to the study of the interface between submerged and emerged surfaces.

Being out of the water, however, the ALB measurements of depth presuppose aknowledge of the vertical reference. For a vessel, it can be identified indirectly by the position on board of the transducer, applying draft, heave, and tide. The aircraft needs an additional channel to measure the position of the water surface. This

channel transmits in the infrared field, which does not penetrate the water. The instantaneous water level measurement is then corrected for the tide.

Acoustic and electromagnetic measurements, in or out of water, can now use the vertical component of GNSS to fix the vertical datum. In this case, the IR channels of the ALB or the transducer immersion data are not useful as they are referred to the ellipsoidal height.

The considerations expressed on the auxiliary sensors for the MBES can be transposed to the ALB. For GNSS and attitude sensors, only operational differences do exist. Aircraft moves faster than ship, so the measurement frequency and the filters to be applied (especially for heave) are different.

Finally, it should be considered that while MBES can be used autonomously by a surveyor, independently from the manufacturer, an ALB survey should be carried out by specialized hydrographic surveyors.

1.4 The Hydrographic Standards

In order to be representative, measures must be collected according to certain common rules, standards, through which the data can be associated to a certain quality standard and then exchanged and used for different needs.

At national and international level, three levels have been consolidated for the management of the rules to be applied in hydrography.

The first level is the international one. The standard is the framework of hydrographic rules and today is represented by the publication of the IHO S-44 “IHO Standards for Hydrographic Surveys” Edition 2020, recently updated to its sixth edition.

The second level, the national one, transposes and applies the international standard to the national level. It can eventually integrate the international standard, giving more detailed and restrictive indications.

The third level includes all residual materials, such as good practices, guidelines, and operating manuals. In practice, this level is useful to apply the standards and make them usable in hydrography.

Hydrographic standards are hierarchically organized among themselves. The definition of hydrography indicates the way forward: the context related to the safety of navigation appears to be only one of the applications, as the collection of data accordingly to the quality rules imposed by the authoritativeness of the BIPM is paramount.

1.4.1 The IHO Standard

The IHO S-44 Edition 6.0.0 "Standard for Hydrographic Surveys" is the international standard that provides the common framework for the execution of hydrographic surveys.

It represents the minimum standard for the execution of surveys agreed by the international hydrographic community. It does not contain procedures for setting up the equipment, as it does not focus on how to conduct surveys, but it defines what is mandatory to achieve high resolution and quality data.

The essential element that guides the standard is obviously the quality of the measure, understood both as Quality Control (QC), i.e., a procedure that operatively allows accompanying the results of the survey quality, and as Quality Assurance (QA), i.e., the declaration of those who conduct the survey that data are representative of reality and therefore interchangeable.

The objective and quantitative value that measures QC and QA are the uncertainties of the measurement. The confidence level is set at 95%. The table that outlines the minimum criteria for each type of survey is organized in orders, and it breaks down the uncertainty into its horizontal component (defined Total Horizontal Uncertainty, THU) and its vertical component (defined Total Vertical Uncertainty, TVU). The uncertainty limit reported in the tables of S-44 should be considered as the uncertainty of processed data, as the final products extracted by the measurements.

Once the quality of the measurement is defined, it remains to understand which types of measurement the standard prescribes for the hydrographic survey.

Starting from the definition of hydrography, the goal is to identify the shape of the seabed through bathymetry measurements. The bathymetric measurements, however, can never be separated from those related to the nature of the bottom, because one parameter influences the other: depth and seabed sampling (directly through samples or indirectly through backscattering) can therefore be read today in an integrated way.

For bathymetric surveys, particular geometric criteria are required: they concern both the bottom features and the shape of the coastline and details of the coastal zone.

For the bottom feature, feature detection and feature search are required. They are mandatory to search and identify the bottom physical shapes with cubic dimensions greater than a certain value. The feature detection is linked to the feature search: it is, in percentage, the extent of an area that has to be surveyed using a systematic method for identifying features.

The last criterion to classify surveys is the bathymetric coverage, the extent to which an area has been surveyed using a systematic method of measuring depth; it is expressed in percentage and it is based on the combination of the survey pattern and the theoretical area of detection of survey instrumentation. For a multibeam system, conducting parallel lines in order to overlap the pattern of the fan beam on the seabed, the bathymetric coverage is larger than 100%. If an area is explored twice by the same system or two independent systems, it is 200%.

Once the minimum criteria have been defined, the S-44 classifies five different groups of minimum criteria, the so-called survey orders.

A different table of the standard is related to other minimum criteria, the THU and TVU of features above the vertical reference and the water flow measures.

Beyond the tables, the real innovation of the new edition of S-44 is related to the new specification matrix. It provides a range of selectable criteria for bathymetric parameters and other hydrographic data types. The matrix alone does not define any standard for hydrographic survey, but its criteria can be used to build up a specification for a particular survey, including those defined in the Tables 1 and 2 of S-44, the so-called preprepared survey orders.

The deep goal of the matrix is to extend the use of S-44 beyond the safety of navigation purpose and the survey orders already detailed, creating a common framework for tasking and assessing hydrographic surveys for a broadband use.

The matrix is organized into four sub-parts, bathymetry, positioning above the vertical reference, water flow and nature of the bottom, which can be integrated in the future by other communities, different from the hydrographic one.

Finally, the standard reports the metadata. This information must comply with appropriate standards. The S100-Universal Hydrographic Data Model implemented by the IHO,[19] that goes well beyond hydrographic measurements, appears to be the reference standard to be followed in the future not only for metadata, but also to integrate the matrix criteria (Fig. 1.3).

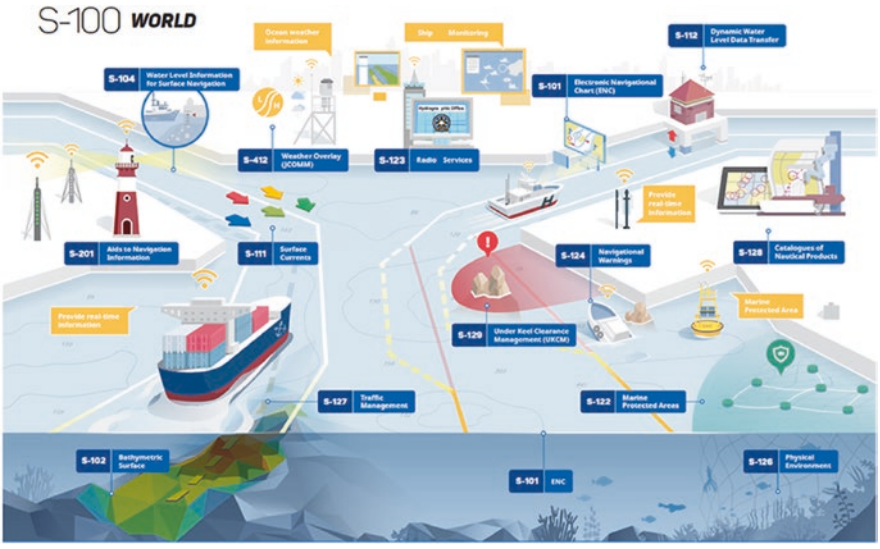

Fig. 1.3 The S-100 based Product Specifications (courtesy of KHOA—Korean Hydrographic and Oceanographic Agency)

[19] See http://s100.iho.int.

1.5 From Marine Data to Information

1.5.1 Data Processing

Data must be combined and reduced to the same space-time reference frame, and then converted into information.

At the basis of data acquisition, there is as follows:

- The spatial reference frame to which the measurements are referred, in order to establish the linear and angular offsets with respect to the body frame of the vector, to which all the measurements are referred in the processing phase.
- The temporal reference frame to which the measurements are referred and the possible shift with respect to those of the other instruments; as already mentioned, data are aligned with UTC time, kept updated, and synchronized by GNSS.

Individual data packages written by the acquisition software in the raw data files.

For bathymetric measurements, raw data are combined to create firstly the soundings, and then the elevation model nodes.

The sounding is an estimation of the depth at a certain position, being the depth reduced to certain spatial and temporal reference frames.

The node is an estimation of the depth at a point, created by number of surrounding soundings.

The elevation model includes ways to interpolate depth among nodes.

For backscattering measurements, raw data are transformed into pixels and then into mosaics.

The pixel is a backscattering measurement at a certain position.

The mosaic is a geo-referenced image of the seabed characterized by a horizontal resolution.

The result of the initial processing is a cloud of geographical and time referenced points (points cloud), being each one the result of a single bottom measurement.

For each point, moreover, the uncertainty is calculated. This uncertainty is also divided into two components, the horizontal uncertainty (THU) and the vertical uncertainty (TVU). The offsets and distances between the instruments are also used in the calculation of uncertainty propagation.

The soundings processed in this way are potentially able to directly represent the depth. However, they have intrinsic limits due to various aspects. The main advantage of multibeam soundings is that they are redundant. Having a redundant number of soundings, therefore, permit to select them or mediate them. Another reason to reduce the data to be selected by post processing is that the sounding points cloud is intrinsically noisy (any error on the single measurement affects the data cloud), as well as having enormous dimension, and it causes very challenging computer management.

Therefore, a certain number of soundings around a point, called node, are mediated by grouping them together. Each node is the result of a geo-statistical

operation, as a consequence its reliability will be greater and its uncertainty smaller respect with the single sounding. In order to be statistically robust, the process of selection must include a good number of soundings per node. Fixed the same uncertainty per sounding, the more soundings are contributing to a node the better the node will be in terms of quality compared to the soundings.

The resolution of the depth surface, characterized by equidistant nodes forming a square mesh, becomes the most important parameter of the processing. It becomes necessary to mediate between the need to bring the nodes closer together in order to be able to represent smaller features through the model, and the need to distance them in order to group more soundings per node and thus improve the uncertainty of the node. The choice should be made according to the specifications of the survey as explained in the previous chapter, and quantity and quality (average distance and uncertainty) of the available soundings. Once the smallest resolution achievable as a function of data and specifications of the survey have been established, there is the possibility of widening the distance among the nodes simply because a higher resolution is not necessary, for example when the survey data are in an area with a relatively regular morphology.

Hydrographic software is developing algorithms that, taking into account the parameters mentioned above, calculate the optimal resolution in the various areas of the survey. They are called auto-resolution algorithms (the software indicates the value of the optimal resolution) and multiresolution algorithms (the software elaborates, on different areas of the survey, grid at different resolutions).

Once the resolution and therefore the horizontal position of the nodes have been established, the soundings that contribute to the estimation of the node depth must be selected. Hydrographic software uses filters based on empirical formulas that calculate the maximum distance around the sounding or node, where the calculation of the node falls. According to the calculation, the same sounding can potentially be used for none, one or more than one node.

The modus operandi for averaging soundings can be classified into two main categories. A category takes the uncertainty into account, the other does not. Assuming that not taking uncertainty into account does not lead to any advantage, the algorithms that do not use it are residual and are simply applied where uncertainty is not available. S-44 also reports:

“omissis.... gridded bathymetric models in presence of survey logs, reports and other metadata are sufficient to serve as the authoritative result and deliverable of the survey.....”.

Using algorithms that use uncertainty is the systematic way to determine whether the survey meets the standard.

One of the uncertainty algorithms used today is the Combined Uncertainty and Bathymetry Estimator (CUBE), which adds a preliminary statistical filter to the calculation of the depth of the node.[20] For various reasons, related to the propagation

[20] See Calder, B., Wells, D. (2007). “CUBE User Manual Version 1.13”. Center for Coastal and Ocean Mapping and NOAA/UNH Joint Hydrographic Center. University of New Hampshire.

and operational aspects of the multibeam, some soundings, called blunders or outliers or spikes, are vertically very far away from the true bottom and the estimation of their uncertainty is not true. If they are used in the calculation, they would lead to unreliable estimates of node depth. The CUBE acts before the node depth calculation; it groups the soundings that have been selected for a certain node in different depth hypotheses, using Bayesian inference. A sounding can only contribute to one hypothesis of a certain node; it follows that sounding in discarded hypotheses does not contribute to the node depth calculation.

The CUBE, therefore, creates for each node one or more hypotheses according to the statistical relevance of the sounding depth differences. The CUBE is therefore a type of model that serves to not only filter data and calculate depths, but also to explore the characteristics of both the data and the background, which can be used to focus the attention on particular areas. Manual processing, which is expensive and complex as well as subjective, is done only where necessary and where it has positive feedback.

Along with bathymetric measurements, backscattering measurements are collected in order to contribute synergistically to the definition of the shape and nature of the seabed.

The raw backscattering data is a time series of signal values accompanied by pitch, roll, heading, and position information.

The georeferenced and equalized pixels are the final representation of the measurements after hydrographic processing. They can be grouped in mosaics in which each node is equidistant from the others (usually from centimeters to meters) and distributed on a regular grid. Grouping several measurements together allows to mediate them and therefore to improve their quality. It is also limited to the desired spatial resolution, avoiding data that are too big and difficult to manage.

A bathymetric grid and a mosaic, aligned with the reference frames of the survey specification, represent the final hydrographic dataset. A detailed technical report of the survey should accompany them; it completes the information that can be inferred from the data and allows tracing all operations and choices of the survey, while a quality assurance statement certifies and confirms the previous quality control operations.

1.5.2 From Data to Marine Spatial Data Infrastructures

Data are integrated into geo-databases and managed by governance that aims the creation of Marine Spatial Data Infrastructures (MSDI). The publication IHO-C17, Spatial Data Infrastructures "The Marine Dimension", reports what today goes beyond the definition of hydrography and looks at the future of the entire sector:

"Hydrography has a vital role in MSDI in providing core "reference" data (such as bathymetry, maritime boundaries, coast line, and geographic areas and names). After all, Hydrography is the branch of applied science which deals with the measurement and description of the physical features of oceans, seas, coastal areas,

lakes, and rivers, as well as with the prediction of their change over time. It does this firstly for the purpose of safety of navigation but also plays a crucial role in the support, through its data and information resources, of all other marine activities, including economic development, security and defense, scientific research, and environmental protection".

Under this idea, the concept "Map once, use many times" appears today as a driver able to indicate how to collect hydrographic measurements and then make them available for various uses. Therefore, nowadays measurements are fundamental to reach the maximum result in terms of representability and knowledge of the marine environment.

Measurements at sea are expensive because they require dedicated knowledge and instrumentation, and the current worldwide situation sees the presence of few data mostly heterogeneous and difficult to use for different applications, as the same data have been collected and oriented mainly to their use. However, there are also factors that, if properly taken into account, can allow orienting future data acquisitions toward a more cost-effective level. In particular, today several sensors can be installed on the same platform at the same time and several environmental parameters can be recorded on the same sensor. From a technological point of view, the parallel acquisition has now surpassed the series acquisition. It is also undeniable that the traditional acoustic measurement carried out in water has been integrated by the electromagnetic one.

Under these strategies, the data collected can be selected into models or charts in order to be more usable for practical application. The hydrographic community is today strongly active not only in data acquisition, but also in the development on how data can be converted into information through products (Fig. 1.4).

MSDI, the way forward for the hydrographic community, has four main pillars, and only one of them is data.

The second pillar is the standard used to manage data and convert it into information. The IHO standard S-100 Universal Hydrographic Data Model provides the data framework for the development of not only the next generation of electronic nautical charts (ENC) products, but also other related digital datasets and products required by the hydrographic, maritime, and GIS communities. Specifications based on S-100 are now being developed for a range of thematic data resources such as S-102 for bathymetry and S-122 for Marine Protected Areas (MPA).

The third pillar refers to policy and governance.

The fourth pillar refers to information and communication technology, because the good use of new discoveries can drive and shape the future of the hydrographic sector (Fig. 1.5).

Only by an integrated development of the four pillars, data and products will be useful for the blue growth and the sustainable use of the ocean.

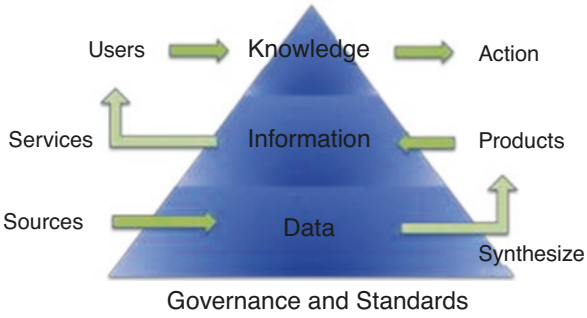

Fig. 1.4 The MSDI Data Information Knowledge triangle (courtesy of International Hydrographic Organization)

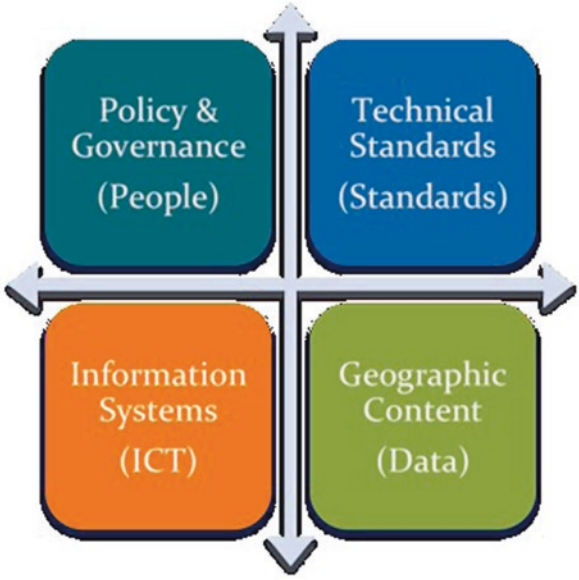

Fig. 1.5 The four MSDI pillars (courtesy of International Hydrographic Organization)

1.5.3 A Look into the Future

The technology has no limits and no controllable speed. Hydrography cannot be subtracted from this dynamic. But technology can make the difference especially in the future.

The hydrographic progress identifies the ability to map the Ocean as one of its top priorities.[21] The niche of safety of navigation, although remaining a fundamental part of the hydrographic world, should be enhanced with other applications,

[21] It is stated in the GOAL 3 "Participating actively in international activities related to the knowledge and the sustainable use of the Ocean" of the new 2021–2026 IHO Strategic Plan approved at the 2nd IHO Assembly in November 2020.

promoting the exchange of hydrographic data and information according to common rules and competencies.

This chapter is a way to introduce how the hydrographic community is expanding the historical approach to assure the safety of navigation to a new one, based on a data centric approach. Through this data centric approach, which is modeled by the S-100 Universal Hydrographic Data Model, the community will be able to better interact with all the Communities and Stakeholders active in the sustainable use of the Ocean.

References

1. Calder B, Wells D (2007) CUBE user manual version 1.13. Center for Coastal and Ocean Mapping and NOAA/UNH Joint Hydrographic Center. University of New Hampshire, New Hampshire
2. Bureau International des Poids et Mesures (2012) International vocabulary of metrology–basic and general concepts and associated terms
3. International Hydrographic Organization (2020) Strategic plan 2021–2026
4. International Hydrographic Organization (2017) C17—spatial data infrastructures: "the marine dimension"—guidance for hydrographic offices
5. International Hydrographic Organization (2020) M3—resolutions of the IHO
6. International Hydrographic Organization (2020) S5—standards of competence for hydrographic surveyors
7. International Hydrographic Organization (2019) S32—hydrographic dictionary
8. International Hydrographic Organization (2020) S44—IHO standards for hydrographic surveys
9. International Hydrographic Organization (2018) S100—IHO universal hydrographic data model

Chapter 2
Measurements for Meteorology

Vincenzo Capozzi, Carmela De Vivo, Yuri Cotroneo, Giuseppe Aulicino, Giannetta Fusco, and Giorgio Budillon

Contents

Abstract Ocean state and sea-air interactions exert a relevant role on the variability of the atmospheric circulation at several timescales from months to decades and centuries. In this framework, marine meteorological observations provide a unique source of information for the description of atmospheric parameters and constitute a key input to numerical models for the prediction of the future state of the atmosphere, as well as an important benchmark for the comprehension of recent trends of global climate. This chapter provides an overview of the meteorological measurements at sea. Sea-based observations involve a great variety of platforms, including ocean weather stations, manned and unmanned light vessels, moored and drifting buoys, and radio soundings. Each platform provides different data and responds to a different scientific need. Here, we provide the main characteristics of the most common instrumentation with some details about measured atmospheric parameters, equipment, and standards (i.e., time of observations and data transmission). Moreover, a paragraph focuses on the importance of marine meteorological services and to their role in supporting safe shipping through the provision of reliable marine observations and forecasting. Finally, we discuss some possible future

V. Capozzi (✉) · C. De Vivo · Y. Cotroneo · G. Aulicino · G. Fusco · G. Budillon
Department of Science and Technology, University of Naples "Parthenope",
Centro Direzionale, Isola C4, Naples, Italy
e-mail: vincenzo.capozzi@uniparthenope.it; carmela.devivo@uniparthenope.it;
yuri.cotroneo@uniparthenope.it; giuseppe.aulicino@uniparthenope.it;
giannetta.fusco@uniparthenope.it; giorgio.budillon@uniparthenope.it

P. Daponte et al. (eds.), *Measurement for the Sea*, Springer Series in
Measurement Science and Technology,
https://doi.org/10.1007/978-3-030-82024-4_2

developments, including the use of unmanned marine vehicles and new strategies to integrate in situ observations with new generation remotely sensed data.

2.1 Introduction

In recent years, the marine meteorology, defined as the monitoring, analysis, modeling, and forecasting of the weather and associated oceanographic conditions at sea, is receiving more and more interest within the scientific community. Nowadays, in fact, it is widely accepted that the meteorological measurements in marine environment provide key information on the comprehension of recent observed climate variability and trends. The most relevant distinguishing features of marine meteorology compared to other subfields of meteorology lie in the ocean-atmosphere interactions. The latter can depend on very complex mechanisms, involving different spatial scale, from microscale to local, regional, and global ones, and can be considered a source of major challenges in the understanding and the prediction of marine weather.

The rapid innovation and growth of technological facilities have offered different options for observations of atmospheric conditions at sea, both along coast and in open sea, including the traditional automatic weather station, the moored and drifted buoys and, from a remote sensing perspective, the satellites. These platforms are able to produce a massive amount of data that are used not only for scientific research purposes, but also in operational contexts dealing with weather forecasting and supporting of the marine meteorological services.

In this chapter, we provide a state of the art of the platforms and instruments currently used to observe weather conditions at sea. A special attention is devoted to surface in situ measurements that constitute the most affordable source of information, used as ground-truth to evaluate and calibrate the performance of alternative measurement techniques, such as remote sensing. A particular emphasis is also dedicated to the marine meteorological service and to their role in managing the available information and observations and in transferring them to different end-users. It is well known, in fact, that a reliable marine meteorological program requires a wide knowledge of the state of the atmosphere and ocean surface, with particular focus on some phenomena triggered by atmospheric dynamics, such as waves, storm surge, and sea ice accretion that may have a relevant impact on navigation.

2.2 Organization of Marine Meteorological Services

Marine meteorological services (MMS) perform two fundamental functions: supporting international shipping and other marine activities on the high sea and serving the various activities that take place in coastal and offshore areas, ports, lakes,

and on the coast [1]. Such services are organized to provide marine users with meteorological and oceanographic information (warnings, forecasts, charts, expert advice, and climatological data) necessary for the safety of the navigation using appropriate dissemination methods. MMS satisfy several basic requirements including the dissemination of information on marine environmental conditions and phenomena (as established by international conventions and national practices in relation to maritime operations), the promotion of the efficiency and economy of navigation. Furthermore, MMS guide the use and interpretation of meteorological and oceanographic information [2]. Open sea MMS include the provision of weather warnings, marine forecasts, and sea ice information services. Members broadcast weather reports through a satellite communication service and on marine radio frequencies. On the other hand, MMS for coastal, offshore, and local waters are focused on services for international shipping in harbor approaches and convergence zones. Information services include coastal community activities, coastal protection, including engineering works, special transport in coastal areas, fishing, as well as fixed or floating installations at sea [2]. Additionally, meteorological services support Search and Rescue (SAR) operations following the internationally specified requirements [2]. Therefore, it seems evident that marine data are used directly and indirectly by a broad community to address operational, commercial, and scientific needs (e.g., from operational oceanography to climate studies). The various sampling and collection strategies, data transmission technologies, metadata and documentation, as well as data quality evaluation differ according to the final users and their use. A primary challenge is effectively managing resources provided by commercial, governmental, and private entities to meet these varied requirements. Most observations made to support operational marine forecasting are funded and managed by *National Meteorological and Hydrological Services* (NMHS), while many other observations are supported by time-limited national or private sector research funding. An important challenge is linked to the management of data that should be used by the scientific community, where users see the need for long-term observations. Equally challenging is ensuring that observations used for climate analyses and researches are of sufficient quality and quantity, are appropriately described by metadata, and have suitable provision for sustained data management [3].

Indeed, oceans cover about 70% of the earth's surface and play an important role in driving atmospheric circulation. The oceanic observations are particularly important for forecasts and warnings to help ships and other offshore operators avoid severe meteorological conditions at sea. An example of ship observations assisting the issuance of a North Atlantic high seas warning occurred on July 29, 2015. A ship observation on the near-west side of an extratropical cyclone reported sustained winds from 65-knot hurricane that was not included in the 6-h forecast of the National Centers for Environmental Prediction Environmental Modeling Center's global forecasting system model. Using the ship observation, a meteorologist at the National Weather Service's Ocean Prediction Center upgraded high seas forecasts to include a hurricane-force wind warning for the cyclone. It is evident that marine observations and human guidance still add value to daily forecasts, watches, and

warnings, especially for high impact events, particularly in the 12–48 h forecast period [3]. Observations are the heart of quality marine services and are collected by several stations. On the mainland, these stations are located to provide adequate coverage of the area of interest, while observations at sea are generally more limited and for this reason, they assume an extraordinary importance. They are generally carried out by ships, buoys, and satellites and sent to the Meteorological and Hydrological Service Centers (NMHS) and inserted in meteorological numerical models from which local and global forecasts start. To coordinate marine meteorological and oceanographic services around the world, the WMO-CIO Joint Technical Commission for Marine Oceanography and Meteorology was established in 1999 (JCOMM), starting with the collaboration of World Meteorological Organization and the Intergovernmental Oceanographic Commission (UNESCO). JCOMM coordinates and recommends standards and procedures for a fully integrated marine meteorology and ocean observation, data management, forecasting, and analysis system. JCOMM is a fundamental element in the implementation of the Global Ocean Observing System (GOOS), the Global Climate Observing System (GCOS), and it is a contributor to the Global Earth Observation System (GEOSS). The main objectives of JCOMM are to improve the provision of marine and oceanographic weather forecasts, promote risk management for economic, commercial, and industrial activities of the marine environment, contribute to the development, improvement, and provision of climate services related to marine atmosphere, coastal, and deep oceans, and to coordinate and improve the provision of data, information, products, and services needed to support climate research, detection, and forecasting of climate variability [1].

2.3 Weather Observations from Ships

For centuries, mariners have contributed to the recording of daily meteorological information essential to navigation. In the logbooks, information about speed of vessel, wind intensity and direction, air pressure, precipitation, the state of the sea and sky, as well as thunder and lightning occurrences were noted. Some of these registers dating back to the seventeenth and eighteenth centuries and preserved in the archives of Great Britain, Holland, France, and Spain have been digitized and made available as part of the Climatological Database for the World's Oceans (CLIWOC) project [4]. These early weather observations now constitute a unique climate record [5]. In recent decades, the key role of the oceans in the global climate system has placed greater emphasis on the importance of marine meteorological and oceanographic observation systems, especially for climatic studies. In this regard, the Voluntary Observing Ships (VOS) scheme of the World Meteorological Organization (WMO) was launched. It is an international program by which ships crossing the world's oceans and seas are recruited by the National Meteorological Services (NMS) for taking and transmitting meteorological observations. In general, the ships participating in the VOS program should be able to

measure some of the main meteorological variables such as wind speed and direction, sea surface temperature (SST), air temperature, humidity, atmospheric pressure, clouds (including types), wave parameters, and significant weather conditions [6]. Some of these observations are visually estimated (such as clouds or weather conditions) while SST, air temperature, humidity, and atmospheric pressure are measured by meteorological instruments. Instruments used by the VOS generally include wet and dry bulb thermometers displayed on marine screens or harness psychrometers, a range of different types of anemometers, barometers, and barographs. Weather reports, at the beginning, were compiled manually and then transmitted to the nearest weather center, typically using Inmarsat communications with a special access code [7]. Observations were distributed between met services and global modeling centers using the global telecommunications system (GTS) established and operated by the WMO. The program can be dated back to 1853, a standard form of ship's log and a set of standard instructions for the necessary observations were defined.

In the recent decades, there has been a substantial increase in the use of automated on-board observation systems and electronic logbooks have increasingly replaced paper versions. Electronic log software is typically used to format manual observations for transmission and storage, calculate derived parameters, and perform simple quality checks, helping to improve the quality of observations and reduce any measurement errors. The VOS scheme is the primary source of real-time weather observations from ships, but the number of VOS observations have decreased over the past 30 years [3]. This decline can be attributed to the increasing dependence of the Numerical Weather Prediction (NWP) models on observations from satellites and drifting buoys and the consequent perception that the observations of ships are not used [3, 6].

Even if the near global coverage of satellite remote sensing helps overcome the problem of the scarcity of in situ data from vast areas of the world's oceans, ship data remain essential as they provide parameters that cannot be retrieved through remote observations (e.g., atmospheric pressure). Furthermore, ships can collect data from regions with gaps in satellite coverage and provide validation data relevant to forecasting operations. In addition, to their use in numerical weather forecasts, ship data are also used operationally in preparing forecasts and warnings, including those for the global maritime safety and rescue system, and to support the routing of ships to avoid adverse weather conditions and transport efficiently goods and passengers [3]. Although the VOS now only comprise one element of the surface marine observing system, their ongoing role in providing marine information is increasingly being recognized. They are widely used to monitor and understand climate change, for the validation, calibration, and analysis of satellite observations of SST, precipitation, wind, clouds, air temperature, and humidity, to provide information on air-sea interaction and atmospheric stability and modeling applications including reanalysis, NWP, and force fields for ocean models. However, there is a need to improve the quality of weather observations from ships [3]. In this regard, the VOSClim project was launched with the goal of providing a high-quality subset of marine meteorological data, with extensive associated metadata, to be available

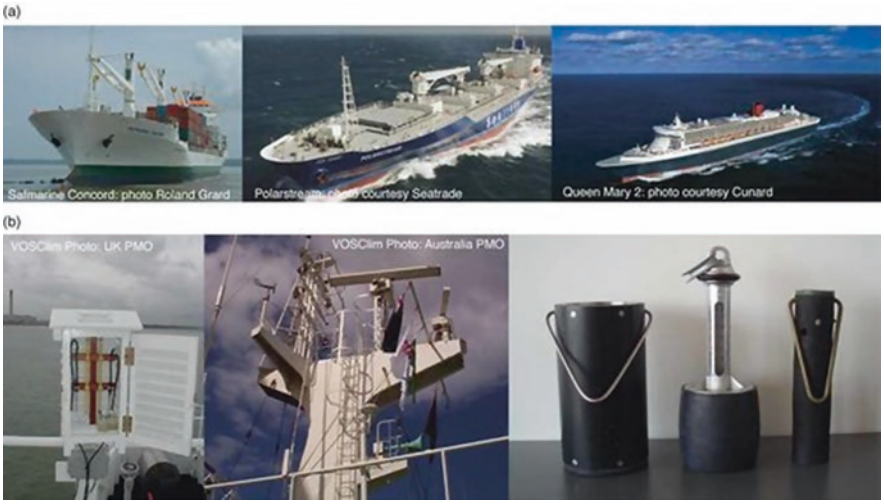

Fig. 2.1 Examples of the types of ships collecting weather observations and the instruments used. (**a**) Left to right Safmarine Concord, Polarstream (both Netherlands VOS) and the Queen Mary 2 (UK VOS). (**b**) Temperature Screen on the Dominica (UK VOS), anemometer on the ANL Australia (Australian VOS), and SST buckets used by VOS from the Netherlands, Germany, and the UK (Copyright Kent and Ingleby, 2010)

in both real-time and delayed mode to support global climate studies. Figure 2.1 shows an example of the types of ships performing meteorological observations and the instruments used in the VOSClim project.

VOSClim is a follow-up to the earlier VOS special observing project North Atlantic (VSOP-NA), which was conducted on behalf of the World Climate Research Project (WCRP) from 1988 to 1990. The data of the VOSClim project are fundamental for climate change studies. They are used as input in the air-sea flow calculations, as part of coupled atmosphere-ocean climate models, for calibration satellite observation and provide high quality data for a possible recalibration of observations from the whole VOS fleet. In terms of benefits to the navy industry, VOSClim supports the development of future marine weather systems which should assist meteorologists in producing more accurate marine weather conditions forecasts. Observations from ships therefore remain a unique and invaluable contribution to all marine meteorological services [7]. However, coverage is inevitably patchy as some regions are not plowed by ships. In these cases, the integration of the VOS observation with other instruments such as buoys and installations on platforms would allow to fill these gaps. New initiatives to improve data quality and integration with other observing programs should ensure that the VOS remain an important contributor to the Global Climate Observing System in decades to come [6].

2.3.1 Automatic Weather Stations (AWS)

In recent years, Automatic Weather Stations (AWS) or partially automated systems on ships are being increasingly used for both purposes of observation and transmission of data [1]. The basic operating modes are essentially three. In the first case, the observations may be performed manually and subsequently entered in an electronic logbook and transmitted through automatic or manual systems. In the second case, observations are performed automatically using AWS; the position, course, and speed of the ship are detected using the on-board satellite navigation system, usually Global Positioning System (GPS). The transmission of such observations may be purely automatic or started manually according to the communication structures. In the third case, the observations are carried out by combining manual and automatic methods [1]. The AWS vary greatly from very simple to more sophisticated installations. Some of the simplest on board AWS are based on technology also used in weather buoys, and basically consist of a barometer package with satellite communications. An example of a low-cost AWS is the mStar-Ship for coastal ship, originally designed by MetService for land application. It gives information about station position, course and speed, wind speed and direction, air temperature, relative humidity, and atmospheric pressure data. Several AWS are completely self-contained, while others require ship's power and may be connected to the ship's navigation system. Other types of AWS developed by Meteo-France include the BATOS and MINOS systems, used by the UK VOS and the Canadian AVOS systems. BATOS gathers data from digital weather sensors (pressure, air temperature, sea temperature, wind speed, and direction) and allows the input of manually observed elements (visibility, sea state, cloud type and height, present and past weather, ice, etc.). The BATOS unit then codes this data into a complete weather observation and transmits it ashore using satellite communications. MINOS weather station consists of a Vaisala PTB 210 barometer, a GPS unit and an Argos transmitter, all located together beneath an antenna dome. An air temperature sensor is located below the dome [7, 8]. The AVOS system collects the data similarly to BATOS, but all the sensors and probes are located on a mast. The position of the instruments on the ship is a very important aspect as it may influence the measurement of the various meteorological quantities [1]. For example, wind measurements are strongly influenced by air flow induced by the structure of the ship. The local effects produced by the superstructure, mast, and the side members should be minimized by placing the tool forward and higher practicable. The top of the foremast is generally the best site for positioning an anemometer. On the other hand, barometers and barographs should be mounted on shock-absorbing material in a position where they are least affected by concussion, vibration or movement of the ship. Generally, the best position is as close to the center of flotation as possible. Additionally, temperature and humidity observations should be made by means of a hygrometer or psychrometer, which has good ventilation. The instruments must be well exposed in a stream of air, directly from the sea and should be adequately shielded from radiation, precipitation, and spray. Sling or aspirated psychrometers

exposed on the windward side of the bridge have been found to be satisfactory. Regarding precipitation, it is difficult to obtain reliable measurements, owing to the aerodynamic effect of the superstructure of the ship, the influence of roll and pitch, the capture of spray, and the changes in ship position. The equipment should be constructed and exposed in such a manner that the first three effects mentioned above are avoided or minimized. As for the sensors for measuring the sea surface temperature, they should be placed forward of all discharges at a depth of 1–2 m below the water line [1]. In this context, the availability of metadata is a fundamental requirement for the correct use of meteo-oceanographic observations. Metadata, in fact, contain information about the type of observation, the type of ship, and the dimensions as well as the position of the instrumentation (where on the ship and at what height). This information allows interpreting the data correctly and increasing data consistency (e.g., bias correction) [1]. The increasing use of automated systems in both measurement and transmission of observations and related metadata has resulted in an improvement in the quality of measurements, maximizing the availability of data for research and climate studies [3].

2.3.2 Radio Soundings

In the mid-1980s, the stationary weather vessel service was replaced with other types of measurements including radio soundings with the ASAP program (Automated Shipboard Aerological Program). The primary goal of ASAP is generation of upper air profile data from sparse ocean areas using automated sounding systems carried on board merchant ships plying regular ocean routes. As part of the global observation system, ASAP data may be used to support many applications, including global climate studies. The radio survey is carried out using an aerostatic balloon capable of reaching 30,000 m in height (three times the flight altitude of an airliner), to which are attached extremely precise instruments capable of measuring pressure, temperature, and the humidity of the air. Thanks to a radio emitter, it is possible to follow the movement of the balloon with respect to the launch point and therefore also calculate the direction and intensity of the wind at various altitudes. The launches take place at the same time as the ground launches, in order to provide a synoptic description of the upper atmosphere on a global scale. A vertical profile of the atmosphere for pressure, temperature, humidity, and wind is thus obtained. Initially, ASAP was part of the program WMO-IOC Joint Technical Commission for Marine Oceanography and Meteorology (JCOMM) and in particular of Ship Observations Team (SOT). In recent years, the responsibility for coordinating program activities, including management and control quality data has shifted to a Ship Observation Team (SOT) established by the WMO/CIO Joint Technical Commission for Oceanography and Marine Meteorology (JCOMM). The original ASAP system was developed as a modular containerized unit that could be quickly installed on, or removed from, a host ship. The system was completely housed within a specially modified standard 6.1 meter shipping container. This container included all

necessary electronics and antennas, the balloon launching system, stowage for consumable supplies such as helium, balloons, and sondes, and adequate operator workspace. In recent years, this configuration has been replaced by a "distributed system". Distributed systems essentially consist of the required electronics that are installed in existing naval spaces accessible to the operator, usually on the bridge or nearby. Manual or remote launch techniques are employed and supplies are stored in an appropriate onboard space. The profile data are all made available in real time on the Global Telecommunication System (GTS), for use by the operations centers. Most of the soundings currently come from the North Atlantic and Pacific Northwest, but the program is also expanding into other ocean basins. ASAP publishes an annual report, which provides program status and statistics on data return and data quality. The quantity and quality of data collected in real time have shown significant improvement since the early years. However, the main problem related to ASAP measures are misplaced reports with some suspect positions. In some cases, in the reports are included missing values for latitude/ longitude or occasionally marked with a wrong sign. Recently, most national programs have adopted the Inmarsat C system for data transmission. This system has a communication efficiency of approximately 99%, enabling data communication as effectively as other flight data worldwide. Nowadays, the Global Positioning System (GPS) and Loran are the most commonly used systems today to determine the speed and direction of radiosondes. The total number of ASAP soundings have increased to around 5000 per year. Every year new ships are introduced and others disappear for many reasons, for example the maintenance of the vessel or its use on other lines [9]. The percentage of successful soundings (i.e., the data have been successfully transmitted to the GTS) is relatively high, despite there are several factors that could compromise the correct use of the radio sounding such as bad sea conditions, errors by the operator or faulty in the instrumentation. Sea radio sounding measurements therefore appear to be of fundamental importance for obtaining information on the vertical profile of the atmosphere in remote and unexplored areas, especially for measurements relating to upper wind. Figure 2.2 shows time series from January 1994 to December 2012 with monthly counts of ASAP reports of wind at 250 hPa included in the Report ECMWF 2012 [10].

2.4 Ocean-Atmosphere Heat Fluxes

The collection of information about how the atmosphere and ocean interact represents an important part of understanding and predicting the Earth climate system. To this aim, it is essential to measure the exchange (or flux) of heat, water, and momentum between the atmosphere and the ocean. These fluxes are sensitive indicators of changes in the climate system, with links to floods and droughts, tropical cyclones and climate indices, e.g., El Niño/Southern Oscillation (ENSO) and North Atlantic Oscillation (NAO). Thus, turbulent and radiative heat exchanges between ocean and atmosphere, ocean surface wind stress, and state variables used to estimate them

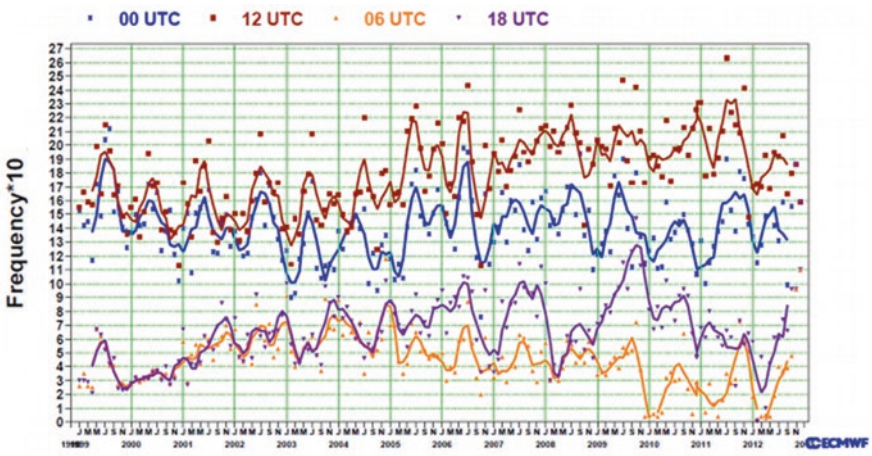

Fig. 2.2 ASAP wind data received at ECMWF 250 hPa (January 1994 to December 2012). Symbols show monthly totals and lines show moving averages (Copyright ASAP Report ECMWF 2012). The content is covered by the Creative Commons Attribution-Non-Commercial-No-Derivatives-4.0-Unported License, as described on https://www.ecmwf.int/en/terms-use [11]

from bulk formulae, have been listed among the Essential Ocean Variables influencing weather and climate. The measurements of fluxes are also critical for successful coupling of ocean-atmosphere (and ice) models to obtain reliable long-term weather forecasts, seasonal-interannual-decadal climate predictions, and regional climate projections [11].

Surface heat flux can be defined as the rate of exchange of heat, per unit area, crossing the sea surface from water to the air. The net heat flux is given by the sum of turbulent (latent and sensible) and radiative (shortwave and longwave) components. Latent heat flux depends on the phase change of water during evaporation/condensation, while sensible heat flux represents heat transferred from the ocean to the atmosphere by conduction/convection. As for shortwave radiation, downward flux is predominantly visible light, while upward is reflected sunlight, often determined by parameterization of surface albedo. Longwave heat flux is given by Earth (ocean) infrared emission. Sensible, latent, and longwave heat fluxes occur at the air-sea interface. The shortwave radiation indeed penetrates seawater, being absorbed with depth along the water column [12].

Sensible and latent heat fluxes have traditionally been estimated through bulk formulae with the aid of the observations of sea surface temperature, near surface air temperature and humidity, surface winds, waves, and mean sea level pressure. Even though it is now possible to infer these bulk variables from satellite observations of the ocean (see Chap. 8), in situ measurements still represent an essential information to monitor ocean conditions and provide ground truth for satellite retrievals calibration/validation.

Locally, sensible and latent heat fluxes can be computed taking advantage of buoys and ships using fast-response, three-dimensional wind sensors together with fast-response air temperature and humidity sensors, through covariance flux methods. As for radiative fluxes, they can be measured directly from buoys, ships, and other ocean platforms using sensors to measure downward shortwave and longwave radiation and meteorological parameters [13].

Prior to 2000, ships have been the primary platform for direct flux observations used by the state of the art bulk flux algorithms. Typically, sensors to estimate the momentum, sensible heat, and latent heat flux on a moving platform, include a 3-axis sonic anemometer/thermometer, a 3-axis motion package and an open path infrared hygrometer. Although they experience some dropouts and occasional spikes, particularly in rain, sonic anemometers/thermometers are generally very reliable in the marine environment [11]. Depending on the experimental focus, additional components can be added to measure fluxes of CO_2, ozone, and all climate-relevant gases, as well as pollutants.

Algorithms using ship-based measurements need to account for several issues (e.g., wind distortion due to the ship profile; ship decks microclimate effect on air temperature, humidity, and barometric pressure measurements; ship motion contribute to turbulence). A major challenge is to limit errors in the observation of momentum, heat, and mass exchange within the wavy boundary layer.

Many of these issues are minimized in moored surface buoys measurements which are equipped with new-generation sensors and radiometers. The instrumentation on these moorings is less affected by flow distortion than ships and collects data on a wider variety of conditions given their longer deployments. They can also compute and transmit flux data in near real-time to shore. Nevertheless, these buoys can be affected by several issues (e.g., battery power limited to 12–24 months, biofouling, extreme weather and wave conditions exposure, damages by vandalism and sea birds) which can determine sensor failures.

A variety of autonomous platforms for observing air-sea interactions have been also developed, e.g., surface drifters and, recently, wave gliders and saildrones (see Chap. 3). Their sensors are usually powered by solar energy and/or batteries, and placed close to the difficult-to-resolve boundary layer, thus improving the accuracy of exchange estimation [11]. On the other hand, problems can arise for meteorology sensors which are indeed best deployed at a height above the wavy boundary layer. These platforms can cover thousands of nautical miles, transported by currents or being piloted by land control station [14]. The latter allows the monitoring of specific areas/transects, as well as the adaptive sampling of target events such as eddies and hurricanes/typhoon [15].

Despite the encouraging results obtained in the last decades, at present the global ocean momentum and heat fluxes estimation does not meet the necessary requirements for oceanography and climate studies, yet. The global coverage of flux observing (fix and drifting) platforms should be expanded and extended over different key regions in order to provide enhanced observations of the coupled boundary layer to be integrated with ship-based measurements.

2.5 Observations from Buoys

The meteorological report from ships has supplied a relevant contribution to the marine observing system over the course of time. However, the coverage of these observations is inevitably patchy, being strictly dependent on ships route. The improvement in technology has offered new opportunities to fill these gaps. In this respect, an alternative to the traditional measurements from ships are the moored and drifted buoys, which provide accurate and very useful information that is often involved in research activities and studies as reference ground truth both for surface and satellite measurements [16]. Drifting and moored buoys are now generally considered as a very affordable option for obtaining meteorological and oceanographic measures from remote ocean areas falling outside the common ships route. This section provides an overview of both moored and drifting buoys, with special emphasis on instruments and data, as well as on strengths and points of weaknesses of these platforms.

2.5.1 Moored Buoys

The moored buoys are defined as large platforms anchored at fixed location that regularly collect meteorological and oceanographic data through different sensors. These buoys are usually part of national monitoring and forecasting centers and serve not only for scientific need but also for maritime safety.

Early, historical, experiments with these types of platforms were performed in the 1940s, when the US Coast and Geodetic Survey investigated the design of a buoy that would measure the tidal currents. The first important deployment of moored buoys was performed in 1950s: it was called Navy Oceanographic Meteorological Automatic Device (NOMAD). On 1962, one of these buoys collected meteorological data at the passage of the hurricane Carla, one of the most severe ever recorded in the Gulf of Mexico. Although the wind speed and pressure values were beyond the calibrations of NOMAD's instruments, the buoy observed a peak gust of 67 m s^{-1}. Other experiments and projects were launched in the 1960s and early 1970s. Different shapes, such as boats, discus, and toroids, were tested in different meteorological and oceanographic scenarios. Such experiments allowed mitigating some troubles and issues, related to failures in mooring sustaining and electronics and sensor problems. The best results, in terms of survivability and sensors performance, were obtained using 10-m hull buoys.

From 1988, an important program financed by main European countries, named European Group Ocean Stations (EGOS), was launched: the main purpose of EGOS was the deployment of a joint network of drifting and moored buoys for the real-time collection of oceanographic and meteorological records in the North-Atlantic, a key area for the large-scale circulation. Other relevant actions were carried out by Canada, Finland, and Australian Bureau of Meteorology.

A critical aspect that must be carefully considered when designing a moored buoy is the hull/mooring system. It is important finding the best compromise between the need of a stable platform to measure wind and an adequate water-surface-following characteristic for sea state observation [17]. The hull configuration must satisfy some logistic requirements: it must be easily installable and transportable both at sea and on land, as well as serviceable at sea by small boats.

As early stated, the moored buoys may be classified according to the hull type, whose choice depends on many factors, related to the location and water depth. Among various hull types, the discus has revolutioned the size buoys design: the discus type proved to be very reliable also in extreme weather conditions. In this respect, it is worth mentioning the experience of National Data Buoys Center (NDBC) of National Oceanic and Atmospheric Administration (NOAA), which designed discus buoys of various sizes (12-m, 10-m, and 3-m). The 12-m discus buoys (Fig. 2.3a) are more rugger in bad weather than smaller ones. However, the latter and in particular the 3-m type (Fig. 2.3b) is very cost-effective and can be easily transportable.

To avoid possible damages to the sensors by the waves and to conform to the standards that regulate the location of sensors above the water surface, a tower or mast is usually deployed above the buoy's deck to support the meteorological sensors. More specifically, the instruments are located at 10 m level for the 10-m and 12-m discus buoys and at a height of 5 m for the 3-m discus buoys. Some sensors, such as the barometer, the water temperature sensor, the magnetic compass, and the accelerometer are generally installed below the buoy's deck, together with the data acquisition/telemetry package. Nowadays, a moored-buoy technology is expected to operate from 6 months up to 2 years even in most critical meteorological conditions.

A typical moored buoy is conceived to measure the following meteorological parameters: wind speed, wind direction, atmospheric pressure, sea surface

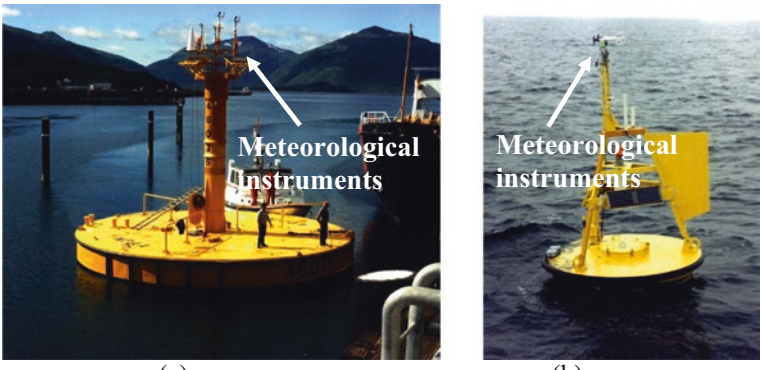

Fig. 2.3 Examples of 12-m (**a**) and 3-m (**b**) discus buoys. The white arrows indicate the position of meteorological instruments. Images are courtesy of National Data Buoys Center (NDBC) of National Oceanic and Atmospheric Administration (NOAA)

Table 2.1 Measurements uncertainties of main oceanographic and meteorological parameters recorded by moored buoys [WMO]

Parameter	Uncertainty
Sea surface temperature	0.2 °C
Air temperature	0.1 °C
Wind speed	1.0 m s^{-1} or 5% above 20 m s^{-1}
Wind direction	10.0°
Dew point temperature	0.5 °C
Sea level pressure	0.2 hPa

temperature, air temperature, dew point or relative humidity; moreover, additional elements recorded are the solar radiation, the precipitation, the atmospheric visibility, and the surface current and salinity. Table 2.1 sketches the measurement uncertainties from operational buoys for some meteorological parameters.

In the following subsections, a description of the meteorological sensors generally hosted by the moored buoys is provided.

2.5.1.1 Anemometers

In operational buoys programs, wind speed and direction are generally measured using a cup-anemometer and wind vane. The cup-type anemometer is widely used as virtue of its simple functioning principle, which is based on a direct relationship between the speed of rotation of the cups and the wind speed. The latter can be determined via different approaches, including mechanical or magnetic switches, small generators, and photoelectric and capacitance choppers. The wind direction from the vane can be retrieved by a potentiometers or shift encoders. Wind measurements from buoys are subjected to various sources of errors and ambiguity. According to marine forecasters' experience, buoys wind speed is generally lighter than ship winds. In the majority of cases, this disparity can be ascribed to the differences in anemometer height and averaging times [18].

The installing of dual anemometers has been found a good strategy to prevent data losses due to anemometer failures as well as expensive service visit involving ships and personnel resources. Moreover, dual anemometers represent an important "added-value" in the framework of quality control procedures, since the measurements of instruments may be compared with each other [19]. The most frequent cause of cup-anemometer failure is the mechanical wear. To increase the longevity and reliability of wind speed measures, alternative sensors have been tested, such as the sonic and dynamic ones. The sonic sensor determines wind speed by computing the time of arrival of acoustic signals transmitted across a fixed path, whereas the dynamic type is engineered to sense the pressure force on an object placed in the wind flow.

2.5.1.2 Barometers

The Rosemont barometer is the most used on-board moored buoys to measure atmospheric pressure. This sensor has a sensing element, a capacitance pressure transducer that converts the atmospheric pressure to an electrical parameter that, in turn, can be processed to have an output signal. One of the most relevant issues affecting barometric buoys observations regards the sensitivity of the transducers both to the accelerations and force of gravity due to the buoys motion. To mitigate this problem, it is recommended installing the sensors with their most sensitive acceleration axis in a direction that is perpendicular to the one of greatest acceleration.

Moreover, an adequate protection must be applied to prevent the intrusion of water and spray into the pressure port.

2.5.1.3 Air-Temperature Sensors

Temperature buoys measurements are generally handled with platinum resistance-wire type or thermistor type sensors. In the design of buoy masts, it is important taking into account the exposure of the air-temperature sensor to the air flow. It is well known, in fact, that wind passing around a nearby surface that is not in thermal equilibrium with air before reaching the thermometer may generate errors in measurements. To reduce imprecisions due to the solar radiation, the temperature sensor is placed in a radiation shield. The latter can be equipped with a fan aspirating to remove the heat.

2.5.1.4 Solar Radiation

Interesting measures of solar radiation were taken by coastal buoys off California for air-quality studies. The sensor used was the LIR-COR Model-200Z pyranometer. The latter consists of a high-stability photodiode that is housed in aluminum case.

2.5.1.5 Relative Humidity

In a campaign carried out through coastal buoys off California for air quality studies, Rotonic hygrometer sensor, which is a capacitive polymer sensor, was tested. The collected relative humidity measurements were found to be accurate and reliable [17]. The United Kingdom Meteorological Office (UKMO) used a different humidity sensor, i.e., a wafer of a chemically treated styrene polymer that has an electrically conducting surface layer: variations in relative humidity cause a change in surface resistance. The long-term survival of the sensor was guaranteed by a protective housing, which allows the passage of water vapor but not of liquid water.

Moreover, this solution proved to very effective in resolving issues related to salt contamination also in most severe sea conditions.

In the same field campaign, interesting measures of solar radiation were also taken, using the LIR-COR Model-200Z pyranometer. The latter consists of a high-stability photodiode that is housed in aluminum case.

2.5.1.6 Precipitation

Several experiments were conducted to determine the rain gauge design that best matches the technical requirement of buoy platform. Such tests highlighted that a rain gauge operating on a buoy should be able to measure the volume and not weight of rainfall, as is usually done by a traditional tipping-bucket gauge. An interesting measurement campaign was conducted by NDBC: it consisted in testing the performance of 13 gauges developed by R.M. Young under the specific suggestions and requirements provided by NDBC. These gauges detect optical irregularities (scintillations) produced by precipitation within a simple volume filling through an infrared light beam. The precipitation rate is proportional to the intensity of the scintillations. The results highlighted that the rainfall records were inaccurate in case of light rainfall rates.

2.5.1.7 Power Source and Data Management

In the first developments, moored buoys were power supplied by diesel generators. Other options, such as nuclear power and wind generators, were also tested with various level of success. Thanks to the progressive miniaturization of on-board electronics and the reduced power requirements, the use of batteries become more and more common. The mean life cycle of batteries is about 2 years; after this limit, they have to be replaced. Such operation may be very hazardous and difficult at open sea, so buoys are usually retrieved and rebatteried in port.

The photovoltaic systems are still a good alternative or complement to batteries, although their efficiency depends on latitude. In most cases, the solar power demonstrated to be able to replace the battery power supply previously used on buoys. However, it is important emphasize that photovoltaic panels may be damaged at sea or during buoy serving.

The meteorological records collected by buoys are generally transmitted by HF and UHF link to the shore or via geostationary or polar orbiting satellites. The transmission relying on geostationary satellites, such as US GOES, the European METEOSAT, and the Japan Geostationary Satellites requires more power than the transmission via polar orbiting satellites. The geostationary satellites are a very useful mean of data transmission for regular messages (send on synoptic basis). In the case of polar-orbiting satellites, data can be received on the ground only when the transmitter and the receiver are simultaneously within the line of sight; otherwise, the data are stored on satellite for a later transmission [17]. Most of buoys data are

transmitted in a standard character code; in this way, the measurements can be easily and rapidly involved on the communication circuits. The procedures of data dissemination are regulated by WMO [20]. Once received, the data from buoys are routinely subjected to a quality control procedure. The latter should not introduce any delay in the onward transmission of the data via Global Telecommunication System (GTS). The quality control check is automatized using common statistical tests, focused on the detection of gross errors (i.e., data that are beyond the physically acceptable limits), outliers (i.e., data that do not satisfy the climatological limits), and other extremes such as unrealistic "jumps" between two consecutive observations. It should be noted that such tests must be applied with caution (e.g., data arriving from station situated along the path of a tropical cyclone may exceed time-continuity limits, but they are still valid). In the majority of cases, these checks are very effective in removing the large errors caused by failures in data transmission and/or in measures recording [17]. Generally, these errors represent the 0% of data and the checks remove the 90% of the errors. However, it is worth mentioning that the statistical test usually applied to control buoys data is not reliable in identifying the errors caused by sensor degradation: an example is the pressure or wind speed drops due to ice accretion, or measurements change due to sensor drift.

2.5.2 Drifting Buoys

Drifting buoys have a long tradition in field of experimental oceanography, especially for the measurements of currents. In the 1990s, accomplice the improvements in satellite tracking and data relay systems, there was a relevant increase in the deployment of these platforms. The evolution of this technology has responded, in the course of time, not only to oceanographic needs, but also to the demands of operational meteorology. According to WMO [20], the drifting buoys can be classified according to the specific application:

1. For oceanographic research, in the framework of the World Ocean Circulation experiment, a lagrangian (i.e., surface-current-following) drifter able to measure the sea-surface temperature has been developed and put into operation into many parts of the world.
2. For operational meteorology, drifting buoys collecting useful data about air pressure, sea-surface temperature, and air temperature were deployed.
3. For polar application, specific ice floats have been designed to observe, in addition to some atmospheric variables, the snow and ice conditions (i.e., ice/snow temperature and temperature profiles in the ice, ice stress, ice thickness, etc.). Using the information about the position of the buoys, it is possible also estimating the ice motion.

A drifter is composed by a surface float, which includes a transmitter for data communication via satellite and by a number of sensors for meteo-oceanographic measurements. The surface float is enshrined to a holey sock drogue (or to a sea anchor),

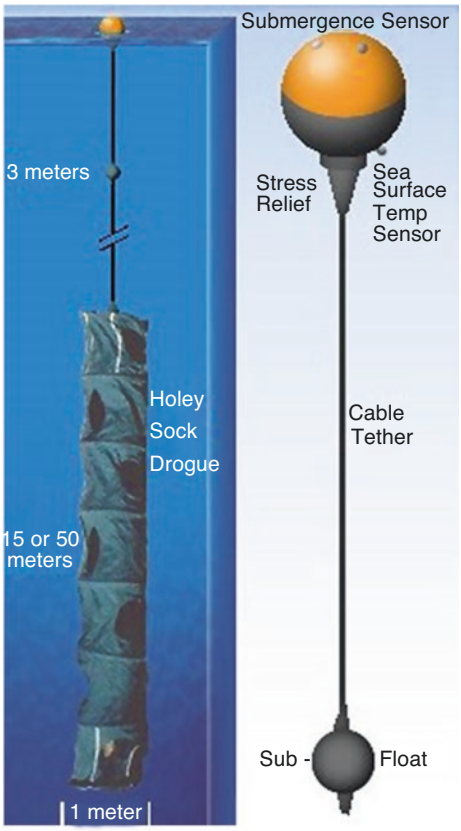

Fig. 2.4 Schematic of a drifting buoy. Image courtesy of U.S. Department of Homeland Security (United States Coast Guard)

centered at a depth of a 15 m (Fig. 2.4). The drifter follows the ocean surface current flow integrated over the drogue depth.

Relevant efforts have been devoted to design of drifting buoys that meet the oceanographic and operational meteorological requirements. In this respect, some examples are represented by:

(1) the SVP-B drifter, which is a lagrangian drifter with an air pressure sensor on-board; (2) the SVP-RW drifter, which is able to measure wind speed using the wind observation through Ambient-Noise (WOTAN) technology; (3) the wind and temperature buoy, which are equipped with meteorological sensors (including wind speed sensor) and with a subsurface thermistor chain for the measurement of temperature profile up to a depth of 100 m; and (4) the SVP with the addition of salinity sensors.

The main advantages in using the drifting buoys for monitoring the marine meteorological conditions relay on the easy deployment and in relatively affordable costs. However, the reliability of some measurements may be questionable: for example, the wind speed observations provided by these platforms are not used in

Table 2.2 Measurements uncertainties of main oceanographic and meteorological parameters recorded by drifting buoys [21]

Parameter	Uncertainty
Sea surface temperature	0.21 °C
Air pressure	0.84 hPa
Wind speed	3.5 m s^{-1} or 10%
Wind direction	18.5°
Subsurface temperature	0.1 °C

operational centers [21]. Table 2.2 summarizes the measurement uncertainties of some oceanographic and meteorological variables collected by drifting buoys [22].

Currently, there are over a thousand drifters operating around the world ocean, measuring both oceanographic and meteorological parameters. Drifting buoys have been deployed in the path of hurricanes to investigate the interactions between ocean and atmosphere during the storm passage, which can be considered a key element for improving forecast skills of such events. In this sense, a nice example is provided by measurement campaign performed during the passage of hurricane Ana, which hits the U.S. State of Hawaii on October 2014. On October 17, during the transition of Ana from tropical storm to hurricane, the Air Force Hurricane Hunters deployed 10 drifters in its path. Very useful and interesting data from nine of the drifters have been successfully collected and retrieved, providing wind speed and direction, atmospheric pressure, ocean temperature up to 150 m depth, and ocean currents in the mixed layer. These data give meaningful information about the strength of the storm and the structure of its ocean wake [23].

Recently, in January and February 2020, 64 drifting buoys have been deployed in the northeast Pacific Ocean (Fig. 2.5), in the framework of an important project, the Atmospheric River Reconnaissance (AR Recon), funded by the U.S. Army Crops of Engineers and the California Department of Water Resources. Two types of drifting buoys are involved in this field campaign: the above-mentioned SVP-B and a new type, the Directional Wave Spectra Barometer (DWSB). Like the SVP-B, the DWSBs measure sea-surface temperature and the atmospheric pressure; moreover, they collect data about the directional wave spectrum using a GPS engine. These buoys, according to the European Center for Medium Range Weather (ECMWF), provide very useful observations in a scarcely monitored area of an essential atmospheric parameter, the sea-level pressure. Such measurements are crucial for different reasons: (i) atmospheric pressure variability at sea level is a very important variable linked to large-scale atmospheric circulation variability and anomalies; (ii) in large part of ocean regions, there are very few in situ observations; and (iii) satellite data provide very limited information about sea-level pressure. The drifting buoys can operate for up 2 years and can represent a relevant and cost-effective opportunity, within the global observing system, for the observation of atmospheric pressure in remote sea-areas. However, it should be noted that only the 50% of the drifting buoys currently operating worldwide is not equipped with a pressure sensor.

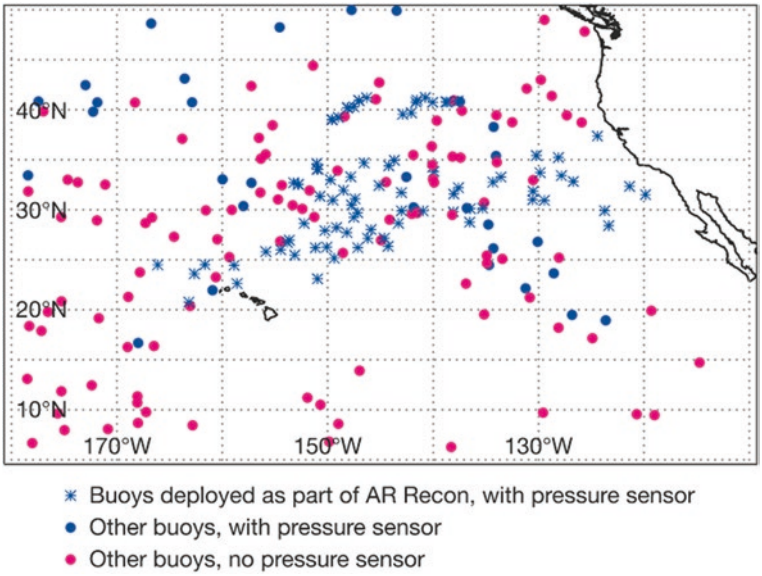

Fig. 2.5 This map shows the location of all drifting buoys in the northeast Pacific Ocean in February 2020. These buoys have been deployed in the framework of Atmospheric River Reconnaissance (AR Recon) project. In this ocean area, 53% of buoys also measure atmospheric pressure. Image adapted from ECMWF [24]. The content is covered by the Creative Commons Attribution-Non-Commercial-No-Derivatives-4.0-Unported License, as described on https://www.ecmwf.int/en/terms-use [25]

This recent deployment in North-Eastern Pacific has reinforced the current monitoring within the AR Recon project; in the precedent deployment (January 2019), 32 SVP-B buoys were launched, of which 24 are still functioning in February 2020. Therefore, the total number of AR Recon launched buoys have raised to 88 in February 2020. The pressure data collected by this network are ingested in the data assimilation framework by the Integrated Forecast System of the ECMWF and promise to improve the forecast skills over Europe in the medium range [24].

2.6 Future Developments

Accurate forecasts and warnings weather and ocean state are nowadays necessary to keep people safe at sea and to study the atmosphere-ocean interaction at all temporal and spatial scales. The realization of reliable numerical models based on large observational dataset is probably the most prominent aspect of the future development of studies focused on the weather at sea and the sea state itself.

Such an ambitious aim first requires large amounts of data collected by multiple organisations from different countries. Furthermore, since the number of

observations at sea are small compared to land-based data, marine observations gain more and more importance.

As described in the previous paragraphs, marine weather observations are increasing in numbers and improving in quality thanks to modern technology and faster and more diffuse communications from ships and unmanned instruments. On the other hand, numerical weather and ocean modeling and forecasting are advancing rapidly, through fully and dynamically coupled systems, involving ocean, atmosphere, and cryosphere. Even the advent of more powerful supercomputers and more advanced algorithms gives to scientists the opportunity of gathering and analyzing more information with a finer precision. Processes at smaller spatial and temporal scales as sea surface temperature filaments, wind speed at various altitudes or rainfall accumulations can now be studied and modeled.

Once become operational, the numerical models and the related forecasts provide assistance to navies and other government agencies. Furthermore, they are gaining increasing space in ocean commerce and industry, transport, fisheries, marine environmental management, and a long list of sea-related sectors.

Due to the typical spatial and temporal scale of atmospheric processes and to the global interest in safe navigation for all the countries, the need of a worldwide coordination of observational, technical, and scientific efforts in the field of sea and weather state observations and forecasts has soon been clear.

Until last century, marine meteorological and oceanographic observations, data management, and service provision programs were internationally coordinated by two separate bodies - the World Meteorological Organization (WMO), through its Commission for Marine Meteorology (CMM), and Intergovernmental Oceanographic Commission of UNESCO (IOC), jointly with WMO, through the Committee for the Integrated Global Ocean Services System (IGOSS).

The emerging need ever closer working relationships between oceanographers and marine meteorologists led to the foundation of Technical Commission for Oceanography and Marine Meteorology (JCOMM), intergovernmental body of technical experts providing a worldwide coordination between WMO and IOC.

The JCOMM provides therefore an international coordination of oceanographic and marine meteorological observing, data management and services, combining different expertise, technologies and capacity building capabilities of the meteorological and oceanographic communities.

The long-term objectives identified by JCOMM are nowadays defining the future steps for marine weather observations and sea state forecasts:

1. To enhance the provision of marine meteorological and oceanographic forecasting and analysis services in support of the safety of life and property at sea and in coastal areas.
2. To contribute to the development, enhancement, and delivery of climate services related to the marine atmosphere, the coastal and deep oceans, to support climate research and the detection and prediction of climate variability.

3. To coordinate the enhancement and long-term maintenance of an integrated global marine meteorological and oceanographic observing and data management system.
4. To manage the evolution of the services through the selective incorporation of advances in meteorological and oceanographic science and technology.

Meteorological and oceanographic scientific community must then face new challenges associated to a deeper understanding of met-ocean processes and to the need of higher reliability, sustainability, affordability, cost effective, real time, global coverage of in situ observations [26, 27].

References

1. WMO (2018) Guide to marine meteorological service
2. WMO (2018) Manual on marine meteorological service–volume I: global aspects, Annex VI to the WMO Technical Regulation
3. Smith SR et al (2019) Ship-based contribution to Global Ocean, weather, and climate observing systems. Front Mar Sci 2019:2
4. Garcìa-Herrera R et al (2005) CLIWOC: a climatological database for the world's oceans 1750-1854. Clim Change 73:1–12
5. Woodruff SD et al (2010) ICOAS release 2.5 and data characteristics. Int J Climatol 31:968
6. Kent E, Ingleby B (2010) From observations to forecasts-part 6. Marine Meteorol Observ Weather 65:231–238
7. Fletcher J (2008) Meteorological observation from ships. Marine Observations Meteorological Service of New Zealand Chair, JCOMM VOS Panel
8. International Maritime Organization [IMO] (2018) Participation in the WMO Voluntary Observing Ship Scheme, MSC.1 Circular 1293
9. The Automated Shipboard Aerological Programme (ASAP website). https://www.ocean-ops.org/sot/asap/. Accessed 25 Nov 2020
10. ECMWF (2012) Summary report on the monitoring of ASAP ship data
11. Cronin MF, Gentemann CL, Edson J, Ueki I, Bourassa M, Brown S et al (2019) Air-sea fluxes with a focus on heat and momentum. Front Mar Sci 103389
12. Fusco G, Budillon G, Spezie G (2009) Surface heat fluxes and thermohaline variability in the Ross Sea and in Terra Nova Bay polynya. Cont Shelf Res 29:1887–1895
13. OOPC (2017) Ocean observations panel for climate Essential Ocean variable specification sheet: ocean surface heat flux, Version 52, Jan 2017
14. Aulicino G, Cotroneo Y, Lacava T, Sileo G, Fusco G et al (2016) Results of the first wave glider experiment in the southern Tyrrhenian Sea. Adv Oceanogr Limnol 7:16–35
15. Cotroneo Y, Aulicino G, Ruiz S, Román AS, Tomàs MT, Pascual A, Fusco G, Heslop E, Tintoré J, Budillon G (2019) Glider data collected during the Algerian Basin circulation unmanned survey. Earth Syst Sci Data 11:147–161
16. Pierson WJ (1990) Examples of, reasons for, and consequences of the poo quality of wind data from ships for the marine boundary layer: implications for remote sensing. J Geophys Res 1990:95
17. Meindl A (1996) Guide to moored buoys and Other Ocean data acquisition systems. Geneva, Switzerland, WMO & IOC, data buoy cooperation panel, 40pp. & annexes. (DBCP technical document no. 8)

18. Wilkerson JC, Earle MD (1990) A study of differences between environmental reports by ships in the voluntary observing Programme and Measurements from National Oceanic and Atmospheric Administration (NOAA) buoys. J Geophys Res 95:C3
19. World Meteorological Organization (1987) Some General Considerations and Specific Examples in the Design of Algorithms for Synoptic Automatic Weather Stations. Instruments and Observing Methods Report No. 19, WMO!TD-No. 230, WMO, Geneva
20. World Meteorological Organization (2008) Guide to Meteorological Instruments and Methods of Observation, 2008 Edition, WMO-no. 8 (7th ed)
21. Ingleby B (2010) Factors affecting ship and buoy data quality: a data assimilation perspective. J Atmos Oceanic Tech 27:1476–1489
22. O'Carroll AG, Eyre JR, Saunders RW (2008) Three-way error analysis between AATSR, AMSR-E, and in situ sea surface temperature observations. J Atmos Oceanic Tech 25(7):1197–1207
23. NOAA's Array of Drifting Ocean Buoys Global Drifter Program. https://www.aoml.noaa.gov/noaas-array-of-drifting-ocean-buoys/. Accessed 1 Dec 2020
24. Drifting buoys deployed in the northeast Pacific. https://www.ecmwf.int/en/newsletter/163/news/drifting-buoys-deployed-northeast-pacific. Accessed 30 Nov 2020
25. ECMWF: Terms of use. https://www.ecmwf.int/en/terms-use
26. Joint Technical Commission for Oceanography and Marine Meteorology. www.jcomm.info
27. Global Weather and Climate Center. https://www.globalweatherclimatecenter.com/

Chapter 3
Measurements for Oceanography

Pierpaolo Falco, Pasquale Castagno, Yuri Cotroneo, Giuseppe Aulicino, Giorgio Budillon, Paola De Ruggiero, Giannetta Fusco, and Enrico Zambianchi

Contents

Abstract This chapter describes the instruments and platforms used to measure the physical properties of seawater to study the density field and dynamics of the ocean. Firstly, instruments used to measure temperature and salinity from ships are introduced: CTD system, XBT/XCTD, and underway probes. Lagrangian (drifters and floats) and Eulerian (single point current meters, ADCP) instruments used to obtain surface and deep ocean current measurements are then described. These instruments are considered the classical tools used to collect observations in the oceans. In the last section, autonomous and/or unmanned vehicles that have had a significant development in the last decade are described. The use of unmanned vehicle has now become more and more widespread. Floats represent the precursor to a new generation of marine drones which include gliders and wave gliders.

P. Falco
Department of Life and Environmental Sciences, Università Politecnica delle Marche, Via Brecce Bianche, Ancona, Italy
e-mail: pierpaolo.falco@staff.univpm.it

P. Castagno · Y. Cotroneo (✉) · G. Aulicino · G. Budillon · P. De Ruggiero · G. Fusco
E. Zambianchi
Department of Science and Technology, University of Naples "Parthenope", Centro Direzionale, Isola C4, Naples, Italy
e-mail: pasquale.castagno@uniparthenope.it; yuri.cotroneo@uniparthenope.it; giuseppe.aulicino@uniparthenope.it; giorgio.budillon@uniparthenope.it; paola.deruggiero@uniparthenope.it; giannetta.fusco@uniparthenope.it; enrico.zambianchi@uniparthenope.it

P. Daponte et al. (eds.), *Measurement for the Sea*, Springer Series in Measurement Science and Technology,
https://doi.org/10.1007/978-3-030-82024-4_3

3.1 Introduction

Ocean and atmosphere can be considered global-scale fluids characterized by analogous physical regimes. Despite the analogies between them and the importance of the ocean in driving atmospheric processes, the understanding of the ocean until recently has lagged.

Observations are essential to understand the mechanisms determining the water masses structure and driving the ocean dynamics. In recent years, with the advent of new ocean observing technologies, significant progress has been made in resolving the spatial and temporal scales ranging from the large dominant oceanic patterns down to the submesoscale processes. The major factor limiting the observational ability is indeed the superposition of motions at different scales that often cannot be separated. In addition, oceanographic cruises and field activities are very expensive in terms of human resources and logistics.

The advent of satellites has greatly improved the ability to observe large areas of the remote oceans in an almost synoptic way. Unfortunately, as the ocean is nearly opaque to electromagnetic radiation compared to the atmosphere, satellite measurements are limited to the thin surface layer ignoring most of the ocean.

Observational technology has evolved to fill the gaps and so did the theoretical understanding of the ocean. Unmanned vehicles represent the last evolution of ocean measurement technology and they are going to strongly improve the observation ability without the ship support. These new platforms are described in the last section of the chapter, whereas the classical instruments are described in the first sections.

3.2 Thermohaline Measurements from Ship

3.2.1 CTD and Rosette

The first oceanographic data recorded below the surface were collected in the Southern Ocean during James Cook's second voyage between 1772 and 1775 [1]. During this voyage, the temperature at the surface and depth of about 180 m were measured discovering that the Southern Ocean surface is colder than the subsurface layer. The second attempt to obtain a vertical profile of an ocean physical parameter was made during the Challenger expedition from 1872 to 1876. During this expedition, discrete temperature profiles were obtained from the surface to the bottom of the ocean using a pressure-shielded thermometer [2]. During the same period, the reversing thermometer was introduced [3]: a mercury thermometer with a constriction which when inverted breaks the column of mercury in the capillary tube fixing the temperature reading. This thermometer measured the temperature at discrete levels and was the standard to measure the temperature below the surface until the beginning of the Second World War.

The reversing thermometer was typically attached to the Nansen bottle [4, 5], a device used to collect water samples at a specific depth. The Nansen bottle, a metal cylinder, was lowered on a cable into the ocean and once the appropriate depth was reached, a weight, named messenger, was dropped on the cable tipping the cylinder upside-down closing the rotary valves at each side of the cylinder trapping the water inside. The water sample was then analyzed in a laboratory to determine the salinity. The Nansen bottle was triggered with the same messenger used for the reversing thermometer, thus, capturing a temperature and a water sample at the same depth with a single action. The Nansen bottles and reversing thermometers system were the standard physical oceanographic practice used from about 1910 to 1970 [6]. This system made observations available at discrete levels along the water column, therefore it was still not adequate to represent the full vertical variability and as an ocean-going temperature/salinity profiling instrument [6]. The first continuous ocean profiling instrument was the bathythermograph (BT) developed by Athelstan Spilhaus in the 1930s [6]. Nevertheless, the BT only measured the temperature; hence a profiler that also measured salinity and pressure was still necessary.

In 1955, Hamon and Brown [7] deployed the Salinity Temperature and Depth (STD) profiling recording system [8–10], which was the first instrument combining pressure with conductivity and temperature measurements. The STD was lowered by a winch and it was equipped with a thermistor as well as conductivity and pressure sensors connected by a sealed cable to an analog strip chart on deck [11]. The STD was further developed into the CTD (Conductivity, Temperature, and Depth) "microprofiler" by [10]. This new instrument, which had a different name to distinguish it from the older, overcomes some previous issues and improves the precision and accuracy of the measurement. Furthermore, by reducing the size of the sensors it pushes the scale of observations from the meter to the centimeter scale [6]. While the original STD had a resolution of 20 m in depth, modern ship-based CTD can reach a resolution of 0.06 m [11].

Nowadays, the CTD has replaced the Nansen cast as a hydrographic tool and represents the standard oceanographic instrument essential for measuring the physical properties of seawater.

The ship-based continuous profiling CTD consists of a set of sensors mounted on a main probe that is lowered through the water via an electrical conductor cable (sea cable) which transmits all the data collected directly to the deck unit on board of the ship. Besides transmitting the data, the sea cable, operated by a winch, is necessary to lower and take the CTD back on board. The deck unit is an analog/digital converter that translates the inputs received from the probe (electric signal) to data that can be received by a computer. The computer allows the real-time visualization of the data profiles (Fig. 3.1) as well as the communication with the probe and the data storage.

Typically, the CTD is located inside a metal cage to protect the sensors from the possible impact with the side of the ship and is often mounted on a larger frame named rosette, or carousel (Fig. 3.2).

The Rosette holds water sampling bottles (Niskin closed remotely as the instrument ascends or Go-flo bottles closed using a messanger) used to collect water

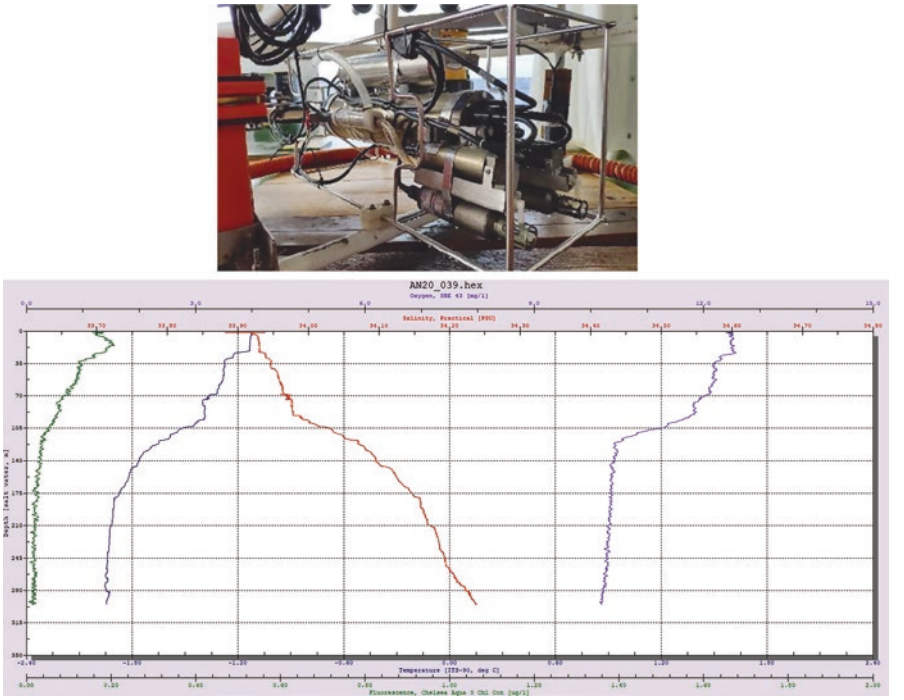

Fig. 3.1 CTD and data profiles: temperature (blue); salinity (red); dissolved oxygen (violet); fluorescence (green). CTD data collected at 78° 40.8' S and 163° 32.06' W in the Ross Sea

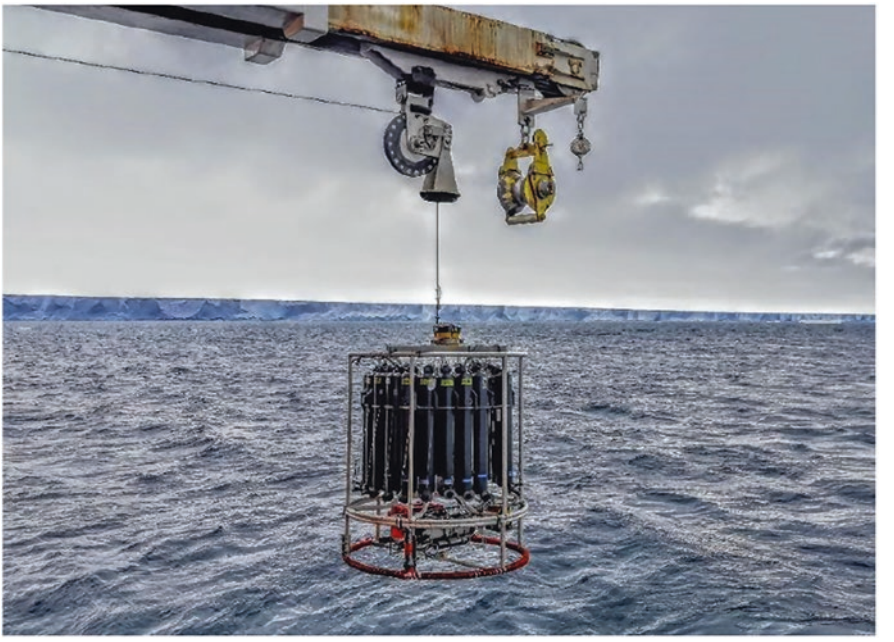

Fig. 3.2 CTD-rosette system during the XXXV Italian Antarctic Expedition in the Ross Sea (Antarctica)

samples at different depths to measure chemical and biological properties. The Niskin bottles are a further improvement of the Nansen bottle designed by Shale Niskin in 1966. Modern ship-based CTDs are often the central element of a complex suite of sensors that measure properties such as dissolved oxygen, fluorescence (used for chlorophyll concentration), pH, optical backscatter (a measure of suspended particles), and irradiance (amount of light from the sun that penetrates the water). Additionally, an Acoustic Doppler Current Profiler (ADCP) can be mounted on the rosette to measure the horizontal velocity of the water.

Nowadays, CTDs can also be used as off ship-based profiling systems and as moored instrumentation. Small, low-powered CTD sensors with internal recording are used on autonomous instruments like moored profiler, gliders, profiling floats, and AUVs.

The CTD laid the groundwork for the current ocean observing system and for the large-scale measurement cruises of the World Ocean Circulation Experiment (WOCE). WOCE Hydrographic Program was a comprehensive global hydrographic survey of physical and chemical properties representing the state of the Ocean during the 1990s (https://www.ewoce.org).

Repeated hydrographic stations obtained with ship-based CTD casts are crucial to establish the role of the World Ocean in the Earth's climate system. For example, a salinity time series created from CTD data have been used to study the variability of the Antarctic Bottom Water (AABW), the coldest and densest water mass that is formed around Antarctica and supplies the abyssal layer of the global ocean. Castagno et al., (2019) [12] analyzed a salinity time series constructed with CTD data in key areas of the Ross Sea (Fig. 3.3) in Antarctica, where the salty dense shelf water (High Salinity Shelf Water; HSSW), precursor to the AABW is formed and is exported from the continental shelf. They highlighted a sharp rebound of the salinity in 2014 following a freshening trend of the HSSW observed since 1958 [13]. This sharp increase in the salinity of the HSSW and consequently of the AABW [14] counters the multidecadal tendency in density decrease and contraction of AABW [13, 15, 16] which have both led to an increase in global ocean heat content and sea level rise [17].

3.2.2 Vertical Profiles Collected from a Moving Vessel: XBT, XCTD, Underway CTD, and Their Evolution

CTD and rosette systems are commonly used to obtain vertical profiles of oceanographic data and water samples from oceanographic research vessels. This activity requires research vessels to stop in the designed stations to carry out the casts and collect the full depth, high resolution data. Thus, long ship time is needed to achieve a high-resolution spatial sampling along the horizontal and vertical dimensions, with a direct effect on the costs of oceanographic cruises. Additionally, sea and weather conditions must be considered before and during each sampling station.

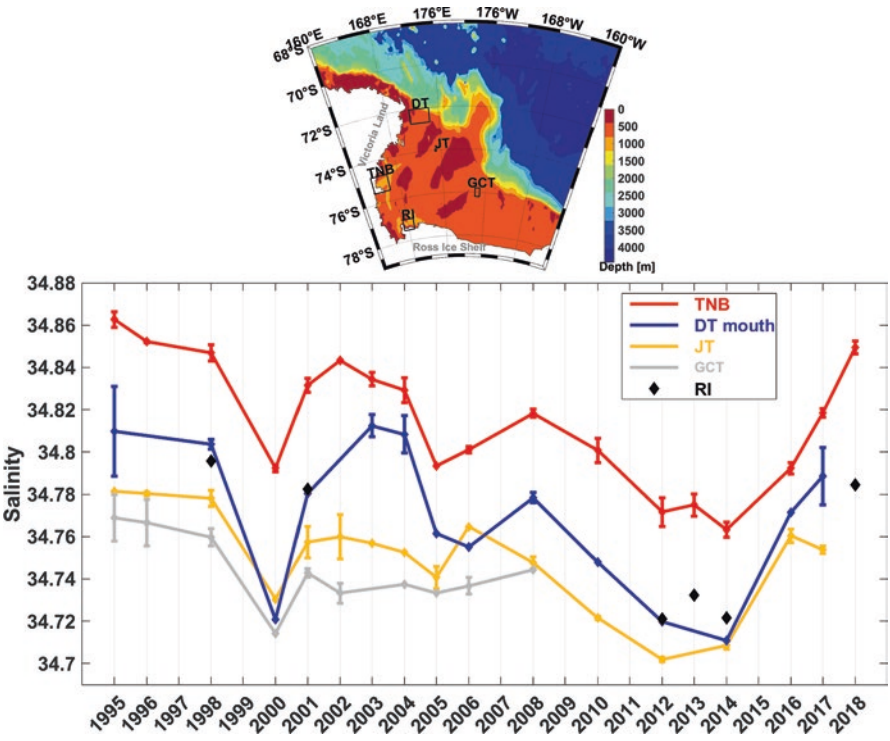

Fig. 3.3 HSSW salinity time series (1995–2018) in five different areas of the Ross Sea (see map above). Salinity averaged in the HSSW between 870 and 900 dbar in Terra Nova Bay (red line), between 850 and 880 dbar at Ross Island (RI, black diamonds), and in the deepest 20 dbar of the water column at Drygalski Trough (DT, blue line), Joides Trough (JT, amber line), and Glomar Challenger Trough (CGT, gray line). From [12]

For these reasons, the oceanographic community has pushed to the realization of a series of low-cost instruments for collecting along depth data from a moving vessel, may it be a research vessel a commercial or a recreational ship crossing a defined area (usually defined as ships of opportunity). The most common example of these instruments is the Expendable BathyThermograph (XBT) (Fig. 3.4).

The XBT is used to measure the water temperature while falling through the water. As the probe falls through the water at a known rate, the temperature/depth data can be inferred from the time of launch. Small wires transmit the temperature data back to the ship where they can be plotted as a function of depth to create a temperature profile of the water column.

The first version of XBT was the bathythermograph (BT) realized between 1935 and 1938 and then used during the II World War by the US Navy. These BTs were commonly used to infer information about the water column temperature variability that is extremely important for submarine activities, to have an exact estimate of the sound velocity speed.

Fig. 3.4 Left panel: an XBT probe out of its canister and the hand launcher. Right panel: an XBT deployment by means of a hand launcher

In the 1960s, the BT was re-designed by the Sippican Corporation of Marion (Massachusetts) to become a single-use instrument that could be operated without a recovery operation. The result is the modern XBT still used in oceanography.

The unit is composed of a probe equipped with a thermistor, a wire link, and a shipboard canister. The cable connection between the probe and the shipboard canister is provided by a pair of fine copper wires which pay out from both a spool retained on the ship and one located in the probe. Once released, the XBT probe falls into the water and the spool inside the probe accounts for the vertical movement, while the onboard spool inside the canister accounts for the horizontal movement of the ship. Accordingly, there is no drag effect produced by the ship motion on the probe or from the probe falling on the wire. When the maximum depth is reached, the wire runs out and breaks, and the XBT sinks to the ocean floor.

The probe and the included thermistor fall freely along the water column at a known speed that changes with time so that its depth can be determined by the timing, providing a temperature-depth correspondence. Ocean temperature profiles are transmitted onboard and constitute the basis for the realization of vertical along track temperature sections.

The deployment of an XBT does not require the ship to stop and thanks to the very simple launch system, it can be easily operated from every kind of vessel. Furthermore, as the instruments are lost after each launch and the collection of data is realized from a moving vessel, the impact of bad sea and weather conditions on oceanographic operations are significantly reduced. XBT is used even in very rough sea conditions where the realization of CTD casts is impossible.

Several XBT probes are available providing different solutions for the underway sampling. The main concern is associated to the ship speed and to the maximum depth that can be reached by the probe: the higher the ship speed the shallower is the maximum depth reached by the XBT.

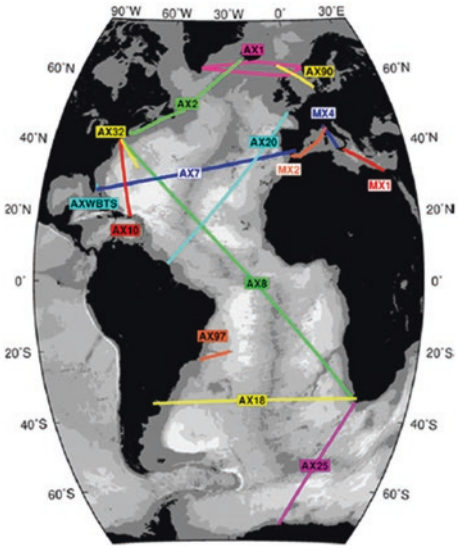

Fig. 3.5 Map of the NOAA/AOML eXpendable BathyThermograph (XBT) network from https://www.aoml.noaa.gov/phod/hdenxbt/index.php

Furthermore, the XBT has also been applied to the measurement of different variables as the sound velocity along depth (XSV) or the conductivity-temperature-depth data (XCTD). Nevertheless, the use of the classical XBT is still the most diffused thanks to the low costs and simple use.

XBT is largely used for real-time monitoring of the oceans [18] or marginal seas [19] mainly realized in the framework of the successful NOAA/AOML eXpendable BathyThermograph (XBT) network (https://www.aoml.noaa.gov/phod/goos/xbt_network/ Fig. 3.5). Here, XBT transects in High Density mode are repeated approximately every 3 months with XBTs deployed 10–35 km apart, in order to measure the mesoscale structure of the ocean and to assess the ocean circulation responsible for redistributing heat and other water properties globally [20].

Since 1994, the Italian National Antarctic Research Program (Programma Nazionale di Ricerche in Antartide - PNRA) has established a repeated monitoring XBT transect between New Zealand and Antarctica. This monitoring has been carried on within several research projects (CLIMA, CLIMA IV, SOChIC, MORSea) focusing on the variability of the Antarctic Circumpolar Current (ACC) and its water masses (Fig. 3.6).

Thanks to the long time series of data available since 1994 and to the high resolution of XBT casts, a description of the temperature distribution of the water masses along depth and along latitude can be realized (Fig. 3.7). This allows studying the location and variability of main Antarctic Circumpolar Current (ACC) fronts and the associated transport as described in [21–23], as well as the properties of mesoscale eddies detaching from the ACC [21].

The XBT concept has been the basis for the development of a large series of modern oceanographic equipment.

These new instruments are based on the idea of retrieving the probe after its use, so allowing the use of more expensive and complete sensors on the probe itself.

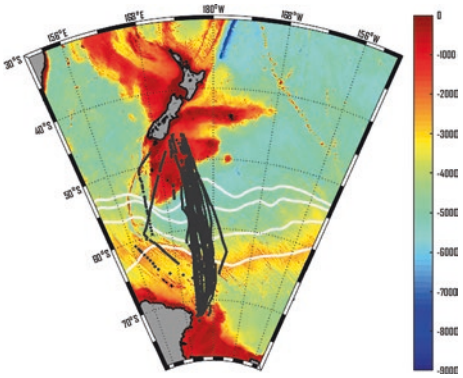

Fig. 3.6 Map of the XBT launches realized from 1994 to 2017 in the framework of the Italian National Antarctic Program. Bathymetry is indicated through color scale, with white lines showing the mean position of the ACC fronts from altimetry data

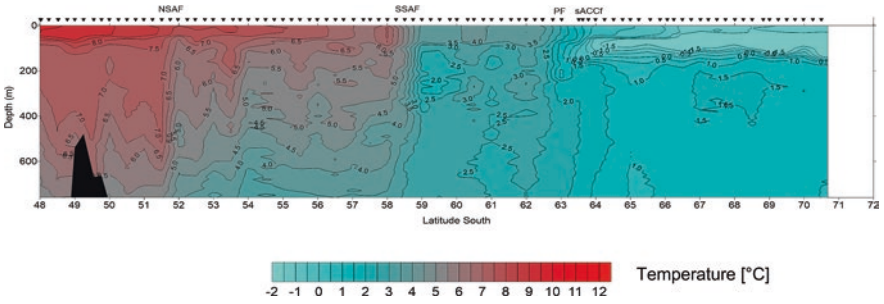

Fig. 3.7 Latitudinal temperature section in the layer 0–800 m between New Zealand and Antarctica. Temperature is indicated through color scale. Black triangles show the location of XBT casts. Northern Sub-Antarctic Front (NSAF), Southern Sub-Antarctic Front (SSAF), Polar Front (PF), and southern ACC front (sACCf) indicate the position of main fronts of the ACC. Modified from [21]

Some examples are provided by the underway CTD/RAPIDCAST or the Moving Vessel Profiler. Vertical profiles of the water properties can also be collected by towed underwater vehicles that can undulate in the upper ocean behind the ship. Nevertheless, all these instruments must still face the compromise between ship speed and maximum depth reached by the instrument, a problem that nowadays seems to be better solved by the 60-years old XBT probes.

3.3 Current Measurement

3.3.1 Lagrangian Instruments

The description of the distribution of any property in a fluid can be obtained with two different approaches: the Eulerian, at fixed point, and the Lagrangian, or particle following (e.g., [24]). The two specifications are in principle equivalent [25] (in

Fig. 3.8 Drifting bottle deployed in 1911 by the Oceanographic Society of San Sebastian (left panel), carrying a message in Spanish, French, and English (right panel). Image from the NOAA Photo Library, originally from the Oceanographic Museum of Monaco, D. Mille photographer

principle means that they would be equivalent if we had access to an infinite Eulerian and to an infinite Lagrangian data set). When it comes to measuring the ocean, the choice of one versus the other is based on the kind of output desired [26], as well as on a number of practical observational issues.

Technological constraints have made Eulerian measurements of the ocean current more popular in the past, but with the advent of accessible localization and data collection, mainly from satellites, Lagrangian current observations have become easier and more widespread. They can be carried out at the surface or at depth; surface instruments are called drifters, while deep ones are called floats [27].

Among the first surface Lagrangian "instruments" ever used were drifting bottles. Figure 3.8 shows an example from 1911. This bottle was used by the Oceanographic Society of San Sebastian, in the Spanish Basque country, and deployed from the vessel MAMELENA in 1911 (Fig. 3.8). It contained a card, marked by a serial number; it was requested to whomever found it to send it back, along with the indication of place, date, and time of recovery. This was encouraged by promising a reward (five pesetas). Such observations were utilized to solve the inverse problem of reconstructing the voyage of the bottle from the deployment (identified based on the serial number) to the recovery location. Many bottles launched in several different but adjacent regions allowed to infer the surface flow pattern with a certain accuracy, as was done, e.g., in the early 1910s in the Adriatic Sea by [28] or [29].

However, by definition, a Lagrangian instrument is a device which moves as a fluid particle. To mimic the motion of an ocean particle, units have to be carefully designed in order to maximize drag by currents and minimize spurious wind, wave, and/or inertia effects. This was obviously not the case for drifting bottles, and such a necessity prompted a technological development which is still going on at present. The awareness that a perfect Lagrangian nature is impossible to achieve leads to implicitly consider all such instruments as quasi-Lagrangian.

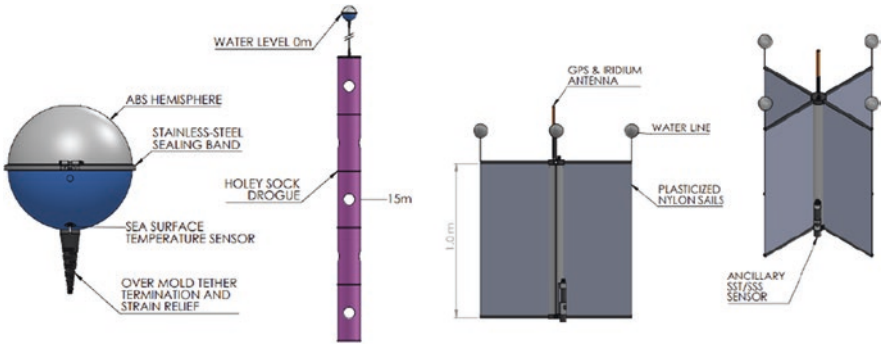

Fig. 3.9 Schematic of an SVP drifter (left) and of a CODE drifter (right panel). Courtesy of the Scripps Institution of Oceanography's Lagrangian Drifter Lab

Modern drifters are composed of a main body carrying the electronics and sensors, and a drogue, which is the structural component needed to "lock" the drifter to the current. Depending on the depth of the surface or subsurface currents investigated, the drogue can be tethered to the central body or built around it.

Figure 3.9 shows an example of the former type, a Surface Velocity Program (SVP) drifter. The SVP drifter design is the result of a standardization process promoted by the WCRP (World Climate Research Program) starting in 1982 (for details [30] and references therein).

An SVP drifter is made of a spherical plastic buoy, a wire tether, and a "holey sock" drogue centered at 15 m depth. It can carry sensors of sea surface temperature and salinity, atmospheric pressure, and wind direction. The latest evolution of the SVP concept is the Directional Wave Spectra Drifter (DWSD, developed by the Scripps Institution of Oceanography's Lagrangian Drifter Lab), an SVP without drogue that computes the directional wave spectrum with a GPS engine; the most common configuration (called SVPB, where B stands for barometer) is equipped with a sea surface temperature and an atmospheric pressure sensor. These instruments provide also real-time information on the sea level pressure field over the ocean at a global scale, thus complying with the specifications requested by the World Weather Watch [31].

Tests carried out by fastening a single point current meter to the top and the bottom of a drogue indicate that for the SVP design, the slip does not exceed 0.7 cm s^{-1} for a wind speed of 10 m s^{-1} [32]. The accuracy of the near-surface current using these drifters is ±1 cm s^{-1} in a 10 m s^{-1} wind [33].

Another type of drifter, specifically designed for coastal studies, is the CODE drifter (Fig. 3.9), named after the Coastal Ocean Dynamics Experiment [34], and presently the most used in the Mediterranean (e.g., [35]). It is a compact unit, composed of a plastic cylinder with four vertical orthogonal drogues stemming from it, positioning its drag center at 0.5 m depth. Smaller versions of the same design are also available on the market, with analogous current tracking accuracy.

Drifters are deployed at sea by vessels, helicopters, and small planes. Positioning is now obtained by GPS, and satellite telemetry is used to exchange location and sensor data.

Drifters have been extensively used to map currents in all corners of the world ocean (see, e.g., the early review [33, 36, 37], and in [38]). The basic information provided by Lagrangian instruments is represented by time series of locations, or trajectories. Simple trajectories can provide extremely useful information on flow features: from the current direction to the presence of inertial oscillations to, as an example, the textbook evidence of a topographic Rossby wave observed at depth by [39] in the framework of the POLYMODE Local Dynamics Experiment. Moreover, multiple trajectories can be plotted on a map, obtaining so-called "spaghetti plots", which can provide preliminary insights on data coverage and on the flow pattern in the sampled area (Fig. 3.10).

One step up in the data treatment is the so-called pseudo-Eulerian analysis that takes advantage of the coverage provided by the Lagrangian nature of drifters as they are carried by currents. It consists of subdividing the basin sampled by drifters into smaller subregions, or bins [41] and in characterizing the flow field in terms of velocity averages (Fig. 3.11) and velocity residuals within each bin. Such a procedure is based on the assumption of a scale separation between these two components of the current field (for a discussion on this aspect see [42–44]). The pseudo-Eulerian analysis thus provides a regularly spaced mean flow and a regular spatial distribution of mean and eddy kinetic energy (MKE and EKE, computed as (<u > 2 + <v > 2)/2 and [<(u- < u>)2 > + < (v- < v>)2>]/2, respectively, as defined [41]. This allows evaluating not only the mutual importance but also the exchange mechanisms between mean and eddy field even in large portions of the ocean, as well as the horizontal eddy momentum fluxes [23, 45, 46].

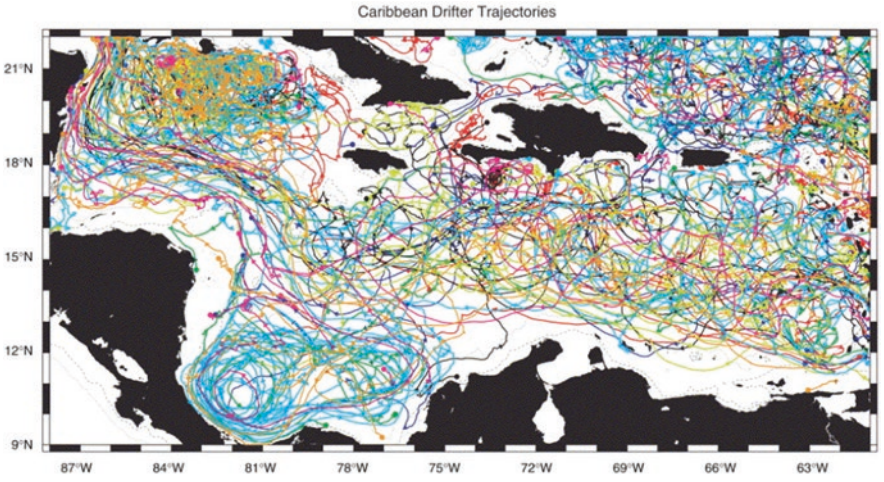

Fig. 3.10 Spaghetti plot of more than 200 surface drifter trajectories in the Caribbean region. Reprinted from [40], by permission

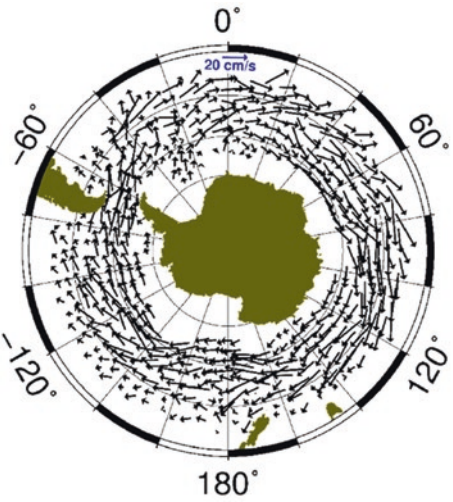

Fig. 3.11 Pseudo-Eulerian near-surface mean velocity field from drifter data. Redrawn from [42], by permission

Last but absolutely not least, the Lagrangian approach finds its most appropriate application in studies of dispersion in the ocean. Diffusivity is best derived from single particle statistics on the basis of Taylor's (1921) theorem, while dispersion due to chaotic advection can be quantified by double particle statistics [47]. The discussion of these aspects is beyond the scope of this chapter, but we refer the interested reader to a recent paper by [48] where dispersion characteristics in the surface ocean are investigated on the basis of information drawn from the largest available drifter data base (https://www.aoml.noaa.gov/phod/gdp/, see [33]). It is worth adding that dispersion information from drifter data can be crucial for two research directions currently under the spotlight: investigations on transport of pollutants, and in particular of plastics [49–51]; and biological connectivity in the ocean [52–54].

3.3.2 Eulerian Oceanographic Observations: Moorings

In physical oceanography, a mooring is the typical example of the Eulerian way to measure currents and many other physical, chemical, and biological parameters at different depths along the water column and over time. Oceanographers require long-term measurements to understand processes and changes occurring in the oceans over seasons, years, decades, or longer, with the ultimate goal of unraveling the ocean's crucial role in shaping our climate.

Moorings consist of a collection of instruments (current meters, CTDs, sediment traps, ph sensors, turbidity sensors, etc.…) attached to a rope at different depths. The rope is anchored to the seafloor and kept vertical by a sufficient number of floating devices.

Moorings can be completely submerged, or they can have a surface component. The latter are used to measure both atmospheric and oceanographic parameters.

Their surface component hosts sensors gathering the main atmospheric parameters (wind, pressure, temperature, solar radiation, etc.…) at sea level, whereas the submerged component is used for ocean observations. Having both atmospheric and ocean observations at the same point and working at similar time resolution, these systems are very efficient for air-sea interactions studies whose results are then incorporated into numerical weather prediction models contributing to significant improvements of weather/ocean forecasts. One of the most outstanding examples of such moorings is represented by the Tropical Atmosphere Ocean (TAO) mooring array (https://tao.ndbc.noaa.gov/), developed to study the El Niño–Southern Oscillation (ENSO) evolution. The TAO array consists of more than 70 surface moorings in the equatorial Pacific and it was completed in 1994. This mooring array helped and is still helping to monitor the ENSO state and to provide early warning of strong events such as the super El Nino event of 1998 and 2015. The typical TAO mooring structure is represented in Fig. 3.12.

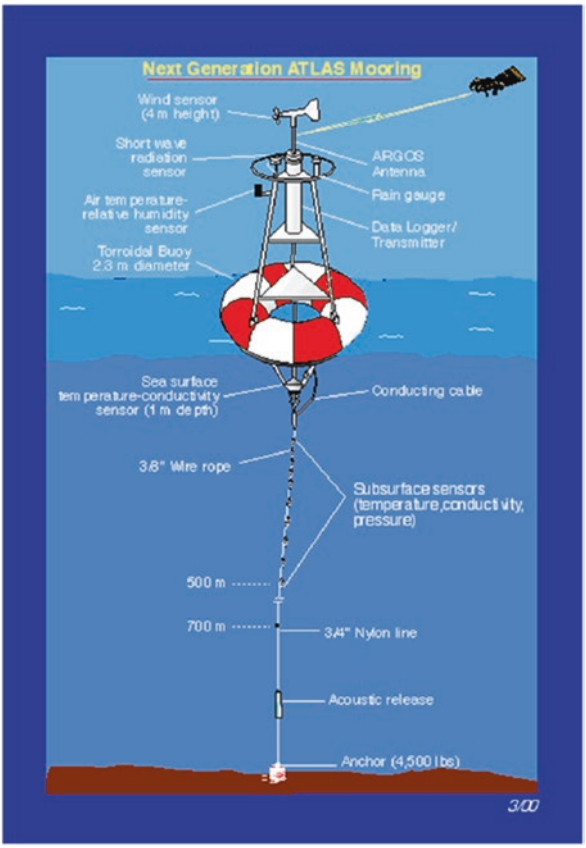

Fig. 3.12 Example of mooring with a surface component From https://www.pmel.noaa.gov/gtmba/moorings

Surface moorings are exposed to ocean storms with high wind and wave conditions and therefore must be constructed to withstand the forces associated with those environmental conditions. Submerged moorings (SMs) instead are more widely used, less exposed to bad weather conditions, but more difficult to recover and to service. SMs (see Fig. 3.13) have three basic structural components: an anchor, some type of wire/rope (sometimes chain) to which instrumentation can be

Anta XXXV (2019-2020) Mooring G

Depth (m)	Component	Length (m)	Weight (kg)	Buoyancy (kg)
218.2	**Orange rope** with a small **black buoy**	10.0		3.0
228.2	Maillon rapide + Shackle (Ω) 14 **+3 Nautilus orange Buoys**	3.0	1.0	75.0
231.2	maillon rapide + **white rope** + maillon rapide	5		
236.2	**SBE37SMP SN 21537 on a yellow rope**	1	3.0	
237.2	Shackle 16+ **Seaguard Currentmeter** +shackle 16	0.7	15.0	
237.9	Maillon Rapide + **yellow kevlar rope**	150.0		
387.9	Maillon Rapide + **yellow kevlar rope** + maillon rapide	100.0		
487.9	**2 Nautilus buoys**	2.0	1.0	50.0
489.9	Maillon Rapide + **yellow rope +SBE37SMP-ODO + Maillon Rapide**	10.0	3.0	
499.9	Shackle 16+ **Aanderaa Seaguard Currentmeter** +Shackle16	0.7	15.0	
500.6	maillon rapide + **yellow rope** + Maillon rapide	4.0		
504.6	**3 orange Nautilus buoys**	3.0	1.0	75.0
507.6	maillon rapide + **yellow rope** + maillon rapide	2.5		
510.1	**Acoustic Releaser**	0.5	50.0	
510.6	2 Shackle (Ω) 14+ Shackle 18 + sweaver 18+ shackle 18 + red iron oval	0.4	2.0	
511.0	Yellow rope	2.0		
513.0	Shackle 20 + chain + shackle 20	3.0	20.0	
516.0	**Ballast (160+160)**		320.0	
516.0	**Bottom depth**			

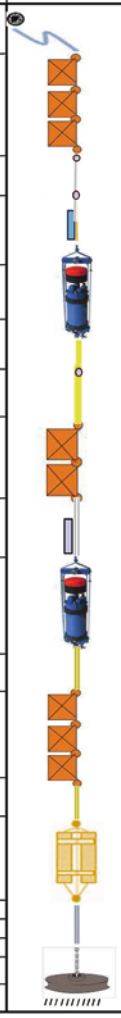

Fig. 3.13 Example of a submerged mooring. Mooring G of the Marine Observatory in the Ross Sea - MORSea - network

attached, and flotation devices that keep the line and instrumentations from falling to the seafloor and allow the mooring to recover.

Shackles and links are used to connect mooring components and to secure instruments. The choice of all components and the size and design of the anchor depends on the type of mooring and the environment in which it is deployed. The choice of the buoyancy devices is related to the total weight in water of all the instruments. Firstly, each weight must be balanced by an equivalent buoyancy and secondly an addition of more buoyancy is necessary to let the mooring rise to the surface. Usually, the buoyancy used on subsurface moorings has the shape of a sphere due to its low drag coefficient. When there is sufficient buoyancy, the mooring can be detached from the anchor through an acoustic releaser and recovered. The acoustic releaser connects all the instrumentation to the anchor by a hook. To recover the mooring, a coded acoustic signal is sent from the vessel to the acoustic releaser which detects the signal and opens the hook disconnecting the mooring from the anchor.

The choice of the instruments and the measurement depths of SMs depends mostly on the scientific targets, but also on other factors including the load the mooring is designed to support and the resources available for instrumenting the mooring.

The Marine Observatory in the Ross Sea (MORSea; http://morsea.uniparthenope.it/) of the PNRA provides an example of SMs network. MORSea currently manages four moorings positioned in key areas on the continental shelf of the Ross Sea, the world's largest marine protected area and one of the few regions of our planet where the Antarctic Bottom Water (AABW) is formed. AABW is formed from the mixing of the dense shelf water and the Circumpolar Deep Water (CDW) that intrudes over the shelf. One of the MORSea moorings is situated in the western Ross Sea, 50 km off the shelf break where the AABW is formed. The time series registered on this mooring show the variability of the measured parameters at different time scales, from hourly to daily, fortnightly, seasonal, and interannual (See Fig. 3.14 [55]) and highlight the importance of the moorings in understanding the oceanographic processes that occur at very diverse time scales.

The analysis of MORSea, USA and New Zealand moorings time series in the Ross Sea, has permitted to understand the central role that the tide plays in governing both the inflow of CDW over the Ross Sea continental shelf [55] and the outflow of AABW from the shelf [56]. The authors [55, 56] not only show the importance of the tides in modulating the exchange of the CDW and AABW across the slope at high frequency (daily and fortnightly), but also at the low frequency (seasonal to interannual). These results were achieved thanks to measurements taken on a long time period and at different time scales that only moorings can provide.

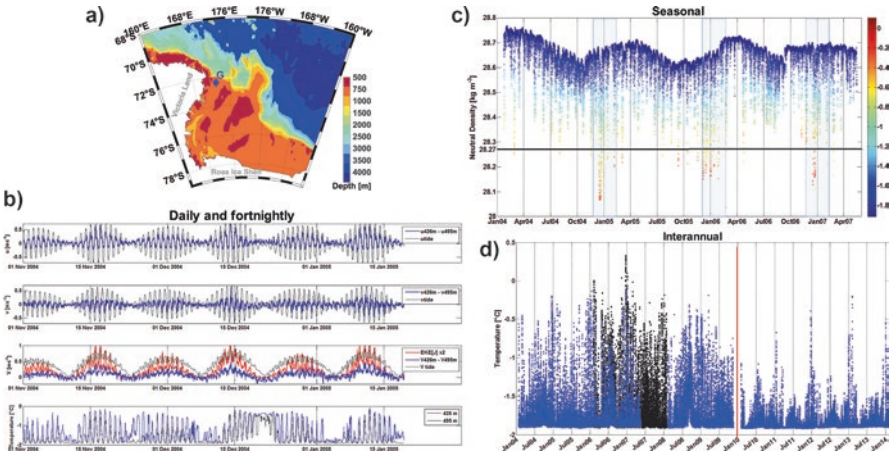

Fig. 3.14 Time series of different oceanographic parameters registered on a MORSea mooring. (**a**) Map of the Ross Sea and position (blue diamond) of the mooring. (**b**) three-months subsets from November 2004 of the zonal component (u, ms−1) differences between the upper and the bottom sensors (thick blue line), tidal component of u (thin black line); meridional component (v, m s^{-1}) differences between the upper and the bottom sensors (thick blue line), tidal component of v (thin black line); current velocity (V, m s^{-1}) differences between the upper and the bottom sensors (thick blue line), tidal component of V (thin black line); Eddy Kinetic Energy (EKE, thick red line) for the bottom sensors scaled for 2; temperature (°C) registered by the bottom (thin black line) and upper (thin blue line) sensors. (**c**) Hourly time series of the neutral density γn (kg m^{-3}) with temperature (°C) color coded. (**d**) Hourly time series of the temperature (°C) registered by the bottom instruments (about 20 m above the bottom; in blue) and by the upper instrument (about 80 m above the bottom; in black). Modified from [55]

3.4 Unmanned Vehicles

3.4.1 Floats

Float technology is part of the Lagrangian techniques for observing and monitoring the ocean, and together with the drifters, they are the most commonly used lagrangian instruments. Floats are profiling and drifting instruments, equipped with CTD and additional sensors. They are becoming one of the major operational platforms to monitor the world ocean and are crucial for the scientific community to deepen the knowledge of many ocean processes. Floats are passively transported by water both at the surface or deeper within the water column and collect chemical and physical observations (direction and speed of water, temperature, salinity, etc...) while moving between the surface and the estabilished depth. The use of this instrument for carrying out subsurface observations in the ocean does not require the presence of a research vessel, the consumption of any propeller, or the work of

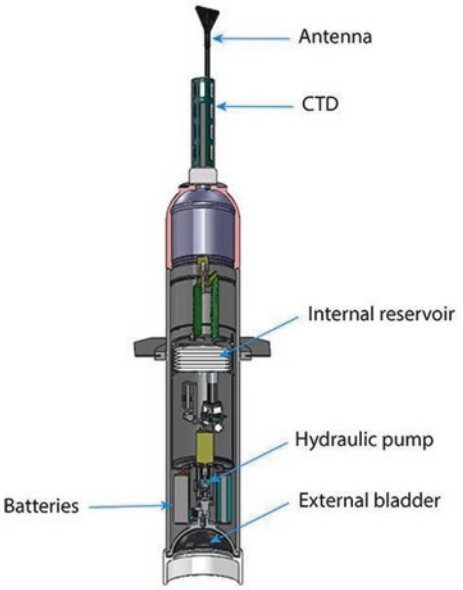

Fig. 3.15 Argo float and its main components (image by Michael McClune of Scripps Institution of Oceanography from https://argo.ucsd.edu/how-do-floats-work/)

operating personnel, so reducing the overall operational costs. On the other hand, the use of a Lagrangian platform is also associated to some disadvantages as the possible errors in determining their position, the difficulty of recovering them in case of any malfunctioning, or their tendency to accumulate in particular areas (i.e., convergence zones) generating an irregular distribution of the data.

Floats usually drift between the sea surface and a defined target depth, spending most of their life at a different depth called "parking depth". These instruments perform a series of cycles during their life at sea. The basic geometry of a float can be described as a structure, typically a cylinder, resistant to high pressure, containing all the scientific instruments, batteries, and communication devices (Fig. 3.15) and an external bladder that is in contact with the environment and can be inflated or deflated.

Floats use a limited quantity of oil contained inside to change the external bladder dimensions and consequently achieve the same density (by change in the volume) as the surrounding water. The way a float moves along the water column is so determined by controlling the buoyancy. Accordingly, when it is time to rise to the surface, the oil is pumped into the external bladder that expands, increasing the volume and the buoyancy of the float. On the contrary, when the float has to sink, the oil is retained entirely inside the hull and withdrawn from the bladder, decreasing the float buoyancy. This working scheme is based on the Archimedes principle and allows the floats to work autonomously for a long time, using the energy from the battery only to change the density, collect and transmit data.

The first generation of Lagrangian floats had a limited autonomy, 36 hours or less [57–59], and hence the impossibility of describing ocean processes on a longer time scale. The technology has been refined over the years to make the floats more

autonomous, aiming at a mission duration of months, and to improve the satellite system to transmit data and help in recovery if necessary. For instance, during the Labrador Sea deep convection experiment of 1997 and 1998 [60], floats have been conceived to realize deep temperature profiles, from surface to 2000 m of depth, through a buoyancy change determined by 30 cc of active volume control on a total volume of about 15,000 cc. The system used to trace these floats drifting in the Labrador Sea was the acoustic RAFOS system [59], while the satellite Argos system was used to retrieve the data.

A second generation of Mixed Layer Lagrangian Float (MLFII) [61] has been used in several studies from 2000 to 2002. This is a larger instrument with enhanced buoyancy control that can also carry larger and heavier instruments such as doppler sonar, altimeter, accelerometers, Photosynthetically Active Radiation (PAR) sensor, and fluorometer. The collection of such a large variety of data was also associated to large amount of data to transmitt or to store inside the float; for this reason the MLFII was usually retrieved after each mission.

Today the Argo floats are the most widely used subsurface floats. The Argo program began in 2000 and has employed and sustained until today, a global array of about 4000 profiling floats (Fig. 3.16). Argo provides continuous temperature (T) and salinity (S) profiles from the surface to 2000 m depth in the global oceans.

At the present, Argo collects about 12,000 profiles each month (400 a day) [62], no other platform is able to collect such a large number of subsurface ocean observations on a global scale. Moreover, these data are made publicly available within a few hours after acquisition. The Argo program aims to achieve a global (from

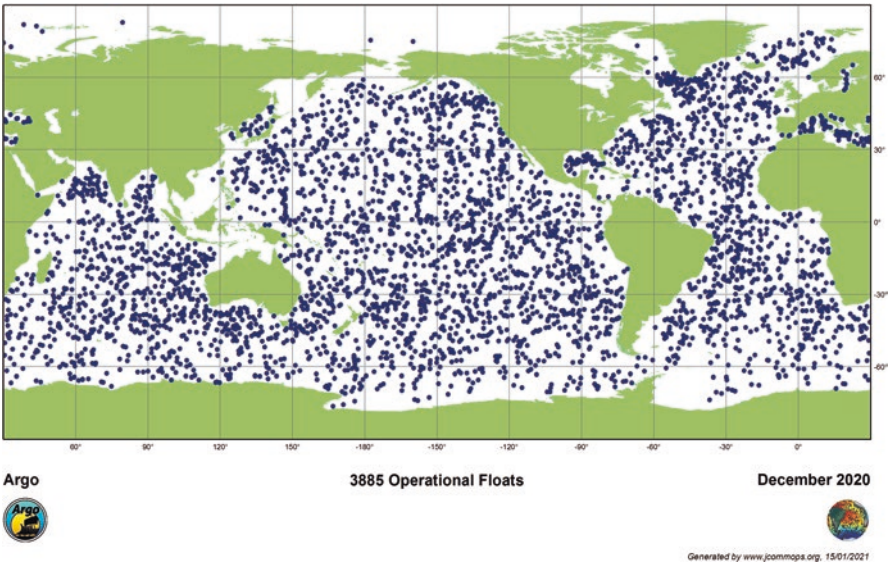

Fig. 3.16 Monthly map of the operational Argo floats positions relative to December 2020 (image from https://argo.ucsd.edu/about/)

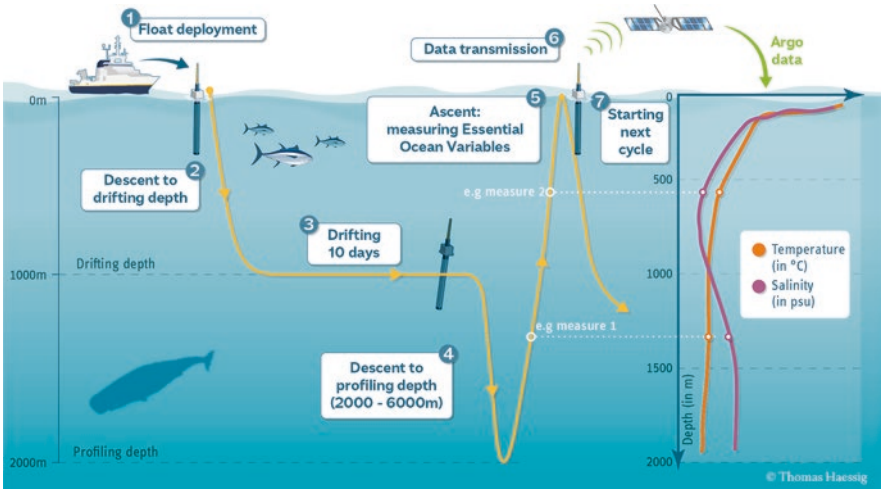

Fig. 3.17 Examples of one float cycle from deployment to data transmission (©Thomas Haessig from https://argo.ucsd.edu/how-do-floats-work/)

surface to the bottom) and multidisciplinary dataset integrating floats acquisition with satellite remote sensing and with other in situ measurements performed by the Global Ocean Observing System (GOOS) [63].

The most common cycle configuration of an Argo float includes five phases (Fig. 3.17). After the deployment, the float sinks to the parking depth at 1000 m below the surface and floats for about 10 days, then it descends to a deeper depth at 2000 m, and soon after starts ascending toward the surface. During the rise, floats measure temperature and salinity as a function of pressure, providing a vertical profile of the water column properties in the rising location. Lastly, the float stays at the surface for transmitting the collected data. When a cycle is terminated, the floats can start another cycle.

Each float can work for many years by repeating this cycle over and over. Currently, subsurface floats can also be designed for drifting at any depth and obtain T and S data also when sinking.

Figure 3.17 shows an example of the Argo floats and their principal components. These floats are equipped with a CTD that measures T with 0.001 °C of accuracy and calculates S within 0.001 psu (practicalsalinity units) and with an antenna that allows them to communicate with the satellites and transmit the acquired data. A small computer governs the Argo float mission and working cycle. The main constraint on a subsurface float lifetime is due to the battery power that feeds the pumps, sensors, controller, and communication system. Today, Argo floats are equipped with modern lithium batteries.

Standard floats are equipped with a CTD but additional sensors can be used, as designed for the Biogeochemical-Argo program (BGC-Argo) [8]. In particular, the scientific community is aiming at measuring key biogeochemical ocean variables at a global scale using the float technology in order to design, coordinate, and collect

oxygen, pH, nitrate, downwelling light, CDOM, chlorophyll fluorescence, and the optical backscattering coefficient measurements at a global scale from profiling floats [64]. To reach its ambitious aims, Argo continues to improve deployment plans and measurement techniques and, as planned for the year 2020, will increase the resolution of floats observations in some critical regions. In the seasonal ice zones, for example, there is a lack of historical data especially in the winter although the polar seas are key areas for studying climate change. Beyond increasing the amount of float profiles in these areas, Argo challenge is to correctly estimate their position under the ice (see e.g., [65, 66]). There are other ocean zones, as the tropical Pacific and Western Boundary Current (WBC) regions [67] that influence global climate variability, where it is also required to double the float density.

Several studies are carried through data collected within the Argo program. Argo data are used in various fields of science and the official web site [63] reports a large list of published papers focusing on large-scale climate change. Argo data contribute to studies focusing on ocean change, affecting temperature and salinity from surface to deep layers. Argo supports the study of ocean at regional scale too, including sea level rise, ocean heat content, fresh and salt water cycle, and ocean circulation. On an even smaller spatial scale, some other applications include the use of Argo floats in-stay-on-the-ground mode: the float depth is programmed to settle on the bottom and maintain position [68] to estimate water mass properties in relatively small and remote areas.

The several T and S profiles measured near real-time by Argo floats allow the computation of global gridded ocean T/S datasets from synoptic in situ data. The scattered data measured by Argo float are preprocessed and quality controlled (for detail see the Argo data management documentation [69]) before being treated with statistical methods (optimum interpolation or more sophisticated variational analysis methods) to be returned on a regular grid. In Fig. 3.18 are shown distributions of annual climatology T and S at 10 m depth from the global ocean Argo grid data set (BOA-Argo) [70].

Today many datasets based on Argo measurements are available, as the Roemmich-Argo [71], IPRC-Argo [72], and WOCE/Argo Global Hydrographic Climatology (WAGHC) [73]. They provide monthly, annual, and climatological maps of T and S increasing the observations and monitoring of the global ocean from the surface to the bottom, moreover the modeling community takes advantage from the Argo dataset assimilation into models to improve ocean and climatological forecasts.

3.4.2 Glider and Wave Glider

The float technology, described in the previous paragraph, has offered oceanographers the possibility to investigate the water column variability, in the range 0–2000 m depth, in total absence of an oceanographic vessel and during every sea and weather condition.

Nevertheless, the floats are passively transported by the currents and cannot acquire data on a selected track or modify their path according to the scientific

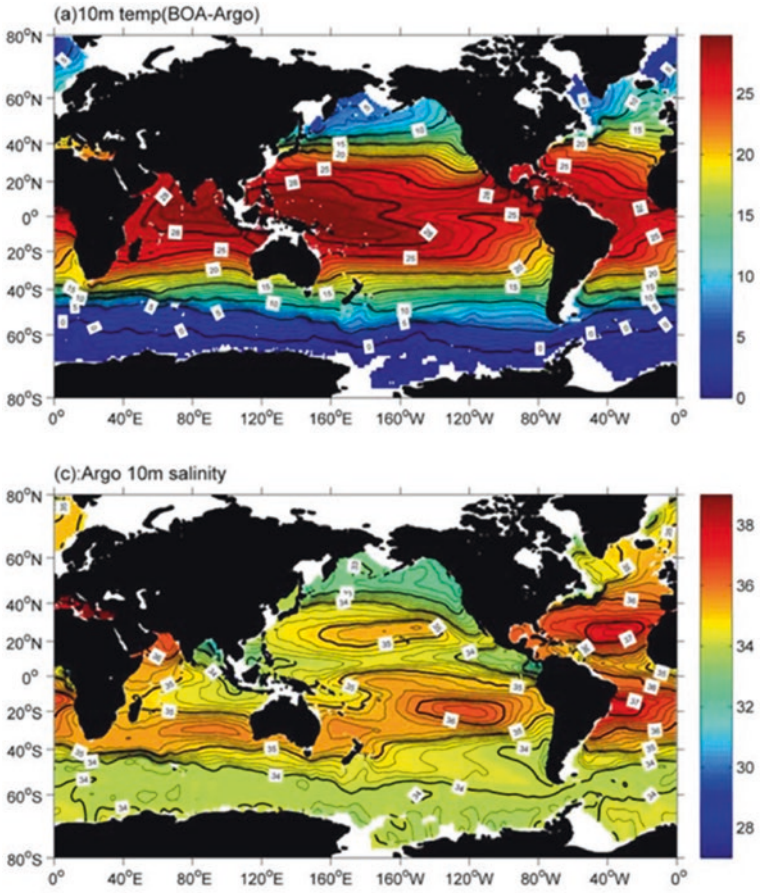

Fig. 3.18 Distribution of annual climatology T (**a**) and S (**b**) at 10 m depth from BOA-Argo (these images are taken from Fig. 3.5 in [70])

targets of an oceanographic study. Additionally, the scientific community has become more aware of the importance of fine space- and time-scales processes whose monitoring over long ranges and durations is a challenge.

For this reason, the oceanographic community worked on the design and realization of Autonomous Unmanned Vehicles (AUV) that can move on a designed track at surface (i.e., using wave or wind energy), or along the water column (i.e., changing its buoyancy for collecting data along depth). The technological solution to this demand can be represented by the Saildrone, the Wave Glider and the Sailbuoy (Fig. 3.19), and several gliders (Fig. 3.20), respectively. These platforms provide valuable surface, subsurface, and water column oceanographic measurements critical for measuring ocean heat content and transport, ocean velocities, thermohaline circulation, and other oceanographic applications. They autonomously navigate

Fig. 3.19 From left to right: a Sailbuoy (http://www.sailbuoy.no – photo credit David Peddie on behalf of Offshore Sensing), a Saildrone (https://www.saildrone.com/ Image courtesy of Saildrone), and a Wave Glider (https://www.liquid-robotics.com – photo credit University of Naples Parthenope)

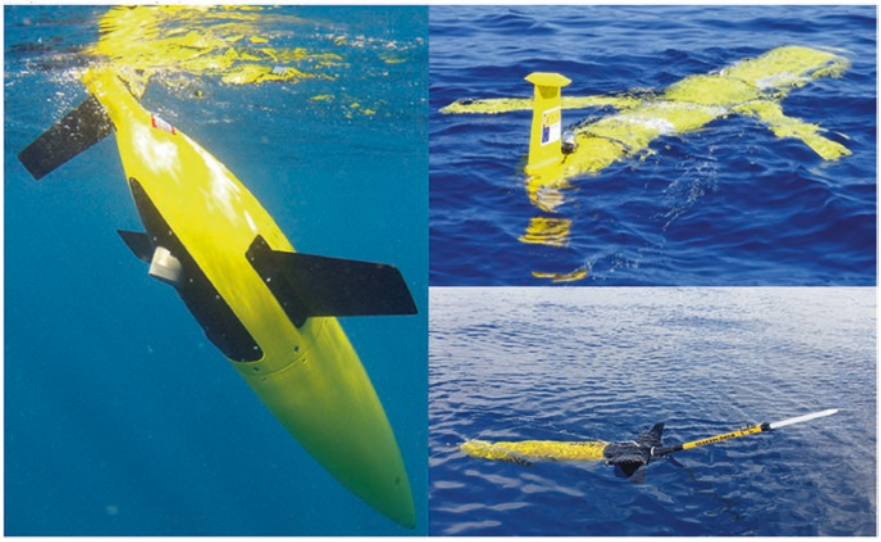

Fig. 3.20 A Seaglider (left panel), a SLOCUM (upper right panel), and a SEAEXPOLRER (lower left panel) gliders (https://eurogoos.eu/gliders-task-team/ credit PLOCAN)

between prescribed waypoints, accounting for wind and currents, and address the need for flexible in situ observations, especially in regions where it is difficult to deploy and maintain other types of observing systems. Moreover, they are also particularly useful for adaptively sampling, under the supervision of a remote human pilot.

Thanks to their speed up to 4 m s^{-1}, the wind-powered Saildrone vehicles are particularly suitable for science applications needing rapid surface and subsurface spatial sampling, e.g., for studying submesoscale variability, air-sea fluxes, ocean fronts, carbon cycling, biophysical interactions. Eventually data can be assimilated in atmosphere-ocean modeling [74].

Each vehicle consists of a 7 m narrow hull, a 5 m tall hard wing, and a keel with a 2.5 m draft, weighing approximately 750 kg [75], and is equipped with

solar-powered meteorological and oceanographic sensors for long-range collection of simultaneous measurements of the lower atmosphere and upper ocean. The sensor payload usually includes sensors measuring atmospheric pressure, air temperature and humidity, wind speed and direction, ocean skin SST, subsurface sea temperature, salinity, chlorophyll fluorescence, Colored Dissolved Organic Matter (CDOM) fluorescence, dissolved oxygen, and subsurface sea temperature at keel (at 0.2–2 m). Data are transmitted in real-time via satellite connectivity, enabling adaptive sampling and real-time data analysis. Although recent studies provided promising results and highlighted their potential contributions as a valuable source of satellite and model validation in certain regions [76, 77], Saildrone instruments need to be further tested in different ocean areas in order to assess the platform's accuracy under a wider range of environmental conditions.

Wave Gliders can harness ocean wave energy to travel at velocities of typically 0.5–0.8 m s^{-1} (depending on sea state) collecting both surface atmospheric (wind speed and direction, atmospheric pressure, air temperature) and subsurface oceanographic observations [78]. A wave glider uses a series of wings located on a subbody at about 6 m below the surface to mechanically propel the vehicle forward exploiting the vertical motion induced by wave motion, independently of wave direction [79]. The vehicle consists of a low-profile surface float equipped with solar panels that provide power for the sampling and navigation systems and of a subsurface board that is connected to the surface payload by a tether (umbilical). The modular payloads usually include: a fluorometer equipped to measure CDOM, refined fuels concentration and turbidity, a CTD and an ADCP. A weather station collecting air temperature, barometric pressure, wind speed, and direction at 1 m height above sea level is installed on the top of the surface component. The collected observations are stored onboard and/or relayed via satellite to a receiving ground station.

Up to 1 year, Wave Gliders surveys demonstrated that they can operate both as a vessel, covering long distances in the ocean, or as a station-keeping platform, representing a cost-efficient strategy for monitoring upper ocean state, studying marine mammals' presence, and validating satellite ocean products [79, 80]. Furthermore, they proved to collect reliable measurements even in presence of severe weather conditions [81, 82] or along very long tracks [83].

Moving to deeper layers, gliders are AUV that collect oceanographic data along oblique paths by diving between two defined depths as a natural development of the float technology previously described.

Henry Stommel recognized the potential of these underwater instruments in 1989. The first ocean deployment longer than a week took place in 1999, after that, the US Office of Naval Research (ONR) supported through a 5-year project and led to the realization of the first commercial and operational gliders, Slocum (Webb Research Corp.), Spray (Scripps Institution of Oceanography and Woods Hole Oceanographic Institution), and Seaglider (University of Washington).

Commercial gliders have converged on a similar design; they have similar size, roughly 50 kg in mass, with a main body equipped with fins, a rudder, and an antenna (Fig. 3.20).

While at sea, they all navigate by dead-reckoning underwater between GPS navigational waypoints. When surfacing, they send data and receive commands via satellite communications.

These gliders are self-propelled by a change in their buoyancy and move with typical horizontal speeds of 30 cm s^{-1}. Movable and rotating internal ballast, typically the battery pack, and a helm or rudder allows it to turn. Vertical movement is realized through a change in the glider buoyancy, as previously described for the ARGO floats. The correct gliding position is achieved through the movement of the internal ballast that can move toward the bow or the poop of the glider. Gliders use their wings to convert their vertical movement into horizontal and to descend and ascend along a see-saw path.

Thanks to their reduced size, gliders can be operated, launched, and recovered from small vessels by two people. Gliders can be used to monitor large basins, move along specific transects or act as a virtual mooring keeping a fixed position in time and moving along depth. They are typically deployed over periods of weeks to months, operate under a wide range of weather conditions, and provide high spatial and temporal resolution measurements. The maximum duration of a glider mission is defined on the maximum capability of the internal batteries, as well as the efforts, in terms of energy, used by the glider to change its buoyancy and then move.

Gliders are suitable for intensive, both in time and space, monitoring of the ocean with a great reduction of costs respect to classical ship operations, nevertheless as most of the AUVs, they can only measure water properties that can be estimated through dedicated electronic or optical sensors.

Thanks to these characteristics, gliders have become an integral component of ocean observation systems, and their use is increasing globally [86, 87]. During the last years, the oceanographic community has identified a series of applications for which gliders are better suited. Generally speaking, gliders are an optimal instrument to monitor small areas at very high spatial resolution. Long monitoring tracks or large study areas monitoring are better realized using faster sampling instruments or oceanographic vessels. Gliders equipped with small electric engines are also used, but the resulting reduced autonomy has, at the moment, a negative impact on their spreading in the oceanographic community. Repeated monitoring from surface to 1000 m depth along limited length defined tracks is an example of successful glider applications.

The ABACUS (Algerian Basin Circulation Unmanned Survey) project supported by European Commission's JERICO-TNA, JERICONEXT and JERICO S3 European calls JERICO TNA third call grant agreement no. 262584, H2020 Framework Programme JERICO-NEXT grant agreement no. 654410, JERICO-S3 Transnational Access program grant agreement No. 871153, and the CANALES Endurance Line initiated in 2011 by the SOCIB (http://apps.socib.es/data-catalog/#/data-products/glider-canales) can be seen as successful examples of glider application in the Mediterranean Sea. In the framework of ABACUS, SLOCUM gliders have been used to monitor the ocean properties along a satellite ground track, providing a significant reference for remote-sensed measurements and reliable water-column data [85, 88]. Mesoscale structures as eddies and filaments in the ABACUS

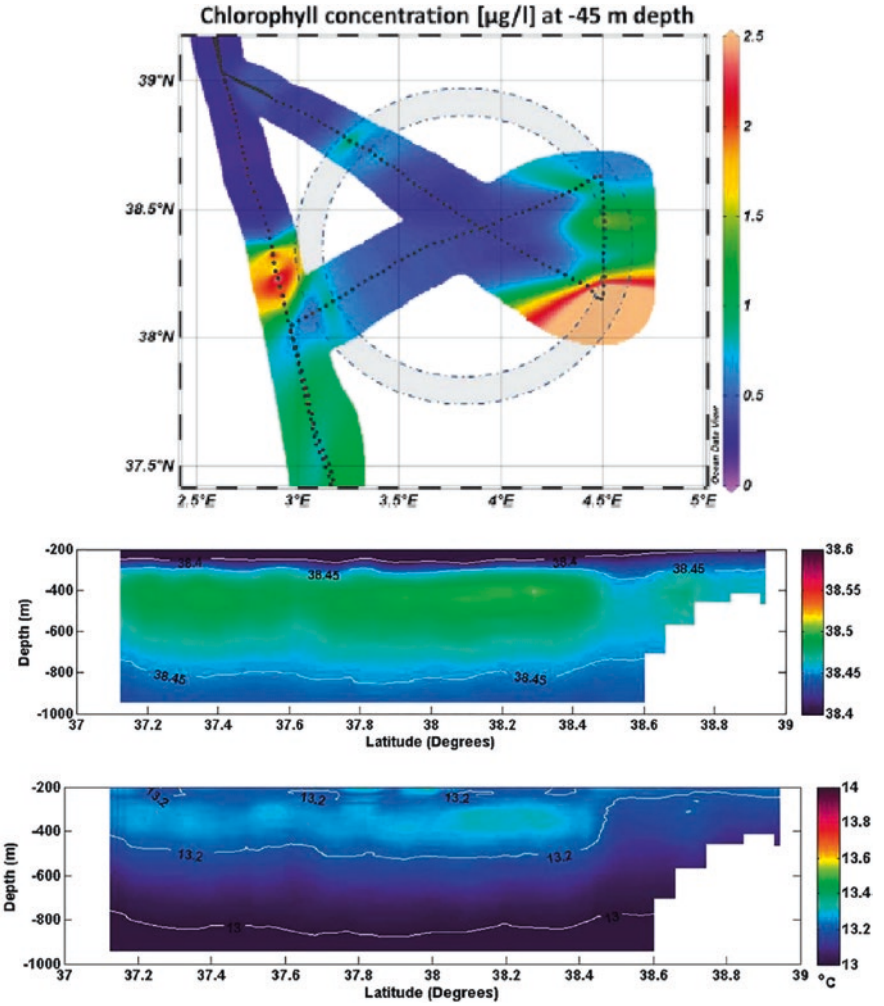

Fig. 3.21 Upper Panel Chlorophyll concentration (µg/l) map at 45 m depth from glider casts (black dots). Gray area identifies the eddy boundary area derived from the estimated radius during the ABACUS mission (From [84]). Lower Panel Vertical sections of glider salinity and temperature in the Algerian Basin in September 2014. Modified From [85]

study area have also been successfully identified and investigated [84], (Fig. 3.21) and data have been published in public repository [89, 90].

Gliders have also been used as a "virtual mooring" in the middle of the Southern Ocean in order to monitor the seasonal and interannual variability of ocean physical and optical properties also due to the storm passage over the monitoring site [91].

In order to overcome some limitation of glider characteristics (i.e., low speed and loss of synopticity during the mission), fleets of gliders are used to monitor long

track or large areas, providing a final high resolution and synoptical description of water column properties.

References

1. Cook J (1777) A voyage towards the south pole and round the world: performed in his Majesty's ships the resolution and adventure, in the years 1772, 1773, 1774 and 1775, printed for W. Strahan and T. Caddell in the Strand, London
2. Roemmich D, Gould WJ, Gilson J (2012) 135 years of global ocean warming between the challenger expedition and the Argo Programme. Nat Clim Chang 2:425–428. https://doi.org/10.1038/nclimate1461
3. Negretti H, Zambra J (1873) On a new deep-sea thermometer. Proc Roy Soc Lond A 22:238–241. https://doi.org/10.1098/rspl.1873.0034
4. Mill RH (1900) The Pettersson-Nansen insulating water-bottle. Geogr J 16:469–447
5. Hellend-Hansen B, Nansen F (1909) The Norwegian Sea: its physical oceanography based upon the Norwegian researchers 1900–1904. Rep Norweg Fishery Marine Investig 11:390
6. Williams AJ (2009) CTD (conductivity, temperature, depth) profiler. In: Steele JH, Thorpe SA, Turekian KK (eds) Encyclopedia of ocean sciences: measurement techniques, sensors and platforms, EDS. Elsevier, Boston, pp 25–34
7. Baker J (1981) Ocean instruments and experiment design. In: Warren BA, Wunsch C (eds) Evolution of physical oceanography. MIT Press, Cambridge, pp 414–419
8. Hamon BV (1955) A temperature-salinity-depth recorder. J du Conseil Int pur l'Exploration de la Mer 21:72–73
9. Hamon BV, Brown NL (1958) A temperature-chlorinity-depth recorder for use at sea. J Sci Instrum 35:452
10. Brown NL (1974) A precision CTD microprofiler, ocean '74 - IEEE international conference on engineering in the ocean environment, Halifax, NS, Canada, pp. 270–278
11. Abraham JP, Baringer M, Bindoff NL, Boyer T, Cheng LJ, Church JA et al (2013) A review of global ocean temperature observations: implications for ocean heat content estimates and climate change. Rev Geophys 2013:450–483. https://doi.org/10.1002/rog.20022
12. Castagno P, Capozzi V, Di Tullio GR, Falco P, Fusco G, Rintoul SR, Spezie G, Budillon G (2019) Rebound of shelf water salinity in the Ross Sea. Nat Commun 5:1–6. https://doi.org/10.1038/s41467-019-13083-8
13. Jacobs SS, Giulivi CF (2010) Large multidecadal salinity trends near the Pacific-Antarctic continental margin. J Climate 23:4508–4524
14. Silvano A, Foppert A, Rintoul SR, Holland PR, Tamura T, Kimura N, Castagno P, Falco P, Budillon G, Haumann FA, Naveira Garabato AC, Macdonald AM (2020) Recent recovery of Antarctic bottom water formation in the Ross Sea driven by climate anomalies. Nat Geosci 2020:11–16. https://doi.org/10.1038/s41561-020-00655-3
15. Rintoul SR (2007) Rapid freshening of Antarctic bottom water formed in the Indian and Pacific oceans. Geophys Res Lett 34:L06606
16. Purkey SG, Johnson GC (2013) Antarctic bottom water warming and freshening: contributions to sea level rise, ocean freshwater budgets, and global heat gain. J Climate 26:6105–6122
17. Johnson GC (2008) Quantifying Antarctic bottom water and North Atlantic deep water volumes. J Geophys Res 113:C05027
18. Auger M, Morrow R, Kestenare E, Salleè JB (2021) Southern Ocean in-situ temperature trends over 25 years emerge from interannual variability. Nat Commun 12:514. https://doi.org/10.1038/s41467-020-20781-1

19. Fusco G, Manzella GMR, Cruzado A, Gacic M, Gasparini GP, Kovacevic V, Millot C, Tziavos C, Velasquez ZR, Walne A, Zervakis V, Zodiatis G (2003) Variability of mesoscale features in the Mediterranean Sea from XBT data analysis. Ann Geophys 21:21–32
20. Goni GJ, Sprintall J, Bringas F, Cheng L, Cirano M, Dong S, Domingues R, Goes M, Lopez H, Morrow R, Rivero U, Rossby T, Todd RE, Trinanes J, Zilberman N, Baringer M, Boyer T, Cowley R, Domingues CM, Hutchinson K, Kramp M, Mata MM, Reseghetti F, Cù S, Bhaskar TVSU, Volkov D (2019) More than 50 years of successful continuous temperature section measurements by the global expendable bathythermograph network, its integrability, societal benefits, and future. Front Mar Sci 6:452. https://doi.org/10.3389/fmars.2019.00452
21. Cotroneo Y, Budillon G, Fusco G, Spezie G (2013) Cold core eddies and fronts of the Antarctic circumpolar current south of New Zealand from in situ and satellite data. J Geophys Res Oceans 118:2653–2666. https://doi.org/10.1002/jgrc.20193
22. Budillon G, Rintoul SR (2003) Fronts and upper ocean thermal variability south of New Zealand. Antarct Sci 15(1):141–152. https://doi.org/10.1017/S0954102003001135
23. Menna M, Cotroneo Y, Falco P, Zambianchi E, Di Lemma R, Poulain PM, Fusco G, Budillon G (2020) Response of the Pacific Sector of the Southern Ocean to wind stress variability from 1995 to 2017. J Geophys Res Oceans 125:e2019JC015696. https://doi.org/10.1029/2019JC015696
24. Batchelor GK (1967) An introduction to fluid dynamics. Cambridge University Press, Cambridge, p 615
25. Csanady GT (1973) Turbulent diffusion in the environment. Springer, p 248
26. Buffoni G, Falco P, Griffa A, Zambianchi E (1997) Dispersion processes and residence times in a semi-enclosed basin with recirculating gyres: an application to the Tyrrhenian Sea. J Geophys Res Oceans 102(C8):18699–18713
27. LaCasce J (2008) Statistics from Lagrangian observations. Prog Oceanogr 77(1):1–29
28. Mazelle E (1914) Flaschenposten in der Adria zur Bestimmung der Oberflächenströmungen. Denkschriften der Kaiserlichen Akademie der Wissenschaften Mathematisch-Naturwissenschaftlichen Klasse 91:335–378
29. Feruglio G (1920) Risultati di esperienze con galleggianti per lo studio delle correnti de1 Mare Adriatico negli anni 1910–1914. R Comit Talass Ital Mem 55:l–92
30. Lumpkin R, Pazos M (2007) Measuring surface currents with surface velocity program drifters: the instrument, its data, and some recent results. In: Griffa A, Kirwan AD, Mariano A, Özgökmen T, Rossby T (eds) Lagrangian analysis and prediction of coastal and ocean dynamics. Cambridge University Press, Cambridge, pp 39–67
31. Centurioni L, Horányi A, Cardinali C, Charpentier E, Lumpkin R (2017) A global ocean observing system for measuring sea level atmospheric pressure: effects and impacts on numerical weather prediction. Bull Am Meteorol Soc 98(2):231–238
32. Niiler PP, Paduan JD (1995) Wind-driven motions in the northeastern Pacific as measured by Lagrangian drifters. J Phys Oceanogr 25:2819–2830
33. Pazan SE, Niiler PP (2001) Recovery of near-surface velocity from undrogued drifters. J Atmos Oceanic Tech 18:476–489
34. Davis RE (1985a) Drifter observations of coastal surface currents during CODE: the method and descriptive view. J Geophys Res Oceans 90(C3):4741–4755
35. Poulain PM, Menna M, Mauri E (2012) Surface geostrophic circulation of the Mediterranean Sea derived from drifter and satellite altimeter data. J Phys Oceanogr 42(6):973–990
36. Niiler PP (2001) The world ocean surface circulation. In: Siedler G, Church J, Gould J (eds) Ocean circulation and climate: observing and modelling the Global Ocean. Academic Press, Oxford, pp 193–204
37. Lumpkin R, Johnson GC (2013) Global Ocean surface velocities from drifters: mean, variance, El Niño–southern oscillation response, and seasonal cycle. J Geophys Res Oceans 118(6):2992–3006
38. Laurindo LC, Mariano AJ, Lumpkin R (2017) An improved near-surface velocity climatology for the global ocean from drifter observations. Deep-Sea Res I Oceanogr Res Pap 124:73–92

39. Price JF, Rossby HT (1982) Observations of a barotropic planetary wave in the western North Atlantic. J Mar Res 40:543–558
40. Richardson PL (2005) Caribbean current and eddies as observed by surface drifters. Deep-Sea Res II Top Stud Oceanogr 52(3–4):429–463
41. Poulain PM (1999) Drifter observations of surface circulation in the Adriatic Sea between December 1994 and March 1996. J Mar Syst 20(1–4):231–253
42. Falco P, Zambianchi E (2011) Near-surface structure of the Antarctic circumpolar current derived from World Ocean circulation experiment drifter data. J Geophys Res Oceans 116:5
43. Zambianchi E, Griffa A (1994) Effects of finite scales of turbulence on dispersion estimates. J Mar Res 52(1):129–148
44. Bauer S, Swenson MS, Griffa A, Mariano AJ, Owens K (1998) Eddy-mean flow decomposition and eddy-diffusivity estimates in the tropical Pacific Ocean: 1 Methodology. J Geophys Res Oceans 103(C13):30855–30871
45. Davis RE (1985b) Drifter observations of coastal surface currents during CODE: the statistical and dynamical views. J Geophys Res Oceans 90(C3):4756–4772
46. Trani M, Falco P, Zambianchi E, Sallée JB (2014) Aspects of the Antarctic circumpolar current dynamics investigated with drifter data. Prog Oceanogr 125:1–15
47. Aurell E, Boffetta G, Crisanti A, Paladin G, Vulpiani A (1997) Predictability in the large: an extension of the concept of Lyapunov exponent. J Phys A Math Gen 30(1):1
48. Corrado R, Lacorata G, Palatella L, Santoleri R, Zambianchi E (2017) General characteristics of relative dispersion in the ocean. Sci Rep 7(1):1–11
49. Maximenko N, Hafner J, Niiler P (2012) Pathways of marine debris derived from trajectories of Lagrangian drifters. Mar Pollut Bull 65(1–3):51–62
50. Van Sebille E, England MH, Froyland G (2012) Origin, dynamics and evolution of ocean garbage patches from observed surface drifters. Environ Res Lett 7(4):044040
51. Zambianchi E, Trani M, Falco P (2017) Lagrangian transport of marine litter in the Mediterranean Sea. Front Environ Sci 5:5
52. Cowen RK, Lwiza KM, Sponaugle S, Paris CB, Olson DB (2000) Connectivity of marine populations: open or closed? Science 287(5454):857–859
53. Carlson DF, Griffa A, Zambianchi E, Suaria G, Corgnati L, Magaldi MG, Poulain PM, Russo A, Bellomo L, Mantovani C, Celentano P, Molcard A, Borghini M (2016) Observed and modeled surface Lagrangian transport between coastal regions in the Adriatic Sea with implications for marine protected areas. Cont Shelf Res 118:23–48
54. Celentano P, Falco P, Zambianchi E (2020) Surface connection between the Ionian Sea and different areas of the Mediterranean derived from drifter data. Deep-Sea Res I Oceanogr Res Pap 166:103431
55. Castagno P, Falco P, Dinniman MS, Spezie G, Budillon G (2017) Temporal variability of the circumpolar deep water inflow onto the Ross Sea continental shelf. J Mar Syst 166:37–49. https://doi.org/10.1016/j.jmarsys.2016.05.006
56. Bowen MM, Fernandez D, Vazquez AF, Gordon AL, Huber B, Castagno P, Falco P (2021) The role of tides in bottom water export from the western Ross Sea. Sci Rep 2246:1–11. https://doi.org/10.1038/s41598-021-81793-5
57. D'Asaro EA, Winters KB, Lien R (2002) Lagrangian analysis of a convective mixed layer. J Geophys Res 107(C5):3040. https://doi.org/10.10291/2000JC000247
58. Davis R, Webb D, Regier L, Dufour J (1992) The autonomous Lagrangrian circulation explorer (Alace). J Atmos Oceanic Tech 9:264–285
59. Rossby T, Dorson D, Fontaine J (1986) The RAFOS system. J Atmos Oceanic Tech 3:672–678
60. Lab Sea Group (1998) The Labrador Sea deep convection experiment. Bull Amer Meteor Soc 79:2033–2058
61. D'Asaro EA (2003) Performance of autonomous Lagrangian floats. J Atmos Oceanic Tech 20(6):896–911. https://doi.org/10.1175/1520-0426(2003)020<0896:POALF>2.0.CO;2
62. https://argo.ucsd.edu

63. Legler DM, Freeland HJ, Lumpkin R, Ball G, McPhaden MJ, North S et al (2015) The current status of the real-time in situ Global Ocean observing system for operational oceanography. J Operat Oceanogr 8:s189–s200. https://doi.org/10.1080/1755876X.2015.1049883
64. Bittig HC et al (2019) A BGC-Argo guide: planning, deployment, data handling and usage. Front Mar Sci 6:502
65. Newman L, Heil P, Trebilco R, Katsumata K, Constable AJ, van Wijk E et al (2019) Delivering sustained, coordinated and integrated observations of the Southern Ocean for global impact. Front Mar Sci 6:433. https://doi.org/10.3389/fmars.2019.00433
66. Lee CM, Starkweather S, Eicken H, Timmermans M-L, Wilkinson J, Sandven S et al (2019) A framework for the development, design and implementation of a sustained arctic ocean observing system. Front Mar Sci. https://doi.org/10.3389/fmars.2019.004
67. Roemmich D et al (2019) On the future of argo: a global, full-depth, multi-disciplinary array. Front Mar Sci 6:439. https://doi.org/10.3389/fmars.2019.00439
68. Porter DF, Springer SR, Padman L, Fricker HA, Tinto KJ, Riser SC et al (2019) Evolution of the seasonal surface mixed layer of the Ross Sea, Antarctica, observed with autonomous profiling floats. J Geophys Res Oceans 124:4934–4953. https://doi.org/10.1029/2018JC014683
69. Argo Data Management (2013) Argo quality control manual version 2.9, p. 54
70. Li H, Xu F, Zhou W, Wang D, Wright JS, Liu Z, Lin Y (2017) Development of a global gridded Argo data set with Barnes successive corrections. J Geophys Res Oceans 122:866–889. https://doi.org/10.1002/2016JC012285
71. https://sio-argo.ucsd.edu/RG_Climatology.html
72. http://apdrc.soest.hawaii.edu/projects/Argo/data/Documentation/gridded-var.pdf
73. https://icdc.cen.uni-hamburg.de/en/waghc.html
74. Gentemann CL, Clayson CA, Brown S, Lee T, Parfitt R, Farrar JT, Bourassa M, Minnett PJ, Seo H, Gille ST, Zlotnicki V (2020) FluxSat: measuring the ocean–atmosphere turbulent exchange of heat and moisture from space. Remote Sens (Basel) 12:1796. https://doi.org/10.3390/rs12111796
75. Meinig C, Burger EF, Cohen N, Cokelet ED, Cronin MF, Cross JN, de Halleux S, Jenkins R, Jessup AT, Mordy CW, Lawrence-Slavas N, Sutton AJ, Zhang D, Zhang C (2019) Public–private partnerships to advance Regional Ocean-observing capabilities: a Saildrone and NOAA-PMEL case study and future considerations to expand to global scale observing. Front Mar Sci 6:448. https://doi.org/10.3389/fmars.2019.00448
76. Cokelet, E. D., Jenkins, R., Meinig, C., Lawrence-Slavas, N., Mordy, C. W., Stabeno, P. J., et al. (2015). The use of saildrones to examine spring conditions in the bering sea: instrument comparisons, sea ice meltwater and Yukon river plume studies. In: Proceedings of the Oceans'15 MTS/IEEE, Marine Technology Society and Institute of Electrical and Electronics Engineers, Washington, DC, pp. 19–22
77. Zhang D, Cronin MF, Meinig C, Farrar JT, Jenkins R, Peacock D et al (2019) Comparing air-sea flux measurements from a new unmanned surface vehicle and proven platforms during the SPURS-2 field campaign. Oceanography 32:122–133. https://doi.org/10.5670/oceanog.2019.220
78. Aulicino G, Cotroneo Y, Lacava T, Sileo G, Fusco G, Carlon R, Satriano V, Pergola N, Tramutoli V, Budillon G (2016) Results of the first wave glider experiment in the southern Tyrrhenian Sea. Adv Oceanogr Limnol 7(16–35):2016. https://doi.org/10.4081/aiol.2016.5682
79. Willcox S, Meinig C, Sabine C, Lawrence-Slavas N, Richardson T, Hine R, Manley J (2009) An autonomous mobile platform for underway surface carbon measurements in open-ocean and coastal waters, Proc. Conf. MTS/IEEE Oceans 2009, p. 1–8
80. Wiggins S, Manley J, Brager E, Woolhiser B (2010) Monitoring marine mammal acoustics using wave glider. In: Proceedings of the MTS/IEEE OCEANS conference, Washington, DC, pp. 1–4
81. Mitarai S, McWilliams JC (2016) Wave glider observations of surface winds and currents in the core of typhoon Danas. Geophys Res Lett 43(11):312–11,319. https://doi.org/10.1002/2016GL071115

82. Tian D, Zhang H, Zhang W, Zhou F, Sun X, Zhou Y, Ke D (2020) Wave glider observations of surface waves during three tropical cyclones in the South China Sea. Water 2020(12):1331
83. Villareal TA, Wilson C (2014) A comparison of the Pac-X trans-Pacific wave glider data and satellite data (MODIS, Aquarius, TRMM and VIIRS). PLoS One 9(3):e92280. https://doi.org/10.1371/journal.pone.0092280
84. Cotroneo Y, Aulicino G, Ruiz S, Pascual A, Budillon G, Fusco G, Tintoré J (2016) Glider and satellite high resolution monitoring of a mesoscale eddy in the Algerian basin: effects on the mixed layer depth and biochemistry. J Mar Syst 162:73–88
85. Aulicino G, Cotroneo Y, Ruiz S, Sánchez Román A, Pascual A, Fusco G, Tintoré J, Budillon G (2018) Monitoring the Algerian Basin through glider observations, satellite altimetry and numerical simulations along a SARAL/AltiKa track. J Mar Syst 179:55–71. https://doi.org/10.1016/j.jmarsys.2017.11.006
86. Liblik T, Karstensen J, Testor P, Alenius P, Hayes D, Ruiz S, Heywood KJ, Pouliquen S, Mortier L, Mauri E (2016) Potential for an underwater glider component as part of the Global Ocean observing system. Meth Oceanogr 17:50–82. https://doi.org/10.1016/j.mio.2016.05.001
87. Rudnick DL (2016) Ocean research enabled by underwater gliders. Ann Rev Mar Sci 8:519–541. https://doi.org/10.1146/annurev-marine-122414-033913
88. Aulicino G, Cotroneo Y, Olmedo E, Cesarano C, Fusco G, Budillon G (2019b) In situ and Satellite Sea surface salinity in the Algerian Basin observed through ABACUS glider measurements and BEC SMOS regional products. Remote Sens (Basel) 11:1361
89. Budillon G, Cotroneo Y, Aulicino G, Fusco G, Heslop E, Torner M, Tintoré J (2018) SOCIB TNA Abacus (version 1.0) [data set]. Balearic Islands coastal observing and forecasting system, SOCIB. https://doi.org/10.25704/B200-3VF5
90. Cotroneo Y, Aulicino G, Ruiz S, Pascual A, Budillon G, Fusco G, Tintoré J (2016) Glider and satellite high resolution monitoring of a mesoscale eddy in the algerian basin: effects on the mixed layer depth and biochemistry. J Mar Syst 162:73–88
91. Swart S, Chang N, Fauchereau N, Joubert W, Lucas M, Mtshali T et al (2012) Southern Ocean seasonal cycle experiment 2012: seasonal scale climate and carbon links. S Afr J Sci 108:1–3. https://doi.org/10.4102/sajs.v108i3/4.1089

Chapter 4
Metrology for the Sea: Physical Quantities

Marc Le Menn

Contents

Abstract This chapter deals with the fundamental physical quantities measured in oceanography, the sensing technology allowing their measurement and the way they are linked to metrological references when available. It starts with the temperature because it is the most commonly measured quantity and also the best mastered. Salinity is the second quantity that oceanographers use to calculate the ocean physical properties. The calculation of salinity is still inseparable today from conductivity measurements, despite the introduction in 2010 of new equations for calculating seawater properties that take into account the notion of absolute salinity. In order to locate measurements in depth, pressure sensors are widely used; pressure is therefore the third quantity described in this chapter. Temperature and salinity changes affect density and thus induce thermohaline circulation and sea currents. Current measurements are part of the essential ocean variables (EOV) and of physical quantities described in this chapter through the operating principle of Doppler current meters and current profilers.

M. Le Menn (✉)
Service hydrographique et océanographique de la marine, Brest, France
e-mail: marc.lemenn@shom.fr

P. Daponte et al. (eds.), *Measurement for the Sea*, Springer Series in Measurement Science and Technology,
https://doi.org/10.1007/978-3-030-82024-4_4

4.1 Temperature

4.1.1 Temperature: A Physical Quantity

Temperature is one of the most measured quantities in the world and one of the fundamental variables used by oceanographers to assess the physical properties of the oceans. It is also a useful indicator of the energy stored in the oceans and of climate changes.

If we place a thermometer in an adiabatic setting, it will show its own temperature. This temperature is that of the medium if there is thermal equilibrium between the thermometer and its surroundings. That is a first aspect of this quantity: It cannot be measured accurately without thermal exchanges between the thermometer and the medium.

Temperature is an intensive quantity; this means that the system in whole or any part of it will have the same value at equilibrium. That is the second aspect of this quantity. It implies that it is not possible to add or subtract two temperatures. It is only possible to classify bodies from the hottest to the coldest according to their temperatures. Therefore, it is not strictly a measurable quantity. Hence, it is treated as a stake out quantity: one can only grade a physical phenomenon in temperature. This is how a temperature scale was developed based on variations of other quantities selected as references.

The first definition of a measurable temperature scale was proposed in 1852 by Sir William Thomson, alias Lord Kelvin, based on experimental work carried out by Carnot. This scale is therefore based on Carnot's principle applied to heat engines:

- dithermal machines that function with a hot and a cold source;
- reversible machines, where the transformations consist of a series of equilibrium states.

This principle establishes a relationship of proportionality between amounts of heat exchanged Q_1 from the hot source and Q_2 from the cold source, and two functions dependent on temperatures T_1 of the hot source and T_2 of the cold source:

$$\frac{Q_1}{Q_2} = -\frac{f(T_1)}{f(T_2)} \tag{4.1}$$

$f(T)$ can be defined by choosing an arbitrary, continuous, and monotonic function. If the simple relation $f(T) = \alpha T$ is chosen, it is just necessary to identify the temperature of observable and reproducible phenomenon. These phenomena are given by phase changing or phase equilibrium points of pure substances. Under some conditions, solid, liquid, and gas phases of a substance can be present. This particular point on the phase diagram is called triple point. During the twentieth century, the physician William Francis Giauque proposed to use the thermodynamic value of the triple point of water to build the temperature scale. This value has been fixed to

273.16 K and the kelvin has been chosen as temperature unit. Until 2018, the kelvin was defined as *the temperature of the fraction 1/273.16 K of the thermodynamic temperature of the triple point of water*.

With this definition and relationship (4.1), it is possible to speak of thermodynamic temperature since we have an origin and a ratio relationship. The thermodynamic temperature becomes a measurable quantity. This principle allowed the creation of International Temperature Scales (ITS) or International Practical Temperature Scales (IPTS), based on the measurement of temperature intervals from a reference origin. The first ITS dates from 1887, and it was called the "normal hydrogen scale." It was revised in 1927, in 1948, in 1968 when it became an IPTS, and then in 1990 (see ref. [1, 2]). All along these revisions, the range and the accuracy of ITSs were improved.

There is another way to define the thermodynamic temperature. It is based on Boltzmann's kinetic theory of gases. Temperature represents the energy of a system, which is related to the kinetic energy of molecules composing it [3]. If we admit that the molecules have 3 degrees of freedom, their mean kinetic energy related to thermal agitation is given by the relation $E_c = 3 \times ½\, k_B T$. k_B is the Boltzmann constant, and since November 2018, the kelvin has been redefined by assigning an exact value to k_B which is expressed in $J.K^{-1}$ [4]:

"1 kelvin is equal to the thermodynamic temperature change resulting from a change in thermal energy $k_B T$ equal to $1.380\,649 \times 10^{-23}$ J."

The kelvin therefore represents the average energy possessed by the atoms and molecules of a substance at a given temperature. With this definition, temperature measurements (re-)become essentially measurements of the energy of molecular motion. As a consequence, the triple point of water is no longer the "reference" of the scale, and its temperature has an uncertainty because it is determined from k_B: $T_{ptH2O} = 273.160\,0 \pm 0.000\,1$ K.

4.1.2 The International Temperature Scale of 1990 or ITS-90

The kelvin has been redefined, but the scale defined in 1990 is still used in practice (for an indefinite period of time). Its principle is based on measuring temperature intervals and on a scale that allows a location from an origin. The values obtained by this marking must be as close as possible to the thermodynamic temperature values.

ITS-90 concerns temperatures between 0.65 K and the highest temperature measurable in terms of the Planck relation using monochromatic radiation. It is composed of overlapping ranges and subranges with limits defined by 18 fixed points. It is vapor pressure points, melting–freezing points, or triple points. Two of them are in the range of oceanographic temperatures: the triple point of water (tpH2O) at 0.01 °C and the melting point of gallium (mpGa) at 29.7646 °C. ITS-90 is also composed of reference instruments to make measurements between fixed points. From 13.8033 K to 961.78 °C, the standard platinum resistance thermometer

(SPRT) composed of a pure platinum coil is the reference instrument. ITS-90 also defines polynomial interpolation relations. These relations are used to calibrate SPRTs.

The WG 4 of the Consultative Committee for Thermometry (CCT) has assessed differences between thermodynamic temperatures T and ITS-90 temperatures T_{90}. To the tpH2O $T - T_{90} = 9.74 \pm 0.6$ mK and to the mpGa, $T - T_{90} = 4.38 \pm 0.4$ mK [5, 6]. It also defined interpolation functions for the ITS-90's ranges. From 273.16 K to 1357.77 K (copper point):

$$\left(T - T_{90}\right) / mK = \left(T_{90} / K\right) \sum_{4}^{i=0} c_i \left(273.16K / T_{90}\right)^{2i} \tag{4.2}$$

with coefficients $c_0 = 0.0497$, $c_1 = -0.3032$, $c_2 = 1.0254$, $c_3 = -1.2895$, and $c_4 = 0.5176$. The accuracy of the different ITSs has improved over the years leading to significant differences between them. BIPM edited in 1989 complex polynomial relations to convert temperatures from one scale to the other [1]. According to the WOCE Hydrographic Program (WHP), simplified relations can be used over the oceanographic temperature range (− 2 °C to 35 °C) [7]. In order to convert IPTS-68 temperature to ITS-90 temperature, it is possible to employ the relationship:

$$t_{90} = 0.9997 t_{68} \tag{4.3}$$

The residual error will be less than 0.5 mK. In order to convert ITS-48 to IPTS-68 temperatures, it is also possible to use the relationship:

$$t_{68} = t_{48} - 4.4 \cdot 10 - 6 \cdot t_{48} \cdot \left(100 - t_{48}\right) \tag{4.4}$$

The use of relationship (4.3) is particularly important to calculate salinities with the practical salinity scale of 1978 (PSS-78). This scale was made with temperatures linked to the IPTS-68, and at 30 °C, the difference can be of 7 mK with ITS-90 temperatures. The same conversion must be made before using algorithms published before 1990 to calculate the speed of sound in seawater.

4.1.3 Temperature Sensing Technology Used in Oceanography and Measurement Errors

The main constraints of temperature measurements in oceanography are the required trueness (or accuracy) and uncertainties. The specifications of the World Ocean Circulation Experiment (WOCE) program are stringent, requiring an accuracy of 2 mK and a precision of 0.5 mK [8]. These specifications are particularly relevant in deep waters where temperature is very stable and where slight changes

must be detected. For surface temperatures, requirements are less important but nonetheless difficult to reach: 0.1 °C for satellites measurements and 0.05 °C for surface buoys.

According to Stephens et al. [9], one must be able to identify a mean temperature change of 10 m°C/decade to detect the anthropogenic heating of oceans. According to Carl Wunsch from Harvard University [10], measurement accuracy should be no worse than 10% of the expected signal or 1 mK/decade! In the same way, satellite estimate of the global mean sea level change is 3 mm/year. If the sea rise level was attributed solely to temperature, according to reference [10], it would correspond to a global mean temperature change of 1.5 mK/decade. Carl Wunsch [10] also calculated that approximate oceanic temperature changes implied by a 1 W/m^2 heating or cooling rate correspond to a temperature change of 2 mK on the full depth over 1 year.

Oceanographic instruments are subject to strong constraints when used in situ from ships or on buoys: chocks, vibrations, and sudden changes in temperature and pressure. If platinum resistance sensors were commonly used a few years ago, this technology is progressively replaced by the technology of thermistors. They are composed of metal oxide ceramics of semiconductors MgO, MgAl2O4, etc. The powdered metal oxides are grouped together by compression, forming disks, pearls, or cylinders of small dimensions (approximately 1 mm^2 or smaller). That makes sensors resistant to shock and vibration, and their sensitivity is around 10 times higher than that of platinum resistance of 100 Ω. However, this sensitivity is not constant in their range of usage. Their response is therefore nonlinear. Relations have been discovered to linearize it in temperature. The more accurate has been found by Bennett [11]:

$$t\left(^{\circ}C\right) = \frac{1}{\left[A + B\ln\left(x\right) + C\ln\left(x\right)^2 + D\ln\left(x\right)^3\right]} - 273.15 \tag{4.5}$$

where A, B, C, and D are the calibration coefficients and x the resistance ratio of the resistance to the temperature t and the resistance to a reference temperature.

Thermistors are passive sensors, and they need to be powered by a constant current. This current leads to a local heating of the medium due to the Joule effect. This self-heating error must be limited by using small currents. The most famous manufacturer of oceanographic instruments, Sea-Bird Scientific, warrants a self-heating error <0.1 mK in still water for its SBE 3 probes mounted on CTD profilers and <200 µK for the SBE 35 thermometers which can be used as reference at sea to make intercomparison. The effect of pressure on these probes has been assessed by Ushida et al. in 2007 [12]. They found pressure sensitivities of 1–2 mK at 6000 dbar.

Dynamic errors can also affect the accuracy of temperature measurements in situ in the first tens of meters. As a temperature sensor measures its own temperature, thermal exchanges are required to acquire the temperature of the medium and these

exchanges need time. The response time τ of a sensor is defined as the product of its mass m by its thermal capacity C_p, divided by the coefficient of exchange by convection h and its surface S. h is very dependent on the relative speed sensor v.s medium and therefore of a ratio called Reynolds number, which implies that τ depends not only on the geometry of the sensor but also on dynamic conditions. Sea-Bird Scientific manufacturer accurately determined τ = 65 ms ± 10 ms (in 1.0 m/s water velocity) for the SBE 3 and fixes this response time by a seawater pumping system which fixes the speed of flow on the CTD profiler SBE 911. That is not the case for all products and manufacturers. Additional software corrections are necessary.

The geometry of sensors is also important in the case of surface temperature measurements. In 2018, de Podesta et al. demonstrated that "the radiative error for an air temperature sensor, in flowing air depends upon the sensor diameter and air speed, with smaller sensors and higher air speeds yielding values closer to true air temperature" [13]. This assertion is also true in seawater at depth where direct or back-scattered solar radiations can be detected. The error due to the irradiance is proportional to the square root of the diameter for a cylindrical sensor [14].

Another dynamic error is due to the viscous heating: the acceleration of flow as it meets the surface of a sensor provokes an increase in temperature related to the fluid viscosity. The viscous heating error can be assessed with the relation $\delta t = 1.263 \times 10^{-4}\ Pr^{0.5}\ U^2$, where Pr is the Prandtl number and U the relative speed. Pr expresses the ability of heat to move through a thermally conductive fluid. It can be calculated by the ratio of the kinematic viscosity by the thermal diffusivity of a fluid. If U = 1 m/s, δt is assessed to be about 1 mK according to Larson and Pedersen [15].

Accuracy and uncertainties of measurements also depend on the instrument calibration. As temperature sensors are attached to probes or instruments, they cannot be calibrated in fixed-point cells. The calibration must be made per comparison in seawater calibration bath of a sufficient volume. The use of seawater allows the conductivity sensors to be calibrated at the same time. The temperature plateaus are made within the temperature range of the instrument to be calibrated. During each plateau, the thermal stability of the bath must be lower than 1 mK peak to peak in order to obtain sufficiently low measurement standard deviations. Temperature gradients in the bath must be reduced in the same way, in order to obtain accurate comparisons between the reference thermometer and the sensor to be calibrated that can be distant. The link to ITS-90 is made by the regular calibration of the reference thermometer in fixed-point cells (fpGa and tpH2O), which are themselves calibrated in national metrology institutes. Uncertainties calculations must be performed, and the results must be communicated to the user in order to assess the expanded uncertainty of the traceability to the SI (unit system) of the data collected with the calibrated sensor. In the best laboratories, with the best instruments, expanded uncertainties close to or better than 2 mK can be obtained, filling the requirements of WOCE program.

4.2 Salinity

4.2.1 The Historical Definitions of Salinity

Salinity is a complex concept that has been the subject of multiple definitions. Absolute salinity S_A refers to the mass fraction of dissolved material per kilogram of seawater. In practice, this mass is difficult to determine because seawater composition is complex, and S_A is a hard-to-define quantity given the complexity of its biogeochemical composition and the imperfections of existing measurement techniques [16]. Although its major inorganic components are well known, its real composition varies in time and space. Table 4.1 gives the concentrations of the major components of standard seawater, as defined by Millero in 2008 [17]. The total sum of dissolved salts gives a total concentration of 35.16504 g kg^{-1}. Nonstandard waters also contain nonionic compounds such as silicates, organic substances, bacteria, chlorofluorocarbons, microplastics, dissolved gases, and other minor components. These compounds modify the density of seawater but at present they are not taken into account in salinity measurements.

Marcet's principle (1819–1822) states that the relative abundances of solute substances are constant in seawater, what allowed Johann Georg Forchhammer to define in 1865 [18] the concept of salinity and to demonstrate that the ratio of major salts in samples of seawater from various locations was constant. However, the first complete study of the composition of seawater was carried out by William Dittmar in 1884 on 77 samples collected during the Challenger Expedition [19].

Table 4.1 Composition of standard seawater as defined by Millero in 2008

Elements	Concentration (g kg^{-1})
Sodium: Na^+	10.78145
Magnesium: Mg^{2+}	1.28372
Calcium: Ca^{2+}	0.41208
Potassium: K^+	0.39910
Strontium: Sr^{2+}	0.00795
Chloride: Cl^-	19.35271
Sulfate: SO_4^{2-}	2.71235
Bicarbonate: HCO_3^-	0.10481
Carbonate: CO_3^{2-}	0.01434
Bromide: Br^-	0.06728
Borate: $B(OH)_4^-$	0.00795
Fluoride: F^-	0.00130
OH^-	0.00014
$B(oh)_3$	0.01944
CO_2	0.00042

In 1902, an Operating Protocol was adopted by an international commission to approximate the value of the mass of dissolved substances. Salinity then became "the mass in grams of solid substances contained in one kilogram of seawater, the carbonates being transformed into oxides, the bromides and iodides replaced by their equivalent in chlorides, the organic matter being oxidized." It is a definition that makes it possible to approach the notion of S_A with a unit of g kg^{-1}. As this definition was impossible to apply in routine measurements, a method based on chlorinity was proposed. Chlorinity Cl is defined as "the mass (in g) of the halogens contained in one kilogram of seawater, with the bromide and iodide ions being replaced by their chloride equivalents." It is also 0.3285234 times the ratio of the mass of pure silver (Ag) needed to precipitate all the chlorine, bromine, and iodine ions to the mass of the seawater sample. For seawater, the halogens are mainly chlorine and bromine [20]. Therefore, from 1902 to 1962, salinity was obtained by the formula:

$$S = 0.03 + 1.8050Cl \text{ in}\% \tag{4.6}$$

Based on work on chlorinity, salinity, and density, a new relationship was proposed in 1962 and used until 1969:

$$S = 1.80655Cl \text{ in}\% \tag{4.7}$$

In order to avoid "chlorinity variations" in relation to the progress in the knowledge of the atomic mass of Cl and Ag molecules, in 1969 another relationship was proposed:

$$S = 1.80655 \cdot 0.32852Ag \text{ in}\% \tag{4.8}$$

While the first reference to the use of conductivity for salinity measurement dates back to 1902 [21], it was not until the late 1950s that measurement of electrical conductivity began to replace the chlorinity titration as a means of estimating salinity, followed by a definition of salinity based on conductivity measurements in 1967 and by the first relationship linking conductivity to salinity in 1969. As electronics and the development of conductivity cells improved, in 1978, a new definition was published by UNESCO in 1981 [22], based on the measurement of conductivity ratio. This definition gave rise to the Practical Salinity Scale of 1978 or PSS-78 stating that "The practical salinity S_P of a seawater sample is the ratio called K_{15} of the electrical conductivity of the sample at a temperature of 15 °C and a pressure of 101325 Pa to that of a potassium chloride (KCl) solution containing 32.4356 g of KCl per kg of solution, under the same temperature and pressure conditions." The relation between S_P and K_{15} is:

$$\begin{aligned} S_p &= 0.0080 - 0.169K_{15}^{1/2} + 25.3851K_{15} + 14.0941K_{15}^{3/2} \\ &-7.0261K_{15}^{2} + 2.7081K_{15}^{5/2} \end{aligned} \tag{4.9}$$

Its domain of validity is $2 < S_P < 42$. Salinity values in g kg^{-1} cannot be obtained using this definition. S_P has no unit because it is the result of a ratio. All waters with the same conductivity ratio have the same practical salinity even if their composition and chlorinity are different, and nonionic compounds like $Si(OH)_4$, NO_3, or CO_2 are not taken into account as they can modify seawater properties.

4.2.2 The Conductivity of Seawater and Its Measurement

In the case of seawater, the electrical conductivity is ensured by the speed of movement of the ions. At constant temperature and pressure, its variation as a function of chlorinity is linear. At constant pressure and chlorinity, an increase in temperature results in a decrease in the density of the water and therefore a decrease in the number of ions per unit volume and in the viscosity. This decrease causes an increase in the mobility of ions and thus an increase in water conductivity.

At constant temperature and chlorinity, an increase in pressure also results in an increase in conductivity. Thus, if the pressure increases from 0 to 10,000 dbar, the relative conductivity $\Delta C/C$ of water with a salinity of 35 at 0 °C increases by 11.5%. This increase is due to a higher volume concentration of the ions, to a decrease of the viscosity and to the dissociation of certain electrolytes under the effect of pressure.

Yet, the definition of S_P is only valid for the temperature of 15 °C. In order to be able to measure salinities in situ, it is necessary to correct the relation (4.9) by replacing K_{15} by a ratio R_t and to add a term Δt to compensate for the effect of temperature. Therefore, the relation (4.9) becomes [23, 24]:

$$\begin{aligned} S_p &= 0.0080 - 0.169KR_t^{1/2} + 25.3851R_t + 14.0941R_t^{3/2} \\ &-7.0261R_t^2 + 2.7081R_t^{5/2} + \Delta S \end{aligned} \tag{4.10}$$

with:

$$\Delta S = \frac{(t-15)}{1+0.0162(t-15)} \left(\begin{array}{l} 0.0005 - 0.0056R_t^{\frac{1}{2}} - 0.0066R_t - 0.0375R_t^{\frac{3}{2}} \\ +0.063R_t^2 - 0.014R_t^{\frac{5}{2}} \end{array} \right) \tag{4.11}$$

In order to take into account the effect of pressure, the ratio R is measured:

$$R = \frac{C(S,t,p)}{C(35,15,0)} \tag{4.12}$$

This ratio can be decomposed into three ratios:

$$R = \frac{C(S,t,p)}{C(S,t,0)} \frac{C(S,t,0)}{C(35,t,0)} \frac{C(35,t,0)}{C(35,15,0)} = R_p R_t r_t \tag{4.13}$$

R_t can be extracted from relationship (4.13) and inserted in relationships (4.10) and (4.11) to obtain the value of S_P. R is the ratio calculated by the instrument, and $C(S, t, p)$ is the conductivity measured by the conductivity cell. $C(35,15,0)$ is a value programmed in the instrument. $C(35,15,0)$ = 42.914 mS/cm according to Culkin and Smith [25], but this value is questionable. In 1980, A. Poisson estimated it to be 42.933 mS/cm. In older instruments (Guildline CTD profilers), the value 42.896 mS/cm was programmed. In 2010, an intercomparison of metrology laboratory measurements yielded 42.9104 mS/cm [26], but the latest [27] yielded 42.8922 ± 0.0074 mS/cm.

In fact, it doesn't matter what value is programmed into the instrument because a ratio is measured, and the instrument is adjusted during calibrations prior to use. The uncertainty of these calibrations can be close to ±0.003 in salinity [28]. However, the difficulties encountered in measuring $C(35,15,0)$ show the limits of what can be done in terms of absolute measurements of conductivity and therefore salinity. The uncertainty of the last measurements (± 0.0074 mS/cm) gives an idea of the limit of salinity linking with respect to the international system of units and therefore of the monitoring of its evolution over the long term from conductivity measurements. In 2011, Seitz et al. [29] estimated that the uncertainty on S_p increases with the number of years N, according to the relationship:

$$\sqrt{\frac{2N}{2N_0 + 1}} x 0.002 \tag{4.14}$$

where N_0 is the life duration of standard seawater bottles or 3 years. Before using R_t in relationships (4.10) and (4.11), it is necessary to determine R_p and r_t. R_p is the ratio used to correct the effect of pressure:

$$R_p = 1 + \frac{p\left(2.07x10^{-5} - 6.370x10^{-10}\, p + 3.989x10^{-15}\, p^2\right)}{1 + 3.42x10^{-2}\, t + 4.464x10^{-4}\, t^2 + R\left(4.12x10^{-1}\, t - 3.107x10^{-3}\, t\right)} \tag{4.15}$$

r_t is the ratio used to correct the effect of temperature in normal conditions of salinity and pressure:

$$\begin{aligned} r_t &= 0.6766097 + 2.00564 \times 10^{-2}\, t + 1.104259 \times 10^{-4}\, t^2 \\ &-6.9698 \times 10^{-7}\, t^3 + 1.0031 \times 10^{-9}\, t^4 \end{aligned} \tag{4.16}$$

In 2010, the relationships for calculating the physical properties of seawater evolved. Since 1980, they have been based on the measurement of practical salinity and

relations called EOS-80 for equations of state of seawater of 1980 [24, 30]. In 2010, the Intergovernmental Oceanographic Commission (IOC) of UNESCO adopted the TEOS-10 or international "thermodynamic equation of seawater" [31]. The TEOS-10 equations are based on the concept of absolute salinity S_A. However, since only S_p can be estimated, it continues to be recorded, but it needs to be transformed into reference salinity S_R:

$$S_R = \left(35.16504 / 35\right) \times S_P \tag{4.17}$$

35.16504 is the salinity of the reference composition described in Table 4.1. It allows the correction of the systematic error of 0.165 that marred S_p measurements. S_A is obtained with the relationship:

$$S_A = S_R + \delta S_A \tag{4.18}$$

δS_A is the salinity anomaly. No instrument is currently available to measure δS_A, and TEOS-10 proposes an empirical method based on silicate concentration measurements to evaluate it [32]. With this algorithm, S_A becomes $S_A(S_p, \phi, \lambda, p)$, where ϕ is the latitude in degrees north, λ the longitude in degrees east and p the pressure to which the sample is calculated.

4.2.3 Technology of Conductivity Sensors

The required uncertainties are as important for conductivity measurements as they are for the temperature. The WHPO specifies an accuracy of 0.002 and a precision of 0.001 for practical salinity [7]. In order to fill these requirements, resistive or inductive technologies can be used.

Resistive technology cells are used in Guildline Autosal and Portasal laboratory salinometers and on Sea-Bird Scientific instruments. Guildline salinometer cells are formed of a glass tube and four platinum spiral electrodes. The water to be analyzed flows into a capillary tube placed in a thermo-regulated bath to acquire the reference temperature of the bath. The capillary tube is connected to the cell that is also immersed in the bath. Two electrodes are used to generate a current field in the cell, and two more are used to measure the voltage variations created by the conductivity variations of the sample to be analyzed.

The Sea-Bird SBE-4 conductivity cell is composed of a tube of glass and three circular platinum electrodes. The tube is 190 mm long, and its external diameter is 7 mm. These platinum rings are covered with black platinum to increase their surface exchange. The electrical resistance of the two water cylinders located between the peripheral electrodes and the central electrode is measured. Like the Guildline cell, it is an internal field cell. The glass is coated with epoxy to seal the wire entry. It is supported by an aluminum plate to enhance resistance to mechanical strain. The SBE-4 cell is used on all Sea-Bird

products but also mostly on all profiling floats of the Argo Network and in OPTIMARE laboratory salinometers.

For these two cells, if l is the distance between the peripheral electrodes, and d the internal diameter of the glass tube, the resistance R_w of seawater is obtained by the relationship:

$$R_w = \frac{1}{\chi}\frac{2l}{\pi d^2} \tag{4.19}$$

where χ is the conductivity of seawater. The term $2\ l/\pi d^2$ is called the cell constant K. Taking into account the geometry of the SBE 4 cell, $K \approx 2000\ \mathrm{m}^{-1}$.

Inductive cells are shaped like a ceramic ring. This ring comprises one or two electric windings forming one or two transformers, in which the secondary coil is simply the liquid that surrounds the ring. In the double transformer configuration, one is used to create an external electrical field in seawater and the second to "read" the induced voltage variations created by the resistance of seawater R_w. They are arranged in such a way that the only coupling between them is the loop formed by the water. The formula between voltage power and voltage induced is very complex (See ref. [33]). The electronic circuit they are connected to must eliminate the inductive component of coils inductance. If the first transformer is powered by a constant voltage U, the current variations I measured by the second transformer are given by the relationship:

$$I = \frac{1}{n_1 n_2}\left(\frac{1}{R_w} - \frac{1}{R_k}\right)U \tag{4.20}$$

where n_1 and n_2 are the numbers of windings of the two coils and R_k a resistance connected to the second coil.

The accuracy of conductivity cells when used at sea decreases due to sensor drift caused by fouling and due to problems in aligning the response time with that of the temperature sensor. The cell constantly drifts over time generally because of the adsorption of organic and inorganic macromolecules by the materials and then because of the deposit of thin layers of biofilm. This phenomenon affects both resistive and inductive cells. For tubular cells, tributyltin (TBT) tablets can be used as an active protection. Antifouling paints composed of TBT are often used for inductive cells. More of that, conductivity cells need to be cleaned with the nonionic detergent Triton X-100 and then rinsed with distilled water and dried. To correct unavoidable drifts, calibrations must be done regularly.

Problems related to the alignment of response times are less trivial. The practical salinity calculation needs temperature, conductivity, and pressure values measured at the same time and in the same space. If this condition is not met, salinity artifacts and differences between up and down casts appear on salinity profiles, in oceanic layers with temperature gradients. It is accepted that variations in the electrical conductivity of seawater are dominated to 80% (or higher) by temperature. The thermal

inertia of the sensors prevents them from adapting instantaneously to the water temperature. As a result, conductivity sensors have a response time that is linked to variations in salinity of the medium (estimated at 30 ms for the SBE 4) and a response time linked to variations in temperature. These two effects combined give a response time in conductivity. As already seen in § 4.1.3, response times are in relation to the convection constant h which depends strongly on the Reynolds number. On the Sea-Bird SBE 9 or SBE 41 probes, seawater is pumped through the conductivity cell at a constant speed of 2.4 m/s using a specially adapted pipe installation. The response time of temperature and conductivity sensors is therefore fixed, and a software alignment of temperature and conductivity data can be made more reliably. From observations made in situ in a region of the ocean where variations in salinity and temperature present staircase profiles, in 1990 Lueck and Picklo [34] determined the equation of a numerical filter to correct the lateness representing the physical distance between the temperature sensor and the middle of the conductivity cell:

$$T^{'}(n) = 0{,}9350\,T^{'}(n-1) + 0{,}5872\,T(n) - 0{,}5222\,T(n-1) \tag{4.21}$$

where $T(n)$ is the temperature of the sample n. From Eq. (4.21), they established the equation of a numerical filter allowing the correction of conductivity value $C_T(n)$ from temperature effects:

$$C_T(n) = -b\,C_T(n-1) + \gamma\,a\left[T^{''}(n) - T^{''}(n-1)\right] \tag{4.22}$$

γ represents the sensitivity of conductivity to variations in temperature ($\partial C/\partial T_{S,P} \approx 0.1$ S m^{-1} °C^{-1}), $a = 4f_n\alpha\beta^{-1}(1 + 4f_n\beta^{-1})^{-1}$, $b = 1 - 2a\alpha^{-1}$, and $T''(n)$ is the temperature corrected by the formula $T''(n) = T'(n-5)$. f_n is the Nyquist frequency or the frequency from which sampling leads aliasing of the spectrum. $f_n = 12$ Hz for an SBE 9, as its sampling frequency is fixed to 24 Hz. α and β are coefficients determined experimentally. Sea-Bird Scientific recommends using the values $\alpha = 0.03$ and $\beta = 0.14$, but earlier studies show that values $\alpha = 0.0132$ and $\beta = 0.0829$ allowed better mitigation of maximal errors in salinity due to temperature gradients [35]. A study of the same type was undertaken in 2007 by Johnson et al., about SBE 41 heads equipping drifting floats [36].

4.2.4 Calibration of Conductivity Sensors

Generally, the calibration of conductivity sensors is made at the same time that the calibration of temperature sensors, in big volume calibration baths containing seawater. During each temperature plateau, conductivity measurements are made with a reference conductivity sensor, or water samples are collected in the bath and measured with laboratory salinometers (Guildline or OPTIMARE) to obtain reference salinity

values. Having reference values of temperature and salinity, by inverting relations (4.10), (4.11), and (4.13) with a Newton–Raphson-type algorithm, it is possible to obtain reference conductivity values. In 2011, Le Menn [28] has shown that with a standard uncertainty between 0.0011 and 0.0023 mS/cm on reference conductivities, it was possible to obtain expanded uncertainties between 0.0032 and 0.0034 on practical salinity values measured with an SBE 9 profiler.

4.2.5 Instruments under Development to Measure Absolute Salinity

As defined by relation (4.18), absolute salinity cannot be measured by conductivity sensors, the salinity anomaly δS_A remaining unknown. Absolute salinity is in direct relation to density. Density can be measured in laboratories thanks to vibrating tube densitometers, pycnometers, or hydrostatic weighing (see ref. [16]), but these techniques cannot be applied for in situ measurements.

In 1869 Ludvig Lorenz and, independently, in 1878 Hendrik Lorentz discovered a formula linking the refractive index of substances and their densities. In 1990, from measurements made on the refractive index of seawater n at different temperature t, salinities S, pressure p, and wavelengths λ, Millard and Seaver [37] proposed an algorithm to calculate n from measurements of t, S, and p in a range of λ varying from 500 to 700 nm. By measuring the refractive index and inverting this algorithm, salinity can be extracted with accuracies close to oceanographic purposes at low pressure, but not at high pressure [16].

Demonstrations have been made of the using of refractometers in situ (see ref. [38]) but several obstacles remain to make of them instruments able to challenge conductivity cells in resolution, precision and compacity. However, recently researchers from JAMSTEC developed and tested with success to 6000 m depth, an interferometric method showing relative accuracy close to conductivity cells [39].

4.3 Pressure

4.3.1 Why and How Do We Measure Pressure?

Pressure refers to the internal energy of fluids or gaz. It can be defined as the capacity of a system to store static mechanical energy per its volume. Absolute pressure P behaves like a force F normal to a surface S:

$$d\vec{F} = P\vec{n}dS \tag{4.23}$$

Pressure is therefore an intensive scalar quantity. Pressure measurements are necessary to calculate several thermodynamic properties of oceans but also to locate

instruments in depth or to measure the sea level. Sensors measure generally an absolute pressure *P,* but some instruments give the sea pressure p defined to be P less the normal pressure P_0 = 101,325 Pa. 1 Pascal (Pa) corresponding to a small quantity, in oceanography, the pressures are expressed in dbar (10^4 Pa). Some instruments give also the gauge pressure which is P less the measured atmospheric pressure p_a.

To locate instruments in low depth (z), a simple formula exists: $z = p$ (dbar) * 0,992. The positioning error will be of 6 cm at 100 m compared to reference relations, but it can be up to 80 cm at 500 m and 2.77 m at a depth of 1000 m. To locate more accurately or to measure sea level or tides, the hydrostatic equation is used:

$$P = p_a + \rho.g.z \tag{4.24}$$

where ρ is the density of seawater and g the gravitational acceleration. For great depth, it is necessary to take into account the relation between g and z and the notion of dynamic height anomaly Ψ:

$$g = g(\phi,z) = g(\phi,0)(1-\gamma z) \tag{4.25}$$

where ϕ is the latitude, and γ the gravitational acceleration average gradient. Ψ is defined with respect to the sea surface by:

$$\Psi = -\int_{p}^{p_0} \left[V(S_A,\Theta,p) - V(S_R,0,p) \right] dp \tag{4.26}$$

where V is the specific volume ($V = 1/\rho$), S_A is defined by relation (4.18), $S_R = 35.165\,04$ g kg^{-1}, and Θ is the conservative temperature. Θ is defined to be proportional to the potential enthalpy $h^0(S_A, t, p)$. $h^0(S_A, t, p)$ is the enthalpy that a fluid parcel would have if its pressure was changed to a fixed reference pressure in an isentropic and isohaline manner ([31], p. 27). $\Theta(S_A, t, p) = h^0(S_A, t, p)/3991.867957119\,63$(j kg^{-1} K^{-1}). The depth Z is obtained by resolving the equation:

$$\int_{z}^{0} g(\phi,z)\,dz = -\int_{p}^{p_0} V(S_R,0,p)\,dp + \Psi + \Phi^0 \tag{4.27}$$

where Φ^0 is the geopotential for $z = 0$. Φ^0 is the gravitational acceleration by the height of the free surface above the geoid. According to the TEOS-10 manual, ignoring the terms $\Psi + \Phi^0$ would lead a difference of up to 4 m at 5000 dbar. Z is given by:

$$Z = \frac{-\int_{p_0}^{p} V(S_R,0,p)\,dp + \Psi + \Phi^0}{\left(g(\phi,0) - \frac{1}{2}\gamma z^2 \right)} \tag{4.28}$$

In this equation, it is possible to replace z by p. The resulting error is about 5 cm at 10000 m.

4.3.2 Pressure Sensors Technologies and Calibration

According to relation (4.23), measuring pressure consists in measuring the force F applied on a surface S. In oceanography, two kinds of technologies are generally used to measure F: the piezoresistive and the piezoelectric.

Piezoresistive sensors use strain gauges to measure the bending of a measuring body. Strain gauges are made of a metallic conducting wire forming a grid pattern, deposited on an insulated support. The support is bonded with a cyanoacrylate adhesive on the surface submitted to pressure. The wire can be also a semiconductor. The resistance of the wire changes with strain and its relative variations are proportional to the length relative variations of the gauge. Strain gauges are connected to a Wheatstone bridge, and the signal is amplified before being digitized.

Very small size piezoresistive pressure sensors can be made also with microelectromechanical systems or MEMS. MEMS pressure sensors are made of a flexible diaphragm that deforms under a pressure difference. This deformation is converted to an electrical signal. The flexible diaphragm is created by bulk micromachining of a silicon substrate. Piezoresistors are made by diffusing boron atoms in selected regions of the diaphragm with maximum stress [40]. These piezoresistors are connected in the form of a Wheatstone bridge.

Strain gauge and silicon elements are sensible to temperature variations, and according to the accuracy class of the pressure sensor, a temperature sensor can be integrated in the body. In this case, the pressure calibration must be made at several temperature values (in calibration bath) and the coefficients of the calibration relationship must be expressed in function of temperature. The best temperature compensated sensors can hold ±0.01% of the full scale (FS) in precision and 0.02% of FS for the typical stability per year at ambient temperature and pressure [41].

In the case of piezoelectric sensors, the sensible element is a blade of piezoelectric material: quartz, PZT ceramic, or PVF_2 polymer. Under mechanical strain, the blade develops a dielectric polarization. Electrical charges are collected by electrodes placed on the longitudinal sides. Electronic circuitry can convert electrical charges in voltage, but the sensitivity is very low (2.32 pC/N for quartz) and the signal is sensible to noise. In addition, quartz is also sensible to temperature. Temperature variations induce volume variations of the blade, small strains, the generation of parasitic charges, and the drift of pressure measurements. A temperature sensor needs also to be integrated in the body of the sensor to compensate this drift.

To solve these issues, Paroscientific pressure sensors are based on an electronic oscillator tuned to the resonance frequency of the quartz blade. When pressure is applied, the frequency changes, and this change can be measured. The sensitivity of this effect is very high, allowing great pressure resolutions to be obtained [42]. To compensate for the temperature effects, the calibration coefficients $C(t)$ and $D(t)$ are polynomials dependent on temperature t [43]:

$$p = C(t)\left[1-\left(\frac{\tau(t)}{\tau_0}\right)^2 - D(t)\left[1-\left(\frac{\tau(t)}{\tau_0}\right)^2\right]^2\right] \tag{4.29}$$

with $\tau_0(t) = K_1 + K_2.t + K_3.t^2$, $C(t) = K_4 + K_5.t$, $D(t) = K_6$. $\tau(t)$ is the oscillation period, τ_0 is the period at zero pressure, and K_1, K_2, K_3, K_4, K_5, and K_6 are coefficients determined during the calibration. This sensor equips Sea-Bird Scientific SBE 911 profiler, with the following specifications: 0.001% of FS for the resolution, 0.015% of FS for the initial accuracy, and 0.02% of FS for the typical stability per year.

The accuracy requirements in oceanography are high. That implies that the calibration must be done with pressure balance also called deadweight testers. Calibrated masses M are placed on the cylinder of a piston of section S. This piston generates a pressure p on an oil tank connected to the sensor to calibrate: $p = M\,g/S$. A screw press allows balancing the pressure applied on the sensor and the pressure generated by the masses and the cylinder. Some balances are equipped with automated mass handlers where the balancing is made automatically by a pressure regulator. Numerous corrections are necessary to obtain a reference pressure. This pressure is not measured but calculated with a complex formula [44]:

$$p_{ref} = \frac{M\dfrac{g(\rho_m - \rho_{la})}{gn(\rho_m - \rho_{na})} + \Gamma c}{S_0\left[\left(1+\alpha\left(t-20\right)\right)\left(1+\lambda p\right)\right]} + \rho g \Delta h \tag{4.30}$$

In this formula, g is the local gravity, g_n the normal gravity (9.80665 ms^{-2}), ρ_m the density of masses material, ρ_{la} the local air density, ρ_{na} the normal air density, ρ the density of oil, Δh the height difference between the standard and the instrument under test, Γ the oil surface tension coefficient in N/m, c the piston circumference, S_0 its effective area at 20 °C and null pressure, t the temperature of the piston-cylinder, α its temperature deformation coefficient, λ the pressure distortion coefficient of the piston, and p the estimated pressure. g must be known with five decimals. When all corrections are properly applied, the expanded uncertainty on P_{ref} can be of 0.03 bar at 600 bar or 0.005%.

4.4 Current

4.4.1 Why and How Do We Measure Currents?

Marine currents are the result of temperature and salinity differences. These differences create changes in seawater densities leading water masses circulation in surface and in depth. Tides and wind forcing create also local variations of water circulation. From a physical point of view, current measurement consists of

measuring its speeds and directions of displacement in a range from 1 m to thousands of kilometers and from 1 s to several decades. This can be done using Eulerian and Lagrangian methods. In this paragraph, we will speak only of one Eulerian method, where current meters are dependent on fixed moorings.

Some 10 years ago, rotor current meters were replaced by Doppler effect acoustic current meters. The marine environment is favorable to the sound wave propagation; thus, the time it takes for the impulses reflected by the particles to return resulted in the creation of current meters. Based on the pulse return times, the profiles obtained are artificially divided into measurement cells by the instrument's software, which gives average velocity values per cell, in relation to the measured Doppler shifts. Water column velocity profiles can be obtained either by placing profilers under the hulls of oceanographic vessels and directing them toward the seabed, or by placing them in cages on the seabed and directing them toward the surface, using mooring cables, or towing them from a boat. Their range depends on their wavelength and can vary from few meters to several hundreds of meters, according to the particle concentrations.

4.4.2 Operating Principles of Doppler Current Meters

The elements given in this paragraph are taken from the publication by Le Menn and Morvan [45] which should be consulted for more details. Current meters and profilers compute velocities (V_1, V_2, and V_3) obtained by Doppler shift measurements of pulses emitted in their beam axes. The transducers are tilted 20°, 25°, or 30° (angle β). With a transformation matrix, it is therefore possible to calculate velocities (V_x, V_y, and V_z) in their own reference frame. They are equipped with "fluxgate," "Hall effect," or magnetoresistive compasses to retrieve the amplitude of current components (*U, V,* and *W*) in reference to magnetic north and considering the magnetic declination, in relation to true north. Moreover, their inclination is corrected by a tilt sensor measuring roll and pitch angles. Taking into account the *cos* and *sin* of these angles, a second matrix allows the transforming of velocities (V_x, V_y, and V_z) in current components (*U, V,* and *W*).

To improve measurement trueness, pulses are repeated at a frequency f_r. The maximum measurable speed V_{max} depends on f_r and on the wavelength λ:

$$\pm V_{\max} = f_r \, \lambda / 4 \tag{4.31}$$

Zedel and Hay [46] explain that "measurements can be made at a prescribed range by considering the time elapsed since a sound pulse is transmitted." It means that f_r determines the maximum profiling range $r_{\max}$, at which a target can be detected without ambiguity concerning its position:

$$r_{\max} = c / \left(2 f_r \right) \tag{4.32}$$

c is the speed of sound. Relationships (4.31) and (4.32) lead to express the range–velocity ambiguity relationship as follows:

$$V_{\max} r_{\max} = \pm c \lambda / 8 \tag{4.33}$$

To overcome the limits imposed by Eq. (4.33), various techniques have been developed, based on the processing of emitted and received signals. Thus, conventional profilers are called "incoherent" or "narrowband" because the received echoes from two different pulses are not correlated. Echoes are measured continuously, allowing the size of measurement cells in the water column to be determined, considering the value of c and the duration t_p of pulses. The lowest uncertainty that can be obtained for the measurements of (V_1, V_2, V_3) is limited by the standard deviation of the Doppler noise σ_δ, which is inversely proportional to t_p. This noise is generated by the random displacement of particles, the multiple echoes, and the detection limits of the instrument electronics. To decrease the uncertainty, it is necessary to multiply the number of pulses n. Another solution is to increase the value of t_p, but this leads to a reduction in spatial resolution.

In order to overcome this ambiguity, "pulse-to-pulse coherent" or "pulse coherent" profilers were created. Their measurement principle relies on series of coherent pulses coded in phase. In order to extract the signal from the noise, the autocovariance function $R(\tau)$ of these pulses is calculated. To improve the extraction, $R(\tau)$ is assessed from the reception of M sequences of two pulses and of the average of M functions $R(\tau)$. Most often, the average Doppler frequency characterizing the Doppler shift δf_i ($i \in \{1, 2, 3\}$) is extracted from the phase $\phi \in [-\pi, +\pi]$ of $R(\tau)$. If f_0 is the emitted frequency, the measured radial velocity is obtained by the relationship:

$$V_i = \pm \delta f_i \cdot c / \left(2 f_0\right) \tag{4.34}$$

According to the Teledyne RD Instrument technical note, if t_l is the time corresponding to pulses going there and back, we have $2\pi\delta f_i = \phi / t_l$. The expression of the velocity becomes:

$$V_i = \pm \phi c / \left(4\pi f_0 t_i\right) \tag{4.35}$$

4.4.3 Calibration Methods of Doppler Current Meters

Rotor current meters were calibrated in test open channels or hydrodynamic channels. In the case of open channels, the device under test (DUT) is fixed on a mobile trolley (see [47]). A speed sensor is mounted on the trolley and is used as a reference to control the speed of the trolley and to calibrate the current meters. If the DUT is a profiler, it can be used in both bottom-track or in water-track modes. In bottom-track, the velocity is obtained over the bed. It is representative of the trolley's speed.

Basin length and time needed to obtain a constant speed and to slow down limit the maximum rating carriage to a speed between 1 and 3 m/s.

In the case of hydrodynamic channels, DUT is in a static position and a turbine allows the variation of the water's circulation speed in the circular channel. A laser velocimeter or an electromagnetic flowmeter gives the reference speed (see [48]). These facilities present the advantage to test instruments in hydrodynamic conditions close to operating conditions, but with some differences, there is no turbulence, the backscatter material is artificial, the bed is smooth, and there are negligible or zero-velocity gradients in the sample volume.

Their measurement uncertainty is principally limited by the time during which the speed can be kept constant in order to be considered as a reference and by the reading uncertainty of the reference sensor. Acoustic reflections on bed and sidewall can also increase the measurement uncertainty of the DUT, and acoustic interferences can introduce negatives bias [49]. Because of these side effects, when deviations are calculated, it remains difficult to determine if they come from the instrument or from experimental bias. The direction of the DUT versus the flow can also cause measurement errors.

These facilities cannot be used for long-range profilers where the size of the first measurement cell is superior to the depth of the channel of water. Clearwater is also an obstacle to make measurements with low noise. Doppler current meters need particles to detect echoes. The lack of particles increases their measurement uncertainties. Lastly, these facilities do not allow the calibration of compass and tilt sensors. Magnetic interferences generally cause systematic errors on compass readings and cannot be used.

To overcome these problems, other methods have been developed where sensors are calibrated separately. According to ref. [50], a platform can be built to calibrate compass and tilt sensors of instruments mounted in mooring cages. Equipments of mooring cages (battery pack, acoustic release, ballast, etc.) can generate magnetic anomalies leading to compass errors in some directions. The platform must be built in an area where the terrestrial magnetic field has been mapped in order to ensure the absence of magnetic anomalies greater than 20 nT/m. The concrete block on which it is rotating can be graduated with a GPS technique in relation to the true north. Knowing the magnetic declination, it is possible to retrieve and correct the systematic errors of compasses. The platform can also be tilted to calibrate tilt sensors.

Another method has been set to calibrate current meters transducers. It is based on the measurement of pulses frequency emitted independently by each transducer of the instrument, and on the simulation of received echoes by a variable frequency sinusoidal signal [45]. The calibration consists in calculating a speed deviation δv such that:

$$V_{ref} - V_i = \frac{c}{2}\left(\frac{\delta f_{ref} - \delta f_i}{f_0}\right) \tag{4.36}$$

where δf_{ref} is the generated frequency shift and δf_i is extracted from relation (4.34).

References

1. BIPM (1989) The International Temperature Scale of 1990 (ITS-90), Procès-Verbaux du Comité International des Poids et Mesures, 78th meeting. https://www.bipm.org/en/committees/cc/cct/publications-cc.html
2. Preston-Thomas H (1990) The international temperature scale of 1990 (ITS-90). Metrologia 27(3):10
3. White DR, Fisher J (2015) The Boltzmann constant and the new kelvin. Metrologia 52:S213–S216
4. Consultative Committee for Thermometry (CCT) (2019) Mise en pratique for the definition of the kelvin in the SI, Version 2.0
5. BIPM 2010. Estimates of the differences between thermodynamic temperature and the ITS-90. https://www.bipm.org/utils/common/pdf/ITS-90/Estimates_Differences_T-T90 2010.pdf
6. Fischer J, de Podesta M, Hill KD, Moldover M, Pitre L, Rusby R, Steur P, Tamura O, White R, Wolber L (2011) Present estimates of the differences between. thermodynamic temperatures and the ITS-90. Int J Thermophys 32:12–25
7. Saunders PM, Mahrt KH, Williams RT (1991) Standards and laboratory calibration, WHP Operations and Methods
8. Joyce TM (1991) WHP operations and methods. Introduction to the collection of expert reports compiled for the WHP Programme
9. Stephens GL et al (2012) An update on Earth's energy balance in light of the latest global observations. Nat Geosci 5:691–696
10. Wunsch C (2016) Global Ocean integrals and means, with trend implications. Annu Rev Mar Sci 8:1–33. https://doi.org/10.1146/annurev-marine-122414-034040
11. Liu G, Guo L, Liu C, Wu Q (2018) Evaluation of different calibration equations for NTC thermistor applied to high-precision temperature measurement. Measurement 120:21–27. https://doi.org/10.1016/j.measurement.2018.02.007
12. Ushida H et al (2007) In situ calibration of the SeaBird 9plus CTD thermometer. J Atm Ocean Tech 24:11. https://doi.org/10.1175/JTECH2093.1
13. de Podesta M, Bell S, Underwood R (2018) Air temperature sensors: dependence of radiative errors on sensor diameter in precision metrology and meteorology. Metrologia 55:229–244. https://doi.org/10.1088/1681-7575/aaaa52
14. Le Menn M, Poli P, David A, Sagot J, Lucas M, O'Carroll A, Belbeoch M, Herklotz K (2019) Development of surface drifting buoys for fiducial reference measurements of sea-surface temperature. Front Mar Sci 6:578. https://doi.org/10.3389/fmars.2019.00578
15. Larson N, Pedersen AM (1996) Proceeding of the 1st IGHEM meeting, Montreal, Sea Bird Electronics, Inc.
16. Le Menn M, Albo PAG, Lago S, Romeo R, Sparasci F (2019) The absolute salinity of seawater and its measurands. Metrologia 56:1. https://doi.org/10.1088/1681-7575/aaea92
17. Millero FJ, Feistel R, Wright DG, MacDougall TJ (2008) The composition of standard seawater and the definition of the reference – composition salinity scale. Deep-Sea Res 55:10–72. https://doi.org/10.1016/j.dsr.2007.10.001
18. Forchhammer G (1865) On the composition of seawater in different parts of the ocean. Philos Trans R Soc London 155:203–262
19. Dittmar W (1884) Physics and chemistry. Rept Scient Res HMS Challenger, 1873-76 1:251
20. Cox CA (1963) The salinity problem. Prog Oceanogr 1:243–261
21. Shkvorets I (2020). https://salinometry.com/implementation-of-the-electrical-conductivity-of-seawater/
22. UNESCO (1981) Background papers and supporting data on the practical salinity scale of 1978. UNESCO Technical Papers in Marine Science 37:144
23. Perkin RG, Lewis EL (1980) The practical salinity scale of 1978: fitting the data. IEEE J Oceanic Eng 5(1):9–16

24. UNESCO (1983) Algorithm for computation of fundamental properties of seawater. UNESCO Technical Papers in Marine Sciences 36:36
25. Culkin F, Smith ND (1980) Determination of the concentration of potassium chloride solution having the same electrical conductivity at 15 °C and infinite frequency, as standard seawater of salinity 35,000 ‰ (chlorinity 19,37394 ‰). IEEE J Ocean Eng 5(1):22–23
26. Seitz S, Spitzer P, Brown RJC (2010) CCQM-P111 study on traceable determination of practical salinity and mass fraction of major seawater components. Accred Qual Assur 15:9–17
27. Zalatarevich A, Olga S, Lopez AR, Sanchez JL, Jakobsen PT, Avnskjold J, Jensen HD, Kozlowski W, Dumańska-Kulpa J, Gonzaga FB (2014) Final report of key comparison CCQM - K105 'Electrolytic conductivity at 5.3 $S \cdot m^{-1}$. Metrologia 5:51
28. Le Menn M (2011) About uncertainties in practical salinity calculations. Ocean Sci 7:1–9. https://doi.org/10.5194/os-7-651-2011
29. Seitz S, Feistel R, Wright DG, Weinreben S, Spitzer P, de Bièvre P (2011) Metrological traceability of oceanographic salinity measurement results. Ocean Sci 7:45–62. https://doi.org/10.5194/os-7-45-2011
30. Fofonoff NP, Millard RC (1991) Calculation of physical properties of seawater, WHP Operations and Methods
31. IOC, SCOR and IAPSO (2010) The international thermodynamic equation of seawater—2010: calculation and use of thermodynamic properties. Intergovernmental Oceanographic Commission, UNESCO, Paris, p 196
32. McDougall TJ, Jackett DR, Millero JF, Pawlowicz R, Barker PM (2012) A global algorithm for estimating absolute salinity. Ocean Sci 8:1123–1134
33. Striggow K, Dankert R (1985) The exact theory of inductive conductivity sensors for oceanographic application. IEEE Journal of Oceanic Engineering 10:2
34. Lueck RG, Picklo JJ (1990) Thermal inertia of conductivity cells: observations with a sea-bird cell. J Atmos Ocean Technol 7:756–768
35. Mensah V, Le Menn M, Morel Y (2009) Thermal mass correction for the evaluation of salinity. J Atmos Ocean Technol 26(3):665–672
36. Johnson GC, Toole JM, Larson NG (2007) Sensor correction for sea-bird SBE 41CP and SBE 41 CTDs. J Atmos Ocean Technol 24:1117–1130
37. Millard RC, Seaver G (1990) An index of refraction algorithm for seawater over temperature, pressure, salinity, density and wavelength. Deep-Sea Res 37(12):1909–1926. https://doi.org/10.1016/0198-0149(90)90086-B
38. Le Menn M, Bougrenet de la Tocnaye JL, Grosso P, Delauney L, Podeur C, Brault P, Guillerme O (2011) Advances in measuring ocean salinity with an optical sensor. Meas Sci Technol 22:8. https://doi.org/10.1088/0957-0233/22/11/115202
39. Uchida H, Yohei K, Maeda Y (2019) Ultra high-resolution seawater density sensor based on a refractive index measurement using the spectroscopic interference method. Nat Sci Rep 9(1):1–8
40. Balavalad KB, Sheeparamatti BG (2015) A critical review of MEMS capacitive pressure sensors. Sensors & Transducers 187(4):120–128
41. Druck, RPS/DPS 8000. High accuracy resonant pressure sensor. https://www.bakerhughesds.com/search?search=DPS8000
42. Polster A, Fabian M, Villinger H (2009) Effective resolution and drift of paroscientific pressure sensors derived from long-term seafloor measurements. Geochem Geophys Geosyst 10:9. https://doi.org/10.1029/2009GC002532
43. Paros JM, Kobayashi T (2009) Mathematical models of quartz sensor stability, Paroscientific, Inc. & quartz seismic sensors, technical note doc. No. G8095 rev. E. http://www.paroscientific.com/pdf/G8095_Mathematical_Models.pdf
44. Budenberg DH (2010) 5200 series user manual, version 07
45. Le Menn M, Morvan S (2020) Velocity calibration of Doppler current profiler transducers. J. Mar. Sci. Eng 8:847. https://doi.org/10.3390/jmse8110847

46. Zedel L, Hay AE (2010) Resolving velocity ambiguity in multifrequency, pulse-to-pulse coherent Doppler sonar. J Atmos Ocean Technol 35:847–851. https://doi.org/10.1109/JOE.2010.2066710
47. International Organization for Standardization (ISO) (2007) Hydrometry—calibration of current meters in straight open tanks, ISO 3455. ISO, Geneva
48. Camnasio E, Orsi E (2011) Calibration method of current meters. J Hydraul Eng 137:386–392. https://doi.org/10.1061/(ASCE)HY.1943-7900.0000311
49. Oberg KA, Mueller DS (2007) Validation of streamflow measurements made with acoustic Doppler current profilers. J Hydraul Eng 133(12):1421–1432
50. Le Menn M, Lusven A, Bongiovanni E, Le Dû P, Rouxel D, Lucas S, Pacaud L (2014) Current profilers and currentmeters compass and tilt sensors errors and calibration. Meas Sci Technol 25:085801. https://doi.org/10.1088/0957-0233/25/8/085801

Chapter 5
Metrology for the Sea: Chemical Quantities

Nineta Hrastelj

Contents

Abstract The chapter »Metrology for the Sea: Chemical Quantities gives an overview of the foundation for measurements in the chemical sciences and in particular those related to the sea. In this context, traceability, validation, and measurement uncertainty are explained, in addition to sampling and quality aspects. An overview of interconnected worlds of the chemical sciences, metrology, policy, standardization, accreditation, and science communication at national, regional, and global levels is provided. How measurements in chemical sciences work on examples that people can relate to, such as quality of bathing waters, classification of olive oils, accumulation of ^{210}Po in coastal waters, and in fish tissue in the Gulf of Trieste is demonstrated. Finally, the difference between a research and an accredited testing laboratory is described and the importance of discourse in a decision-making process is briefly explained.

N. Hrastelj (✉)
The European Chemical Society (EuChemS), Brussels, Belgium

P. Daponte et al. (eds.), *Measurement for the Sea*, Springer Series in Measurement Science and Technology,
https://doi.org/10.1007/978-3-030-82024-4_5

5.1 Measuring in the Chemical Sciences

Welcome to gripping science of measurements (metrology) in the field of chemical sciences and its applications. Let us start at the beginning, by setting the scene and getting familiar with the cornerstones on which the entire system for measurements in the chemical sciences is built. In order to do so, we have to look at some of internationally agreed definitions published in the *International Vocabulary of Metrology—Basic and General Concepts and Associated Terms* (VIM) [1] and the *Compendium of Chemical Terminology, the IUPAC Gold Book* [2].

5.1.1 Definitions Are Not Boring, but Highly Exciting

Do you know that agreeing on international definitions is a thrilling lengthy process? Even when those definitions get officially approved, some of them may have different interpretations. Additional notes, guidelines, and examples are thus developed to get them consistently implemented in real life.

For thorough understanding of measurement science, one needs to understand not only individual definitions, but also their relationships. The aim of this chapter is to help you to accomplish the necessary fundamental knowledge on which measurement science is built by going through key definitions and describing, step-by-step, their relationships, illustrated by examples and anecdotes.

Metrology [VIM3] 2.2
science of measurement and its application.
Measurement [VIM3] 2.1
process of experimentally obtaining one or more quantity values that can reasonably be attributed to a quantity

Before starting any measurement, one shall carefully think about the following questions:
What is the *quantity* in my case?
What is the *analyte*?
What is the *measurand*?
What is the *measurement unit* in which the measurement result will be expressed?
What is the *measurement scale* in my case?
What is the *measurement result*?

Let us first have a look at some more definitions and their applications.

Quantity [VIM 3] 1.1

property of a phenomenon, body, or substance, where the property has a magnitude that can be expressed as a number and a reference.

Analyte

In chemistry, "analyte" is the name of a substance or compound, which is sometimes erroneous used for "measurand."

Measurand [VIM3] 2.3

quantity intended to be measured.

Measurement unit [VIM3] 1.9

real scalar quantity, defined and adopted by convention, with which any other quantity of the same kind can be compared to express the ratio of the two quantities as a number.

Measurement scale [VIM3] 1.27

ordered set of quantity values of quantities of a given kind of quantity used in ranking, according to magnitude and quantities of that kind.

Measurement result [VIM3] 2.9

set of quantity values being attributed to a measurand together with any other available relevant information.

NOTE 2 A measurement result is generally expressed as a single measured quantity value and a measurement uncertainty.

Defining the measurand

Do you know that some measurands are operationally defined?
Find the definition of »operationally defined measurand« online and think of an example; they are plenty.

We are now ready to dive deeper into *quantity* and *measurement unit* related aspects and have a closer look at the *amount of substance* and *mole*.

The *amount of substance* is one of seven *base quantities* of the International System of Quantities (ISQ), the others being length, mass, time, electric current, thermodynamic temperature, and luminous intensity. It is the youngest of the seven base quantities.

The International System of Units (SI), which is based on the International System of Quantities, therefore includes one base unit related to measurements in Chemistry, namely *the mole*.

The mole

The mole, symbol mol, is the SI unit of amount of substance. One mole contains exactly 6,022,140 76 x $x10^{23}$ elementary entities. This number is the fixed numerical value of the Avogadro constant, N_A, when expressed in the unit mol^{-1}, and is called the Avogadro number.

The amount of substance, symbol *n*, of a system is a measure of the number of specified elementary entities. An elementary entity maybe an atom, a molecule, an ion, an electron, any other particle or specified group of particles [2].

Note: The formulation of this definition was agreed upon by the 26th CGPM in November 2018 with effect from May 20, 2019.

How old is the mole? Still very young!

The development of the concept of amount of substance was coincidental with, and vital to, the birth of modern chemistry. By the turn of the twentieth century, the concept of atomic and molecular entities was generally accepted, but many questions remained, for example, the size of atoms and their number in a given sample. The concurrent development of mass spectrometry, starting in 1886, supported the concept of atomic and molecular mass and provided a tool of direct relative measurement. Here are the historical milestones:

1893 First recorded use of the term *mole* to describe a unit of amount of substance by Ostwald in a university textbook.
1959/1960 Unified atomic mass unit scale based on 12C = 12 adopted by IUPAP and IUPAC.
1968 The mole is recommended for inclusion in the International System of Units (SI) by the International Committee for Weights and Measures (CIPM).
1972 The mole is approved as the SI base unit of amount of substance.
2019 The mole is redefined in the SI as "the amount of substance of a system that contains $6.02214076 \times 10^{23}$ specified elementary entities" (the Avogadro constant N_A). This redefinition was part of the landmark decision made at the twenty-sixth meeting of the General Conference on Weights and Measures (CGPM). The landmark decision means that from May 20, 2019, *all SI units are defined in terms of constants that describe the natural world*. This was a somewhat disruptive birth of new scientific models, which are not yet finished.

However, in addition to the basic quantities, there are other *derived quantities* that apply to measurements in the chemical sciences. Some examples are given in the Table 5.1.

According to Ref. [4], the concept of the *amount of substance* underpins much of chemistry, yet remains challenging to many students and teachers. Successful application of the concept depends on the ability to move seamlessly between macroscopic, microscopic, and symbolic levels of representation. The use of terminology also presents an obstacle to many students embarking on chemistry studies. This confirms the importance of internationally accepted definitions and basic terms,

Table 5.1 Some examples of quantity–analyte–measurand–unit–measurement scale in the chemical sciences (modified, first published in Ref. [3])

Quantity	Analyte	Measurand	Unit	Measurement scale
Mass fraction w	DDT	w(DDT) in soil	ng kg^{-1}	SI
Mass concentration ɣ	Pb	ɣ(Pb) in wastewater	ng L^{-1}	SI
pH	H_30^+ ions	a(H_3O^+) in freshwater	pH unit	pH scale
Octane rating	Antiknocking behavior	Research octane number	RON	Octane number scale
Enzyme activity	Amylase	A(amylase)	Kat (Katal) $mols^{-1}$	SI

together with consistent implementation. To successfully implement internationally agreed definitions, close collaboration between those involved in decision making, researchers, and experts in the field is essential from an early stage.

Emergency plane landing
In 1983, Canada was in the process of switching from imperial units to metric units. A new Air Canada plane used metric units only; the crew and the airport were more used to imperial.

In calculating how much fuel was required, the units were mixed up and the calculations were done in pounds (lb) instead of kilograms (kg). As there are 2.2 lb to kg, this meant that the plane had half as much fuel as the pilot thought that it did. When the fuel ran out halfway through the flight, the pilot had to land the plane on an abandoned air base. Surprisingly, the only injuries were sustained when passengers were leaving the plane.

5.1.2 From Sampling to Measurement

To do any measurement in the chemical sciences correctly, one needs to be knowledgeable and consider all the following aspects:

- Sampling
- Metrological traceability
- Validation of analytical (measurement) procedure
- Measurement uncertainty
- Quality measures (internal quality control and external quality measures)
- Reporting of measurement result

All measurements start with a sampling as the first step. Depending on the request, the corresponding measurement result can refer to the sample or to the bulk from which the sample has been taken.

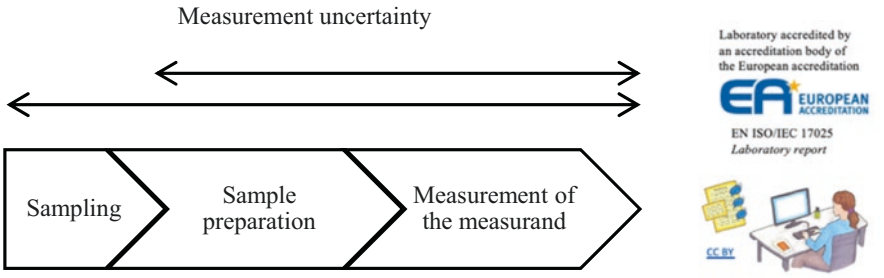

Fig. 5.1 Steps of an analytical (measurement) procedure in the chemical sciences. An analytical procedure includes measurements of different quantities. All of them should be done according to the best measurement practices. Each measurement result is associated with measurement uncertainty and is reported together with the measurement unit. When the measurement result is reported for the bulk and not only for the sample in the laboratory, then measurement uncertainty for sampling should be taken into account as well

Measurement procedure [VIM3] 2.6
detailed description of a measurement according to one or more measurement principles and to a given measurement method, based on a measurement model and including any calculation to obtain a measurement result.

In the chemical sciences, science of measurement goes beyond traceability, calibration and reference values, which are traditionally the core of metrology for physical measurements. In the chemical sciences, we rarely, if ever, deal with measurement of only one quantity.

Each measurement (analytical) procedure has the following key steps (Fig. 5.1):

- Sampling
- Sample preparation
- Measurement of the measurand

Each of the above three steps is a complex interdisciplinary/multidisciplinary subject. In order to take a representative sample, knowledge of (bio)chemistry is important when it comes to stability of e.g., a water sample. Also, volume, mass, or flow measurements shall typically be done during sampling phase.

The sample preparation phase is the one which is covered by what is known as analytical chemistry: it requires a thorough knowledge of chemistry as well as laboratory skills. It also includes measurements of various quantities such as mass (of the sample), volume (e.g., pipetting), concentration of extraction reagents, and temperature (e.g., dry matter, melt).

Measurement of the measurand is the last step of a measurement procedure done in a laboratory. Typically, it includes preparation of calibration standards and calibration of a measuring instrument prior to measuring the measuring in the sample.

Eq. (5.1) describes a measurement process in mathematical language:

$$\text{Measurement result} = \int_{\text{sampling}}^{\text{measurement}} x dx = \tag{5.1}$$

$$\left(\text{measured value} \pm \text{measurement uncertainty}\right)\text{measurement unit}$$

5.1.3 Calibration and Metrological Traceability

A measurement implies comparison of quantities or counting of entities. For any comparison, one needs a reference. If a reference is not the same for two or more measurement results, any comparison is, of course, meaningless.

Metrological traceability[1] [VIM3] 2.41
property of a measurement result whereby the result can be related to a reference through a documented unbroken chain of calibrations, each contributing to the measurement uncertainty
Calibration [VIM3] 2.39
operation that, under specified conditions, in a first step, establishes a relation between the quantity values with measurement uncertainties provided by measurement standards and corresponding indications with associated measurement uncertainties and, in a second step, uses this information to establish a relation for obtaining a measurement result from an indication.

As explained earlier, in the chemical sciences, we are dealing with measurements with more than one input quantity in the measurement model. For each and all input quantities, values should itself be metrologically traceable. The calibration hierarchy involved may form a branched structure or a network. The effort involved in establishing metrological traceability for each input quantity value should be commensurate with its relative contribution to the measurement result.

[1] The abbreviated term "traceability" is sometimes used to mean "metrological traceability" as well as other concepts, such as "sample traceability" or "document traceability" or "instrument traceability" or "material traceability," where the history ("trace") of an item is meant. Therefore, the full term of "metrological traceability" is preferred if there is any risk of confusion.

A measurement: a concert

Have you ever paid attention to tuning of an orchestra on stage, just before a concert starts? I am still fascinated by it, and throughout years of enjoying concerts I have drawn parallels between tuning of the orchestra and calibration in the chemical and physical sciences. I published my observation in "A measurement: a concert" in 2009 [5], and I invite you to read an updated version of it below.

It is the oboist who gives a tone with a specific frequency to all others in the orchestra (strings, wind, and brass instruments). This frequency is always a middle A, but can be geographically slightly different; e.g., it is 440 Hz in the USA and 443 Hz in Europe. The frequency of the middle A has risen throughout the centuries. For instance, in the Baroque period, 1700s, the middle A was 438 Hz, but what matters is that the entire orchestra is tuned to the same frequency regardless how much exactly this is. The orchestra makes the unorganized sound on the stage until they get tuned.

However, there is one instrument which does not get tuned by the musician just before a concert. Do you know which one? This instrument gets tuned well before the concert, when nobody is in the concert hall yet, by a professional tuner. Yes, this is the piano.

And how does all this relate to calibrations?

The piano tuning is how calibrations are done for physical quantities (mass, volume, temperature, etc.); e.g., an expert from an accredited calibration laboratory comes to calibrate the balance, which you then use for mass measurements.

On the contrary, it is an analytical chemist who calibrates a spectrophotometer *each time just before* doing a measurement, which is the same as tuning all other instruments on stage just before the concert starts.

Now, we have all the instruments calibrated, musicians seated, lights are on, and it is time for the conductor to enter the stage. Here he/she comes! And what is her/his role now? Well, if the dress rehearsal (validation of a measurement procedure) went well, it is very likely the concert is going to be a great success. Keep reading.

Having it by now all theoretically clear, let us try to implement it in an actual measurement procedure in a laboratory. The question is the following: How to tune all these different input quantities, as well as other parameters that are part of a measurement procedure, in such a way that we get a measurement result which is adequate for a given purpose? Find the answer in the concert anecdote.

As with most things, establishing metrological traceability is easier to do theoretically than in practice. Ideally, it starts with an internationally recognized Calibration and Measurement Capability (CMC). CMCs can be found in the Key Comparison Database (KCDB) which is freely available Web resource related to the Mutual Recognition Arrangement of the International Committee for Weights and

Table 5.2 Excerpt from the KCDB on CMCs related to the sea

Meas. serv. category	Meas. serv. subcategory	Matrix	Analyte or component	Quantity
Food	Contaminants	Seafood	Cadmium	Mass fraction
Food	Nutritional constituents	Seafood	Iron, zinc	Mass fraction
Food	Contaminants	Fish oil	p,p'-DDT, gamma-HCH, p,p'-DDE, alpha-HCH, trans-nonachlor, beta-HCH, hexachlorobenzene, aldrin, heptachlor epoxide, gamma-chlordane, beta-chlordane, endrin, dieldrin, p,p'-DDD, mirex, cis-nonachlor	Mass fraction
Food	Contaminants	Olive oil	Benz(a)anthracene, chrysene, benzo(b) fluoranthene, benzo(a)pyrene	Mass fraction
Water	Seawater	Seawater	Arsenic, cadmium, cobalt, chromium, copper, iron, mercury, manganese, nickel, lead, selenium, vanadium, sodium, magnesium, strontium, chloride, and sulfate	Mass fraction

Measures (CIPM MRA). The CIPM MRA is the framework through which National Metrology Institutes demonstrate the international equivalence of their measurement standards and mutual acceptance of the calibration and measurement certificates they issue. The comparison and CMC data in the KCDB have been approved through a peer-review process within the CIPM MRA. The KCDB provides users with reliable quantitative information on the comparability of national metrology services and provides the technical basis for wider agreements negotiated for international trade, commerce, and regulatory affairs. In Table 5.2, extract from the KCDB is given on sea-related matrices (Ref. [6], as on September 26, 2020).

In the chemical sciences, a reference value is most often carried by a reference material, more precisely, by a certified reference material (CRM). A certified reference material is accompanied by a certificate, which shall include all relevant information, such as how traceability of the reference value was assured, measurement uncertainty, homogeneity, stability, etc.. Ideally, a CRM is produced by an accredited reference material producer (EN ISO/IEC 17034, General requirements for the competence of reference material producers).

5.1.4 Validation of Analytical (Measurement) Procedure

Let us now proceed to the dress rehearsal, i.e., validation of an analytical (measurement) procedure.

Validation [VIM3] 2.45
verification, where the specified requirements are adequate for an intended use

Regardless whether you are developing your own measurement procedure or you are about to use a standardized procedure, before releasing any measurement result, one shall validate the procedure, i.e., confirm that it works in your laboratory and that it is fit for the intended use. This is a rather straightforward thing to do; one needs to apply the following steps:

1. Define a measurand.
2. Select a measurement (analytical) procedure.
3. Depending on the type of the measurement (analytical) procedure, decide on the degree of validation. The degree of validation depends on whether you are using a standardized procedure (e.g., ISO, EN) or not. In the first case, a simple confirmation that it works in your laboratory is sufficient, else a more thorough validation is needed.
4. Draft a list with all characteristics of (1) an analytical (measurement) procedure and of (2) a measurement result; these are the same for all procedures, e.g., limit of detection (LOD), sensitivity, and linearity, while traceability and measurement uncertainty are characteristics of a measurement result, not of a procedure.
5. Think critically which ones from the list are important in your particular case.
6. Define the expected values for the selected characteristics, or apply the ones defined in legislation, or other specifications, when this is the case. The requested (maximum or minimum) values for the selected characteristics of your measurement (analytical) procedure and the measurement result are typically set by the customer, but not also necessarily for research purposes. The customer's requirements are usually set either in legislation or in a product's specification (see below example on olives).
7. Perform a measurement according to the procedure and use the experimental data for calculations for the selected characteristics; once you have done the evaluation of the selected characteristics in your laboratory, compare them with the expected (requested) values.
8. Release a statement (report) about suitability of the procedure in your laboratory for the intended use (fit for purpose).

Measurements of pesticides in olives

A *pesticide* is something that prevents, destroys, or controls a harmful organism ("pest") or disease or protects plants or plant products during production, storage, and transport. The traces pesticides leave in treated products are called *residues*. A maximum residue level (MRL) is the highest level of a pesticide residue that is legally tolerated in or on food or feed when pesticides are applied correctly (good agricultural practice). One such example is a legislation for MRL for pesticides in olives.

Which steps a laboratory has to take in this case before starting measurements of pesticides in olive samples?

First, a laboratory has to decide which analytical (measurement) procedure they will use for measuring pesticides in olives. In some cases, the method and/or the procedure can be prescribed by the legislation.

The laboratory then has to validate its analytical procedure. In this case, the following parameters of the chosen analytical procedure are especially important: (1) limit of detection (LOD), (2) limit of quantitation (LOQ), and (3) linearity up to max 500 μg kg^{-1}.

Once the laboratory has their own experimental data for these parameters, the experimentally obtained LODs and LOQs are compared with MRL stated in the legislation for a particular pesticide. If MRL is higher, then one can claim that this analytical procedure is fit for purpose. When this is the case, the laboratory can proceed with measurements of the pesticides in samples.

Tuna fish and heavy metals

About two decades ago, I was the Slovenian national contact point for a European interlaboratory comparison on heavy metals in tuna fish samples. Each participating laboratory has received few grams of tuna fish to measure mass fraction of heavy metals in the samples. Tuna fish samples were sent from Belgium to laboratories all around Europe and shall be kept at low temperature until analyzed. However, I faced a challenge explaining to the custom officers why few grams of tuna fish have arrived to Slovenia as well as why they have to urgently put them in refrigerator, until laboratory representatives come and pick them. I had to make lots of phone calls on this particular day to get it done properly by the Slovenian customs. I was so concerned that measurement results in Slovenian laboratories will go wrong due to inappropriate sample handling at customs that I vividly explained my scientific frustration at home. Since then, my daughters keep reminding me about few grams of tuna fish, as they found the situation entertaining.

To summarize a dress rehearsal (i.e., validation of an analytical procedure) in a simplified way, one should try a new recipe at home first, before preparing it for a gala dinner.

Never forget that important decisions are made based on laboratory results. If measurement results are not reliable, wrong decisions with wide societal implications can be taken.

5.1.5 Measurement Uncertainty

There is one thing left to do before we can eventually report our measurement result, i.e., the evaluation of measurement uncertainty. Regardless which approach to measurement uncertainty evaluation one applies, measurement evaluation process goes through the following steps:

1. Specifying the measurand[2]
2. Specifying the measurement procedure and model function
3. Identifying the sources of uncertainty
4. Quantifying the uncertainty components
5. Calculating the combined standard uncertainty
6. Calculating the expanded uncertainty
7. Examining the uncertainty budget

Depending on data one has and on the intended use of the measurement result, one can choose from the following three approaches for the evaluation of measurement uncertainty:

- Model approach: It gives measurement uncertainty of an individual result of a measurement for a measurement procedure in the laboratory.
- Validation and internal quality control data approach: This one is applied when using validation data and data from internal quality control from the laboratory for measurement uncertainty evaluation; one gets typical uncertainty of results obtained by this particular measurement procedure in this laboratory.
- Interlaboratory comparison data approach: When using data from interlaboratory comparison for measurement uncertainty evaluation, evaluated uncertainty gives an indication for the same measurement procedure in different laboratories.

Clearly, measurement uncertainties for the same result obtained by different approaches differ, as they do not apply to the same measurement conditions.

Inevitably, the evaluation of measurement uncertainty requires some mathematical knowledge. Let us have a look at simple examples of its application.

In general, measurements uncertainties can be acquired by a statistical analysis of measured quantity values obtained under defined measurement conditions (type A uncertainty) or by other means (type B uncertainty). A typical example of the latter is data from calibration certificates or other literature data.

In the chemical sciences, a typical model equation looks as follows:

$$Y = k * x_a / x_b \tag{5.2}$$

where Y is concentration (g mL^{-1}), k stoichiometric factor, x_a mass, and x_b volume. For any such equation, measurement uncertainty is calculated through corresponding relative standard uncertainties:

[2]You will recall that the first and the second steps have already been done at the very beginning, before starting an actual measurement; however, they are listed here for the sake of completness.

$$\frac{u(Y)}{Y} = \sqrt{\left(\frac{u(x_a)}{x_a}\right)^2 + \left(\frac{u(x_b)}{x_b}\right)^2} \tag{5.3}$$

When applying the validation approach for measurement uncertainty evaluation, the following equation applies:

$$u = \sqrt{u(\text{bias})^2 + u(R)^2} \tag{5.4}$$

where R is within laboratory reproducibility and u combined standard uncertainty. In some cases target measurement uncertainties (TMU) are defined. For those interested in more details on this aspect, see [7].

Target measurement uncertainty [VIM3] 2.34
measurement uncertainty specified as an upper limit and decided on the basis of the intended use of measurement results.

5.1.6 Reporting Measurement Result

Reporting measurement result may sound trivial, but it is a quick indicator of a laboratory's competence: If the measurement result is not reported correctly, one can have justifiable doubts about the overall knowledge of measurement science in this particular laboratory. The rules that shall be applied when reporting a measurement result are the following:

- The expanded measurement uncertainty (U) shall be reported with maximum two significant figures following adequate rounding number rules.
- The measured quantity value shall be reported with the same number of decimal places as reported measurement uncertainty.
- The units, coverage factor, and confidence level shall also be clearly reported.

For c(Y) = 19.63 mg L^{-1} and U(Y) = 1.23 mg L^{-1},
the result shall be reported as
(19.6 ± 1.2) mg L^{-1} k = 2 (for a confidence level of approximately 95%)

5.1.7 Errors

To complete this short overview on basics of measurements in the chemical sciences, relationship between errors and measurement uncertainty shall also be explained. Both types of errors, systematic and random, are embraced in the process of measurement uncertainty evaluation; however, this shall not be mistakenly related to type A and type B evaluation of measurement uncertainty. While distinguishing

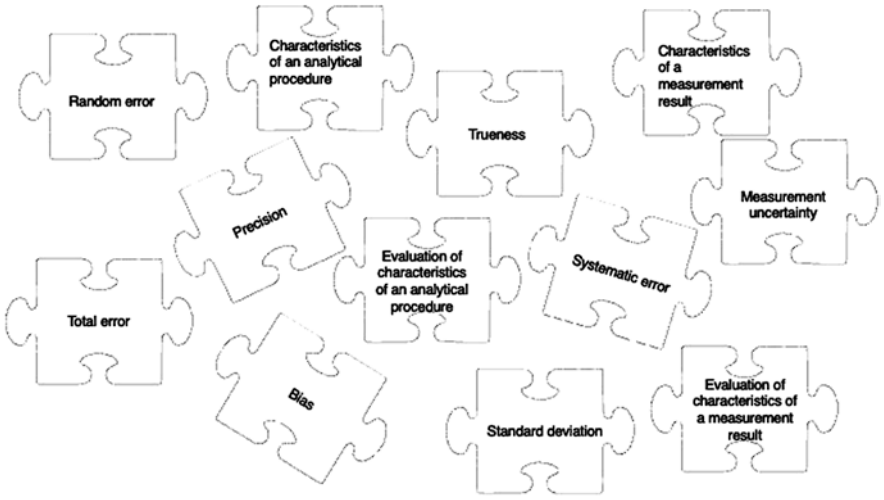

Fig. 5.2 Thorough understanding of errors, characteristics of an analytical procedure and of measurement results as well as of their quantitative evaluation, together with relationships/interconnections among them is the key for getting the measurement framework correct.

between random error and systematic error is relevant for (measurement) scientists and experts, this is not the case for users of measurement results. For the latter, it is measurement uncertainty that should be of their interest. It is of course a matter of their, i.e., end users of measurement results/laboratory customers' knowledge to understand measurement uncertainty to sufficient degree. It is, however, up to experts to make an effort to help their customers properly understanding measurement results. This brings us already to the role of science communication, which is becoming increasingly important (Fig. 5.2).

Now, we have validated our measurement procedure, evaluated measurement uncertainty, and reported the measurement result. But how do we know that when we measure other samples in the coming days, weeks, and months, all remains to be well in place? And how well do our results compare to other laboratories? For this, additional quality tools are in place. Most commonly used ones are known as *internal quality control* and *interlaboratory comparisons*. Furthermore, implemented *quality management system* and *third-party assessment* (accreditation) have an important role too. This interconnected multidimensional landscape which I have described in my article [8] as »jungle of pyramids with here and there a horizontal social network, when it comes to communication" is briefly addressed in the next section.

5.2 Quality Criteria for the Seawater and Seafood

We are now going to leave the world of science for a while and make a short visit to the policymaker landscape, where, legislation is discussed, set and decided. Once approved, it shall be implemented. The policy world is different than science

landscape in many respects, which does not make collaboration between scientists and policy makers easy. Due to such intrinsic differences between both worlds, the key prerequisite for a successful collaboration is learning each other's "language" and developing a respectful and trustworthy communication. All parties in such dialogue should listen, hear, and understand each other and aim to find optimal solutions for society, powered by science.

In the European Union, most of the technical legislation is prepared and approved at the European level and then implemented at the national level. For scientists, it is important to have basic knowledge of EU legislative process in order to provide timely input. For a sneak peek on how the ordinary legislative process works, you might want to consult the following short video available on this link https://www.consilium.europa.eu/en/council-eu/decision-making/ordinary-legislative-procedure/. There is plenty of information on the EU legislative process available online; one simplified graphics is shown in Fig. 5.3.

When it comes to the sea-related legislation, one may typically think of those on quality of seawater and quality of food, while there are also many others related to trade. Let us examine a few scenarios.

You might be heading on holidays and are wondering about the quality of the bathing water across Europe. To allow Europeans to make informed decisions on where to go to best enjoy Europe's inland and coastal bathing sites, an annual assessment briefing has been prepared by the European Environment Agency (EEA) in cooperation with the European Commission's DG Environment. You can find the annual reports on this link http://ec.europa.eu/environment/water/water-bathing/index_en.html or check an interactive map https://eea.maps.arcgis.com/apps/ops-dashboard/index.html#/f9cecd95b1b44c88ac6ed3a9dc4d51b2

Criteria for assigning a certain quality label to the particular seawater bathing site are set in the Bathing Water Directive (BWD). In the BWD, you will read that the bathing waters shall be inspected visually for pollution such as tarry residues, glass, plastic, rubber, or any other waste, in addition to two parameters which shall be measured, namely intestinal enterococci and Escherichia coli. For both parameters, the BWD states that the measurements shall be done according to international standards (ISO).

Once you have chosen your favorite beach, you surely want to order some high-quality seafood. What does EU say and do on food quality?

The European Union (EU) is by far the world's biggest importer of fish and other seafood and aquaculture products. Import rules for these products are harmonized, meaning that the same rules apply in all EU countries. On behalf of all EU member

Fig. 5.3 Ordinary EU legislative process

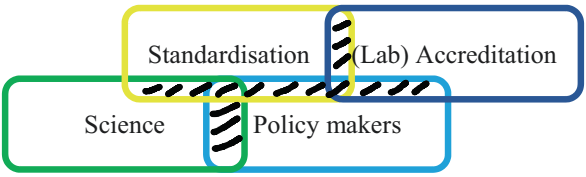

Fig. 5.4 Simplified sketch of interaction between science, policy, standardization, and accreditation. Importance of scientific advice to policymakers is emphasized nowadays; however, it is often just a one-way communication, i.e., from researchers to policymakers. A transparent feedback to experts would increase trust of citizens in policymakers as well as improve the final outcome through several iterations in a consultation process.

states, the European Commission is the sole negotiating partner for all non-EU countries in questions related to import conditions for seafood and fishery products.

The European Commission's Directorate-General for Health and Food Safety establishes import conditions for fishery products and shellfish (bivalve molluscs). By following these rules, non-EU countries can guarantee that their exports of such products fulfill the same high standards as products from the EU member states—not only with respect to hygiene and consumer safety but, if relevant, also to their animal health status.

Non-EU countries which are interested in exporting seafood and seafood products to the EU must be aware of the fundamental principles and philosophy of European food law, which forms the basis for the EU import conditions.

In the case of aquaculture products, a residue monitoring plan which includes testing for residues of veterinary drugs, pesticides, heavy metals, and contaminants must be in place to verify compliance with EU requirements. The plan (and results from the previous year's monitoring) must be submitted to the European Commission annually for approval.

Clearly, science and policy go hand in hand, intervening with standardization and accreditation (Fig. 5.4). In these intervened interactions, science communication between experts, citizens, and policymakers has an important role.

In such demanding and diverse communication process, a discourse as a communication action is a key to get an optimal output from the processes. A proper professional discourse is shown in Fig. 5.5. It tells us that in general, we can never conclude what we should do if there is no ought premise.

Translations

Have you ever thought that an official translation of a piece of European legislation can go wrong? Here is one such example:

"Commission Implementing Regulation (EU) No 661/2012 of July 19, 2012, correcting the Slovenian version of Commission Regulation (EEC) No 2568/91 on the characteristics of olive oil and olive-residue oil and on the relevant methods of analysis https://eur-lex.europa.eu/legal-content/EN/TXT/?uri=celex:32012R0661

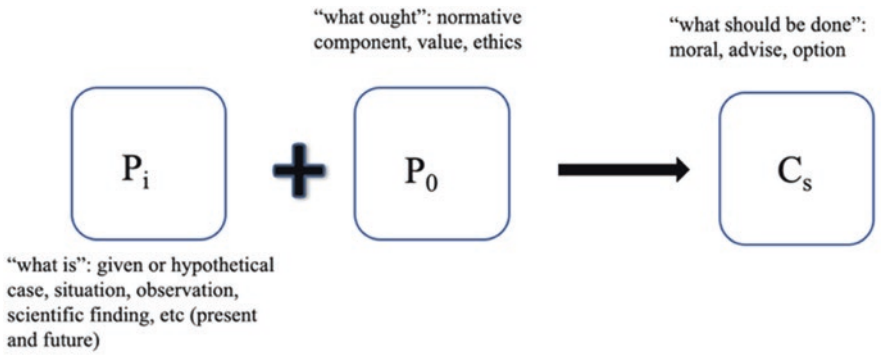

Fig. 5.5 Professional discourse [9]

The European cooperation for Accreditation (EA)
EA has been appointed by the European Commission (EC) as the official European accreditation infrastructure. The appointment of EA follows the adoption of Regulation (EC) No 765/2008 by the European Parliament and the European Council which establishes the legal framework for accreditation in the EU and sets out the requirements for accreditation.

This regulation came into effect from January 1, 2010.

The regulation promotes a harmonized approach to accreditation in the EU member states so that, ultimately, one accredited certificate (or report) should be sufficient to demonstrate the technical competence of the accredited conformity assessment bodies.

There is another legislative document that should be mentioned here, the Marine Strategy Framework Directive 2008/56/EC (MSFD), which aims to protect the marine environment across Europe and includes parameters that should be measured and monitored for this purpose.

Finally, there is a rather comprehensive description of interactions between analytical laboratories, accreditation, and standardization bodies in Ref. [10].

Overall, education remains to be the key to improve, foster, and further develop mutual understanding among all of the above stakeholders, including citizens.

Let us now go back to science.

5.3 Measuring ^{210}Po in the Gulf of Trieste and Acidity in Olive Oils

Imagine you are working in a laboratory analysing different types of samples, amongst other samples of olive oil and fish. One day a customer knocks on your laboratory door and says: Here is a sample of olive oil and fish. Could you please measure all that is requested by legislation in the olive oil sample and report the quality of the olive oil sample. As for the fish sample, I am interested in ^{210}Po concentration.

First, we shall clarify that the above two requests are essentially different. One is required by legislation, the other not, even more it is a matter of research. Having said this, it is unlikely that the same laboratory can do both. Let us examine the main differences between an accredited testing laboratory and a research laboratory.

Typically, a testing laboratory, which is doing measurements requested by legislation, is accredited, while accreditation rarely applies to a research laboratory. An accredited testing laboratory is applying measurement procedures, for which they are accredited, in their daily work. Saying differently, they measure the same measurands in the same type of samples on a (almost) daily base. They shall report measurement results to customers as soon as possible.

In a research laboratory, they develop new measurement procedures, and when sufficient research data are available, scientists publish an article in a scientific journal. They do not, or rarely, report their measurement results to a concrete customer.

Measurements of ^{210}Po in the Gulf of Trieste are a matter of research work. The element was discovered in 1898 by Marie Sklodowska Curie and is named after her native country, Poland. It is a silver-grey, radioactive semimetal and an alpha emitter. A single gram of polonium will reach a temperature of 500 °C as a result of the alpha radiation emitted. This makes it useful as a source of heat for space equipment; however, polonium has no biological role. It is highly toxic due to its radioactivity. It thus makes sense to measure it in different matrices, also in the sea. The researchers found out by measuring that the natural alpha-emitting radionuclide ^{210}Po can be accumulated to relatively high levels in tissues of a variety of marine organisms, well above levels of the parent radionuclide ^{210}Pb. Moreover, ^{210}Po and other radionuclides as well as trace elements can concentrate to a relatively high degree in the tissues of marine organisms, depending on their food habits (filter-feeding organisms). The data obtained in the study [11] showed higher ^{210}Po levels in all matrices (water, plankton, sediment) analyzed in the Gulf of Trieste compared to the central Adriatic and western Mediterranean areas. Higher levels were encountered in sediments influenced by local rivers. The increase in ^{210}Po concentrations was very pronounced in particulate matter and plankton. The ^{210}Po/^{210}Pb ratios greatly increased at higher tropic levels (fish, shellfish).

On the contrary to ^{210}Po in the sea, quality of olive oils is defined by legislation. One of many parameters which shall be measured in oils is measurement of acidity, expressed as percentage of oleic acid. This parameter, i.e., acidity, is indicator for quality of the olives. When the acidity is smaller or equal to 2,0%, oil is categorized

as virgin oil. When acidity is smaller or equal to 0,8%, oil belongs to extra virgin olive oil category.

Let us say that our laboratory is accredited for measuring acidity of olive oils. This means that before measuring acidity of the sample, we shall only verify that the analytical procedure that we are using in our laboratory to measure acidity is fit for purpose; there is no need to do a validation.

Interesting fact
The physical, chemical, and organoleptic characteristics of olive oils and the relevant methods of analysis are regulated by the European Union (EU) by Reg. (EEC) 2568/91. You may be surprised to find out that such legislation is signed by the President of the European Commission. Google and learn more.

Acidity, expressed as percentage of oleic acid, is calculated by applying the following equation:

$$V \times c \times \frac{M}{1000} \times \frac{100}{\mathrm{m}} = \frac{V \times c \times M}{10 \times \mathrm{m}} \tag{5.5}$$

V the volume of titrated potassium hydroxide solution used, in milliliters, c the exact concentration in moles per liter of the titrated solution of potassium hydroxide used, M the molar weight in grams per mole of the acid used to express the result (= 282), m the weight in grams of the sample.

For our sample, 0,7% acidity was measured. This classifies the olive oil sample as extra virgin oil, providing also all other parameters comply with the limits fixed in this regulation. If the sampling was done appropriately, this also means that the bulk of the olive oil, from which the sample was taken, falls in the same category as the sample that was analysed.

We have come to the end of a tutorial on measurements in the chemical sciences. If it triggered your scientific curiosity and have now more questions than before starting to read this chapter, then you are well on the way toward unveiling remaining scientific challenges related to measurements in chemical sciences. A list of references is a good starting point; however, please note that it is not at all comprehensive. If you are interested in a structured approach for traceability, validation, and measurement uncertainty in the chemical sciences, then I recommend having a look at freely available first volume of "Examples" [12]. This structured approach has been developed in the first decade of the twenty-first century within a pan-European program. At that time, measurements in chemical sciences were high on a scientific and political agenda, as chemistry was positioning itself as a scientific discipline in relation to metrology, which is traditionally owned by physics. Finally, note that there are continuous developments in the measurement sciences, such as Ref. [13].

Alcohol measurements and the sea

I've been asking those who eagerly spend their holidays on the sea and do not have scientific background what they would like to read about in my chapter of this book which is dedicated to the sea. Apart from serious proposals, most of them have been addressed in this chapter, there was one less sober, namely on alcohol measurements. Alcohol measurements are certainly as thoughtful as any other; however, the proposed topic was put in a humorous context. The question I got was the following: "How to appropriately distribute alcohol consumption across several days when going out for sailing?" My immediate answer was that volume measurements are not part of this chapter, but I promised to explain chemistry behind alcohol measurements.

In many countries, there is legislation in place which prescribes legal drinking limits. These measurements are then a subject of legal metrology. For this purpose, alcohol can be measured in breath and/or in blood.

A breathalyzer is a device for estimating blood alcohol content (BAC) from a breath sample. Two breathalyzer technologies are most prevalent. Hand-held field testing devices are generally based on electrochemical platinum fuel cell analysis and, depending upon jurisdiction, may be used by officers in the field as a form of "field sobriety test" commonly called "preliminary breath test" or "preliminary alcohol screening" or as evidential devices in point of arrest testing. Desktop analyzers generally use infrared spectrophotometer technology, electrochemical fuel cell technology, or a combination of the two.

Alcohol breath-testing devices use the amount of alcohol in exhaled breath to calculate the amount of alcohol in a person's blood, also known as blood alcohol concentration (BAC). To fulfill requirements of legal metrology, such devices are a subject of test approval and verifications.

When the user exhales into a breath analyzer, the overall reaction is the oxidation of ethanol to acetic acid and water.

$$CH_3CH_2OH(1) + O_2(g) \rightarrow CH_3COOH(aq) + H_2O(1)$$

The electric current produced by this reaction is measured by a microcontroller and displayed as an approximation of overall blood alcohol content. Mind you that measurement units for alcohol in breath sample are usually different than measurement units for alcohol in blood. Results for the first are usually expressed in mg of alcohol per liter of exhaled breath, while for the latter in gram of alcohol per kilogram of blood (also known as "promile"). A factor of 2,1 can be used for approximate conversion between both units. In-depth science behind these measurements unveils many interesting scientific issues, which may be worth your curiosity to discover them in papers describing this topic in more detail.

References

1. International vocabulary of metrology—basic and general concepts and associated terms (VIM 3rd ed) JCGM 200:2012 (JCGM 200:2008 with minor corrections) VIM3 https://www.bipm.org/en/publications/guides/vim.html
2. McNaught AD, Wilkinson A (1997) IUPAC, Compendium of chemical terminology, 2nd edn. Blackwell, Oxford
3. Robouch P et al (2003) EUR 20841 EN, Euromet/Eurachem project 693. European Communities, Brussels
4. Resources. RSC Education. https://edu.rsc.org/resources
5. Majcen N (2009) A measurement: a concert? Accred Qual Assur 14:565–566. https://doi.org/10.1007/s00769-009-0517-8
6. KCDB database https://www.bipm.org/kcdb/
7. Majcen N, Skubic I, De Bièvre P (2004) Target measurement uncertainties for results of chemical measurements in Slovenia. Part I. Legislation related to quality of food Accred Qual Assur 9:106–111. https://doi.org/10.1007/s00769-003-0723-8
8. Majcen NH (2017) Circular citizens research. Environ Sci Pollut Res 24:7867–7868. https://doi.org/10.1007/s11356-016-7926-0
9. Mehlich J (2018) Good chemistry–methodological, ethical and social implications. http://www.elearning-euchems.eu
10. Papadakis I, Krokos FD, Trapalis C (2017) Interaction of analytical chemistry with accreditation/certification. Environ Sci Pollut Res 24:7872–7879. https://doi.org/10.1007/s11356-016-6638-9r
11. Faganeli J et al (2017) Accumulation of ^{210}Po in coastal waters (gulf of Trieste, northern Adriatic Sea). J Environ Radioact 174:38–44
12. Majcen N, Taylor P (2010) Practical examples on traceability, measurement uncertainty and validation in chemistry, 2nd edn. European Union, Luxembourg
13. Prenesti E, Gosmaro F (2015) Trueness, precision and accuracy: a critical overview of the concepts as well as proposals for revision. Accred Qual Assur 20:33–40. https://doi.org/10.1007/s00769-014-1093-0

Chapter 6
Sensors, Measurements, and Analysis for Underwater Acoustic Investigation

Mirko Stifani, Michele Andreini, Lorenzo Bazzarello, Vincenzo Manzari, and Daniele S. Terracciano

Contents

Abstract Sensors, Measurement, and Analysis for Underwater Acoustic Investigation is a chapter dedicated to deepen why underwater acoustics is the key reference of underwater investigation. This chapter provides the basis for understanding the challenges of the underwater domain, starting with a dissertation on the historical and philosophical connection between human beings and acoustics. Over the course of human history, people have tried to learn from nature and replicate its phenomena through the development of technologies to support investigation. Following the presentation of some fundamental acoustic terminology, a picture of the noise levels and frequencies of anthropogenic and naturally occurring sound sources and basic mathematical terms of SONAR (SOund NAvigation and Ranging) equations are given. Transducer principles and complex active and passive sensors as a basement for multiple applications, from localization, through tracking methodologies, to imaging classification for both civilian and military scopes are also introduced, including some references to measurements and performance test and evaluation capabilities. Finally, this chapter provides the integration of such principles into autonomous systems as a continuous improvement process to replicate

M. Stifani (✉) · M. Andreini · L. Bazzarello · V. Manzari · D. S. Terracciano
Centro di Supporto e Sperimentazione Navale (CSSN), La Spezia, Italy
e-mail: mirko.stifani@marina.difesa.it; michele.andreini@marina.difesa.it; lorenzo.bazzarello@marina.difesa.it; vincenzo.manzari@marina.difesa.it; danieles.terracciano@marina.difesa.it

P. Daponte et al. (eds.), *Measurement for the Sea*, Springer Series in Measurement Science and Technology,
https://doi.org/10.1007/978-3-030-82024-4_6

nature, with a particular focus on the scientific and technological challenges to increase the autonomy of systems for longer range and time missions, enabling exploration of more remote environments.

6.1 Introduction

6.1.1 Why Acoustics

The link between human life and the sense of hearing is probably the closest to the one known as sixth sense. Natural amplifier of this perception is the water. If we want to start a path on the way to understand the role of this sense, above all under the water or sea, we have to start from those who, able to leave a track of their thought, used the investigation (i.e., to study carefully something to discover the truth behind it) as a tool for the elevation of human being, making acoustics a science: the ancient Greek world and its philosophers.

From an archeological point of view, acoustics, as a branch of physics, is the legacy of the experimental and empiric considerations of Pitagora and pitagorici in music. But one step more was done by Archita, one of the last representatives of Pythagorean thought, investigating not only the music, but also acoustics in general, bringing to considerations like distinction between sound versus noise, audible versus not audible, and severe versus acute sounds.

From this experience, the first who discussed the relation between acoustics and the soul mentioning the application in the water has been Aristotle in De Anima "... Further, sound is heard in air, and in water, though less so. But it is not the case that either air or water is chiefly responsible for sound …" [1] opening the way to the concept of the "perception" through the mean of propagation, and elevating the hearing sense like the one that (as Plutarco in the De recta ratione audiendi attributed to Teofrasto) "move" passions more than any other, making auditory a multimodality sense that bears on theorizing perception.

We can simplify further the concept, sentencing that we can hear and perceive the means of sound and the messages it takes, through the entire body. Nowadays, new acoustic devices have been developed with new technologies to change the way we listen to music, like bone conduction devices or listening through haptic feedback devices, which applied the concept of "multimodal" perception moving the hearing sense toward, as said in our premises, the sixth sense. Moreover, marine mammals themselves use "auditory perception involving many other factors beyond merely hearing or detecting sounds" [2]. That is why acoustics, using a philosophical language, makes the sixth sense a substance: "a foundational or fundamental entity of reality" [3], and why human beings try to replicate its principles to better understand the undersea and marine life on which our existence is strictly dependent. From ancient Greek to nowadays, acoustics became a science, passing from scientists of high value for the undersea world, like Leonardo da Vinci that in 1490 noticed that "... place the head of a long tube in the water and place the outer extremity to your ear, you will hear ships at a great distance from you."

6.1.2 Terminology, Units, and Measurements Parameters

Different scientists worked to mathematically formulate the theory and physics of sound in the sea, from Sir Isaac Newton to Ernst Chladni, Lord Rayleigh, Hugo Lichte, and many others. Thanks to those people we can today benefit from notations, formulas, definitions, units, procedures, and standards that supported the development of underwater acoustics (as we are not using only the ears to "listen" or "see"). That is why we need a short definition corner to support the following reading.

The Decibel (dB) It is a unit commonly used in electroacoustic. The dB derives from the Bel unit (in honor of the scientist Alexander Graham Bell) for comparing two power levels with logarithm to the base ten of the ratio of the two powers you want to compare. In fact, some of our senses require us to manage a huge variety of intensity that is needed, for example, if you want to hear the sound of leaves moved by the breeze in a forest or a gunshot. We are speaking about double or ten times a reference level, but to be able to change 6 orders of magnitude, from 1 dB, accepted as the smallest change of level that is generally perceptible to the human ear, to the human hearing threshold of pain. This is possible because ears have a natural logarithmic response. It was more useful to move from the Bel scale to the dB scale, ten times smaller, for practical reasons. If we want to compare acoustics intensities,

$$\mathrm{SPL} = 10\log\left(I / I_{\mathrm{ref}}\right) = 10\log\left(P^2 / P_{\mathrm{ref}}^2\right) = 20\log\left(P / P_{\mathrm{ref}}\right) \tag{6.1}$$

where $P_{\mathrm{ref}} = 1\mu Pa$ and the sound pressure level (SPL) is expressed in [dB re $1\mu Pa$]. $1\mu Pa$ is the root-mean-square pressure value that in water is equivalent to a sound intensity of $6.5 \cdot 10^{-19} W/m^2$, conventionally defined as source level (SL) indicated as dB re $1\mu Pa$ @1 m (at 1 meter of distance from the source).

Spectrogram Spectrogram in acoustics is a visual representation of the frequency spectrum of sound as a function of time. It means to represent graphically how the spectrum varies in time in intensity (expressed in dB). Spectrogram is also possible to determine frequency evolution effects like Doppler or other shapes connected to artifacts or natural behavioral sounds that can be classified through artificial intelligence (or human operator evaluation connected with listening) and assigned to specific subjects.

Frequency, Bandwidth, and Third-Octave Band A frequency is the number of repetitions per second of a recurrent event. It is measured in Hertz (Hz) which is equal to one occurrence of a repeating event per second, and it is the inverse of the period that is the duration of time of one cycle in a repeating event. Bandwidth is the difference between upper frequency and lower frequency in a continuous range of frequencies. As a difference of frequencies, it is measured in Hertz. Bandwidth is one of the characterization parameters of the capacity of a given communication channel; in fact, it establishes the amount of information that can be carried, regard-

less of where that band is located in the frequency spectrum. Third-octave band: As per acoustic levels, it was necessary to recur to the dB scale, and the frequency bandwidth of the spectrum of interest is wide enough to require a similar representation that is again connected with natural behavior. As we said before, the whole frequency range can be divided into sets of frequencies called bands. For this reason, scales of octave and one-third octave bands have been defined: In octave band, the upper band frequency is twice the lower one; in one-third octave band, the upper band-edge frequency is the lower band frequency times the cube root of two. This last definition simply recognizes a natural behavior, as in each third octave there are 4 semitones, clearly distinguishable by people with perfect pitch.

6.1.3 How to See the Sound

Following the introduction of some basic useful terms, it is the moment to give pictures of noise levels and frequencies of anthropogenic and naturally occurring sound sources to provide an overview of the dynamics of the underwater acoustic spectrum and relations. Some representations use marine mammals sound sources distribution in frequency and body mass weight [4], while some others represent the distribution of natural sounds per level versus frequency (like the Wenz curve [5, 6]). Thanks to these representations, it is possible to understand acoustics overlapping, e.g., the impact of an anthropogenic source's emission in the marine mammals' spectral domain, as mammals use sound for communications, feeding, and orienteering (Fig. 6.1).

Moreover, other representations show the evolution of the sound in the water taking care of parameters that contribute estimating the expected signal at e specific point (radiated noise) in the water volume also through predictive simulation of the behavior of a sound source in a particular region depending on range, directivity, bathymetry, bottom characteristics, etc. (Figs. 6.2 and 6.3):

6.1.4 Fundamental Concepts of SONAR Equation

Before introducing the behavior of acoustics in the water, we need to specify that sound travels about 1500 meters per second in seawater (five times faster than in the air). The speed of sound in seawater is not a constant value and varies from place to place, time to time (daily and seasonally), and with water depth (through variation of pressure, salinity, and temperature). Such variations have important effects on how sound travels in the ocean. An empirical formula for the computation of the sound speed is proposed by Mackenzie [7]. Another important factor is the propagation (or transmission) loss (PL), that is, the process "loss of intensity" [8] caused by geometrical spreading and absorption loss:

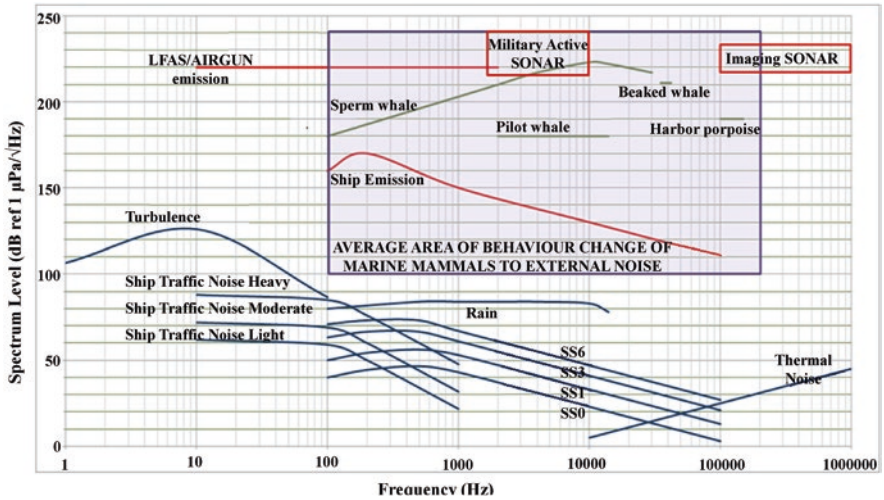

Fig. 6.1 Noise levels and frequencies of anthropogenic and naturally occurring sound sources

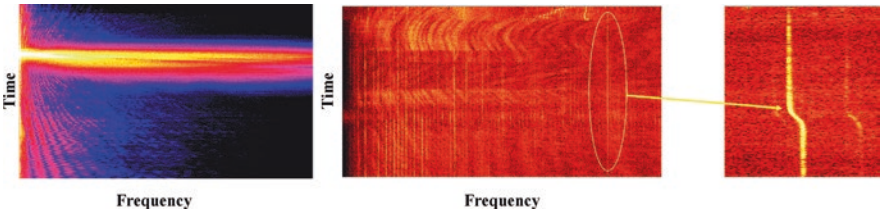

Fig. 6.2 (**a**) Example of radiated noise spectrogram frequency vs. time; (**b**) with Doppler effect

$$PL = X \cdot \log(R) + \alpha(f)R; \tag{6.2}$$

where the first term represents spreading losses ($X = 20$ in spherical spreading; 10 in cylindrical spreading; and other values depending on geometrical condition); the second term denotes absorption losses. α is the absorption attenuation coefficient defined accordingly to the Thorp equation as:

$$\alpha\left(\frac{d\mathrm{B}}{km}\right) = \frac{0.11f^2}{1+f^2} + \frac{44f^2}{4100+f^2} + 2.75 \cdot 10^{-4} f^2 + 0.003\left(f\ in\left[kHz\right]\right) \tag{6.3}$$

Then, we are going to show the active and passive SONAR equation, on which the systems we are going to describe are based on, and look their representation through the use of complex underwater acoustic performance predictors like Acoustic Toolbox User interface and Postprocessor (ACTUP [9]), MultiStatic Tactical Planning Aid (MSTPA [10]), and many others [11]:

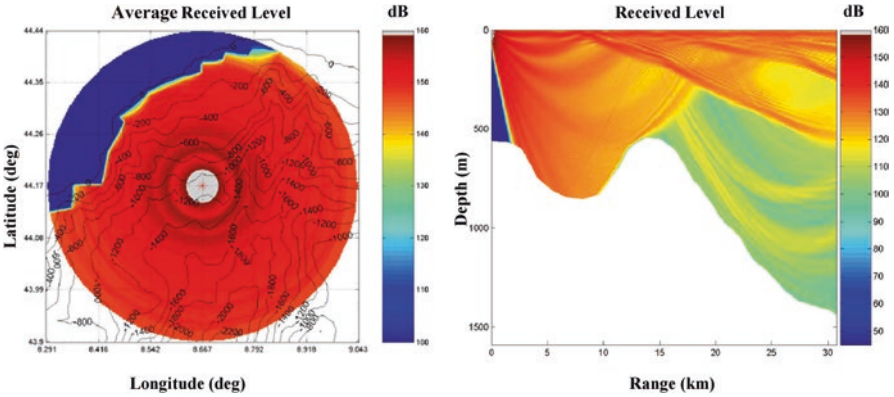

Fig. 6.3 (**a**) Radiated noise average level in range vs bearing; (**b**) and level received in range vs bathymetry

$$\text{Passive SNR} = SL - PL - \left(NL - DI\right) \tag{6.4}$$

$$\text{Active SNR} = SL - PL_1 - PL_2 + TS - \left(NL - DI\right) \tag{6.5}$$

SNR is the ratio between signal level and noise level at the entrance of the receiver and, thus, is independent from the sensor used.

SL is the original level of the source;

PL as per definition in (6.3) is the propagation loss. In the active SONAR formula, PL_1 is the propagation loss from source to target and PL_2 the loss of return path, valid also in bistatic solution when transmitter and receiver are geographically separated. Ambient noise as seen by the receiver is denoted by *NL* (noise level). Directivity index (*DI*) represents the amount of noise reduction due to the receiver's directivity capabilities. Target strength (*TS*) refers to the echo returned by a target and is defined as the log of the ratio, in dB, of the intensity of the echo 1 m from the target relative to the intensity of the sound hitting the target.

SONAR systems use acoustic signals propagated through the water to detect, track, localize, and classify underwater targets. Such systems can be installed on surface ships, submarines, or maritime unmanned systems (MUSs) and can be active, passive, monostatic, bistatic, and multistatic. This last system consists of a combination of active and passive SONAR sensors mounted at different locations. Following paragraphs introduce sensor technologies, data analysis, and data processing to support measurements and applications (including communications, echolocation, and orienteering), with an emphasis on the unmanned approach to acoustic investigation, which is a new approach to performing measurements and applications with new technologies and for new technologies.

6.2 Acoustic Sensors

We now need to understand in which way we can receive acoustic waves. To do this, we have to start from principles of acoustic transduction, going through the state of the art of transducer, concluding with the most common SONAR used on metrology, and how they work in different applications.

6.2.1 Transducer

The term "transducer" indicates a mechanism capable of transforming one type of energy into another. The acoustic transducer is the component that transforms an electric energy into acoustic energy and vice versa. As a result, the role of electro-acoustic transducers in the transmission and reception of acoustic energy in water is inextricably linked.

Thus, a transducer can be defined as a "hydrophone" if it is only a receiver; as a "projector" if it is only transmit; and "reciprocal transducer" for both properties.

A summary (Table 6.1) [12] gives a panoramic of different types of transducers related to their behavior, bandwidth, the material of which they are made, and the yield.

Table 6.1 Different types of transducers with their main characteristics

Transducer type	Behavior and acoustic bandwidth	Material and note
Piezoeelectric (electric field)	Linear reversible 5Hz–50 MHz<230 dB	Crystal Quarts, Rochelle salt, Ammonioum di-hydro phosphate, Lithium sulphate, Tourmaline Yields between 0.4 and 0.8
Electrostrictive (electric field)	Liner reversible Up to 50 kHz<240 dB	Yields between 0.6 and 0.8
Electrodynamic (magnetic field)	Linear reversible Up to 50 kHz<100 dB	Wraps that require a diaphragm Small powers
Magneto strictive (magnetic field)	Reversible quadratic; linear If polarized 10 – 200 kHz<230 dB	Nickel, cobalt alloys (Ni-Fe, Ni-Cu, ferrite) Yields between 0.2 and 0.3
Hydraulic	Linear with harmonics Up to 1000 Hz<240 dB	Hydraulically controlled diaphragm Transmitter only low freq

6.2.2 Ceramics Measurement and Usage

Parameters required to technically describe a transducer are resonance frequency (in relation to the specific application), bandwidth (narrow and wide), output power, electroacoustic efficiency, receiving sensitivity (electrical voltage generated, related to pressure accident), dimensions, and weight, resistance to static pressure (related to quote of work). Considering the possibility to have custom geometry and cost-effective devices, ceramic is the current state of art technology.

Typically, measurements performed to characterize acoustic transducers are electrical impedance, electroacoustic sensitivity, and the directivity pattern; to better understand the mechanism, please refer to Sect. 6.4. In particular, free-field "receiving sensitivity" M_t is expressed as a function of frequency. Mathematically, it is defined as the ratio $M_t = e/p$ where e is electrical output voltage and p is the sonic pressure acting on the hydrophone, the unit being V per N/m^2 or V per μPa. Suppliers deliver hydrophones together with receiving sensitivity (dB re 1 $V/\mu Pa$) and often with radiation diagram (on horizontal and vertical plane). Similarly, for projectors, the most important parameter is the "transmission sensitivity" (dB re $1\mu Pa@1\ m/V$): When a hydrophone is used as a projector, a useful parameter to define it is its impedance.

Since now, we have considered a single transducer, but in SONAR systems, a transducer is normally part of an array. Why? Small transducers are easily to be built, mounted, and substituted; the array can increase the overall gain, provide diversity reception, steer the array so that it is most sensitive in a particular direction, determine the direction of arrival of the incoming signals, and increase the directivity index.

6.2.3 SONAR Sensors

The role of sense organs is to transform external and internal stimuli into nerve impulses transmitted to the brain. SONAR replicates some of these senses: hearing with passive systems, sight with imaging SONAR, and touch with sub-bottom profilers. The human operator, or the artificial intelligence, is the brain of the system. So, the acoustic wave, transformed and elaborated, becomes strings of bits that can be interpreted to extract many information. In passive SONARs, the radiated noise emitted by a target becomes the source of signals. The sound radiated by ships and submarines is of most interest in the military application of passive SONAR [13], but it is also of interest to shipyards for maintenance and "Green Ship" design. Typically, the radiated noise is composed of discrete and continuous components. The discrete components are narrowband and are produced by propellers and engines. Flow noise phenomena play an important role in the continuous components. As a passive SONAR detects a signal from a target, a measure of the target's

bearing and how it varies over time is given [14]. Active SONAR instead emits acoustic pulse of various lengths and waveforms and listens to backscatter coming from different targets. Following paragraphs give a short explanation of SONAR sensors mentioned in this book; to have an exhaustive explanation of them, you can refer to [15].

6.2.4 Single–Multi-Beam Echo Sounder

The echosounder has only a transducer, looking to the seabed. In this case, it is considered the time lag between the istant of the emitted sound and the returning echo to calculate the water depth. An evolution of the echosounder is the multibeam, where multiple beams are transmitted to map the seafloor. By reconstructing all the echoes back, you get a 3D map of the seabed. Remaining on the single beam but going down in frequency (below 70 kHz), you can also measure the echo reflected from the inner layers of the bottom, obtaining precise information on a possible structure of the bottom; in this case, we speak of a sub-bottom profiler.

6.2.5 Side-Looking SONAR

Normally, there are two transducers mounted each on one side of the ship/vehicle or in a dedicated tow fish. Each transducer has a very narrow horizontal directivity (around 1° or less). The signal backscattered by the seabed, recorded over time, reproduces the structure of small irregularities on the seabed that scatter acoustic waves at grazing incidence, so the echo received a long time represents the bottom reflectivity along the swath. The image of the seafloor is re-constructed by combining the data acquired line by line. The resolution of SSS is strictly connected to the transducer dimension and the pulse duration. In synthetic aperture SONAR (SAS), a solution is given utilizing a synthetic huge transducer. The principle is very simple, with the realistic hypothesis that what you are looking at, if steady, you can imagine to look at from different angles at different times, using a low-resolution transducer (in relation to the frequency used). Choosing the right pulse rate, so the right spacing between transducers, you can create a synthetic (because it is only in the signal elaboration) big array of transducer that has the same resolution of the single transducer footprint. So, the resolution can reach the order of a few centimeters, and it remains constant for the whole across track.

6.2.6 Acoustic Baseline

Transducers can be used also like transponder to perform underwater acoustic positioning. The lack of GPS into the water makes necessary the use of these solutions. The main acoustic positioning methods are now described.

Long Baseline (LBL) LBL systems consist of underwater transponders fixed on the bottom and a transceiver installed on the target. The transceiver interrogates the beacons which will transpond and be used as underwater references for target positioning. The position of the target is then determined via trilateration by measuring the two-way travel time from each transponder. The precision of the target position will depend on the accuracy of the positioning of the transponders. In reference [16], the authors discuss the influence of transponder location in the performance of the LBL navigation. Such method presents the following advantages: The system is able to provide high potential accuracy; such accuracy is preserved over a wide operating area. Against advantages, the system requires multiple underwater transponders that need to have two-way ranging. In addition, the known problem of acoustic ray bending is present, especially at long slant range from the target.

Ultra-Short Baseline (USBL) USBL systems rely on a small transducer array that can be mounted on the bottom of a surface vessel or small asset. Unlike LBL, USBL measures the target distance from the transducer by using two-way travel time and the target direction by measuring the phase shift of the reply signal at the elements of the transducer array. The target position is then estimated by combining distance and direction measurements. Such systems can be equipped with additional sensors: GPS, gyro, or electronic compasses and vertical reference units in order to compensate for pitch, roll, and bearing of the surface vessel. They do not require a seafloor transponder array. The position accuracy is not as good as for LBL systems due to angle estimation errors of the target.

Short Baseline (SBL) SBL method uses a transponder installed on the target to track and at least three transducers that are placed on board ships, AUVs, or buoys. Such method is based on measurement of time difference of arrival (TDoA) of signal between the target and the transducers, and it offers the advantage of not requiring the deployment of bottom anchored transponders.

GPS Intelligent Buoys Also written as GIB (GPS intelligent buoy), such a system is composed of at least three buoys equipped with GPS receivers and underwater hydrophones. The buoys measure the times of flight (ToF) of acoustic signal emitted from the transponder fitted on the target to the buoys. The ToF is then translated into ranges between the buoys and the transponder if the sound of speed in the water is assumed to be known. Then, the target position can be determined by trilateration. The main advantages of such systems are relatively simple operation costs and no need to deploy transponders on the sea bottom. GIB positioning is very stable and accurate and offers real-time GPS tracking underwater.

6.3 Localization, Processing, and Analysis

6.3.1 Target Motion Analysis

Target motion analysis (TMA) is a method to estimate the state of a target (position and velocity) from noise measurements collected by a single passive receiver [17]. TMA is achieved by marking the direction of arrival (DoA), or bearing, of the acoustic wave at various times, and matching the motion with that of the passive receiver (on a ship or other asset).

The efficiency of any bearing-only TMA method depends on the receiver's maneuver strategy [18]. A typical issue in applying TMA methods is the fact that the target could be not observable from the measurements [19]. In literature, several estimation methods have been applied with different results to the bearing-only TMA problem [20, 21]. The extended Kalman filter (EKF), the unscented Kalman filter (UKF), and the maximum likelihood estimator (MLE) seem to be the most commonly accepted solutions.

6.3.2 Triangulation

The technique called triangulation belongs to bearing-only analysis methods. The principle is essentially based on the spatial separation of at least two receivers. In fact, given two well-separated directional receivers capable of estimating individually the DoA of a target, the range of interest can be estimated through a simple trigonometry calculation.

6.3.3 Time Difference of Arrival or Cross-Correlation Method

The conventional approach of obtaining the direction of a target is to use the technique called TDoA. Often, terms such as cross-correlation and phase difference method are used to name this technique.

The principle of operation is quite simple: The receiver is composed of at least two omnidirectional hydrophones, and their outputs are compared to estimate the phase difference or the time delay difference. This can be done using the cross-correlation function between each hydrophone's signal.

Let us consider the case of an array composed of two hydrophones acting as passive receivers. A layout of the receiver model is shown in Fig. 6.4:

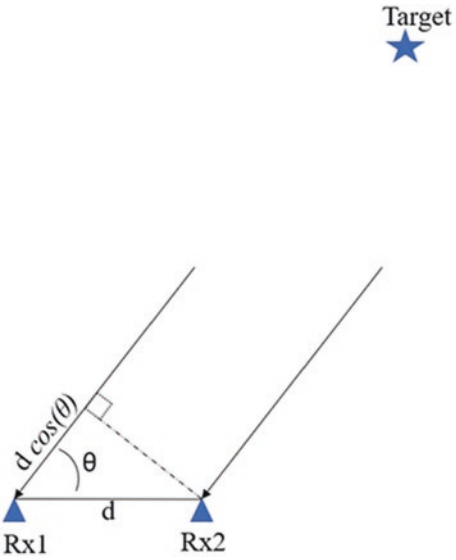

Fig. 6.4 Plane waves coming from the target incident on a 2-element array

where d is the distance between the two hydrophones and θ is the DoA of the signal emitted by a target of interest. Let us consider the target in the array's far-field. For this case, the source emits a plane wave so that the normal to the wavefront makes an angle θ with the line joining the sensors.

The cross-correlation function between the signals at the two sensors is defined as:

$$R_{x1x2}(\tau) = \int_{-\infty}^{+\infty} x_1(\tau)\, x_2(t+\tau)\, d\tau \tag{6.6}$$

and gives the correlation degree between the two sensors output x_1 and x_2, implying that for a high correlation degree the argument τ is comparatively similar to the real TDOA. After computing the signal delay τ between the two sensors, which will correspond to the peak of the correlation function, the DOA estimation of the emitting target can be obtained according to the following equation:

$$\tau = d\cos\theta / c \Rightarrow \cos\theta = c\tau / d \Rightarrow \theta = \cos^{-1}(c\tau / d) \tag{6.7}$$

where c is the speed of sound in water.

An efficient algorithm to compute the DoA from TDOA making use of the cross-spectral method through the use of the fast Fourier transform (FFT) is described in [22]. Several representative localization algorithms that use TDOA method are addressed in [23], whose authors point out that the errors in such methods can be

complicated, depending on signal-to-noise ratio (SNR) at the receiver, integration time, signal bandwidth, and multipath phenomena.

6.3.4 Multipath Passive Ranging

The sound radiated by an acoustic source can be reflected by the bottom and surface, especially in shallow water environments. If we assume constant sound speed along the vertical water column, sound rays travel in straight lines. Under these assumptions, the acoustic field can be modeled simply by using geometry. In an isotropic channel, the arrival structure at the receiver consists of a direct eigenray and multiple reflected rays from sea bottom and surface. In some conditions, it is possible to extract the arrival times. A multipath scenario is depicted in Fig. 6.5.

Differences in arrival times between rays at the receiver (i.e., hydrophone array) can be estimated with TDOA method. Sometimes, the time difference between the direct arrival and multipath arrivals is defined as time difference of multipath arrival (TDOMA) [24]. Known also as the vertical direct passive ranging (VDPR) method, measurements of the vertical angles of arrivals at the receiver from a radiating target and the time differences between signals reaching the receiver can be used to estimate the range and depth of the target.

In the case of only three paths as shown in Fig. 6.5, a closed formula for estimating the target range and depth can be obtained [25].

6.3.5 Conventional Beamforming

Beamforming has been studied and applied in a variety of fields, such as radar, SONAR, seismology, and communications. In the underwater environment, the detection of targets and DoA estimation often go through the application of beamforming. A beamformer is historically formulated as a spatial filter which operates in order to shape a desired directivity pattern of hydrophones array. Typically, conventional beamforming operations can be divided into two suboperations: time synchronization and weight-and-sum. Time synchronization is necessary to temporally align the signal components at the hydrophones. This is basically done through the use of the TDoA method described in the previous paragraphs. Then, the next step is to weigh the aligned signals and sum all the components of each hydrophone in order to form one output. A particular attention has to be kept in order to decide the coefficients of the weighting operation, which typically are determined on a preimposed array beam pattern.

Let us consider an equispaced linear array which consists of N omnidirectional sensors, as illustrated in Fig. 6.6. The spacing between two neighboring sensors is denoted by d. We always assume that the target is in the far-field and acoustic waves are planes at the hydrophones.

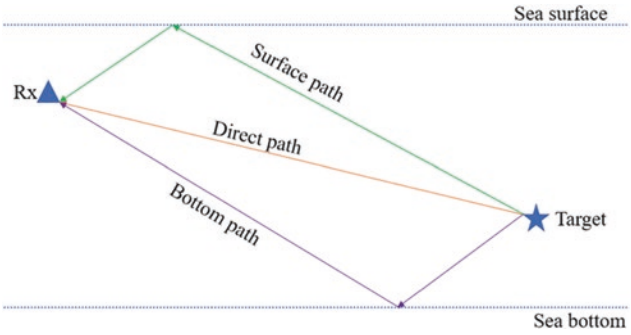

Fig. 6.5 Illustration of a simplified scenario of underwater multipath propagation

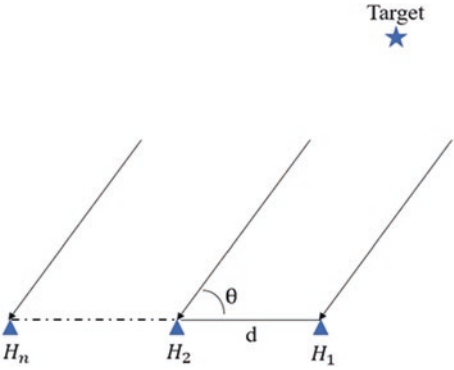

Fig. 6.6 Plane wave incident on a uniformly spaced array from direction θ

If the waves reach the array with an incident angle denoted by θ, the TDOA between the nth and the reference sensors is:

$$TDoA(\tau) = (n-1)\tau = (n-1)d\cos\theta / c \tag{6.8}$$

where c denotes the sound velocity in the medium. Let us consider the generalized form of delay-and-sum method, called weighted delay-and-sum beamforming. The output signal can be written as follows:

$$b(kT) = \sum_{i=0}^{N-1} w_i \, x_i\left[kT - \tau_i\right] \tag{6.9}$$

where signal samples at each hydrophone H_i are denoted by $x_i(kT)$ delayed by τ_i samples, which are then multiplied by weights and summed. T is the sampling time.

6.3.6 *Spectral Analysis*

LOFAR Analysis The LOFAR (low-frequency analysis and recording) is a broadband analysis. This technique provides the machinery noise to the SONAR operator, and it can be explained as follows: After DoA, the signal is multiplied by a Hanning window and separated in blocks of samples. Then, a short-time Fourier transform (STFT) algorithm is applied [14]. Typically, LOFARGRAMs (low-frequency analysis recording gram) are used to display the outputs from all DoA (beams) or a selected group of beams. They are displayed in a frequency versus time format and contain information useful for classification and analysis of contact motion. An example of LOFARgram is represented in Fig. 6.2, consisting of a waterfall display representing a frequency–time analysis for one run of a vessel.

DEMON Analysis DEMON (detection envelope modulation on noise) analysis is a technique used to detect and classify targets allowing to separate the cavitation noise from the overall signal spectrum and to estimate number of shafts, rotation frequency, and the blade rate through narrowband analysis [26]. Let us consider a single omnidirectional hydrophone. The signal received at the hydrophone is band-limited by a band-pass filter, in order to select the frequency band where cavitation is more emphasized. Then, the envelope signal is extracted, and a FFT is applied. Typically, a waterfall spectrogram, or DEMONgram in this case, is obtained, that is, a time–frequency spectrum of the signal, and it shows the harmonics associated with the rotating components of the propeller. This kind of processing supports vessel classification. The main challenge of this method is the selection of the bandwidth which requires good operating skills. Figure 6.7a shows a DEMONgram obtained from real data.

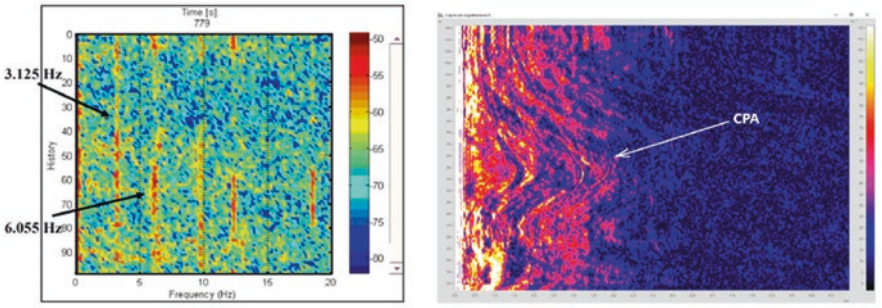

Fig. 6.7 (**a**) DEMONgram of a vessel. Estimation of shaft modulation of 3.125 Hz. (**b**) Cepstrogram of a fishing boat crossing the hydrophone at CPA

Cepstral Analysis From a mathematical point of view, the cepstrum is defined as the inverse Fourier transform (IFT) of the logarithm of the estimated signal spectrum. The term cepstrum was derived by reversing the first four letters of the spectrum, as the operations on the spectra (called "cepstra") are labeled "quefrency" analysis or "cepstral" analysis. This technique can be applied to a variety of applications, such as radar, SONAR, speech analysis, and medical and machine vibration analysis. Different variants of the CEPSTRUM exist: They are power, complex, and real cepstrum. Over the years, the definition of cepstrum has changed. The most common definition that is used and implemented in SONAR applications is as follows:

$$C(\tau) = FFT^{-1}\left[\log F_{XX}(f)\right] \tag{6.10}$$

where $F_{XX}(f) = |FFT[f_x(t)]|^2$ and $f_x(t)$ is the signal of interest. Cepstrum approach can be used for example in shallow water environments characterized by multipath effects. This technique is able to nullify such effects [27] or mitigate the effects of the channel distortions and the ambient noise on the received signal [28]. Figure 6.7b shows a cepstrogram obtained from real data.

6.3.7 Image Processing

SONAR imaging systems (SAS, SSS, and forward-looking SONAR—FLS) generate a significant amount of data during operations. Such data must be analyzed. For this purpose, various image processing approaches are used to find targets quickly and accurately. Convolutional neural networks (CNNs) can be considered the state-of-the-art performance of image classification tasks. Many recent studies show that with well-trained networks, their use of both side-looking SONAR and FLS [29] achieves good performance. The difficulty of collecting precisely geo-referenced images and therefore the subsequently locating detected objects is one of the main problems of the underwater domain. A useful technique to avoid such limits is the change detection (CD) method, based on the process of identifying objects or other phenomena of interest as temporal differences by observing a scene at different times.

6.4 Measurements and Applications

Ships, submarines, torpedoes, anthropic activities (coastal and underwater), and marine mammals are examples of sources of radiated noise. Generally, the propulsion, its components (engines, turbines, gear trains, pumps, rotating parts, and propellers), and their auxiliary systems are the principal sources of noise and emit signals with very complex features. Passive SONARs are designed to exploit

radiated noise and to recognize it from interfering noises as, for example, platform self-noise (propulsion and hydrodynamics), array self-noise, and environmental noise. In the military branch, high level of noise means early highly probable detection and classification: Control and mitigation of noise are necessary in order to improve "invisibility" against passive SONAR and hostile sensor and surveillance systems.

Propulsion noise is generated by thermal machines but also by the wrong balance of rotating axes or bearings. Hull roughness is a source of hydrodynamics noise too, and it increases with velocity.

Periodically, military units (surface and submarine) are subjected to radiated noise measurement to know if their characteristics are degraded. Often, also accelerometric measurements are carried out, setting up sensors on machinery and platform components under investigation. In addition, cavitation of propellers is one of the most critical items under control: The blade must be designed in order to avoid this effect, and, during the service life of the unit, periodical inspection of the hull and propellers is necessary.

In military application, classification was born as a branch of the radiated noise measurement. Every acoustic source has a spectrum with shape or feature defined and more or less recognizable. Obfuscation of this feature is one of the aims of the military naval design.

For civil applications, regulation fixes less strong constraint to the acoustic radiated noise from ships. EUROPEAN DIRECTIVE 2008/56/CE and later Decision 2017/848 give criteria (descriptor 11) to ensure that "introduction of energy, including underwater noise, is at levels that do not adversely affect the marine environment," without a limit of noise: Each nation can choose own way to apply directives to avoid acoustic pollution in order to preserve marine environment.

Other important measurements are connected with the evaluations of the performance of active and passive sensors, in range and bearing estimation using calibrated active source device and echo repeater transducers and on *dual-use* point of view: oceanography/hydrography and intelligence surveillance reconnaissance, seabed monitoring/archeology and mine counter measures, sub-bottom profiling and buried mine detection, search and rescue operations, marine mammals monitoring, and anti-submarine warfare, through systems and techniques in Sects. 6.2 and 6.4.

6.4.1 Underwater Radiated Noise

Modern acoustic radiation calculation and measurement of underwater sources can be executed by means of transducers, which transform, as seen in the chap. 6.2, acoustic signals (pressure waves) into electric tension.

Underwater acoustic sources are characterized by measuring the SL, acquiring the signal level (L) with a hydrophone at a distance R and adding the propagation loss as per (2). During measurement campaigns, signals, coming from the source of interest, and ambient noise (not desired) are acquired together. Such noise, or

interference, depends on factors that are generally beyond our control. Potential sources of this noise could have environmental and anthropic origin as described in Fig. 6.1. In order to estimate and localize the SL emitted by the source under test, it is important to discriminate noise from the signal. Generally, it means to acquire an optimized SNR.

Many international standards exist to describe acoustic radiation measurement criteria; some of these are as follows: NATO STANAG 1136 and AMP-15, ANSI/ASA S12.64–2009 part I, and ISO 17208-1:2016, DNV (Det Norske Veritas) SILENT class noise notation, American Bureau of Shipping (ABS) Guide for the classification notation of underwater radiated noise, and BUREAU VERITAS NR614. Only STANAG 1136 and AMP-15 also consider procedures and best practices for submarines and mine warfare vessels and do not exclude the possibility to include other configurations delving into uncertainty and repeatability aspects. In short, all standards for civil or military applications range from the use of at least 3 hydrophones to linear array, from deep to shallow water, that require to take care of a specific propagation loss estimation, from d_{CPA} of 100 m to increasing distances (1, 1.5 or 2 times the lenght of the unit under test), looking also at different frequency bandwidth.

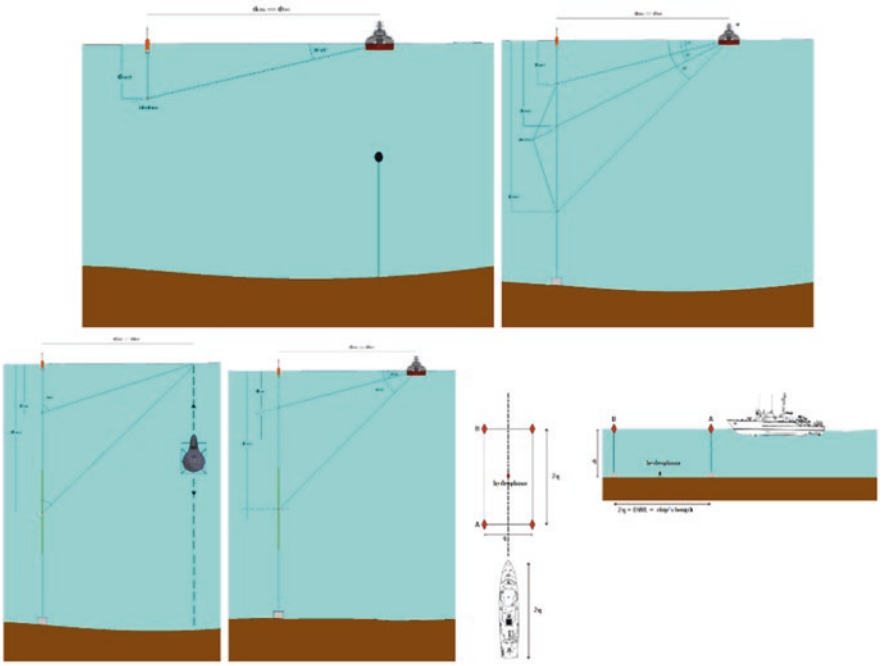

Fig. 6.8 Sensors possible configuration for underwater radiated noise measurements

Using the average among the signals acquired from three hydrophones (at different depths), instead of one, gives more accuracy to the measurement, thanks to the decrease of surface reflection interferences [30]. In the same way, a more advanced method of acoustic radiation calculations is represented by a vertical linear array, able to give excellent SNR thanks to beamforming and beam steering capabilities to eliminate some of the environmental noise and surface reflection interferences. In addition, extremely positive advantages may be obtained with the use of directional sensors, such as vector sensors, to localize potential noisy sources onboard the UUT. STANAG 1136 is the only that adds a hydrophone on the bottom for low-frequency analysis that is a must for mine warfare vessels (Fig. 6.8).

6.4.2 *Transducer Evaluation and Measurement*

Periodical transducer calibration is mandatory in order to ensure accuracy in test procedure. Several kinds of methods are used. Among these, the accurate results can be achieved either by using the comparison method or by reciprocity method. A free-field environment is required. To use a test site, high attention must be paid to ensure a low environmental noise. This problem can be overwhelmed using an anechoic water tank, whose inner surfaces are able to absorb interferent echoes. However, dimensions of a water tank are related to the lowest frequency to be tested: The lower the frequency is, the bigger the water tank dimensions are, when continuous waves are used. This makes the anechoic water tank too large and expensive. Using the pulse technique can allow to calibrate the hydrophone in a smaller water tank.

The following factors should be considered when designing a calibration test in a water tank (Fig. 6.9a): pulse duration (τ ms), which should be short enough to avoid echoes; distance between transducers (Fig. 6.9d), which should be large enough to account for the free-field requirement; and pulse repetition rate, which should vary depending on the reverberation time.

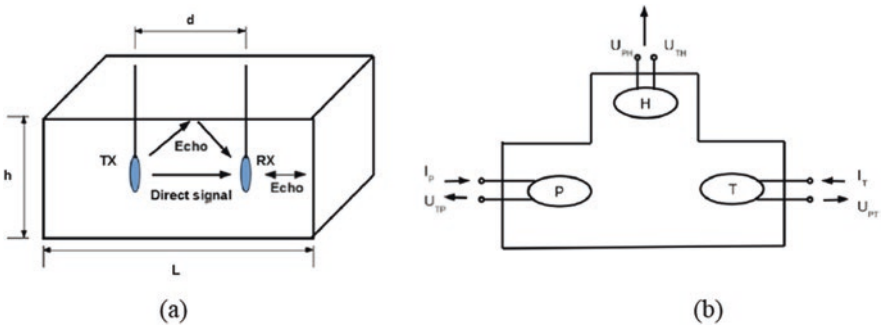

Fig. 6.9 (**a**) Water tank setup for pulse technique; (**b**) measurement reciprocity scheme

Elements involved in determining the reverberation time are frequency, water tank shape and dimensions, and the acoustic features of the inner surface material.

Reciprocity calibration method can be carried out with piezoelectric and electrodynamic (moving coil) hydrophones [31]. In this procedure, three reciprocal transducers are embedded into the water and, thanks to mutual mathematical relationship among their current, voltage, transfer impedance, and sensitivity, each transducer can be calibrated at the same time by only three measurements. Setup and procedure are displayed in Fig. 6.9b. Measurements are as follows: (1) input of current I_P and measurement of U_{PH} at the hydrophone H (under calibration); (2) input of current I_P and measurement of U_{PT} at the reciprocal hydrophone T; (3) input of current IT and measurement of U_{TH} at the hydrophone H (under calibration). At the end of this procedure, parameters of all transducers are known.

The comparison calibration approach uses a hydrophone under test and another calibrated hydrophone as a reference (sensitivity M_R): A projector is used to activate both transducers, and their output voltage is measured. Sensitivity (free-field) is known from the equation $Mx = M_R\, v_x/v_R$. This procedure does not depend on the calibration accuracy of the projector.

6.5 The Unmanned Way to the Acoustic Investigation

The trend of going toward unmanned systems for dangerous, dull, and dirty tasks includes the maritime domain, which is distinguished by specific challenges presented in the previous sections that make underwater robotics very different from air and land counterparts. The maritime domain is hard since the sea is a hostile

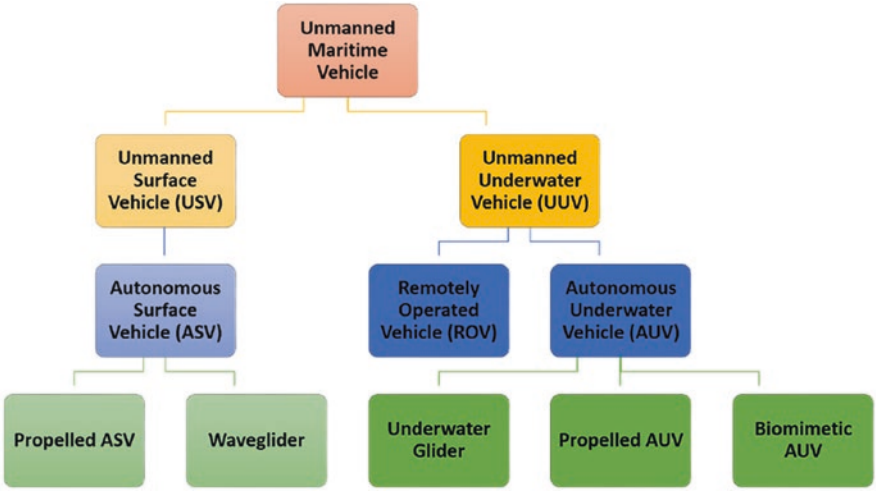

Fig. 6.10 High-level unmanned maritime vehicle classification

environment where unmanned maritime vehicles (UMVs) could operate in (the comparison with space-type operations is not a far-fetched one).

Figure 6.10 illustrates the most commonly agreed general classification of UMVs, recently formalized by the European Defense Agency (EDA) in the context of Unmanned Maritime Systems Program (https:/www.eda.europa.eu/). Every class of vehicle can have different temporal and spatial resolution and can cover different extensions of the operating area with their own methods of movement and power source for its propulsion.

Marine robotics has been an important branch of robotics since its beginning in the early 1970s [32], and nowadays, the world's commercial fleet consisted of almost 100,000 vessels [33]. In particular, fully autonomous robotic systems are envisioned to be able to operate completely independent of humans, using a variety of sensors and communication systems to assess the situation and make decisions and changes during operation [34]. Under the sea surface, the use of remotely operated vehicles (ROVs) and AUVs is rapidly increasing for all the applications presented before, both civil and military.

In general, from a state-of-the-art analysis, it can be stated that four research macro trends are currently aiming at improving UMV operations while integrating them with manned legacy platforms:

- Command, control, and communication systems (C3S) suitable for complex missions;
- Interoperability between heterogeneous assets, both manned and unmanned;
- Reliable autonomous behavior and precise autonomous navigation required for correct georeferencing of the collected data and for effective data processing;
- Improvement of the system endurance and energy capacity onboard the vehicle to carry out long-term missions.

In order to keep the discussion concise, these four themes will be quickly illustrated in the following subsections, underlining their link with underwater acoustic measurements and investigation. Notice that all these scientific and technological challenges are highly interconnected with each other to increase the autonomy of a vehicle and of manned-unmanned system of systems. The overall envisioned goal for achieving greater autonomy in robotic vehicles is to enable longer missions without the need for human intervention. This ability would further allow for longer range missions, enabling exploration of more complex environments (see Fig. 6.11).

6.5.1 Manned-Unmanned C3S and the Security Issue

Despite the proliferation of UMVs, the traditional approach is still mostly centralized nowadays, which means that they must communicate their known position and measurements to a specific C3S when on the surface, which fuses all this information and sends back new waypoints or tracklines [36].

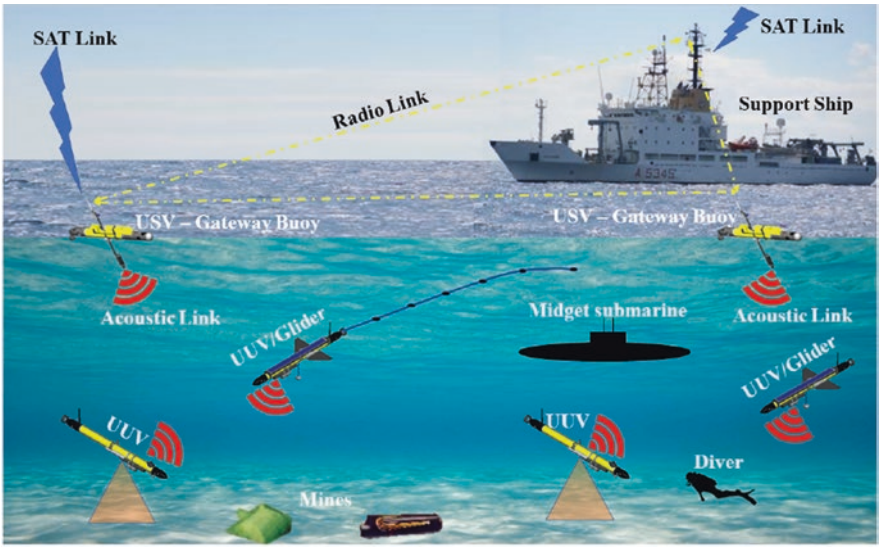

Fig. 6.11 Futuristic underwater surveillance scenario centered on unmanned systems. A manned-unmanned hybrid network composed of several UMVs, each carrying different payloads and performing specific missions, could ensure intersystem communication, heterogeneous data collection, and real-time display onboard processed data. The communication infrastructure between the underwater and the aerial domain is provided by USVs serving as gateways, i.e., fitted with acoustic and radio modems. Figure from [35] (Creative Commons License)

Indeed, the scientific community, military end users, and industry are steadily paying attention to aspects of multivehicle operations and (cyber)security [37] that are increasingly dependent on the capacity of vehicles to intercommunicate.

In this context, recent works have shown how it is possible to exploit the flexibility of the upcoming underwater software-defined open-architecture modem (SDOAM) technology [38] according to network requirements and vehicle mission profiles, considering fundamental channel metrics [39]. For the efficient use of SDOAMs, a cognitive and adaptable approach is also required for the upper layers of the communication protocol stack. These solutions were also successfully implemented on AUVs and tested during sea trials [40].

C3S needs to be correctly designed to perform autonomous collaborative tasks. In addition to developments in underwater acoustics communications, both field-based and theoretical works on UMVs have made substantial progress in collaboration with a range of projects funded by the EU [41–43].

Finally, the inherent broadcast of an underwater acoustic channel presents major cybersecurity risks in sensitive missions, such as autonomous robotic surveillance, since an intruder is easily able to interrupt or intercept communications within such a network. The use of the spread spectrum signals [44] was one of the first approaches to confront this issue. An innovative idea is that of physical protection, where the signal itself can be manipulated to produce confidential keys according to channel

variability [45]. Finally, it is important to point out that a cooperative robotics network can use its own flexibility and adaptability to respond to cyberthreats [46].

6.5.2 Interoperability Between Heterogeneous Assets

Another obstacle to the diffusion and application of underwater robotic platforms is the lack of widely agreed standards that undermine systems' interoperability [47]. Even if software middlewares (e.g., MOOS-IvP or ROS [48]) are becoming increasingly popular in the robotics community to promote the integration of software modules, much needs to be achieved in the field of payload interface and hardware standardization. It should be emphasized that interoperability depends on several interconnected issues, such as the C3S of the robotic system of systems mentioned above [49] is an important review reference to deepen this research topic, providing many recent notable cases of interoperability-focused experimentation.

Finally, in the authors' opinion, the current operating culture is also a brake on interoperability between UMVs. Even if out of the field, human operators are still very engaged in UMV missions; i.e., a point-to-point contact and command line are required and usually implemented. An interoperable system-of-systems of autonomous UMVs would require human intervention only at the supervisory level and only in limited time windows. Acceptance of this principle of operations can be accomplished by a progressive approach, minimizing human oversight step-by-step by creating confidence in the system's efficiency. This system reliability must be accompanied by robust and mature interoperability, allowing autonomous UMVs to reach their maximum capability.

6.5.3 Autonomous Behavior and Navigation

UMVs are outstanding technologies that have revolutionized the method of data collection autonomously in rugged maritime environments. In their early years, launching costly vehicles operating autonomously in a dangerous environment and trusting them to return safely was a genuine act of faith in engineering. Over the last decade, with successful advances in computing capacity, miniaturization of electronic devices, and power supply technologies, UMVs have been suitable for use as testbeds for emerging data processing techniques and advanced navigation algorithms. Indeed, the accuracy of the data obtained during the UMV missions depends heavily on the navigation system's efficiency. UMVs must understand their environment, recognize targets, avoid barriers, autonomously manage, and adjust routes to achieve their goal and navigate safely.

Basic navigational radio frequency signals such as the GPS cannot be received directly by a submerged vehicle, whereas acoustic communications work better

with all the limitations presented in the previous sections. However, the research in this field is advancing at an unprecedented pace due to recent developments [50].

In general, underwater dead-reckoning devices use speed and acceleration measurements to approximate the vehicle's state vector over time. Since these observations are generally noisy, their integration results in an accumulation of error over time known as drift. Inertial navigation system (INS) refers to a system that uses a mixture of measurements and sensors along with filtering algorithms to estimate the vehicle's inertial dynamics in all six degrees of freedom. Higher-performing INS devices usually utilize very precise accelerometers and gyroscopes, preferably fiber-optic gyroscope (FOG), and implement optimal fusion sensor technology. Although with low drift rates, a very reliable INS does not solve the issue of underwater robotic navigation. The longer range missions desired for these vehicles, up to thousands of kilometers, will result in a navigation error unsustainable for sensitive tasks and applications. Furthermore, extremely precise INS systems can be prohibitively costly.

Various methods have been proposed based on incorporating high-performance navigation sensors with powerful fusion sensor algorithms that can maintain navigation error bounded. For example, in [51], a novel underwater navigation technique based on the UKF is described and tested at sea.

For effective long-range and sensor-limited navigation, dead-reckoning systems must be also complemented by acoustic positioning systems (Sect. 6.3). For the interested reader, a hybrid USBL/LBL acoustic navigation system has been extensively demonstrated at sea in [52].

In general, experimental demonstration of navigation methods is frequently reported, but a formal evaluation of vehicle navigation accuracy is difficult to achieve in many situations due to the lack of accurate ground-truth and, in general, of standardized testing procedures and facilities. With this in mind, the authors of [53] deal with the design, deployment, and testing of the easily deployable Underwater Test Range (UTR) for the verification and validation of AUV's autonomous navigation. The UTR performance assessment concept provides a framework for evaluating the AUV's capability to satisfy long-range mission performance criteria in constrained domains, with methodology and analytical techniques generally applicable to any UMV.

6.5.4 Long-Endurance Vehicles for Long-Term Missions

As the autonomy of UMVs increases, the energy efficiency of vehicles is becoming a vital issue. Progress in endurance has so far been related to progress in electrical batteries; new generation batteries allow for more energy storage while at the same time reducing the size and weight of the battery [54]. However, this is not yet enough to ensure mission times of more than a few days. The example of glider actuation shows that a smart design will lead to a much higher efficiency leap [55].

A complementary solution is the recharging of the vehicle's internal batteries during the mission at dedicated off-shore docking stations [56]. This approach poses the significant pitfalls of the suspension of the primary mission of the vehicle to reach the installation and charge the batteries.

On the contrary, environmental energy harvesting is a whole different way to fuel underwater vehicles. Solar energy, ocean thermal energy, and wave energy are massive, clean, and renewable sources, with both advantages and disadvantages (e.g., solar-powered AUVs [57] and the wave glider vehicle [58]).

Wave energy is more promising than solar energy and ocean thermal energy, primarily because it is not bound by time or place. However, wave energy harvesting is a difficult operation, since it is dispersive and chaotic; i.e., the conversion efficiency is very poor due to the energy loss incurred during the energy delivery period.

A more versatile, almost unexplored concept would be to configure the vehicle with a portable unit capable of gathering energy from the surrounding environment. The last line of study involves the WAVE initiative, which was concluded in October 2017 in the framework of the Italian National Research Projects of Military Interest. The final aim of the WAVE project was to research, build, and test a novel method for both wave energy harvesting and low-energy propulsion, to be installed into a generic, modular, torpedo-shaped AUV with hybrid propulsion. A preliminary evaluation of the system was carried out at sea in April 2016, demonstrating its realistic viability [59]. A comprehensive experimental characterization of the module capabilities was then carried out in a controlled setting at the Italian National Research Council—National Institute for Naval Architecture Studies and Experiences (CNR-INSEAN) test tank facility in Rome, Italy [60].

6.6 Conclusion

This chapter provided a picture of sensors, measurements, and analysis in support of the investigation of the undersea world. The attention is mainly focused on how to carefully study and understand the underwater environment and to discover the truth behind it. It is well understood how human beings are directly connected with marine habits; 60% of people live in the first 100 km from the coast, and seawater occupies 71% of the earth's surface, representing one of the natural engines of life in the world (natural climate catalyst). Furthermore, the natural link between human life and the sense of hearing is clearly described: Through technology, innovation became a modern sixth sense confirming how visionary have been the thoughts of the ancient Greek philosopher considering that this perception stimulates passions more than any other involving more factors beyond merely hearing. The water itself helps to match the entire body to perceive acoustics not only through ears.

All marine innovation technologies need to take into account this relation to integrate such principles into its development strategy. The same should be on the emerging autonomous unmanned systems concept to replicate nature, as main

scientific and technological challenges enabling a more efficient sustainable exploration of the seas.

Fundamental concepts of SONAR equations and a survey of typically used methods and technologies for electroacoustic measurements are provided in the chapter.

A new approach to perform acoustic measurements and relevant applications with maritime robots is also presented. Such robots can host onboard a wide variety of sensors that, in addition to the integration with the more traditional manned solutions, makes them a solution able to lower the overall operational costs.

The chapter also provides a short review of the macro trends, documented within the state of the art, of unmanned vehicles aiming at improving their involvement in real operations. In such analysis, the reader is critically guided through the recent bibliography on the topic.

References

1. Shields C (2016) De Anima, Aristotle (4th century BC). Translated with an introduction and commentary of Christopher Shields
2. Branstetter B, Finneran J (2013) Effects of noise on sound perception in marine mammals
3. The Stanford Encyclopedia of Philosophy (2020) The metaphysics research lab, Center for the Study of language and information (CSLI), Stanford University Library of Congress Catalog Data: ISSN 1095-5054
4. Erbe C et al (2019) The effects of ship noise on marine mammals—a review. Front Mar Sci 6:606. https://doi.org/10.3389/fmars.2019.00606
5. Knowlton CW, Morin H, Scowcroft G, Vigness-Raposa K (2016) Discovery of sound in the sea book I: importance of sound. University of Rhode Island Research Foundation, Kingston
6. Morin H, Knowlton CW, Scowcroft G, Vigness-Raposa K (2018) Discovery of sound in the sea book II: science of underwater sound. University of Rhode Island Research Foundation, Kingston
7. Mackenzie KV (1981) Nine-term equation for the sound speed in the oceans. J Acoust Soc Am 70(3):807–812
8. Urick RJ (1983) Principles of underwater sound, 3rd edn. McGraw-Hill, New York
9. Maggi A, Duncan A (2005) Underwater acoustic propagation modelling software-AcTUP v2. 2l. Center for Marine Science and Technology, Curtin University of Technology, Perth
10. Strode C, Mourre B, Rixen M (2012) Decision support using the multistatic tactical planning aid (MSTPA). Ocean Dyn 62(1):161–175
11. Wang L et al (2014) Review of underwater acoustic propagation models. Teddington National Physical Laboratory, Teddington
12. Vives A (2008) Piezoelectric transducers and applications. Springer, Berlin Heidelberg
13. Havelock D, Kuwano S, Vorlaender M (2009) Handbook of signal processing in acoustics. Springer, Berlin Heidelberg. https://doi.org/10.1007/978-0-387-30441-0
14. Waite AD (2002) SONAR for Practising engineers. Wiley, London
15. Lurton X (2010) An introduction to underwater acoustics. Springer, Berlin Heidelberg
16. Matos A, Cruz N, Martins A, Pereira FL (1999) Development and implementation of a low-cost LBL navigation system for an AUV. In: Oceans 1999 MTS/IEEE, Seattle
17. Stergiopoulos S, Pan X, Sidky E (2003) Advanced signal processing handbook: theory and implementation for radar, SONAR, and medical imaging real-time systems. Med Phys 30:995. https://doi.org/10.1118/1.1569271

18. Nardone S, Lindgren AG, Gong K (1984) Fundamental properties and performance of conventional bearings-only target motion analysis. IEEE Trans Autom Control 29(9):775–787
19. Nardone SC, Aidala VJ (1981) Observability criteria for bearings-only target motion analysis. IEEE Trans Aerosp Electron Syst 2:162–166
20. Aidala VJ (1979) Kalman filter behavior in bearings-only tracking applications. IEEE Trans Aerosp Electron Syst 1:29–39
21. Aidala VJ, Hammel SE (1983) Utilization of modified polar coordinates for bearings-only tracking. IEEE Trans Automat Control 28:283–294
22. Li P, Zhang X, Zhang W (2019) Direction of arrival estimation using two hydrophones: frequency diversity technique for passive SONAR. Sensors 19:9
23. Li X, Deng Z, Rauchenstein L, Carlson T (2016) Contributed review: source-localization algorithms and applications using time of arrival and time difference of arrival measurements. Rev Sci Instrum 87:4
24. Gebbie J, Siderius M, McCargar R, Allen JS III, Pusey G (2013) Localization of a noisy broadband surface target using time differences of multipath arrivals. J Acoust Soc Am 134(1):EL77–EL83
25. Dubrovinskaya E, Nissen I, Casari P (2016) On the accuracy of passive multipath-aided underwater range estimation. In 2016 IEEE third underwater communications and networking conference (UComms), IEEE, Lerici
26. Trees V, Harry L (2001) Detection, estimation, and modulation theory-part l-detection, estimation, and linear modulation theory. Wiley, New York
27. Kiran R, Verma AK, Naidu GA (2012) Application of cepstrum in passive sonar. Int J Eng Res Appl 2:3
28. Das A, Kumar A, Bahl R (2013) Marine vessel classification based on passive sonar data: the cepstrum-based approach. IET Radar, Sonar Navig 7(1):87–93
29. Ridolfi A, Franchi M, Zacchini L (2018) A forward-looking sonar-based system for underwater mosaicing and acoustic odometry. IEEE/OES AUV, Porto
30. Turkmen S, Atlar M, Sasaki N (1997) Full-scale measurements of underwater radiated noise of a catamaran research vessel. Measurements 1141:16–13
31. Bobber RJ (1970) Underwater electroacoustic measurements. Naval Research Laboratory, U.S. Government Printing Office, Washington
32. Zhang F, Marani G, Smith RN, Choi HT (2015) Future trends in marine robotics. IEEE Robotics Autom Mag 22:14
33. United Nations (2018) Conference on trade and development. Rev Maritime Transp 2018:5
34. Parasuraman R, Sheridan TB, Wickens CD (2000) A model for types and levels of human interaction with automation. IEEE Trans Syst Man Cybern 30(3):286–297
35. Terracciano D, Bazzarello L, Caiti A et al (2020) Marine robots for underwater surveillance. Current Robotic Rep 1:159
36. Ferri G, Cococcioni M, Álvarez A (2016) Mission planning and decision support for underwater glider networks: a sampling on-demand approach. Sensors 16(1):28
37. Caiti A, Munafò A, Petroccia R (2020) Underwater communication. In: Ang M, Khatib O, Siciliano B (eds) Encyclopedia of robotics. Springer, Berlin, Heidelberg
38. Potter J, et al (2014) Software defined open architecture modem development at CMRE. In: 2014 Underwater communications and networking (UComms), Sestri Levante
39. Pelekanakis K, Baggeroer AB (2011) Exploiting space–time–frequency diversity with MIMO–OFDM for underwater acoustic communications. IEEE J Ocean Eng 36:502
40. Petroccia R et al (2018) Development of a software-defined and cognitive communications architecture at CMRE. OCEANS 2018 MTS/IEEE, Charleston
41. Birk A, et al (2011) The CO3AUVs (cooperative cognitive control for autonomous underwater vehicles) project: overview and current progresses, in OCEANS 2011 IEEE, Madrid
42. Abreu P et al (2016) Widely scalable mobile underwater SONAR technology: an overview of the H2020 WiMUST project. Mar Technol Soc J 50:42–53

43. Kalwa J et al (2016) The European project MORPH: distributed UUV systems for multimodal, 3D underwater surveys. Mar Technol Soc J 50:26–41
44. Park JH (1986) LPI techniques in the underwater acoustic channel. MILCOM1986 - IEEE military communications conference: communications-computers: teamed for the 90's, Monterey
45. Huang Y, Zhou S, Shi Z, Lai L (2016) Channel frequency response-based secret key generation in underwater acoustic systems. IEEE Trans Wireless Commun 15:5875
46. Munafò A, Sliwka J, Alves J (2015) Dynamic placement of a constellation of surface buoys for enhanced underwater positioning. OCEANS 2015 - Genova, Genoa
47. Ferri G et al (2017) Cooperative robotic networks for underwater surveillance: an overview. IET Radar Sonar Navig 11(12):1740–1761
48. Li X, Martínez JF, Rodríguez-Molina J, Martínez NL (2016) A survey on intermediation architectures for underwater robotics. Sensors 16(2):190
49. Costanzi R et al (2020) Interoperability among unmanned maritime vehicles: review and first in-field experimentation. Front Robotics and AI 7:14
50. Paull L, Saeedi S, Seto M, Li H (2014) AUV navigation and localization: a review. IEEE J Ocean Eng 39(1):131–149
51. Allotta B et al (2016) A new AUV navigation system exploiting unscented Kalman filter. Ocean Eng 113:121–132
52. Caiti A et al (2014) Experimental results with a mixed USBL/LBL system for AUV navigation. In: 2014 underwater communications and networking (UComms). IEEE, pp. 1–4
53. Costanzi R et al (2018) Towards an autonomous underwater vehicles test range: at-sea experimentation of bearing-only tracking algorithms. Annu Rev Control 46
54. Wang X et al (2012) Reviews of power systems and environmental energy conversion for unmanned underwater vehicles. Renew Sustain Energy Rev 16(4)
55. Glenn S et al (2011) The trans-Atlantic Slocum glider expeditions: a catalyst for undergraduate participation in ocean science and technology. Mar Technol Soc J 45(1):52–67
56. Hobson BW et al (2007) The development and ocean testing of an AUV docking station for a 21" AUV. In: OCEANS 2007 MTS/IEEE. Vancouver
57. Blidberg D, et al (2005) The SAUV II (solar powered AUV) test results 2004. In: OCEANS 2005 MTS/IEEE
58. Manley J, Willcox S (2010) The wave glider: A persistent platform for ocean science. In: OCEANS 2010 MTS/IEEE, Sydney
59. Fenucci D et al. (2016) WAVE: A wave energy recovery module for long endurance gliders and AUVs. In: OCEANS 2016 MTS/IEEE, Monterey
60. Caiti A et al (2018) Wave module for hybrid oceanographic autonomous underwater vehicle–prototype experimental validation and characterisation. In: International ship control systems symposium (iSCSS), Glasgow

Chapter 7
Measurement of Sea Waves

Vincenzo Piscopo, Giovanni Battista Rossi, Francesco Crenna, Salvatore Gaglione, Antonio Scamardella, Marco Uttieri, and Enrico Zambianchi

Contents

Abstract This chapter focuses on the analysis and measurement of sea waves. After a brief review about the generation and propagation of ocean waves, the most common wave spectra are briefly described. Subsequently, the spectral analysis of sea waves is discussed focusing on the most promising techniques that allow obtaining the sea state parameters starting from the wave elevation time history. Finally, two techniques useful to measure the sea wave parameters are outlined. The former is based on the reverse analysis of the motions a ship advancing at a constant speed in a seaway, and the latter focuses on the employment of coastal high-frequency radars.

V. Piscopo (✉) · S. Gaglione · A. Scamardella · E. Zambianchi
Department of Science and Technology, University of Naples "Parthenope", Centro Direzionale, Isola C4, Naples, Italy
e-mail: vincenzo.piscopo@uniparthenope.it; salvatore.gaglione@uniparthenope.it; antonio.scamardella@uniparthenope.it; enrico.zambianchi@uniparthenope.it

G. B. Rossi · F. Crenna
Department of Mechanical, Energy, Management and Transportation Engineering, University of Genova, Genoa, Italy
e-mail: g.b.rossi@unige.it; francesco.crenna@unige.it

M. Uttieri
Department of Integrative Marine Ecology, Stazione Zoologica Anton Dohrn, Naples, Italy
e-mail: marco.uttieri@szn.it

P. Daponte et al. (eds.), *Measurement for the Sea*, Springer Series in Measurement Science and Technology,
https://doi.org/10.1007/978-3-030-82024-4_7

7.1 Modelling and Measuring of Sea Waves

7.1.1 Ocean Waves: A Brief Review

Ocean waves are generated by the interaction of wind and the water surface, based on two main physical processes, namely the friction between air and water and the local pressure field associated with the wind blowing over the wave surface [1]. In this respect, even if the mechanism that is on the basis of the energy transfer from wind to sea is not completely satisfactory, it is reasonable to assume that a storm wave system is the sum of many local interactions between wind and water distributed over space and time. Hence, during a storm, ocean waves grow with time depending on two main parameters, namely the fetch and duration. The former is the reference dimension of the storm area where the wind speed is steady, while the latter is the time interval between the storm inception and decay. Subsequently, ocean waves propagate from the storm area with a given celerity, depending on the water depth and the wavelength, namely the distance between two consecutive crests of the ocean wave. Indeed, if the wave amplitudes are small, if compared with the wavelength, the principle of linear superposition can be applied for the propagation and dispersion of the wave systems outside the storm area. In this respect, if wind speed is steady for a sufficiently long period and the fetch length is wide, ocean waves take on a stable structure, which is named fully developed sea state condition. On the contrary, if the fetch length or the storm duration is not sufficient to achieve a stable wave generation, the sea state condition is partly developed. The ocean waves inside the storm area are obtained by the superposition of a very large number of separate random and independent contributions, with different celerity and wavelength, that resemble a short-crested sea state condition. Anyway, as previously said, ocean waves propagate outside the storm area at different velocities, as longer waves travel faster than the shorter ones, producing at a great distance from the storm area a long-crested sea state condition, generally named swell.

In the last decades, a variety of theories have been developed to properly describe the wave kinematics [2]. The simplest and most applied wave model is the Airy theory, according to which the wave has the form of a sine curve and the free surface profile, representing the elevation as regards the undisturbed sea water level, is written in the following form:

$$\varsigma(t) = \varsigma_0 \cos\left[k\left(x - v_c t\right)\right] \tag{7.1}$$

where ς_0 is the wave amplitude, k is the wave number, connected to the wave celerity v_c by the equation $v_c^2 = g/k$ valid for the deepwater condition, and x is the distance of the measurement point, as regards a given reference system. The wave number and celerity are also connected to the wave circular frequency ω by the condition $\omega = kv_c$ valid for deepwater. Further details about the Airy wave theory are available in Ref. [1, 2].

7.1.2 Wave Spectra

Ocean waves are irregular and random in shape, height, length, and speed of propagation, so as they need to be described by random models based on frequency-dependent wave spectra, with given significant wave height, peak period, and shape function [3]. In this respect, real sea state conditions are generally obtained by the superposition of wind sea and swell components. The former is generated by local wind, while the latter has no relationship with the in situ met-ocean conditions and comes from areas located far from the measurement point.

The first pioneering studies on wave spectra were performed in the 50s by Neumann [4], Roll and Fisher [5], and Darbyshire [6] that developed the first frequency-dependent analytical formulations for single-peaked wave spectra. Nevertheless, these theoretical formulations are nowadays substantially unused as more refined wave spectra were developed for both fully and partly developed sea state conditions. Particularly, in 1964, Pierson-Moskowitz [7] provided a new analytical wave spectrum for fully developed wind seas, based on the analysis of a large amount of data collected in the Atlantic Ocean. The Pierson–Moskowitz (PM) wave spectrum S_{PM} is currently embodied for the design of ships and offshores structures, located in sea areas where fully developed sea state conditions are expected to occur as follows:

$$S_{PM}(\omega) = \frac{5}{16} H_s^2 \omega_p^4 \omega^{-5} \exp\left(-\frac{5}{4} \left(\frac{\omega}{\omega_p} \right)^{-4} \right) \tag{7.2}$$

having denoted by ω the circular wave frequency, by $\omega_p = 2\pi/T_p$ the spectral peak frequency depending, in turn, by the wave peak period T_p, and by H_s the significant wave height. In the subsequent years, an extensive wave measurement programme, also known as Joint North Sea Wave Project (JONSWAP), was carried out in the North Sea to derive a new analytical formulation, representative of wind-generated seas with limited fetch conditions. The JONSWAP spectrum S_J is currently formulated as a modification of the PM spectrum for a developing sea state in a fetch limited condition (7.3):

$$S_J(\omega) = A_\gamma S_{PM}(\omega) \gamma^{\exp\left(-0.5 \left(\frac{\omega - \omega_p}{\sigma \omega_p} \right)^2 \right)} \tag{7.3}$$

where γ is the nondimensional peak shape parameter, $A_\gamma = 1 - 0.287\ ln\ (\gamma)$ is the normalizing factor, and σ is the spectral width parameter, generally assumed equal to 0.07 and 0.09 if $\omega \leq \omega_p$ and $\omega > \omega_p$, respectively. The peak shape parameter mainly depends on the fetch length, and it is generally taken equal to 3.3 for the North Sea area. Besides, the condition $\gamma = 1$ resembles the fully developed sea state, corresponding to the PM wave spectrum. Fig. 7.1a reports a typical example of PM and JONSWAP spectra with H_s =4.0 m and T_p = 8.0 s.

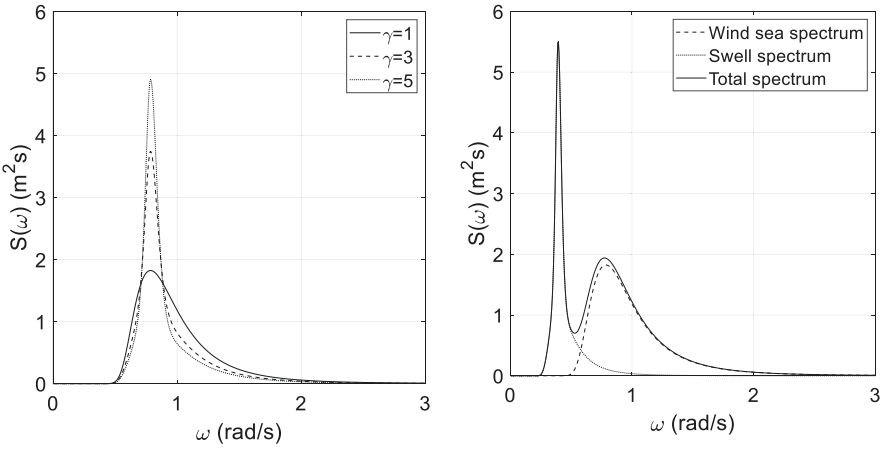

Fig. 7.1 Example of single-peak (**a**) and double-peak (**b**) spectra

In the same years, further studies were performed in order to develop theoretical models suitable for double-peaked wave spectra, obtained by combining wind sea and swell components. In this respect, in the 70s, Ochi and Hubble [8] provided a general spectral formulation, obtained as the sum of two gamma distributions, each one with the same three parameters of the JONWAP spectrum. Nevertheless, a simplified approach can be embodied, so as the double-peaked wave spectrum is regarded as the sum of two uncorrelated single-peaked wave spectra, representative of the wind sea S_{wind} and swell S_{swell} components, respectively, as follows:

$$S(\omega) = S_{\text{wind}}(\omega) + S_{\text{swell}}(\omega) \tag{7.4}$$

In Eq. (7.4), the wind sea spectrum is generally described by Eq. (7.2 and 7.3), while the swell component can be described by either a generalized JONSWAP spectrum or a normal function [9]. Figure 7.1b provides an example of double-peaked wave spectrum. The wind sea component has the same values as the fully developed PM spectrum depicted in Fig. 7.1a, while the swell spectrum is characterized by the following values: H_s =3.0 m and T_p = 16.0 s and γ = 5.0. By Fig. 7.1b, it is gathered that the swell component is generally much more peaked if compared with the wind sea one, as it is representative of past storm conditions, located quite far from the measurement point. Assuming a specific spectrum, sea wave observation can be simulated by generating times series in agreement with assumed spectrum, according to:

$$\varsigma(t) = \sum_{i=1}^{n} \sqrt{2S(f_i)df_i}\cos\left[2\pi f_i t + \varphi_i\right] \tag{7.5}$$

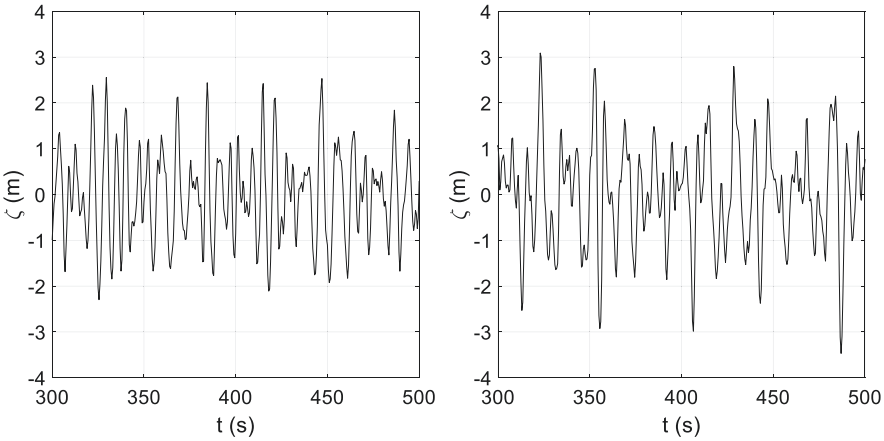

Fig. 7.2 Simulated sea wave elevation for the spectra of Fig. 7.1a, b

after partitioning the theoretical wave spectrum into a discrete set of components. In Eq. (7.5), ς denotes the wave amplitude, while f_i is the ith wave frequency component, with uniform random phase φ_i in the interval $[0,2\pi]$. Example of simulated time series, corresponding to the spectra depicted in Fig. 7.1, is shown in Fig. 7.2. In the case of Fig. 7.2b, the presence of low-frequency components, related to the swell phenomenon, can be noted.

7.1.3 Sea Wave Monitoring Techniques

Different sea wave monitoring techniques are available to measure the wave elevation and monitor the sea state condition. The most applied method involves the wave buoys that are generally connected in a network, whose working principle has been discussed in Chap. 2. Besides, different techniques are available to measure the sea state condition. Particularly, the two different techniques are discussed, in Subsections 7.3 and 7.4, respectively. The former is based on a reverse analysis technique of the motion of a floating buoy, namely a ship, which advances at a constant speed in a seaway. The latter instead involves one of more high-frequency wave radars, generally located along the coastline or, in some cases, being part of the measurement system installed onboard a ship.

7.2 Spectral Analysis of Sea Waves

7.2.1 Spectrum Estimation

Once an elevation record has been obtained, for example, by an inertial sensor mounted on a wave buoy, the useful information is best expressed by the estimated wave spectrum or by the estimated sea state parameters. Since the latter are typically obtained by the spectrum, spectrum estimation plays a key role in wave monitoring.

Along the years, several estimation methods have been proposed that can be parsed in two main groups, namely nonparametrical and parametrical [10]. The seminal idea under the first group was Schuster's "periodogram" [11], that is, the square of the Fourier transform (FT) of the series of observations, normalized in respect of the observation duration, T_0. Originally proposed for identified hidden periodicities in noisy signals, the periodogram constitutes a rough estimate of the power spectral density (PSD), since it is both biased and it has a large variance that does not decrease even by increasing the observation time. Yet, the basic periodogram can be improved both to reduce bias, which is usually accomplished by data tapering or prewhitening, and by reducing variance, by averaging in the time domain or smoothing in the frequency domain. An important method that moves along these lines was proposed by Welch [12] that will be discussed in the following.

Another important method was proposed by Thomson [13], whose basic idea was to taper the data with an orthonormal series of tapers, each of which highlighting different and complementary aspects of the signal, hence denomination of multitaper method (MTM).

Lastly, an approach alternative to the above nonparametrical methods is called parametrical and consists of considering parametrical models of the observed time series, such as the autoregressive (AR) or the autoregressive-moving average (ARMA) ones [14]. Once such a model has been fitted to the observations, the PSD can be obtained analytically. For brevity, we will not deal with these methods here.

Let us now discuss Welch's method in greater detail. The first step of the analysis procedure consists in parsing the overall data record, having an observation duration T, in n smaller segments of duration T_0, with partial overlap, typically from 20% to 50%. Each segment is pretreated by multiplying it by a smooth observation window, to limit the edge effect due to the *cutting* of the time series at the edges of the segment. (Such effect consists, in the spectral domain, in some *spectral leakage*. This effect can be simply described as follows. Consider a discrete spectrum: in consequence of the sharp truncation of the signal at the edges of the considered segment, part of the energy associated with each spectral component spreads around that component, causing not only an inexact estimation of the energy associated with it, but also some smearing of the components close to it, which is even more annoying. For a continuous spectrum, the effect is similar. Since this is an edge effect, it is intuitive that tapering can reduce it since it weights decreasingly data as long as they approach the edges.) Then, for each segment, the (modified) periodogram is

calculated and the spectrum is finally obtained by averaging over such periodograms. Therefore, spectral leakage is reduced by tapering and variance is reduced by averaging. Let us now consider the procedure in greater detail. Let us then denote the series of measurements by $x_i = x(i\Delta t)$, where Δt is the sampling interval, and $i = 1, \ldots N$, with $T = N\Delta t$, and $T_0 = N_0\Delta t$. Let $w_1,\ldots,w_{N_0}$ be a data taper, then the modified periodogram for the l th segment is as follows:

$$\hat{S}_l(f) = \Delta t \left| \sum_{i=1}^{N_0} w_i x_{i+l-1} e^{-j2\pi fi\Delta t} \right|^2 \tag{7.6}$$

where j is the imaginary unit. The spectral estimator is then:

$$\hat{S}(f) = \frac{1}{n} \sum_{k=0}^{n-1} \hat{S}_{km+1}(f) \tag{7.7}$$

where n is the number of segments and m is an integer-valued shift factor, satisfying $0 < m \leq N_0$ and $m(n-1) = N - N_0$.

To apply the method, a proper choice of the analysis features is required. The total observation time, T, is typically fixed by general experimentation constraint. The remaining features include the kind of taper, the degree of overlap, and the duration of individual segments, T_0. The goal is to optimize the main "metrological" characteristics of the method, namely its spectral resolution and its variance, or standard deviation. The spectral resolution can be understood as the capability of properly representing spectral components, i.e., peaks or, more generally, local maxima, in terms of localization of the peak/maximum and of restitution of its bandwidth. Spectral resolution is (inversely) related to the effective bandwidth, in that a large effective bandwidth implies a poor spectral resolution. Variance instead is a measure of statistical (in)stability. More practical a high variance results in a "noisy" spectrum. For example, in the spectrum of Fig. 7.2, there are two peaks, physically corresponding to the two superimposed sea states, the swell peak is narrowband, and the wind one is broadband. Spectral resolution will be more critical for the former, variance for the latter. Coming back to Welch's method, the choice of the degree of overlap is related to the kind of taper adopted, in that the smoother the taper is, the higher the degree of overlap can be adopted, which results in a larger number of segments, with a reduction of the variance. On the other hand, the smoother the window is, the larger its bandwidth is and, consequently, the worse its spectral resolution results. Welch suggested that a 50% overlap, with a cosine (Hanning) window, should be adopted, as it is carried out in current analysis. Concerning the effective bandwidth, for Welch's method, it can be expressed as $\Delta f_e = \alpha_w T_0^{-1}$ where α_w is a factor that depends upon the kind of the selected taper and on the way bandwidth is defined. In the case of the Hanning window and considering a half-power bandwidth, we obtain $\alpha_w = 1.44$. Concerning the variance of the estimator, with a 50% overlap, a relative standard uncertainty (standard deviation) $u_S(f)/S(f) = \sqrt{(11/18)N_0N^{-1}}$ can be assumed, where $S(f)$ is the PSD and

$u_S(f)$ is the absolute standard uncertainty. An example of the application of design of the estimator will be provided in the next subsection.

Let us now briefly consider Thomson's multitaper approach. Basically, this method generalizes the tapering issue by adopting multiple orthogonal tapers, with the aim of recovering information that may be lost when using a single taper. The estimator is the average of K direct spectral estimators, each acting on the whole data record (rather than on a signal segment, as happens in Welch method) and applying a different taper. Each (partial) estimator is defined by:

$$\hat{S}_k(f) = \Delta t \left| \sum_{i=1}^{N} h_{i,k} x_{i+l-1} e^{-j2\pi fi\Delta t} \right|^2 \tag{7.8}$$

where $h_{i,k}$ is the k th data taper, usually chosen as the k th discrete prolate spheroidal sequence with parameter W, where $2W$ is the normalized bandwidth of the tapers, i.e., the bandwidth for $\Delta t = 1$ s. The final estimator is thus:

$$\hat{S}(f) = \frac{1}{K} \sum_{k=0}^{K-1} \hat{S}_k(f) \tag{7.9}$$

where K is typically chosen to be equal to $2NW - 1$. The metrological characteristics of the procedure can be kept under control by assuming an effective bandwidth $\Delta f_e = 2W/\Delta t$ (Hz) and considering that the estimator is approximately equal in distribution to $S(f)\chi^2_{2K}/2K$, which yields a relative standard uncertainty equal to $K^{-\frac{1}{2}}$. Therefore, with respect to Welch method, there is here much less arbitrariness, since, for a fixed observation time, T, the only parameter to be chosen is the half-bandwidth W, which influences both spectral resolution and relative standard uncertainty. Again, examples of application will be provided in the next section.

7.2.2 *Spectral Analysis of Simulated Sea Wave Measurement Data*

The performance of different methods of spectrum estimation can be compared by simulating observations, i.e., signals, from a given PSD, and applying to them and comparing the results, keeping the assumed spectrum as the reference one. Form a metrological standpoint, spectrum measurement can be seen as a kind of indirect dynamic measurement, developed in two steps: the measurement of the time history of the phenomenon and the processing of the acquired signal by a spectrum estimation procedure [15]. Dynamic calibration of the overall measurement process is often quite difficult. Therefore, it makes sense to calibrate the two parts separately. In this perspective, assessing the performance of the spectrum estimator by simulated signals of the same kind as those that are likely to be encountered in actual application may be seen as a (partial) dynamic calibration.

To illustrate this procedure, signals from both the single-peak spectrum of Fig. 7.1a [16] and the double-peak spectrum of Fig. 7.1b, were generated, assuming a sampling rate of $f_s = 2.0$ Hz [17], and a total duration $T = 3600\ s$, and both Welch's and Thomson's spectra were calculated. For doing that, the design considerations presented above must be applied. In the case of the single-peak spectrum, an optimum trade-off between spectral resolution and relative uncertainty of the spectrum estimate was reached by assuming a duration of the observation window, $T_0 = 120$ s = 2 min, which corresponds to an effective bandwidth $\Delta f_e = 0.012$ Hz and to a relative standard uncertainty $u_S(f)/S(f) = 0.14$. The resulting spectrum is presented in Fig. 7.3a. For applying the Thomson method, the same effective bandwidth was selected, which yielded a design parameter $NW = 21.6$, corresponding to a relative standard uncertainty $u_S(f)/S(f) = 0.15$. The corresponding spectrum is reported in Fig. Fig. 7.3b.

In the case of the double-peak spectrum, a better spectral resolution is required, for the presence of peaky swell component. Therefore, with Welch's method, a larger observation duration was selected, namely $T_0 = 360\ s = 6\ min$, corresponding to an effective bandwidth $\Delta f_e = 0.0o4\ Hz$ and to a relative standard uncertainty $u_S(f)/S(f) = 0.25$. The result is shown Fig. 7.1a.

Again, for the multitaper approach, the same effective bandwidth was selected, resulting in a design parameter $NW = 7.2$, corresponding to a relative standard uncertainty $u_S(f)/S(f) = 0.27$. The corresponding spectrum is reported in Fig. 7.4b.

It appears that both methods provide a consistent estimation of the spectra, yet Thomson method, despite its "noisy" appearance, provides a better reconstruction of the "shape" of the spectrum, which is what really matters. This is reflected also by the recovering of the sea state parameters, as it will be briefly outlined in the next subsection.

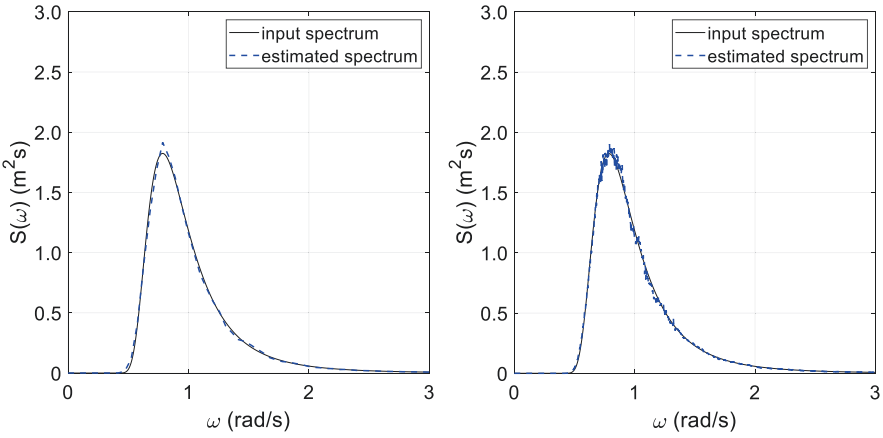

(a) Welch method (b) Thomson method

Fig. 7.3 Spectrum estimation of a signal generated from the spectrum of Fig. 7.1a: (**a**) Welch method, (**b**) Thomson method

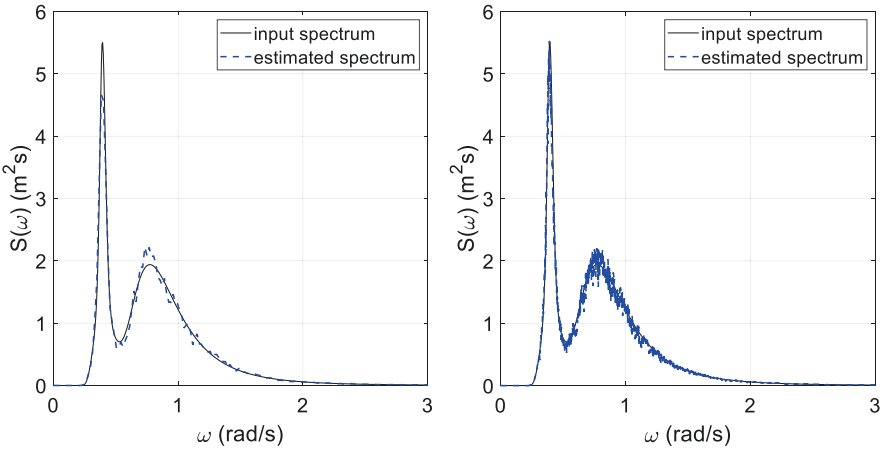

(a) Welch method (b) Thomson method

Fig. 7.4 Spectrum estimation of a signal generated from the spectrum of Fig. 7.1b: (**a**) Welch method, (**b**) Thomson method

7.2.3 Estimation of Sea State Parameters from Estimated Spectra

The sea state parameters, namely the significant wave height H_s, the wave peak period T_p, and the peak enhancement factor γ, are determined by the nonlinear least square method (NLSM), embodied by Rossi et al. [16] and generalized [17] to fit double-peak wave spectra, obtained by combined wind sea and swell components. In the general, bimodal case, the fitted wave spectrum is assessed by a two-step procedure. Firstly, the peak frequencies, corresponding to the swell and wind wave components, are preliminarily detected, as they correspond to the relative maxima of the smoothed estimated spectrum. Then, the remaining spectral parameters, namely the significant wave height and the peak enhancement factor of the two components, are obtained by the NLSM, based on the iterative trust-region-reflective algorithm and the interior-reflective Newton method [18]. Particularly, it allows detecting the unknown parameters by iteratively solving a large set of linear equations by the method of the preconditioned conjugate gradients.

The application of this method to the spectra presented in the previous subsection is presented in Tables 7.1 and 7.2.

It can be noted that both methods yield consistent estimations, yet Thomson methods prove to be more accurate, especially for the estimation of the peak enhancement factor of the swell component.

Table 7.1 Assessment of sea state parameters through the two spectrum estimation methods (JONSWAP)

Parameter	Input wave spectrum	Method	
		Welch	Thomson
H_s (m)	4.00	3.99	4.01
T_p (s)	8.00	8.00	7.94
γ	1.00	1.00	1.00

Table 7.2 Assessment of sea state parameters through the two spectrum estimation methods (bimodal)

Parameter	Input wave spectrum		Welch		Thomson	
	Wind wave	Swell	Wind wave	Swell	Wind wave	Swell
H_s (m)	4.00	3.00	4.01	2.99	4.01	2.95
T_p (s)	8.00	16.00	8.00	15.65	8.22	16.06
γ	1.00	5.00	1.00	4.00	1.00	4.77

7.3 Sea Wave Monitoring Based on Ship Motion Measurement and Analysis

7.3.1 A Brief Theoretical Review

A possible way to reliably monitor the sea waves is based on the measurement and analysis of ship motions in a seaway. This topic was widely investigated since the 70s when Takekuma and Takahashi [19] developed the first reverse analysis technique to detect the wave spectrum parameters based on the analysis of ship motions without forward speed. Subsequently, a variety of attempts were performed to include the ship speed and, consequently, the Doppler shift, for vessels advancing in head and bow seas [20, 21] and more recently in quartering and following seas [22]. Based on these pioneering works, in the last two decades, the interest of the scientific community on this research topic grew fast, as proved by the variety of research activities carried out throughout the world [23–26].

The wave spectrum resembling procedures are generally based on the frequency-domain analysis of ship motions, based on the following main assumptions [27]: (1) the ship motions are linear with the incident wave amplitude; (2) the incoming waves resemble an ergodic random process [28], so as all sea state parameters are stationary, in a stochastic sense, in a short time interval; and (3) the ship speed and course are kept constant during the ship motion measurements. Hence, the wave spectrum is subsequently detected by parametric or nonparametric modelling techniques. In the first case, the main sea states parameters are obtained assuming a priori a certain analytical formulation of the wave spectrum in order to subsequently detect the best-fit parameters. In the latter case, instead, the spectral shape is not specified a priori, and the wave spectrum is detected by the energy equivalence principle, so equating the 0th-order spectral moments of

the measured and resembled wave spectra. Only few attempts have been performed to detect the sea state parameters by time-domain techniques mainly based on Kalman filtering [29, 30], mainly due to the high numerical effort required to detect the unknown sea state parameters. In this case, in fact, the ship motion measurements are converted into the wave elevation time history, based on the ship response amplitude operators (RAOs) that, in any case, need to be preliminarily assessed in the frequency domain.

As concerns the selection of the ship motions embodied in the wave spectrum resembling procedure, different attempts and selections were embodied in the past, combining single and multiple motions with different weighting factors, in order to apply a robust sea state measuring procedure. Based on the main outcomes of past research activities, heave and pitch motions seem to be the most promising selection to detect the sea state parameters, eventually combined with sway [31] or roll [32] motions if the prevailing wave direction is not known a priori. In the following, the parametric procedure, recently developed by Piscopo et al. [28], is briefly discussed.

7.3.2 *Assessment of Sea State Parameters*

The sea state assessment procedure outlined in [28] is based on two subsequent steps. At the first step of the procedure, the wave peak period and the peak shape parameter are determined by an iterative procedure that allows detecting the best-fit parameters of the JONSWAP spectrum, as depicted in Fig. 7.5.

Particularly, at the first step the heave S_{ξ_3} and pitch motion S_{ξ_5} motion spectra are preliminarily assessed in the encounter frequency domain ω_e by spectral analysis of ship motions recorded by the onboard measuring equipment. In this respect, the heading angle between the vessel route and the prevailing sea waves is obtained by independent systems, such as wave radars. Hence, the unknown wave spectrum parameters, namely the wave peak period and the peak shape parameter, are iteratively varied to maximize the following parameter:

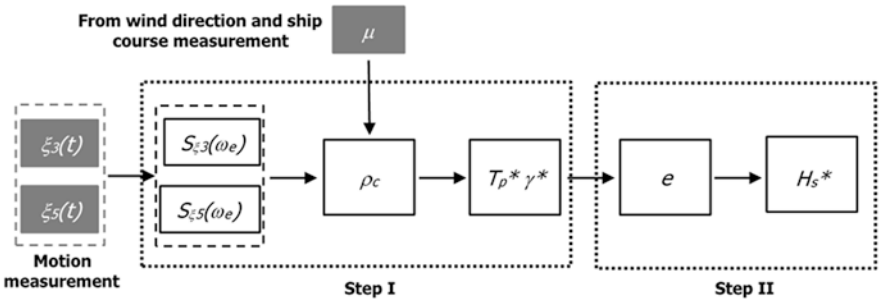

Fig. 7.5 Flow chart of the two-step iterative procedure [28], reprinted by permission

$$\varrho_c\left(T_p^i,\gamma^j\right)=\sqrt{\sum_{k=3,5}\left[\rho\left(\frac{S_{\xi_k}\left(\boldsymbol{\omega_e}\right)}{\int_0^\infty S_{\xi_k}\left(\omega_e\right)d\omega_e},\frac{\left|H_k\left(\boldsymbol{\omega_e}\right)\right|^2 S_J\left(H_s,T_p^i,\gamma^j,\boldsymbol{\omega_e}\right)}{\int_0^\infty\left|H_k\left(\omega_e\right)\right|^2 S_J\left(H_s,T_p^i,\gamma^j,\omega_e\right)d\omega_e}\right)\right]^2} \tag{7.10}$$

having denoted by ρ the Pearson correlation coefficient and by H_k the complex ship motion transfer function for heave (3) and pitch (5) motions. At the second step of the procedure, the significant wave height is assessed based on single or combined heave and pitch motion:

$$H_s^*=\begin{cases}\dfrac{\xi_{5,s}}{4\sqrt{\int_0^\infty\left|H_5\left(\omega_e\right)\right|^2 S_J\left(1,T_p^*,\gamma^*,\omega_e\right)d\omega_e}} \; if\; e\le 1/2\\ \sqrt{\prod_{k=3,5}\dfrac{\xi_{k,s}}{4\sqrt{\int_0^\infty\left|H_k\left(\omega_e\right)\right|^2 S_J\left(1,T_p^*,\gamma^*,\omega_e\right)d\omega_e}}} \; if\; 1/2<e<2\\ \dfrac{\xi_{3,s}}{4\sqrt{\int_0^\infty\left|H_3\left(\omega_e\right)\right|^2 S_J\left(1,T_p^*,\gamma^*,\omega_e\right)d\omega_e}} \; if\; e\ge 2\end{cases} \tag{7.11}$$

having denoted by e the ship kinetic parameter:

$$e=\frac{\left(\Delta+A_{33,\infty}\right)\ddot{\xi}_{3,s}^2}{\left(I_{55}+A_{55,\infty}\right)\ddot{\xi}_{5,s}^2} \tag{7.12}$$

In Eq. (7.12), Δ (I_{55}) denotes the ship displacement (pitch moment of inertia), $A_{33,\infty}$ ($A_{55,\infty}$) is the heave (pitch) added mass at infinite frequency and $\ddot{\xi}_{3,s}$ ($\ddot{\xi}_{5,s}$) is the heave (pitch) motion significant velocity, as obtained by the onboard measurements.

7.3.3 Assessment of Sea State Parameters

The procedure outlined in Subsect. 7.3.2 allows efficiently measuring the sea state parameters of single peaked wave spectra, as proved by the numerical investigation reported in the benchmark study performed by Piscopo et al. [28] with reference to the well-known S175 containership [33, 34]. Particularly, the heave and pitch motion time histories, obtained by time-domain simulations after solving the relevant coupled nonlinear equations, were subsequently embodied as input for the two-step procedure. In this respect, Figs. 7.4 and 7.5 report a comparative analysis between the input and resembled parameters for a fully developed sea with 3.0 m

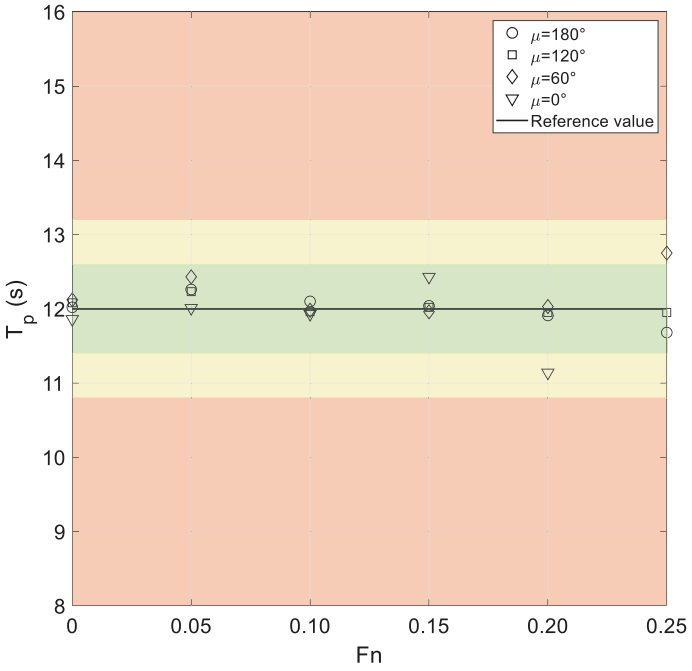

Fig. 7.6 Assessment of the wave peak period [28], reprinted by permission

wave height and 12.0 s peak period, at different vessel speeds corresponding to a Froude number (Fn) ranging from 0 up to 0.25. The green area represents the set of values with a percentage error, as regards the reference one, less than 5%, while the yellow and red areas refer to percentage errors up to and beyond 10%, respectively. As it can be gathered from Figs. 7.6 and 7.7, the resembled values of the wave peak period and significant wave height almost always lie in the green area, so proving the effectiveness of the proposed procedure.

7.4 Sea Wave Monitoring by Coastal HF Radars

Over the last decades, HF (high-frequency) radars (3–50 MHz) have been increasingly used for monitoring the surface current field in coastal areas, with a wide spectrum of applications ranging from maritime safety to coastal zone management, including operational purposes such as oil spill response and pollution assessment [35]. The functioning principles of coastal HF radars are very briefly described in chap. 9 of this same volume [36]. As explained in [36], HF radar signals are backscattered by the sea surface roughness induced by the presence of gravity waves [37]. In presence of Bragg scattering, the backscattered signal yields a Doppler shift owing to the underlying currents [38]; these are the strongest signals reflected by the

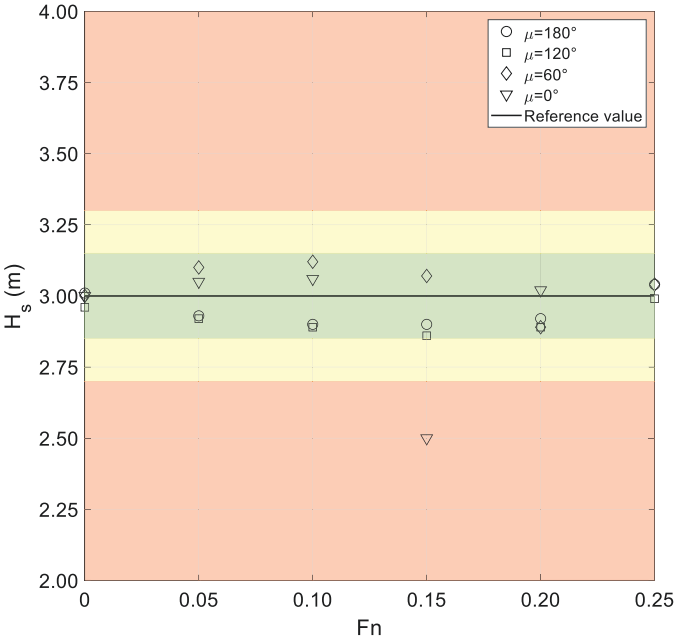

Fig. 7.7 Assessment of the significant wave height [28], reprinted by permission

sea surface, the first-order echoes, which provide information on the surface current field. Nonlinear wave interactions and double scattering processes [39], on the other hand, give rise to second-order echo spectra, the source of information on surface waves (see Fig. 7.8) [41–44]. identified a relationship between the HF backscattered Doppler spectrum and the ocean wave directional spectrum, thus enabling to derive wave height and dominant wave period from HF radar data. Stemming from this result, several techniques have been developed to reconstruct the wave directional spectrum from HF data (see [45] for a review of early reconstruction methods; [46] for a recent summary of inversion techniques).

Thus, HF radars have the potential of measuring the surface wave field by proper analysis of the second-order echoes. This peculiarity makes them ideal platforms for the study of a wide range of processes in coastal areas, including year-long monitoring of coastal basins [46, 47], sea storms [48], or tsunamis [49]. It is worth underlining that, differently from other systems that give single-point information (e.g., wave buoys, ADCPs), HF radars provide measurements of surface gravity waves over larger areas of the basin of interest, thus allowing for a more accurate description of the development of the wave field.

Despite such a great potential, wave retrieval from HF radars has received less attention compared to surface current measurements [46]. This is mostly due to inherent technical limitations. Second-order spectra are much less straightforward to handle than first-order ones, as they are typically much weaker and often disturbed, at least partly, by the measurement noise. This occurs, in particular, in the

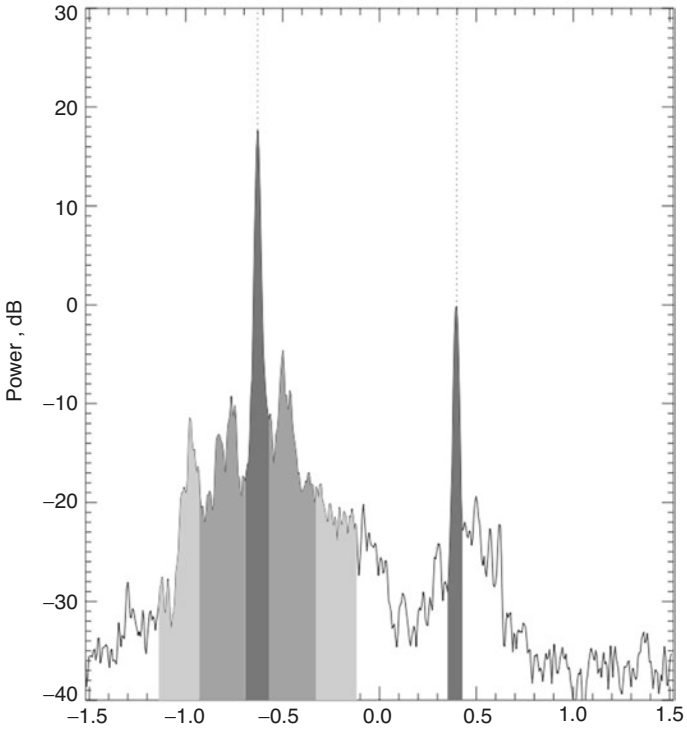

Fig. 7.8 Example of a typical low sea state Doppler spectrum measured by a coastal HF radar. Dark grey: first-order Bragg peaks, used for surface current estimation (theoretical positions shown with dotted lines); medium grey: second-order spectrum used for significant wave height and directional spectrum estimation; light grey: additional part of the second-order spectrum used in mean period estimation. From [40], reprinted by permission

case of intense surface currents: in this case, the first-order peaks may mask at least in part the second-order ones. Moreover, limits to the minimum and maximum detectable wave heights exist. The former is due to the low signal-to-noise ratio in case of low sea state conditions; the latter is due to the fact that the maximum detectable wave height depends on the radar frequency as follows [39, 50–52]:

$$h_{sat} = \frac{2}{k_0}[m] \tag{7.13}$$

where k_0 is the radar wavenumber, yielding an underestimation or overestimation of wave heights above h_{sat}. It is worth noticing that this upper limit decreases in shallow water conditions.

However, even though in the awareness of the above caveats, the use of HF radars to estimate surface wave parameters is becoming more and more widespread as this kind of instruments has started to be clustered in local and larger-scale networks

[36], even though we are still far from being able to deliver HF radar-derived wave data on an operational basis (even though steps are being taken in this direction: see [53, 54]). Such measurements have been carried out so far in various coastal areas of the world ocean, spanning from California to New Jersey, from northwestern Spain to the British and Irish coasts, to Norway, and in the Mediterranean in the Malta–Sicily Channel and in the Gulf of Naples [55–64]. On the northern coast of Cornwall, UK, a specific HF radar site has been installed expressly to measure waves in a test site for offshore renewable energy studies (the Wave Hub, [39]).

Obviously, in order to provide reliable data, measurements must be validated; this is always true, but assumes a special importance in the case of remotely sensed data. This is routinely carried out for all HF radar installations. In particular, for wave observations, this has been done by comparing HF radar data with wave buoy measurements, ADCPs and/or with wave model outputs [39, 52, 61, 64].

HF radars can be roughly divided into two categories: direction-finding and beam-forming (or phased array, for a recent assessment of the performance of both kinds of systems see [65]). In order to exemplify the potential of a coastal HF radar for measuring waves, we will look at results obtained with systems belonging to the first group, and in particular with SeaSonde ones, manufactured by CODAR Ocean Sensors (where CODAR originally stands for Coastal Ocean Dynamics Applications Radar [66]), which are compact radars that compare phases and amplitudes of back-transmitted signals using direction-finding inversion algorithms. In such systems, as explained, e.g., by [52], wave spectra are derived from HF radar data fitting them to a locally optimized Pierson–Moskowitz spectrum (see above, Sect. 7.1.2). This allows to indirectly derive directional and nondirectional wave parameters such as significant wave height, centroid period, and direction. In SeaSonde radars, these parameters are averaged along evenly distributed annuli (range cells, RCs) centred on the antenna. RCs spacing depends on the operating frequency of the radars, ranging from 5 km for long-range systems (5 MHz) [52] to 1 km for short-range ones (25 MHz) [46]. This feature allows the reconstruction of the wave field along a radial transect, permitting the evaluation of the coast-offshore changes in the parameters. In the following, the characterization of the wave field in two different environments is illustrated, with the aim of highlighting the potentialities of these systems and their possibilities of improvement.

The Gulf of Naples (Tyrrhenian Sea) is site to the oldest, presently running European HF radar network, managed by the Department of Science and Technology of the Parthenope University [67]. Over the years, this system has been exploited to reconstruct seasonal circulation patterns and transport dynamics [68–71]. In recent times, its potential use in wave retrieval has been investigated as well [40, 46, 53, 64]. The HF radar-derived measurements have been compared with historical data from the Gulf of Naples [46] and with model results [64], returning good consistency among the different platforms. Annual [46, 53] and interannual [47] investigations allowed the identification of specific seasonal patterns, linking the wave field characteristics to the prevailing meteorological forcing acting over the area, as well as illustrating specific directional prevalence in different subsectors of the basin.

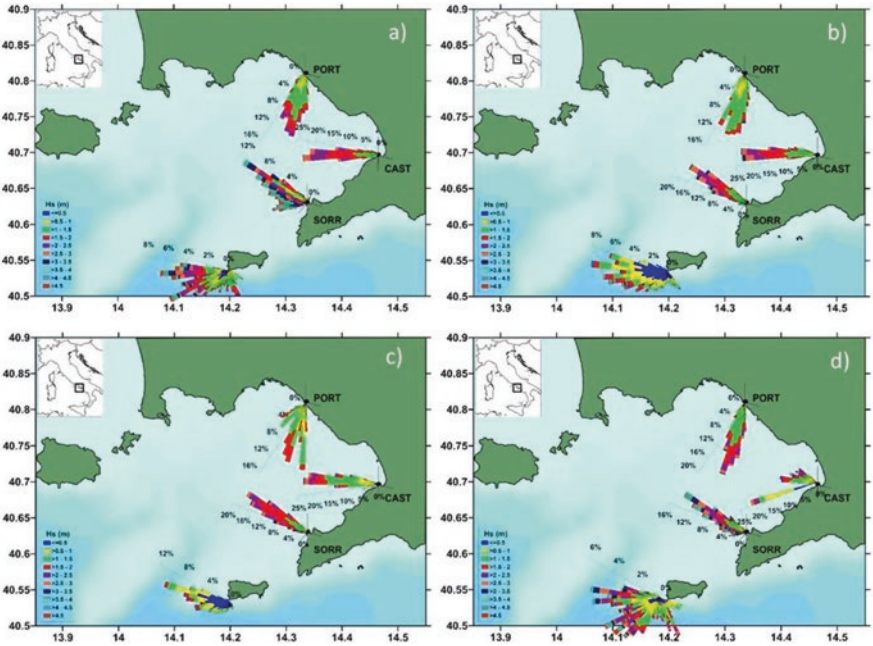

Fig. 7.9 Seasonal rose diagrams of significant wave heights for the year 2010 measured in the Gulf of Naples by three HF radar stations (Portici, Castellamare, and Sorrento, from north to south) and by a wave buoy off the island of Capri (farthest south): (**a**) winter, (**b**) spring, (**c**) summer, (**d**) autumn. From [46], redrawn by permission

This can be seen in Fig. 7.9, where seasonal rose diagrams of significant wave height for the whole year 2010 are shown along with in situ wave buoy measurements collected off the Island of Capri. The radar system was composed of three short-range 25 MHz transceiving stations, whose measurements showed a site-dependent pattern: provenance recorded at RC 5 (5 km from the station) was fairly constant for each site (including the wave buoy location) but different from one site to another, thus underlining the ability of the HF radar observations to resolve the spatial variability of the wave field over even such a small basin.

Another example of utilization of wave data from HF radars in the framework of a synoptic multiplatform wave regime observation network is shown in Fig. 7.10. The map displays wave and wind observations gathered along the Galician coast (NW Spain) over approximately 16 months (January 2014–April 2015). Waves were measured at RC 2 (10 km from the stations) by two long-range HF systems transmitting at 5 MHz approximately (SILL and VILA on the map), two wave buoys (SB and VB on the map), estimated in three points with a model (SO2, S20 and S24 on the map), while wind data were collected by two weather stations (CW on land, VBW on the VB buoy). Also in this case, the results returned robust validations and the HF radar-derived measurements improved the knowledge of the wave field dynamics in a particularly energetic area of the coastal eastern Atlantic Ocean.

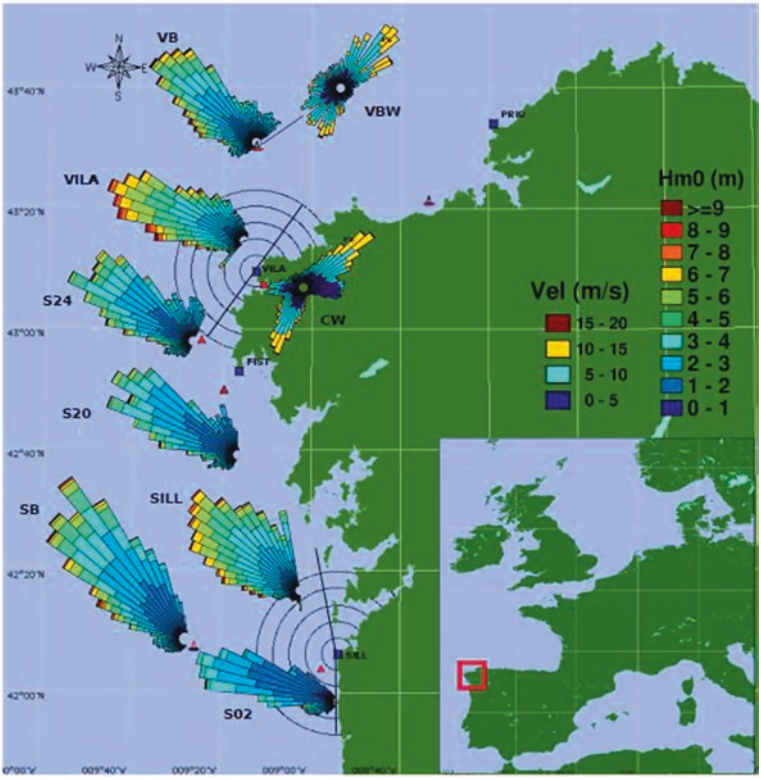

Fig. 7.10 Rose diagrams of significant wave heights for the period January 2014–April 2015 measured off the northwestern coast of Galicia by two HF radar stations (VILA = Vilàn and SILL = Silleiro), two wave buoys (VB and SB), estimated in three sites by a numerical model (S24, S20 and S02), along with wind roses measured by two weather stations (CW on land, VBW on the VB buoy). From [52], reprinted by permission

7.5 Future Developments

The applied advanced sea spectrum reconstruction methods seem to be promising for future developments, mainly related to: (1) reduce the time duration of the wave history, without penalizing the effectiveness of the sea spectrum reconstruction method, and (2) extend the above-mentioned techniques to the sea spectrum reconstruction methods, based on onboard ship motion measurement and analysis. Finally, the positive results gathered over the last years have demonstrated that HF radars can realistically retrieve surface wave parameters in different environments. As discussed in [46], the functioning and performance of these systems need some future improvement and refinement, such as standardization of QA/QC protocols, and optimization of inversion methods and of wave retrieval algorithms. Nonetheless, HF radars can potentially qualify as effective operational tools [72], supporting and integrating already existing observation networks.

References

1. Lewis E (1989) Principles of naval architecture—volume III: motions in waves and controllability. Society of Naval Architects and Marine Engineers, NJ
2. Chakrabarti SK (2005) Handbook of offshore engineering. Elsevier, Amsterdam
3. Det Norske Veritas (2010) Environmental conditions and environmental loads. Recommended Practice DNV-RP-C205
4. Neumann G (1953) On ocean wave spectra and a new method of forecasting wind-generated sea. In: Technical memory 43. Beach Erosion Board, US Army Corp of Engineers, Washington
5. Roll H, Fischer G (1956) Eine Kritische Bemenkung Zum Neumann-Spektrum der Seeganger. Deutsche Hydrografische Zeitschrift 9:9–14
6. Darbyshire J (1957) Eine Bemerkung über den Vergleich von Formeln verschiedener Autoren zur Berechnung von Wellenspektren. Deutsche Hydrografische Zeitschrift 10:184–190
7. Pierson WJ, Moskowitz L (1964) A proposed spectral form for fully developed wind seas based on the similarity theory of S.A. Kitaigorodski. J Geophys Res 69(24):5181–5190
8. Ochi MK, Hubble EN (1976) On six-parameters wave spectra. In: Proceedings of the 15th coastal engineering conference, Honolulu, Hawaii, pp. 301–328
9. Torsethaugen K, Haver S (2004) Simplified double peak spectral model for ocean waves. In: Proceedings of the 14th international offshore and polar engineering conference, Toulon
10. Percival DB, Walden AT (2020) Spectral analysis for univariate time series. Cambridge University Press, Cambridge
11. Schuster A (1898) On the investigation of hidden periodicities with application to a supposed 26 Day period of meteorological phenomena. Terr Magn 3:13–41
12. Welch PD (1967) The use of fast Fourier transform for the estimation of power spectra: a method based on time averaging over short modified periodograms. IEEE Trans Audio Electroacoust 15:70–73
13. Thomson DJ (1982) Spectrum estimation and harmonic analysis. Proc IEEE 70:1055–1096
14. Marple SL (1987) Digital spectral analysis. Prentice—Hall, Englewood Cliffs
15. Rossi GB (2012) Towards an Interdisciplinary Probabilistic Theory of Measurement. IEEE Trans. Instrum. Meas. 61(8):2095-2106
16. Rossi GB, Crenna F, Piscopo V, Scamardella A (2020) Comparison of spectrum estimation methods for the accurate evaluation of sea state parameters. Sensors 20:1416
17. Rossi GB, Crenna F, Berardengo M, Piscopo V, Scamardella A (2020) In: Proc. 2020 IMEKO TC-19 international workshop on metrology for the sea, Naples, Italy, October 5–7
18. Coleman TF, Li Y (1996) Trust region approach for nonlinear minimization subject to bounds. SIAM J Optim 6:418–445
19. Takekuma K, Takahashi T (1973) On the evaluation of sea spectra based on the measured ship motions. Trans West-Japan Soc Naval Arch 45:51–57
20. Isobe M, Kondo K, Horikawa K (1984) Extension of MLM for estimating direction wave spectrum. In: Proceedings of the symposium on description and modeling of direction seas, volume A-6
21. Kobune K, Hashimoto N (1986) Estimation of directional spectra from the maximum entropy principle. In: Proceedings of the 5th international offshore mechanics and Arctic engineering (OMAE) symposium, Tokyo, pp. 80–85
22. Iseki T, Ohtsu K (2000) Bayesian estimation of directional wave spectra based on ship motions. Control Eng Pract 8:215–219
23. Iseki T, Terada D (2002) Bayesian estimation of direction wave spectra for ship guidance systems. Int J Offshore Polar Eng 12:25–30
24. Nielsen UD (2006) Estimations of on-site direction wave spectra from measured ship responses. Mar Struct 19:33–69
25. Nielsen UD, Andersen IMV, Koning J (2013) Comparisons of means for estimating sea states from an advancing large containership. In: Proceedings of the 12th PRADS, Changwon, South Korea

26. Montazeri N, Nielsen UD, Jensen JJ (2016) Estimation of wind sea and swell using shipboard measurements – a refined parametric modelling approach. Appl Ocean Res 54:73–86
27. Ochi MK (1990) Applied probability and stochastic processes in engineering and physical sciences. Wiley, New York
28. Piscopo V, Scamardella A, Gaglione S (2020) A new wave spectrum resembling procedure based on ship motion analysis. Ocean Eng 201:107137
29. Pascoal R, Guedes Soares C (2009) Kalman filtering of vessel motions for ocean wave directional spectrum estimation. Ocean Eng 36:477–488
30. Pascoal R, Perera LP, Guedes Soares C (2017) Estimation of directional spectra from ship motions sea trials. Ocean Eng 132:126–137
31. Tannuri EA, Sparano JV, Simos AN, Da Cruz JJ (2003) Estimating directional wave Spectrum based on stationary ship motion measurements. Appl Ocean Res 25:243–261
32. Nielsen UD (2006) Estimations of on-site direction wave spectra from measured ship responses. Mar Struct 19:33–69
33. ITTC (1978) Report of the seakeeping committee. In: Proceedings of the 15th international towing tank conference, the Hague, 1, 55–114
34. Kim M, Hizir O, Turan O, Day S, Incecik A (2017) Estimation of added resistance and ship speed loss in a seaway. Ocean Eng 141:465–476
35. Paduan JD, Washburn L (2013) High-frequency radar observations of ocean surface currents. Ann Rev Mar Sci 5:115–136. https://doi.org/10.1146/annurev-marine-121211-172315
36. Ferla M, Nardone G, Orasi A, Picone M, Falco P, Zambianchi E (2021) Sea-monitoring networks
37. Crombie DD (1955) Doppler spectrum of sea echo at 13.56 Mc/ s. Nature 175:681–682
38. Barrick DE, Evans MW, Weber BL (1977) Ocean surface currents mapped by radar. Science 198:138–144
39. Lopez G, Conley DC, Greaves D (2016) Calibration, validation, and analysis of an empirical algorithm for the retrieval of wave spectra from HF radar sea echo. J Atmos Oceanic Tech 33(2):245–261
40. Wyatt LR (2002) An evaluation of wave parameters measured using a single HF radar system. Can J Remote Sens 28(2):205–218
41. Barrick DE (1972a) First-order theory and analysis of MF/HF/VHF scatter from the sea. IEEE Trans Antennas Propag 20:2–10
42. Barrick DE (1972b) Remote sensing of sea state by radar. In: Derr VE (ed) Remote sensing of the troposphere. GPO, Washington
43. Barrick DE (1977a) Extraction of wave parameters from measured HF radar sea-echo Doppler spectra. Radio Sci 12:415–424
44. Barrick DE, Weber BL (1977) On the nonlinear theory for gravity waves on the ocean's surface. Part II: interpretation and applications. J Phys Oceanogr 7:11–21
45. Wyatt L (1986) The measurement of the ocean wave directional spectrum from HF radar Doppler spectra. Radio Sci 21:473–485
46. Saviano S, Kalampokis A, Zambianchi E, Uttieri M (2019) A year-long assessment of wave measurements retrieved from an HF radar network in the Gulf of Naples (Tyrrhenian Sea, Western Mediterranean Sea). J Operat Oceanogr 12(1):1–15
47. Saviano S, Cianelli D, Zambianchi E, Conversano F, Uttieri M (2020) An integrated reconstruction of the multiannual wave pattern in the Gulf of Naples (south-eastern Tyrrhenian Sea, Western Mediterranean Sea). J Marine Sci Eng 8(5):372
48. Lipa B, Barrick D, Alonso-Martirena A, Fernandes M, Ferrer MI, Nyden B (2014) Brahan project high frequency radar ocean measurements: currents, winds, waves and their interactions. Remote Sens (Basel) 6:12094–12117
49. Lipa BJ, Barrick DE, Bourg J, Nyden BB (2006) HF radar detection of tsunamis. J Oceanogr 62:705–716
50. Lipa BJ, Barrick D, Isaacson J, Lilleboe PM (1990) CODAR wave measurements from a north sea semisubmersible. IEEE J Ocean Eng 15:119–125

51. Wyatt LR, Green JJ (2009) Measuring high and low waves with HF radar, OCEANS 2009-EUROPE. IEEE Bremen 1:1–5
52. Basañez A, Lorente P, Montero P, Álvarez-Fanjul E, Pérez-Muñuzuri V (2020) Quality assessment and practical interpretation of the wave parameters estimated by HF radars in NW Spain. Remote Sens (Basel) 12(4):598
53. Falco P, Buonocore B, Cianelli D, De Luca L, Giordano A, Iermano I et al (2016) Dynamics and sea state in the Gulf of Naples: potential use of high-frequency radar data in an operational oceanographic context. Jf Operat Oceanogr 9:33–45
54. Lorente P, Varela SP, Soto-Navarro J, Ruiz MI, Álvarez-Fanjul E, Montero P (2016) The high-frequency coastal radar network operated by Puertos del Estado (Spain): Roadmap to a fully operational implementation. IEEE J. Ocean. Eng. 42(1):56-72.
55. Long RM, Barrick D, Largier JL, Garfield N (2011) Wave observations from Central California: SeaSonde systems and in situ wave buoys. J Sens 2011
56. Beckenbach E, Washburn L (2004) Low-frequency waves in the Santa Barbara Channel observed by high-frequency radar. J Geophys Res Oceans 109:2
57. Kohut J, Roarty H, Licthenwalner S, Glenn S, Barrick D, Lipa B, Allen A (2008) Surface current and wave validation of a nested regional HF radar network in the mid-Atlantic bight. In: 2008 IEEE/OES 9th working conference on current measurement technology, IEEE, pp. 203-207
58. Lorente P, Sotillo MG, Aouf L, Amo-Baladrón A, Barrera E, Dalphinet A et al (2018) Extreme wave height events in NW Spain: a combined multi-sensor and model approach. Remote Sens (Basel) 10(1):1
59. Lorente P, Basañez Mercader A, Piedracoba S, Pérez-Muñuzuri V, Montero P, Sotillo MG, Álvarez-Fanjul E (2019) Long-term skill assessment of SeaSonde radar-derived wave parameters in the Galician coast (NW Spain). Int J Remote Sens 10:9208–9236
60. Wyatt LR, Green JJ (2009) Measuring high and low waves with HF radar, OCEANS 2009-EUROPE. IEEE Bremen 1:1–5
61. Wyatt LR, Green JJ, Gurgel KW, Borge JN, Reichert K, Hessner K, Reistad M (2003) Validation and intercomparisons of wave measurements and models during the EuroROSE experiments. Coastal Eng 48(1):1–28
62. Atan R, Goggins J, Hartnett M, Nash S, Agostinho P Assessment of extreme wave height events in galway bay using high frequency radar (CODAR) Data. In: Proceedings of the 1st international conference on renewable energies offshore (RENEW), Lisbon, 24–26 November 2014
63. Orasi A, Picone M, Drago A, Capodici F, Gauci A, Nardone G et al (2018) HF radar for wind waves measurements in the Malta-Sicily Channel. Measurement 128:446–454
64. Saviano S, De Leo F, Besio G, Zambianchi E, Uttieri M (2020) HF radar measurements of surface waves in the Gulf of Naples (southeastern Tyrrhenian Sea): comparison with hindcast results at different scales. Front Mar Sci
65. Hardman RL, Wyatt LR, Engleback CC (2020) Measuring the directional ocean spectrum from simulated bistatic HF radar data. Remote Sens (Basel) 12(2):313
66. Barrick DE, Lipa BJ (1985) Mapping surface currents. Sea Technol 26:43–48
67. Rubio A, Mader J, Corgnati L, Mantovani C, Griffa A, Novellino A et al (2017) HF radar activity in European coastal seas: next steps toward a pan-European HF radar network. Front Mar Sci 4:8
68. Uttieri M, Cianelli D, Nardelli BB, Buonocore B, Falco P, Colella S, Zambianchi E (2011) Multiplatform observation of the surface circulation in the Gulf of Naples (southern Tyrrhenian Sea). Ocean Dyn 61(6):779–796
69. Cianelli D, Falco P, Iermano I, Mozzillo P, Uttieri M, Buonocore B et al (2015) Inshore/offshore water exchange in the Gulf of Naples. J Mar Syst 145:37–52
70. Iermano I, Moore AM, Zambianchi E (2016) Impacts of a 4-dimensional variational data assimilation in a coastal ocean model of southern Tyrrhenian Sea. J Mar Syst 154:157–171

71. Cianelli D, D'Alelio D, Uttieri M, Sarno D, Zingone A, Zambianchi E, d'Alcalà MR (2017) Disentangling physical and biological drivers of phytoplankton dynamics in a coastal system. Sci Rep 7(1):1–15
72. Wyatt LR, Thompson SP, Burton RR (1999) Evaluation of high frequency radar wave measurement. Coast Eng 37(3–4):259–282
73. Hasselmann K, Barnet TP, Bouws E, Carlson H, Cartwright DE, Enke K, Ewing JA, Gienapp H, Hasselman DE, Kruseman P, Meerburg A, Müller P, Olbers DJ, Richter K, Sell W, Walden H (1973) Measurements of wind-wave growth and swell decay during the joint North Sea wave project (JONSWAP). Deutschen hydro-graphischen Institut, Hamburg
74. Fonseca N, Guedes Soares C (1998) Time-domain analysis of large amplitude vertical ship motions and wave loads. J Ship Res 42(2):139–153

Chapter 8
Remote Sensing Applications in Satellite Oceanography

Giuseppe Aulicino, Yuri Cotroneo, Paola de Ruggiero, Andrea Buono, Valeria Corcione, Ferdinando Nunziata, and Giannetta Fusco

Contents

Abstract Satellite remote sensing provides repeated global observations of key ocean surface variables. These observations are complementary to in situ measurements. In fact, remotely sensed information fills some in situ gaps in temporal and spatial coverage, while in situ measurements, being a point-wise source of information, provide critical ground-truth for satellite retrievals calibration and validation. Advances in satellite ocean technology and algorithm research make satellite remote sensing an indispensable tool for environmental monitoring of the open and coastal ocean. Moreover, remotely sensed products support the interpretation and the prediction of oceanic phenomena that occur at regional and mesoscales in a synoptic way. In this chapter, we introduce basics of satellite oceanography, including the most used satellite orbits, the range of frequencies involved, and the processing levels related to the remote sensed products. Then, selected ocean products and their

G. Aulicino (✉) · Y. Cotroneo · P. de Ruggiero · G. Fusco
Department of Science and Technology, University of Naples "Parthenope", Centro Direzionale, Isola C4, Naples, Italy
e-mail: giuseppe.aulicino@uniparthenope.it; yuri.cotroneo@uniparthenope.it; paola.deruggiero@uniparthenope.it; giannetta.fusco@uniparthenope.it

A. Buono · V. Corcione · F. Nunziata
Department of Engineering, University of Naples Parthenope, Naples, Italy
e-mail: andrea.buono@uniparthenope.it; valeria.corcione@uniparthenope.it; ferdinando.nunziata@uniparthenope.it

P. Daponte et al. (eds.), *Measurement for the Sea*, Springer Series in Measurement Science and Technology,
https://doi.org/10.1007/978-3-030-82024-4_8

applications, from ocean color to infrared observations of sea surface temperature, passive microwaves, and altimetry, are addressed. Finally, a special attention is devoted to synthetic aperture radars (SARs) and the emerging role of microsatellites in observing ocean variables and, in particular, wind speed.

8.1 Introduction

During the past five decades, rapid technological growth has advanced the ability of satellites to observe and monitor the global ocean and its overlying atmosphere. Besides several pioneer activities experimented after the invention of photography (e.g., cameras mounted on balloons or pigeons), satellite remote sensing of the ocean began between 1960s and 1970s of the last century, when the USA launched the first meteorological observational satellites [1]. Since that time, many countries have launched satellites that carry instrumentations that allow us to observe several oceanic variables, including sea surface temperature (SST) and salinity (SSS), the concentrations of phytoplankton, sediments and suspended and dissolved material, the changes in sea surface height associated with current systems, the global distribution of ocean waves, the wind speed and direction, the extent of polar sea ice, and many other derived information. In recent years, international agreements among different countries also favored the constellations of smaller satellites that usually focus on a specific ocean feature or phenomenon flying in complementary orbits, so that the coverage by a single satellite is enhanced by observations from the other constellation members. The multi-instrument Envisat mission, equipped with ten instruments operating at both microwave and optical frequencies, for example, has been replaced by the European Space Agency (ESA) Sentinel series of satellites, each one specialized on a different topic.

Prior to satellite oceanography, sea surface properties were determined only from dedicated and expensive ship expeditions, so that the ocean could be surveyed only slowly and incrementally. Earth-orbiting satellite sensors can indeed achieve large-scale synoptic observations that, therefore, enable the monitoring of several oceanic variables at different spatial scales and with a dense temporal sampling. This information is usually provided at short time delays and is used to produce time series several years long. The immediate availability of simultaneous data over large ocean areas is essential for assimilation into numerical models that contribute to weather and climate forecast.

Satellite oceanography is of course limited by a number of issues. Firstly, the penetration depth resulting from the range of frequencies used to collect remotely sensed measurements limits ocean monitoring to surface and near-surface parameters. However, there is limited possibility to get direct information about the underlying water column. Hence, remotely sensed information can be completed by measurements performed by moored and drifting buoys, or by 3D reconstructions inferred through machine learning and statistical techniques applied to satellite observations [2, 3].

Generally, in situ and satellite data should be viewed as an integrated system in order to enhance our knowledge of the physical and biogeochemical characteristics of the four-dimensional ocean. Several studies already demonstrated that the combination of in situ observational networks enhanced spatial and temporal coverage of space-born remote sensing, and numerical simulations booted a number of oceanographic applications to address major concerns like global monitoring, disaster management support, and climate change issues [4]. To ensure that its effect will be pervasive, in science, industry, and social welfare, the satellite oceanography community is working to strengthen the networking among different measurement technologies, provide a more efficient management of the processing chain—from the sensor to the user, improve the assessment of the different available observations and the combination of the different types of measurements (especially for coastal applications), and enhance data management and mining techniques to fully exploit the large amount of available information.

In this chapter, we provide a brief understanding of the rationale that underpins satellite remote sensing—from orbits to generic data processing (Sect. 8.2). Then, an overview of the main satellite oceanography techniques is provided focusing on the main aspects of ocean color (Sect. 8.3), thermal infrared temperature detection (Sect. 8.4), passive microwave radiometry (Sect. 8.5), altimetry (Sect. 8.6), and SAR (Sect. 8.7).

8.2 Technical Background

8.2.1 Electromagnetic Radiation

Ocean remote sensing can be defined as the use of electromagnetic radiation to collect information about the ocean without being in physical contact with the sea surface under investigation [1]. Sea properties are inferred by analyzing the properties (e.g., the intensity and frequency distribution and the polarization) of the electromagnetic radiation received by the satellite-based sensors. This received radiation depends on a number of geophysical variables that—at once—affect the radiation emitted by the ocean, the reflected solar radiation, and the backscattered energy. Remote sensing instruments can be divided into imaging tools (e.g., the SAR, which natively provides measurements arranged as two-dimensional maps that are also known as images) and nonimaging tools (e.g., the microwave radiometer, which provides measurements in a swath-based fashion). The frequency that characterizes the remote sensing instrument must be selected to trade off a number of issues, e.g., capability of penetrating the atmosphere and sensitivity to the geophysical parameter of interest. Accordingly, the bands commonly adopted include visible (VIS), infrared (IR), and microwaves (MW); see Fig. 8.1a. VIS and near-IR (NIR) observations strongly depend on reflected sunlight so that they are restricted to daytime cloud-free periods. IR can be also performed during nighttime, but they are affected

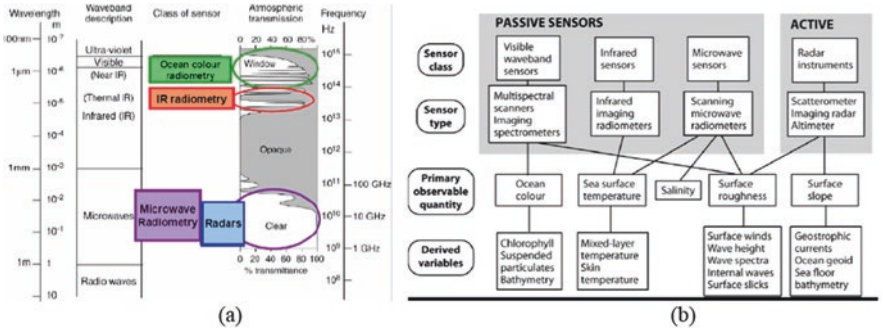

Fig. 8.1 (**a**) Electromagnetic spectrum and the bands used for satellite oceanography according to atmospheric transmission windows; (**b**) an overview of the sensors used for satellite oceanography and the derived ocean variables (adapted from [5])

by clouds. Conversely, the MW part of the spectrum allows all-day and almost all-weather observations. Remote sensing tools can be also divided into passive and active. The passive microwave (PMW) instruments measure the naturally emitted blackbody radiation, while the active sensors transmit bur of signals and receive the electromagnetic wave that—after the interaction with the ocean—reaches the antenna. The latter can be the same antenna used in the transmission phase (monostatic configuration) or an antenna hosted by a different satellite (bistatic configuration or multistatic configuration when multiple antennas are used). Figure 8.1b provides a useful summary of the different remote sensing groups of sensors used in satellite oceanography, along with their applications, as previously reported in [6].

8.2.2 Satellite Orbits

Ocean observation sensors are usually equipped onboard of Earth-orbiting (either geostationary or near-polar) satellites. The geostationary orbit is characterized by a period of one sidereal day (about 23.93 h), being located over the Equator at a height of about 35,800 km to ensure that the satellites always observed a fixed target area on the ground. The sensors onboard of these satellites can observe only part of the Earth that is limited to lower latitudes. Near-polar orbits call for lower altitude (typically 700–1350 km), and they are characterized by an orbital period of about 100 min, so that satellites usually complete 14–15 orbits per day. Since the Earth rotates itself, satellites flying on these orbits cover the ground about 14 times along both descending (northeast–southwest) and ascending (southeast–northwest) tracks. Frequently, low near-polar orbits used for Earth observation are also arranged to be sun-synchronous in order to cross the Equator always at the same local solar time. This is important to boost interoperability among different sensors (e.g., to verify SAR-based wind estimations using nearly timely colocated scatterometer-based winds), to provide daily observations of SST or ocean chlorophyll at the same time

in their diurnal cycle and to minimize cloud cover disturbance through the choice of a specific crossing time. Conversely, according to this orbit, the satellites do not pass directly over the poles reducing the coverage of these regions and giving rise to the famous "hole at the pole." Besides the constraints of the platform on which it is placed, it is important to emphasize that every instrument has its own space-time sampling capabilities which can usually depend on the sensor itself [1].

8.2.3 Imaging Techniques and Data Processing

Remotely sensed satellite products consist of millions of individual measurements collected by a specific sensor over a short length time interval by exploiting a sampling pattern over the observed scene. This scene is referred to as instantaneous field of view (IFOV). Generally, each measured value represents the average of a variable property over the IFOV region observed during a finite time. Some sensors simply make downward-looking observations at periodic intervals, while the satellite moves over the ground, and others scan sideways across the satellite track direction. The former class of sensors provides an average value of the variable in the IFOV that is typically centered at the nadir (i.e., the point on the ground placed immediately below the satellite). The latter gives a wide swath usually centered on the satellite ground track. The scanning and imaging mechanisms are different from sensor to sensor, as fully discussed in [6].

The raw data received by the sensor are converted into scientific units with a proper precision and accuracy which describe an observed geophysical variable. The processing of the swath data includes several steps which are extremely relevant for the interpretation and application of the final ocean products. Thus, the users should be aware of all calibrations, corrections, analyses, and resampling that may have been applied to the satellite data before being released as quantitative information about an ocean variable. The main steps which are generally used to describe the processing tasks can be summarized into four stages of data processing which correspond to different levels of satellite products [7]:

- Level 0—unprocessed raw data acquired by the sensor, in standard binary format;
- Level 1A—Level 0 data processed and converted into an estimate of the electromagnetic property which the sensor is intended to detect, with related ancillary data (e.g., time, calibration coefficients, and geolocation information);
- Level 1B—Level 1A data converted into sensor units (e.g., radiances and brightness temperatures) and organized through along-track swaths;
- Level 2—geophysical products (e.g., SST, SSS, and sea ice cover) in a swath format with same resolution of Level 1 products. They can represent the physical interpretation of the Level 1 units, usually derived from the combination of data from multiple channels and including an atmospheric correction;
- Level 3—geophysical data mapped to uniform grids. Even though averaged in space and time from several Level 2 passes, they may still have gaps associated

with no data due to the swath geometry and/or the cloud cover. The pixel size is usually larger than the native Level 2 one. These products are useful to extend the ocean monitoring beyond the space-time constraints of a single overpass.
– Level 4—Level 3 products combined with information from multiple platforms (e.g., different satellites, in situ measurements, and model outputs) to obtain a gap-free product on uniform grid.

8.3 Visible Imagery

8.3.1 Ocean Color Measurements

Satellite remote sensing of ocean color (OC) is today an indispensable tool for environmental monitoring of the open and coastal ocean. When solar radiation hits the surface of the water, it is absorbed, transmitted, scattered, or reflected by water molecules and by other optically active particles in suspension in the upper layer of the ocean. OC radiometers detect the fraction of sunlight reemitted by the ocean surface after interaction with the water and any suspended matter and allow the retrieval of all the geophysical parameters that can be estimated through the observation of the sea surface at the visible wavelength bands of the electromagnetic spectrum [8].

This signal provides a reliable basis for estimating the concentration of chlorophyll associated with the phytoplankton of the upper ocean, that is, the main contribution of remote sensing to ocean biological science. Phytoplankton are the primary producers of organic matter and the base of the food web in the ocean. They include all the marine algae that absorb light in the blue and red regions of the spectrum and reflect green light, thanks to the presence of chlorophyll pigments. Accordingly, as the concentration of phytoplankton increases in the water, the color of the water (blue) shifts toward the green [5]. For this reason, OC observations are used for monitoring large-scale seasonal and interannual phytoplankton dynamics, analyzing its role in the global carbon cycle, and studying the response of marine ecosystems to climate change [9].

In coastal areas, chlorophyll contribution needs to be distinguished from that of resuspended particulates, colored dissolved organic matter not associated with phytoplankton, and terrestrial suspended particulates due to river runoff. Several specific algorithms permit their identification, proving to be an excellent tool for monitoring coastal eutrophication, algal blooms, sediment plumes, and pollution, as well as their evolution due to coastal currents, storms, and tides, and provide reliable data which can also be assimilated in biogeochemical models [9].

8.3.2 Sensors and Platforms

The OC observations from the space began in the 1970s with the launch of the multichannel scanning radiometer Coastal Zone Color Scanner (CZCS) onboard NASA Nimbus 7 satellite. Since then, several sensors have monitored the global ocean with a spatial and temporal sampling depending on the type of satellite mission and platform. A summary of main OC instruments is reported in Table 8.1.

Given the biological, oceanographic and atmospheric constraints that characterize Earth observation in the visible bands (see Sect. 8.2.1), similar wavelengths, atmospheric corrections, and resolutions characterize the different available instruments [1].

Generally, the operating OC sensors have several spectral bands spanning the visible wavelengths (400–700 nm), which are carefully selected on the specific response of several targets, e.g., the reflectance of open ocean waters and the phytoplankton pigment absorption. Additional bands in the NIR and the short-wave infrared (SWIR) are used indeed to provide atmospheric corrections. Among others, the recent Ocean and Land Color Imager (OLCI) sensor, flown on ESA Copernicus Sentinel-3 satellites since 2016, has even 21 spectral bands from 400 to 1020 nm which measure reflected solar radiation at a ground spatial resolution of about 300 m [10].

Most of the current and defunct sensors were mounted on sun-synchronous polar orbiting satellites (e.g., CZCS, SeaWiFS, VIIRS, and MODIS) and were conceived for having wide sampling swaths in order to provide a global coverage of the Earth surface, at about 0.25–1 km resolution, every 3 days (at the equator) and more frequently at the poles. Nevertheless, to overcome the limitations due to cloud cover, OC data are frequently used as L3/L4 averaged (weekly, monthly, and seasonal) or aggregated (4–9 km pixels) products to obtain continuous and reliable representations of the global ocean and marginal seas.

The observed geophysical parameters usually include chlorophyll concentration, cyanobacterial pigments, total suspended matter, colored dissolved organic matter, diffuse attenuation coefficient, and turbidity. Suitable and potential use from different sensors is reported in Table 8.1.

OC sensors are also mounted on geostationary orbiting satellites, e.g., the Geostationary Ocean Color Imager (GOCI) instrument launched by the Korea Institute of Ocean Science and Technology (KIOST) in June 2010. Thanks to their repeated high-resolution observations over specific regions, these platforms improve the mitigation of the effects of cloud cover and provide biological parameters variability over daily or subdaily temporal scales [11].

Additionally, new requirements from user communities (e.g., a detailed monitoring of coastal and estuarine areas) promoted the development of a new generation of hyperspectral radiometers which are able to sample the full visible spectrum and provide very high-resolution observations for selected areas with more than one sampling per day. In this framework, even though designed for terrestrial applications, the US Geological Survey Landsat 8 OLI sensor and the ESA Copernicus

Table 8.1 A summary of relevant operating OC sensors (adapted from [8]). Potential and suitable geophysical parameters are listed as chlorophyll concentration (Chl), cyanobacterial pigments (CYP), total suspended matter (TSM), colored dissolved organic matter (CDOM), diffuse attenuation coefficient (Kd), and turbidity/Secchi disk depth (Turb/SD)

Type	Platform	Sensor	Pixel size	Spectral bands	Revisit frequency	Launch	Variables					
							Chl	CYP	TSM	CDOM	Kd	Turb/SD
Sun-sync	Terra/Aqua	MODIS	1 km	9	Daily	1999/2000	✓	✓	✓	✓	✓	✓
Sun-sync	Suomi NOAA-20	VIIRS	750 m	7	Daily	2011/2017	✓	✓	✓	✓	✓	✓
Sun-sync	SENTINEL 3 A/B	OLCI	300 m	21	Daily (2 satellites)	2016/2018	✓	✓	✓	✓	✓	✓
GEO	KOMPSAT	GOCI	500 m	8	Half hourly	2010	✓	p	✓	✓	✓	✓
GEO	KOMPSAT-3B	GOCI	500 m	8	Half hourly	2019	✓	p	✓	✓	✓	✓
Sun-sync	Terra/Aqua	MODIS	500 m	2	Daily	1999/2002	p		✓	p	p	p
Sun-sync	LANDSAT 8	OLI	30 m	5	16 days	2013	p	✓	✓	p	✓	✓
Sun-sync	SENTINEL 2	MSI	10–60 m	10	10 days per sensor; 5 days with two S-2	2015	✓	✓	✓	✓	✓	✓

✓ = suitable, p = potential.

Sentinel-2 MSI provide high-resolution (10–60 m) data which allow the monitoring of coastal floating vegetation, suspended particulates, and inland water color, as well as the identification of different types of phytoplankton, including those responsible for harmful algal blooms [8].

8.3.3 Ocean Color Applications

OC remote sensing has many biological applications linked to the estimation of chlorophyll concentration, primary productivity, phytoplankton physiology and distribution, and their linkage at multiple trophic levels of the ocean food web. Marine ecology studies on *Posidonia oceanica* meadows, fish species like anchovies and sardines, which eat phytoplankton in their life cycle, as well as distribution, movement, and migration of various marine species (e.g., whales, dolphins, pinnipeds, penguins, and turtles), have been developed analyzing chlorophyll patterns. OC data also demonstrated that the recruitment success of the fish planktonic larvae, usually transported by ocean currents, is directly related to the degree of timing between spawning and the seasonal phytoplankton blooms. Still, even studies on the distribution of other species as invertebrates, pteropods, pelagic molluscs, and cephalopods have been supported by satellite OC observations [9].

In physical oceanography, OC products are successfully used for the detection and analysis of basin-scale structures and regional dynamics, including eddies, oceanic fronts, and convergence zones in different areas of the global ocean [12, 13]. Since the visible radiation captures better the frontal features than SST data alone, thanks to the effect of dynamical processes on biological life, satellite-derived OC information represents a useful indicator to readily identify the upwelling regions in the oceans. The upwelling processes bring cold, nutrient-rich waters up to the surface, so time series of chlorophyll concentration can easily describe their temporal and spatial variability.

Another OC parameter profitably used in coastal oceanography is the diffuse attenuation coefficient (Kd), which is representative of the total water turbidity and provides valuable information about the dispersion and transport of turbid coastal waters [14].

These applications are extremely useful for several economical and societal activities, such as fishery and aquaculture management, marine protected area monitoring, ecosystem models improvement, and hazard monitoring due to water quality, eutrophication, and harmful algal blooms. In South Africa, for example, the availability of regular OC hyperspectral data assists in discrimination of certain harmful algal species which have previously provided negative impacts on aquaculture and which can be distinguished from spectral features. Along Indian coast, OC data have been proficiently used for location of productive regions through the analysis of oceanographic processes important for enrichment of nutrients (e.g., upwelling and convective mixing) and for creation of maps of potential fishing zones which help to optimize fishery and contrast overfishing [9].

8.4 Infrared Radiometry

8.4.1 Sea Surface Temperature Infrared Observations

IR satellite observations consist of measurements of the blackbody radiation emitted from the top few micrometers of the sea surface. Thus, the retrieved SST should be considered as a measure of the ocean skin temperature. A complete description of thermal skin effects, diurnal variability, and atmospheric corrections can be found in [15].

The first reliable quantitative satellite observations of SST started in 1979 when the first radiometers with multiple IR and MW channels were deployed and allowed corrections for the effects of the atmosphere. From the advanced very high-resolution infrared radiometer (AVHRR) on, satellite measurements provided exceptional information to study global climate change and regional ocean dynamics (e.g., eddies and filaments, upwelling/downwelling, and ocean fronts), and support anthropic sea activities (e.g., fisheries, ship routing, and forecasting). To this aim, since 2002, an important role has been played by the Group for High-Resolution SST (GHRSST) which includes scientists and operational practitioners to discuss issues and results, and coordinate research and operational activities [16]. Besides AVHRR on METOP satellites series and NOAA polar orbiting platforms, at present, IR observations are also collected by MODIS (since 2002) and VIIRS (since 2011) which provide broad swath (2300–3000 km) daily observations at 0.75–1 km resolution, as well as by several instruments flown by India, Japan, and China space agencies and Earth observation centers. A technical and historical description of IR instruments is provided by [15].

Several geosynchronous satellites also collect IR observations, e.g., the Spinning Enhanced Visible and Infrared Imager (SEVIRI) on the Meteosat Second Generation satellite, and the Japanese MTSAT VIS/IR imager and the Advanced Baseline Imager (ABI) on the GOES-R. They all operate with resolutions of 1–4 km and impressive (up to 30 minutes) revisit time [5].

Although information is acquired at different bands of the IR spectrum, MODIS, VIIRS and the geosynchronous instruments use similar algorithms to retrieve SST from pixels which are not affected by clouds or aerosols. Given the strong correlation existing between the atmospheric water vapor content and SST, these algorithms usually involve two bands to remove or minimize the effects of the atmosphere and include different series of diurnal and nighttime empirical regression coefficients (a_n) derived from matchup observations [17]. This split-window technique is implemented as a simple nonlinear combination of measured brightness temperatures [18] having the form of

$$SST\left(^{\circ}C\right) = a_0 + a_1 T_{\lambda_1} + a_2 T_R \left(T_{\lambda_1} - T_{\lambda_2}\right) + a_3 \left(T_{\lambda_1} - T_{\lambda_2}\right)\left(\sec\theta - 1\right) \qquad (8.1)$$

where T_{λ_1} and T_{λ_2} are the temperatures (in K) measured at wavelengths where the atmosphere is relatively transmissive (11–12 μm), T_R is the daily "first-guess" estimate of the SST in the area (in °C), and θ is the satellite zenith angle measured at surface. It is important to emphasize that for nighttime retrievals, observations at mid-IR bands (3.5–4 μm) can also be used for obtaining more accurate products.

The along-track scanning radiometer (ATSR) equipped onboard of the ERS-1/2 and the Advanced ATSR (AATSR) flown on Envisat used an approach different from the split-window technique to remove the atmospheric effect on the observed radiances and, therefore, to obtain reliable SST retrievals at 1 km resolution and about 0.3–0.4 K standard deviation [19]. In fact, those instruments are designed to acquire multichannel information with a dual-look-angle technique [20], that is, observing the same element of ocean surface through two different atmospheric path lengths in an interval of time short enough so that the SST and atmospheric conditions do not change. The dual-look successor to AATSR is the sea and land surface temperature radiometer (SLSTR) that operates in a similar manner on ESA Copernicus Sentinel-3a and Sentinel-3b since 2016 and 2018, respectively. This instrument uses two scan mechanisms and a flip mirror to enable wider swath and takes advantage of an accurate self-calibration of the measured radiances that is achieved using two onboard blackbody cavities [15].

8.4.2 Ice Surface Temperature

Split-window technique has been also adapted to retrieve ice surface temperature (IST) over ice fields that cover the sea surface in polar regions. To this purpose, specific Arctic and Antarctic sets of regression coefficients have been derived in order to consider the unique polar ocean characteristics [21]. An interesting IST application has been devoted to the monitoring of polynyas [22], the recurring and quasi-permanent highly dynamic areas of open water which interrupt the continuous ice cover regulating the exchange of heat, energy, mass, and momentum between the ocean and the atmosphere, and represent important hot spots for ice production, deep-water formation, and ventilation of the global oceans [23].

The polynyas extent variability is probably the most useful variable that can be retrieved from satellite imagery to study these areas. The presence of strong gradients of temperature, associated with the transition between open water and ice field, makes IST information an excellent variable to detect polynyas edges with a good accuracy [24], independently from the exact IST value that is retrieved (Fig. 8.2). Despite the constraints of necessary clear-sky scenes and the better estimations provided by high-resolution SAR imagery [25, 26], the availability of multiple IR observations a day (e.g., from MODIS acquisitions) usually reduces gaps in daily monitoring of several polynya areas [22].

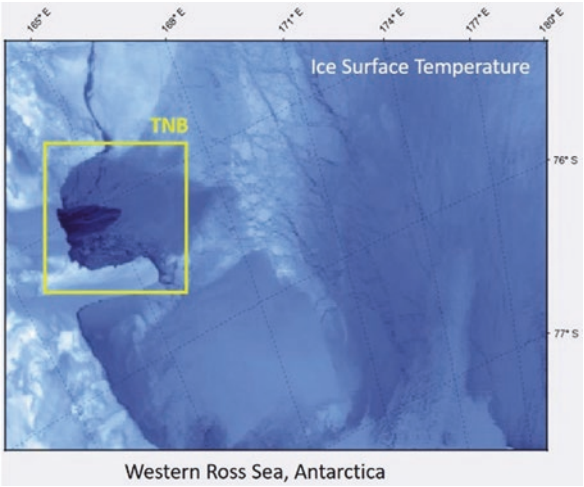

Fig. 8.2 Terra Nova Bay (TNB—yellow square) polynya area (dark blue) observed through MODIS derived ice surface temperature retrievals on September 15, 2014. Estimated polynya extent is about 1428 km^2

8.5 Passive Microwave Radiometry

8.5.1 Physical Aspects

MW radiometers are passive instruments that observe the radiation naturally emitted by the sea surface and that can be used to retrieve several atmospheric and ocean properties, such as SST, SSS, the extent and concentration of sea ice cover, the wind speed, and the rain rate over the ocean. These sensors provide global all-weather coverage, both day and night. Since the atmosphere is much more transparent than in the VIS and IR (VIR), especially in the range between 1 and 10 GHz, MW instruments can view the surface through clouds and gather data under almost all-weather conditions except heavy rain.

At the MW frequencies, the Planck's function can be approximated to the Rayleigh–Jean law [15], so that the emitted radiance varies linearly with the surface physical temperature (T_S) within a frequency interval. As in the IR, the MW brightness temperature (T_B), i.e., the temperature of the black body source that would generate the measured radiance, is related to the physical temperature by the sea surface dielectric properties of the sea surface, which are described by its emissivity (ε), as summarized by the radiative transfer equation [27].

$$T_B = \varepsilon\, t\, T_S + (1-t)\overline{T} + (1-t)(1-\varepsilon)\, t\, \overline{T} + (1-\varepsilon)\, t^2 \left(T_{\text{sun}} + T_{ext}\right) \tag{8.2}$$

where (1–ε) represents reflectivity, t is transmissivity, $\overline{T}$ is the vertical average of the tropospheric temperature profile, T_{sun} is the solar T_B, and T_{ext} is the extraterrestrial brightness temperature exclusive of the sun.

Its approximation in the polar atmosphere

$$T_B\left[\lambda,p\right]=\varepsilon\left[\lambda,p\right]\cdot T_S \tag{8.3}$$

also suggests that T_B is a function of polarization (p). In fact, ocean MW emission is strongly polarized, as it depends on the orientation of the electric field in the plane of incidence with the emitting surface. Since the emissivity changes as the wavelength and polarization vary, the T_B measured at different wavelengths and at different polarizations can be used to retrieve information about the characteristics of the seawater that is emitting the radiation. Considering how each factor differentially affects different MW frequencies, multifrequency and multipolarization radiometers can be used to observe sea surface and retrieve several geophysical parameters by using empirical algorithms, calibrated and validated versus in situ observations. Frequencies used in PMW retrieval of oceanic variables are restricted to specific windows in the range 1–90 GHz to avoid interference from other users, as modern telecommunications and broadcasting infrastructure. These signals would swamp background radiation from natural sources, but by international agreement certain bands are preserved for passive radiometry [5].

Finally, since less energy is available in the MW than in the VIR, a larger aperture or a larger FOV is needed at the long MW wavelengths to obtain the same spatial resolution. Despite significant improvements in swath width, spatial resolution, and spectral diversity have occurred in the last decades, due to size constraints that limit antenna diameters to 1–4 m, at present the resolution of PMW-derived products is usually in the range 3.125–100 km [28].

8.5.2 Wind Speed and Sea Surface Temperature

As mentioned above, the radiation emitted by the sea surface at MW wavelengths depends not only on water temperature and its dielectric properties, but also on the orientation and shape of the sea surface [5]. Consequently, wind speed is one of the parameters that can be retrieved from a multifrequency MW radiometer using empirical algorithms that exploit wind sensitivity at frequencies between 6 GHz and 37 GHz [29]. The first wind speed retrievals date to 1987, thanks to the information collected by the Special Sensor Microwave Imagers (SSM/I) series of instruments carried on the U.S. Defense Meteorological Satellite Program (DMSP). The microwave imager (TMI) on the Japanese–U.S. Tropical Rainfall Measuring Mission (TRMM) satellite and the Japanese Advanced Microwave Scanning Radiometer (AMSR-E) on the NASA Aqua near-polar orbit satellite also provided daily maps of wind speed, since 1997 and 2002, respectively. However, it is important to remark that none of these sensors provide wind direction information as they do for speed (see Chap. 2).

A first fully polarimetric microwave radiometer is indeed the experimental WindSat instrument. It was launched on 2003 onboard the Coriolis spacecraft with

the main purpose of retrieving both speed and direction of the wind from V-pol and H-pol measurements, and provides a cheaper alternative to scatterometers [30].

As for SST, the use of the 6.6 GHz channel, which is sensitive over the full range of sea temperatures, including cold waters, only began in 2002 with the AMSR-E. This sensor provided routine, high-quality, cloud-free, and global mapping of SST over a 1450 km swath, with an accuracy of about 0.4 K and a spatial resolution of about 25 km. Composite daily, weekly, and monthly maps at 1/4°, which are extremely useful to complement infrared radiometers L4 products, are provided as well. In 2012, AMSR-E has been replaced by a second-generation AMSR2 on the Japanese Global Change Observation Mission—Water (GCOM-W) satellite.

SST observations from PMW are also available since 1997 through the TRMM TMI microwave imager but using only the 10.7 GHz channel. Although limited to latitudes lower than 40°, TMI provided continuous observations of the tropical oceans with a resolution of up to 25 km, which allowed the first mapping of mesoscale eddies [31]. As for next-generation satellites, ocean scientists usually suggest SST sensors that could combine the IR and MW channels to provide all-weather SST fields with higher resolution.

8.5.3 Sea Surface Salinity

Sea surface salinity (SSS) is a key component of the water cycle. Its role in ocean density makes it an essential driver of oceanic circulation, a critical parameter for recognizing water masses and understanding their variability and biogeochemical properties, and a tracer of precipitation/evaporation as well as ice melt/freeze.

The retrieval of SSS from microwave radiometry is based on the emissivity of the ocean surface, which depends on the sea surface roughness, and on the dielectric constant of seawater that is a function of temperature and salinity. In such context, three L-band missions, i.e., the ESA Soil Moisture and Ocean Salinity (SMOS) mission [32], the NASA Aquarius mission [33], and Soil Moisture Active Passive (SMAP) observatory [34], provided an unprecedented source of salinity information over the global oceans, which are very useful to improve models and compensate for the scarcity of in situ observations. Since notable differences exist in the instrumental approaches, as well as in the retrieval algorithms and in the dielectric constant models, the three satellite products exhibit SSS errors with a strong dependence on the SST that generally varies with the sensor and version of the products [35].

SMOS satellite was launched in late 2009 and carries aboard an electronically focusing synthetic aperture instrument named MIRAS (Microwave Imaging Radiometer using Aperture Synthesis) operating in L band (1.413 GHz), a protected band at which artificial emissions are forbidden and atmospheric disturbance is negligible. SMOS SSS products are collected over swath of approximately 1000 km with a spatial resolution of 35–50 km and demonstrated good sensitivity of the

ocean surface T_B to SSS in the tropics and subtropics [32]. However, the sensitivity decreases rapidly in cold waters and over areas in which additional undesired effects are due to land–sea and ice–sea contaminations, as well as radio-frequency interference (RFI). Even though L band was supposed to be reserved to science, after the first SMOS data retrievals, the presence of contaminating unlawful sources was indeed noticed [36]. RFI and coast contamination are also challenging in semi-enclosed seas (e.g., the Mediterranean Sea) and represent serious limitations also in Aquarius and SMAP measurements. Nevertheless, several strategies have been developed to overcome these issues and provide new sets of SMOS SSS enhanced data [37, 38]. These enhanced products have been already used, for example, to describe SSS variability at high latitudes [39] or to detect mesoscale structures and reconstruct coherent currents in the Mediterranean Sea [40].

It is important to remark that other than the nominal uses, SMOS has proved to be a versatile satellite, as its data have been used also for additional applications, like wind speed estimation inside tornadoes [41], or the monitoring of the extent and thickness of sea ice [42, 43].

The Aquarius L-band radar/radiometer collected data from August 2011 to June 2015 over a 390 km wide swath with a spatial resolution of about 100–150 km. A complete overview of the progressive improvement obtained in the final version of the released products (i.e., Version 5) and a discussion of the unsolved issues can be found in [44]. Several authors showed that Aquarius data provide reliable information over different areas through comparison with in situ observations and model outputs [45]. Like in SMOS, major issues arise in proximity of coastlines, over areas affected by heavy rain or high RFI and at high latitudes where the L band is less sensitive to SSS. Although the SMAP mission was originally conceived for acquiring direct observations of soil moisture and freeze/thaw, it has been demonstrated that the Aquarius retrieval algorithm can be adapted to retrieve SSS also from this dataset [45].

Future missions are also being planned to enable continuity in the regular and global observation of SSS. Unfortunately, at present SSS products are characterized by a coarse spatial resolution. Next generation of ocean salinity satellite instruments should achieve a much finer spatial resolution (i.e., an order of magnitude) in order to support better the oceanographic, meteorological, and climatological applications [36]. Such improvements cannot be achieved with classical interferometry, so improved techniques should be considered, including the use of a long baseline spatio-temporal interferometer and that of multiple frequencies.

8.5.4 Sea Ice Applications

Sea ice cover has a central role in the albedo feedback mechanisms that regulates climate response at high latitudes and influences the exchange of heat, gases, and momentum between ocean and atmosphere over the polar regions [46, 47]. The monitoring of sea ice extent, concentration, and types represents nowadays a

reliable product of PMW imagers. The dielectric properties of sea ice vary during different stages of growth and decay and are affected by thickness, desalinization, snow cover, roughness, and surface wetness. Thus, the MW emissivity of sea ice is more variable and less predictable than that of seawater, which increases with frequency. The simple formulation of radiative transfer equation in polar regions (Eq. 8.3) and the large differences in open water and sea ice emissivity (T_B contrast is usually >100 K) favored the retrieval of continuous and remarkable ice information on a daily basis. This information allows us to produce composites of the sea ice extent (defined as areas with at least 15% ice coverage) and sea ice concentration variability during the last 40 years and to describe the seasonal to interannual behavior, and the multidecadal trends, in both the Northern and Southern Hemispheres sea ice coverage (Fig. 8.3).

The different responses of the emissivity of open water and sea ice categories to frequency and V/H polarization represent the basis for the algorithms that combine the multifrequency and multipolarization data collected by SSM/I and AMSR-E (and their successors) instruments. SSM/I and SSM/IS (Special Sensor Microwave/Imager Sounder) operate since 1987 (2003) collecting MW observations at 19.35 (V, H), 22.235 (V), 37.0 (V, H), and 85.5 (V, H) GHz. Continuity is available back to 1978, thanks to the scanning multichannel microwave radiometer (SMMR) onboard the NASA NIMBUS-7 spacecraft. Since 2002, AMSR-E (and then AMSR2) employ similar, but not identical, channels at 6.9 (V, H) 10.7 (V, H), 18.7 (V, H), 23.8 (V, H), 36.5 (V, H), and 89.0 (V, H) GHz, with an improved spatial resolution (6.25 km) respect to SSM/I (12.5–25 km). Technical details, issues, and limitations of main empirical algorithms used for sea ice extent and concentration monitoring (e.g., Nasa Team, Bootstrap) are discussed in [48].

Additionally, it is important to remark that first-year ice is saline, while the surface of multiyear ice is nearly fresh and contains many air bubbles (Martin, 2014). Thus, measuring emissivity at different MW frequencies and polarizations also provides valuable information about ice types and thickness as demonstrated in several studies [48–51].

8.6 Synthetic Aperture Radar

8.6.1 Basics of Synthetic Aperture Radar Imaging

SAR is an off-nadir active microwave imaging sensor that allows obtaining fine-resolution images of the Earth's surface day and night under almost any weather conditions latitudes [52]. SAR sensors are usually equipped onboard of aircrafts or satellites in order to exploit the platform's motion to synthesize an antenna longer than its physical dimension. This mechanism makes the spatial resolution of SAR imagery much finer than the one provided by real aperture radars. The image formation process relies on the transmission of modulated microwave pulses while

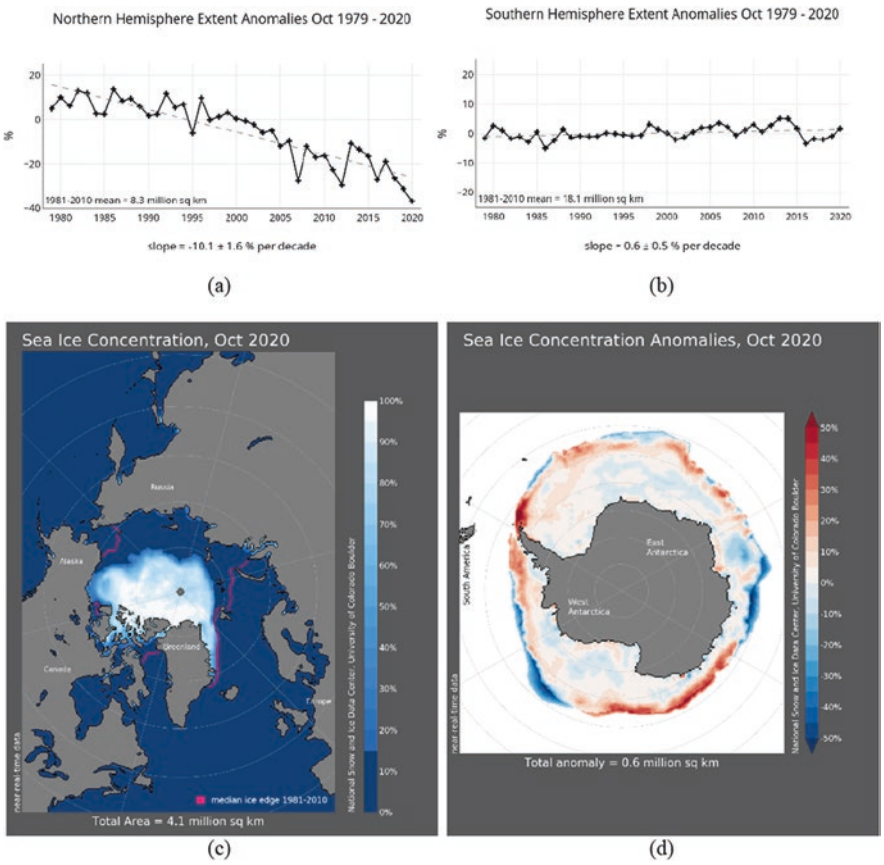

Fig. 8.3 PMW daily and monthly ice extent and concentration products provide a quick look at Arctic- and Antarctic-wide changes in sea ice since 1979. These examples show sea ice extent anomalies during the month of October in the (**a**) Northern and (**b**) Southern Hemisphere since 1979; (**c**) October 2020 sea ice average concentration in the Arctic with an outline of the 30-year (1981–2010) median extent for that month (magenta line); (**d**) October 2020 sea ice concentration anomalies in the Southern Ocean (National Snow and Ice Data Center, University of Boulder Colorado, https://nsidc.org/data/seaice_index)

receiving coherently the echoes scattered off by the observed target. Hence, the SAR image represents a two-dimensional estimation of the target reflectivity which can be linked to the normalized radar cross section (NRCS)—also termed as back-scattering coefficient, σ^0—for each resolution cell [52]. The latter depends on both SAR imaging parameters (wavelength, incidence angle, etc.) and target properties (roughness, moisture, electric permittivity, etc.).

The SAR acquisition geometry is shown in Fig. 8.4. The antenna beam, pointing toward the Earth's surface, illuminates an area termed as footprint, whose width is called swath. The observed area spans two directions: azimuth and range, which are parallel and orthogonal to the platform flight direction, respectively. The ground

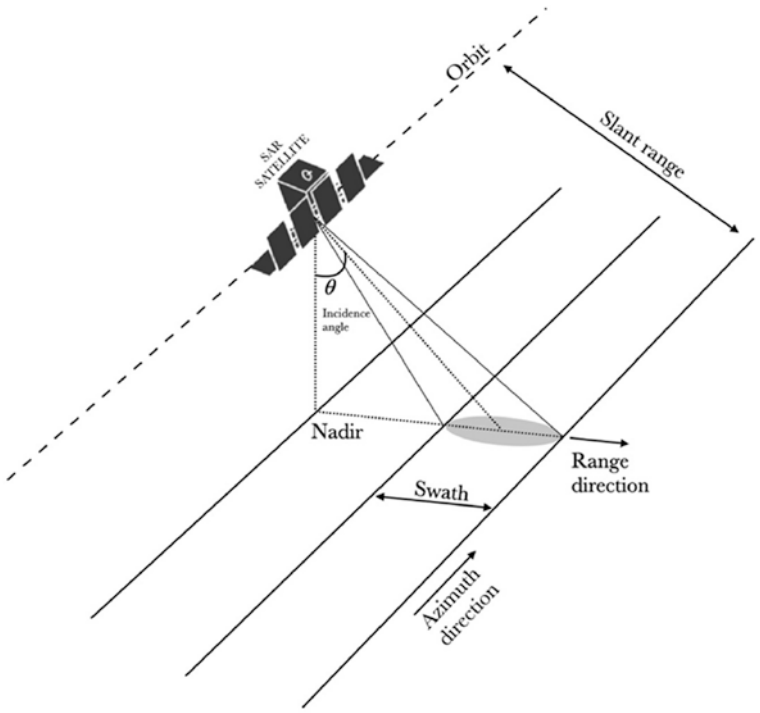

Fig. 8.4 Sketch of the SAR acquisition geometry

area closer to the nadir direction of the SAR sensor is termed near range, while the further one is known as far range. With respect to the nadir, the pointing of the antenna beam defines the incidence angle, which spans from near to far range. When dealing with SAR, the off-nadir looking geometry needed to solve range ambiguities results in a slant range along the line-of-sight direction and a ground range along the Earth's surface, which are related to each other by the incidence angle.

The interpretation of SAR imagery is hampered by the geophysical multiplicative noise that affects any coherent sensor [52]. In fact, the coherent superposition of the backscattered fields due to elementary scatters that lie within each resolution cell results in statistical fluctuations, also known as fading. As a result, gray-tones NRCS SAR images are characterized by a "salt and pepper" appearance termed speckle, which is a random noise that needs to be reduced, at the expenses of the spatial resolution, to improve the capability of extracting reliable information from SAR imagery.

Together with the wavelength of the microwave pulses, an important property that characterizes SAR imaging modes is the polarization. SAR sensors used for Earth observation purposes usually transmit linearly polarized signals, horizontal (H) and/or vertical (V) with reference to the polarization plane, while receiving

coherently in an orthogonal linear H-V basis. The simplest SAR architecture—termed as single-polarization SAR—consists of transmitting a linearly polarized signal while receiving along the same component. When dealing with SAR imaging of the oceans, according to the Bragg/tilted Bragg scattering theory, the vertical polarization is considered to maximize the received signal. Hence, single-polarization SAR operating with a vertical polarization measures the NRCS under vertical transmission and vertical reception, i.e., the VV co-polarized channel σ^0_{VV}. Nevertheless, advanced but more demanding SAR imaging modes, i.e., polarimetric architectures, allow observing the scene under polarization diversity, increasing the geophysical information retrieval capability [53].

The SAR sensors are able to acquire images of the Earth's surface under different imaging modes; each of them is characterized by different spatial resolution, polarization, area coverage, and incidence angle among the various parameters. The most common imaging modes are Stripmap, ScanSAR, and Spotlight [52]. The Stripmap mode consists of illuminating the ground with a continuous sequence of pulse, while the antenna beam is fixed in both azimuth and elevation directions; i.e., a homogeneous scan is made that results in an image quality which is constant along the flight direction. The ScanSAR mode consists of moving the antenna beam along the swath, therefore covering different incidence angles. This results in a reduced azimuth bandwidth and, hence, in a coarser spatial resolution. The Spotlight mode consists of using an observation time as long as the synthetic aperture, resulting in a finer resolution if compared to the Stripmap mode. Spotlight is the finest resolution SAR imaging mode, even if it provides information over a very limited area on the ground.

The main data format for SAR data processing to generate added-value products are single-look complex (SLC) and ground range detected (GRD):

- SLC (Level 1A in Subsect. 8.2.3): SAR images are stored, after raw data focusing, in complex format (real and imaginary part). They are represented in radar coordinates, i.e., over the slant range azimuth plane centered in the zero Doppler point. The product needs radiometric calibration to obtain the NRCS value for each pixel of the image. SLC products are suggested for data processing that needs phase information.
- GRD (Level 1B in Subsect. 8.2.3): SAR images are stored, after raw data focusing, in real format (amplitude). They are represented over the ground range azimuth plane using a reference model for the Earths' ellipsoid. The product needs radiometric calibration to obtain the NRCS value for each pixel of the image. GRD products are suggested for data processing that exploits intensity.

Nowadays, it has been widely demonstrated that SAR satellites represent a key source of information for a broad range of ocean applications including coastline extraction; wind field retrieval; target detection; oil spill monitoring; observation of ocean features as eddies, internal waves, currents; sea ice classification; and extreme weather phenomena observation.

8.6.2 Small-Size Satellites Technology

In very recent years, with the goal of providing a cost-effective and broader access to the space segment even for small companies and universities by trading off satellite planning constraints and launch costs, small-size lighter Earth observation satellites have been launched. This was boosted by the growing developing of engineering technologies in the fields of nano-electronics, micromechanics, solar cells, positioning systems, and telecommunications. In fact, before the beginning of the small satellite era, typical satellite mass was in the range 500 kg–2000 kg, for a cost in the range of 40–170 billion euros, making this market restricted to space agencies and well-established governmental agencies [54]. When dealing with small satellites, mass and cost were dramatically reduced down to few kilograms and few thousand euros, respectively, welcoming into this market many other aerospace operators and private small companies as ICEYE, XpressSAR, and OptiSAR. In addition, the limited costs allow launching experimental space instruments to be tested and validated for research purposes.

Satellites can be grouped according to their mass since it has a direct impact on the launch cost when placed as payload onboard of space vehicles. Small satellites are classified as minisatellites (100–1000 kg), microsatellites (10–100 kg), nanosatellites (1–10 kg), picosatellites (0.1–1 kg), and femtosatellites (0.001–0.1 kg); see Table 8.2.

The fundamental element of most the small-size satellites is the Cubesat, a small-size satellite composed by one or more 10 cm^3 modular units. An "XU" Cubesat indicates a small satellite composed by "X" modular units. The use of Cubesat allows optimizing the hosting capabilities of large launchers; i.e., Cubesat modular units are so small that can be placed as a secondary payload in the extraspace present in large space vehicles in order to put in orbit several small-size satellites with a single launch. Furthermore, the whole Cubesat project from the original idea to the launch takes no longer than 24 months with a total cost that does not exceed 1 billion euros. Several Italian (BlackSky, PlaTino) and international (Quakesat-1, Genesat-1, PRISM, NovaSar, ICEYE) space missions used Cubesat with different payloads depending on the goals of the mission. In 2016, the NRC NASA report found that 34 Cubesat were operating along with 18 space missions, while 46 more

Table 8.2 Satellite classification based on dimension and mass [55]

Satellite class	Mass (kg)
Large	>1000
Mini	100–1000
Micro	10–100
Nano	1–10
Pico	0.1–1
Femto	0.001–0.1

Cubesat were already planned. In 2017, 8 Cubesat missions for Earth observation equipped with optical spectrometers and microwave sensors were developed (three 3 U and five 6 U satellites) by the Earth Science Technology Office (ESTO) under two different NASA space programs: Inflight Validation of Earth Science Technology (InVEST) and Earth Venture Technology [56, 57].

The main planning criteria to be satisfied by the small-size Cubesat satellite can be summarized as follows: minimizing the deployment costs and the risks associated with the instruments; standardizing the modular units; using electronics which is robust to space radiation; and optimizing pointing and propulsion systems. Nowadays, the small-size satellite technology was exploited to host SAR sensors in several space missions. The main mini-SAR satellite (see Table 8.2) missions for Earth observation are as follows [55]:

- NovaSAR-1 (UK, 400 kg);
- TecSAR (Israel, 260 kg);
- SmallSat InSAR (USA/India, 180 kg);
- Micro-XSAR (Japan, 135 kg).

The main micro-SAR satellite (see Table 8.3) missions for Earth observation are as follows:

- ICEYE (Finland, 85 kg);
- Micro-SAR (Norway, 65 kg);
- Capella-XSAR (USA, 48 kg).

8.6.3 The ICEYE Constellation Mission

ICEYE is a Finnish commercial company that was born in 2012 from a research team of the Aalto University. The ICEYE company planned to launch a constellation of 18 sun-synchronous circular orbit (570 km height, 97° inclination)

Table 8.3 Main ICEYE microsatellite characteristics

Satellite characteristic	Value
Carrier frequency (GHz)	9.65, X band
Look direction	Right and left
Antenna size (m)	3.2 × 0.4
Pulse repetition frequency (kHz)	2–10
Range bandwidth (MHz)	10–300
Polarization	VV
Microwave peak power (kW)	4
Total mass (kg)	85

microsatellites in the next few years, offering an unprecedented dense revisit time of 3 h on average, worldwide. Actually, 7 out of the 18 satellites are operating.

The first satellite of the constellation was launched on January 2018 by the Indian rocket PSLV-C40, while the second one was launched in California on December 2018 by the VAFB (Vandenberg Air Force Base) SpaceX Falcon-9 Block 5 launcher, during the SSO-A Spaceflight mission. The last satellite was launched on September 28, 2020, from the Russian Plesetsk Cosmodrome as secondary payload of the Roscosmos Rideshare Soyuz-2.1b/Fregat.

ICEYE satellites are equipped with X-band SAR sensors (carrier frequency around 10 GHz, corresponding to a wavelength of about 3 cm) to keep a small size since the transmitted wavelength is comparable to the actual antenna size [52]. Each SAR belonging to the ICEYE microsatellite constellation is identified by the label "ICEYE-XN," where "N" stands for the satellite identifier. ICEYE-X1 was the first micro-SAR satellite. The main technical features of ICEYE-X2, ICEYE-X4, and ICEYE-X5 are listed in Table 8.4.

It can be noted that they are all equipped with single-polarization VV SAR sensors characterized by a small 3.2 m × 0.4 m phased array antenna, an incidence angle range spanning from 10° to 35° depending on the imaging mode, and total satellite mass of 85 kg. The ICEYE micro-SAR satellites acquire images under two different imaging modes, Stripmap and Spotlight modes, that call for a spatial resolution up to 2.5 m and 0.25 m, respectively. A ScanSAR imaging mode is also planned to be implemented in the near future; see Table 8.3. Note that, independently on the imaging mode, the noise equivalent sigma zero (NESZ), i.e., the noise floor of the SAR instrument, is always better than −19 dB, which is comparable with NESZ values of same imaging modes of conventional X-band SAR satellites as the German TerraSAR-X. As an example, a SAR image collected by ICEYE-X5 over the coast of Port Hedland (Australia) in Stripmap mode is shown, overlapped on the Google Earth map (Fig. 8.5).

Several studies assessed the small-size satellite constellation, including ICEYE, performance with respect to satellite mass, and total cost of the space mission (satellite development and launch); see Fig. 8.6 [54, 58].

Table 8.4 Main features of the ICEYE SAR imaging modes

SAR parameter	Spotlight high	Spotlight	Stripmap high	Stripmap
Area coverage (km^2)	5 × 5	5 × 5	30 × 50	30 × 50
Range × azimuth ground resolution (m)	1 × 1	1 × 1	3 × 3	3 × 3
Range × azimuth slant resolution (m)	0.5 × 0.25	0.5 × 0.5	0.5 × 2.5–3	0.5–1.5 × 2.5–3
NESZ (dB)	≤17	≤17	≤17	≤19
Incidence angle range (°)	20–35	20–35	15–30	15–30

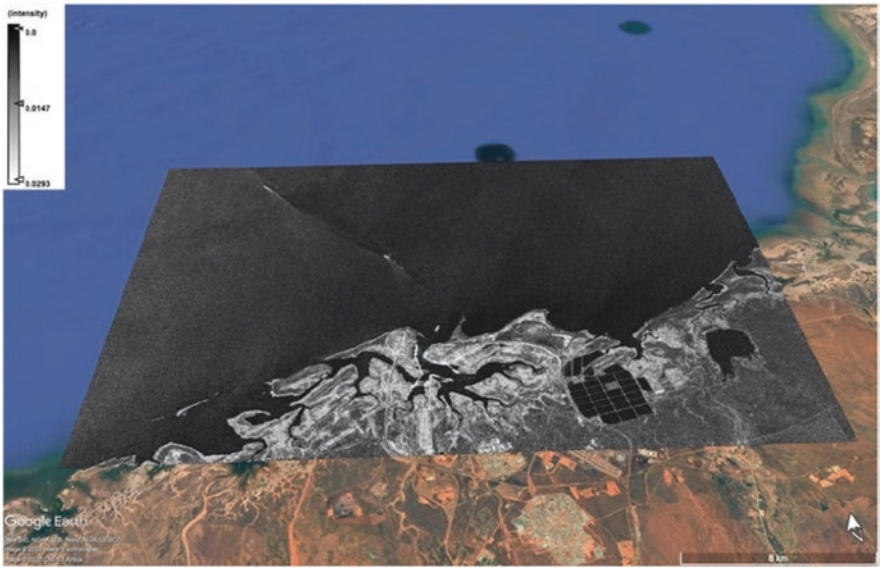

Fig. 8.5 A gray-tones intensity image collected by ICEYE-X5 over the coast of Port Hedland (Australia), superimposed on the Google Earth map

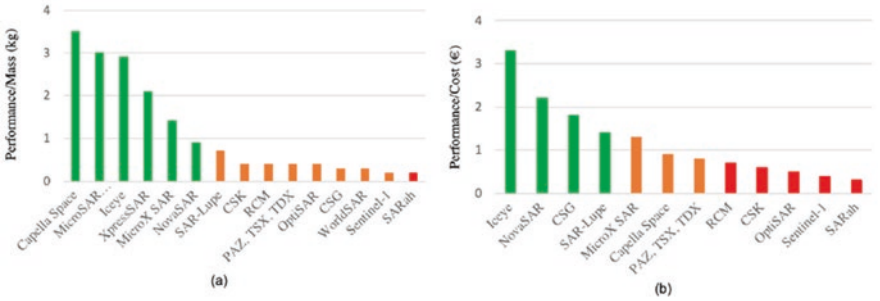

Fig. 8.6 ICEYE performance analysis with respect to (**a**) mass and (**b**) cost [54]

8.6.4 SAR Wind Speed Retrieval

The scattering of the electromagnetic waves from the ocean surface is mainly ruled by the electrical and geometrical properties of the ocean layer involved in the interaction between electromagnetic waves and ocean. At microwave frequencies, the scattering from the wind-roughened ocean surface is the main mechanism. It results from complex nonlinear interactions which are time-dependent and affected by the atmospheric boundary layer [59]. Generally speaking, when the wind blows, short waves that are aligned to the wind direction are generated first, and then, while it continues to blow, large waves are generated until equilibrium is reached. This

reference case, usually assumed in SAR ocean modeling, is known as a fully developed sea [58]. Whenever the fully developed sea case is in question and no swell or coastal effects are present, it is possible to relate the ocean roughness to the local wind speed and direction, i.e., wind field, by a proper modeling, which is at the basis of the scatterometer, i.e., a multibeam real aperture radar that is designed to provide mesoscale estimations of sea surface wind field (see Chap. 2). These sensors offer limited possibility for wind estimation in coastal regions due to land/sea contamination arising from their coarse spatial resolution.

Within this context, the SAR is a key tool to generate high-resolution (up to 1 km) wind maps that are used in local forecasting, typhoon monitoring, and coastal engineering applications. However, unlike the scatterometer, the SAR was not designed for ocean surface wind retrieval, and, therefore, it is impossible to derive both the wind speed and direction based on NRCS values alone. Several approaches have been proposed to deal with wind direction retrieval based on the use of additional wind data sources, e.g., operational meteorological models and wind-aligned features observed in the SAR images (typically in coastal zones) or measurements from other in situ or remote sensors. With respect to wind speed, empirical geophysical model functions (GMFs), originally developed to exploit C-band VV-polarized scatterometer measurements [60, 61], have been tuned and recalibrated to deal with SAR measurements at different frequencies and polarizations. However, when retrieving wind speed using those GMFs, wind direction information must be provided in the retrieval process [60]. This means that errors in the wind direction estimation are propagated into the wind speed estimation.

An alternative approach to the GMF is the so-called azimuth cutoff methodology [62]. It is a spectral method that does not need neither calibration of the data nor any a priori information on wind direction [10] and, therefore, has recently gained more attention [63, 64]. According to [62], the azimuth cutoff λ_c is linked to the directional sea spectrum $S(\omega,\delta,\varphi)$ as follows:

$$\lambda_c = \pi\beta\sqrt{\int_0^\infty \omega^2 S\left(\omega,\delta,\varphi\right) d\omega} \tag{8.4}$$

where ω is the angular frequency of sea waves, δ is the incidence angle, φ is the relative direction of the ω-component of the sea surface spectrum, and β is the ratio between the slant range distance and the velocity of SAR platform.

The retrieval of λ_c from SAR imagery consists of some key steps: (a) The SAR image is partitioned into a number of tails; (b) the autocorrelation function (ACF) is estimated by evaluating the inverse fast Fourier transform (IFFT) of the PSD computed for each tail; (c) speckle noise peaks are mitigated by median filtering; (d) λ_c is estimated as follows [64]:

$$\lambda_c = \sqrt{2\pi\sigma} \tag{8.5}$$

where σ is the standard deviation of the Gaussian bell that best fits the estimated ACF; e) the sea surface wind speed at 10 m above sea level (U) is estimated from the linear relationship [62]:

$$\lambda_c = a + bU \tag{8.6}$$

where a and b are coefficients to be determined from data. Once the azimuth cutoff algorithm was detailed, the sea surface wind speed estimation from ICEYE micro-SAR satellite imagery is showcased to demonstrate the potential of small-size SAR satellites for ocean monitoring. An image collected on September 7, 2019, by the ICEYE-X5 SAR over the coastal area of Port Hedland, northwestern part of Australia, is considered. The fine-resolution image (3 m), covering an area of about 800 km^2, was acquired in VV-polarization Stripmap mode under an incidence angle of 28.5° at midrange.

A multilooked Level 1.1 product with a pixel spacing of 10 m is processed to obtain U on a 1.5 km × 1.5 km grid. The sea surface wind speed map is shown in Fig. 8.7, where the land is masked out in white. It can be observed that low-to-moderate sea state conditions apply over the Port Hedland coastal area at the SAR acquisition time. On average, a wind speed of about 5.45 m/s is estimated. This is consistent with the wind speed information provided by a collocated ASCAT scatterometer product (12.5 km spatial resolution) that results in an average sea surface wind speed of 5.35 m/s.

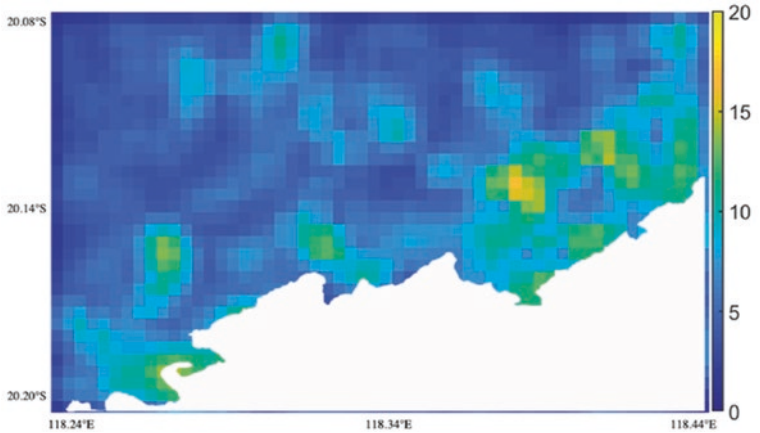

Fig. 8.7 Sea surface wind speed (m/s) map obtained from the ICEYE SAR using the azimuth cutoff approach

8.7 Radar Altimetry

Since 1992 [65], radar altimeters monitor the sea surface topography along the satellite's ground track in order to provide near-global high-precision record of the temporal and spatial scales of ocean variability, the meridional transports of heat, and the distribution and properties of ocean eddies [1]. To this goal, the altimeters transmit short pulses of energy vertically downward toward the surface and then receive the reflected signal. The measure of the time difference between the transmitted and received very short radar pulses gives an estimation of the distance between the satellite and the ocean surface, i.e., of the sea surface height (SSH) associated with tides, geostrophic currents, seafloor topography, and other oceanic phenomena. The shape of the returned electromagnetic signal gives indeed an estimation of the significant wave height (SWH) and the wind speed [31]. Present studies focus on improving resolution and accuracy when approaching the coasts, since the extraction of correct sea level information is still challenging due to corrupted waveforms and imprecise auxiliary information used in the data processing [66, 67]. Additional insights on sea level measurements are provided in Chap. 10.

References

1. Martin S (2014) An introduction to ocean remote sensing, 2nd edn. Cambridge University Press, Cambridge.
2. Sammartino M, Marullo S, Santoleri R, Scardi M (2018) Modelling the vertical distribution of phytoplankton biomass in the Mediterranean Sea from satellite data: a neural network approach. Remote Sens (Basel) 10:1666
3. Nardelli B et al (2020) A deep learning network to retrieve ocean hydrographic profiles from combined satellite and in situ measurements – personal communication. J Geophys Res 12:3151
4. Le Traon PY, Reppucci A, Fanjul EA, Aouf L, Behrens A, Belmonte M et al (2019) From observation to information and users: the Copernicus marine service perspective. Front Mar Sci 6:234
5. Robinson IS (2010) Discovering the ocean from space: the unique applications of satellite oceanography. Springer, Berlin, p 685
6. Robinson IS (2004) Measuring the ocean from space: the principles and methods of satellite oceanography. Springer, Berlin, p 669
7. Parkinson C, Ward A, King M (2006) Earth science reference handbook: a guide to NASA's earth science program and earth observing satellite missions. National Aeronautics and Space Administration, Washington, p 277
8. Groom et al (2019) Satellite Ocean colour: current status and future perspective. Front Mar Sci 6:485
9. Dierssen HM, Radolph K, Lewis E (2013) Remote sensing of ocean colour. In: Orcutt J (ed) Earth system monitoring: selected entries from the encyclopedia 439 of sustainability science and technology. Springer, New York
10. Donlon C, Berruti B, Buongiorno A, Ferreira MH, Femenias P, Frerick J et al (2012) The global monitoring for environment and security (GMES) Sentinel-3 mission. Remote Sens Environ 120:37–57

11. Ruddick K, Neukermans G, Vanhellemont Q, Jolivet D (2014) Challenges and opportunities for geostationary ocean colour remote sensing of regional seas: a review of recent results. Remote Sens Environ 146:63–76
12. Cotroneo Y, Aulicino G, Ruiz S, Pascual A, Budillon G, Fusco G, Tintoré J (2016) Glider and satellite high resolution monitoring of a mesoscale eddy in the algerian basin: effects on the mixed layer depth and biochemistry. J Mar Syst 162:73–88
13. Rivaro P, Ianni C, Langone L, Ori C, Aulicino G, Cotroneo Y, Saggiomo M, Mangoni O (2017) Physical and biological forcing of mesoscale variability in the carbonate system of the Ross Sea (Antarctica) during summer 2014. J Mar Syst 166:144–158
14. de Ruggiero P, Napolitano E, Iacono R, Pierini S (2016) A high-resolution modelling study of the circulation along the Campania coastal system, with a special focus on the Gulf of Naples. Cont Shelf Res 122:85–101
15. Minnett PJ et al (2019) Half a century of satellite remote sensing of sea-surface temperature. Remote Sens Environ 2019:233
16. Donlon CJ et al (2007) The global ocean data assimilation experiment high-Resolution Sea surface temperature pilot project. Bull Am Meteorol Soc 88:1197–1213
17. Kilpatrick KA, Podestá G, Walsh S, Williams E, Halliwell V, Szczodrak M, Brown OB, Minnett PJ, Evans R (2015) A decade of sea surface temperature from MODIS. Remote Sens Environ 165:27–41
18. Walton CC, Pichel WG, Sapper JF, May DA (1998) The development and operational application of nonlinear algorithms for the measurement of sea surface temperatures with the NOAA polar-orbiting environmental satellites. J Geophys Res 103(27):999–928,012
19. Berry D, Corlett G, Embury O, Merchant C (2018) Stability assessment of the (a)ATSR Sea surface temperature climate dataset from the European Space Agency climate change initiative. Remote Sens (Basel) 10:126
20. Llewellyn-Jones DT, Minnett PJ, Saunders RW, Zavody AM (1984) Satellite multichannel infrared measurements of sea surface temperature of the N.E. Atlantic Ocean using AVHRR/2. Q.J.R. Meteorol Soc 110:613–631
21. Hall DK, Key JR, Casey KA, Riggs GA, Cavalieri DJ (2004) Sea-ice surface temperature product from MODIS. IEEE Trans Geosci Remote Sens 42:1076–1087
22. Preußer A, Willmes S, Heinemann G, Paul S (2015) Thin ice dynamics and ice production in the Storfjorden polynya for winter seasons 2002/2003–2013/2014 using MODIS thermal infrared imagery. Cryosphere 9:1063–1073
23. Aulicino G, Sansiviero M, Paul S, Cesarano C, Fusco G, Wadhams P, Budillon G (2018a) A new approach for monitoring the Terra Nova Bay polynya through MODIS ice surface temperature imagery and its validation during 2010 and 2011 winter seasons. Remote Sens (Basel) 10:366
24. Sansiviero M, Morales Maqueda MÁ, Fusco G, Aulicino G, Flocco D, Budillon G (2017) Modelling Sea ice formation in the Terra Nova Bay polynya. J Mar Syst 166:4–25
25. Parmiggiani F (2006) Fluctuations of Terra Nova Bay polynya as observed by active (ASAR) and passive (AMSR-E) microwave radiometers. Int J Remote Sens 27:2459–2467
26. Aulicino G, Wadhams P, Parmiggiani F (2019a) SAR pancake ice thickness retrieval in the terra nova bay (Antarctica) during the PIPERS expedition in winter 2017. Remote Sens (Basel) 11:2510
27. Stewart RH (1985) Methods of satellite oceanography. University of California Press, Berkeley
28. Brodzik MJ, Long DG, Hardman MA, Paget A, Armstrong R (2018) MEaSUREs calibrated enhanced-resolution passive microwave daily EASE-grid 2.0 brightness temperature ESDR, version 1. NASA National Snow and Ice Data Center Distributed Active Archive Center, Boulder
29. Wentz FJ (1997) A well calibrated ocean algorithm for special sensor microwave/imager. J Geophys Res 102:8703–8718
30. Ricciardulli L, Wentz FJ (2015) Ascatterometer geophysical model function for climate-quality winds: QuikSCAT Ku-2011. J Atmos Oceanic Tech 32:1829–1846

31. Fu LL, Lee T, Liu WT, Kwok R (2019) 50 years of satellite remote sensing of the ocean. Meteorol Monogr 59:1–46
32. Mecklenburg S et al (2012) ESA's soil moisture and ocean salinity Mission: Mission performance and operations. IEEE Trans Geosci Remote Sens 50:1354–1366
33. Le Vine DM, Lagerloef GSE, Colomb FR et al (2007) Aquarius: an instrument to monitor sea surface salinity from space. IEEE Trans Geosci Remote Sens 45:2040–2050
34. Entekhabi D et al (2010) The soil moisture active passive (SMAP) mission. Proc IEEE 98:704–716
35. Soldo Y, Cabot F, Rougé B, Kerr YH, Al Bitar A, Epaillard E (2013) SMOS-NEXT: a new concept for soil moisture retrieval from passive interferometric observations. Eur Astron Soc Publ Ser 59:203–212
36. Alvera-Azcarate A, Barth A, Parard G, Beckers J-M (2016) Analysis of SMOS Sea surface salinity data using DINEOF. Remote Sens Environ 180:137–145
37. Olmedo E, Martínez J, Turiel A, Ballabrera-Poy J, Portabella M (2017) Debiased non-Bayesian retrieval: a novel approach to SMOS Sea surface salinity. Remote Sens Environ 193:103–126
38. Olmedo E, Taupier-Letage I, Turiel A, Alvera-Azcaràte A (2018) Improving SMOS Sea surface salinity in the Western Mediterranean Sea through multivariate and multifractal analysis. Remote Sens (Basel) 10:485
39. Aulicino G, Cotroneo Y, Olmedo E, Cesarano C, Fusco G, Budillon G (2019b) In situ and Satellite Sea surface salinity in the Algerian Basin observed through ABACUS glider measurements and BEC SMOS regional products. Remote Sens (Basel) 11:1361
40. Grodsky SA, Reul N, Lagerloef G, Reverdin G, Carton JA, Chapron B, Quilfen Y, Kudryavtsev VN, Kao H-Y (2012) Haline hurricane wake in the Amazon/Orinoco plume: AQUARIUS/SACD and SMOS observation. Geophys Res Lett 39:L20603
41. Kaleschke L, Tian-Kunze X, Maaß N, Mäkynen M, Drusch M (2012) Sea ice thickness retrieval from SMOS brightness temperatures during the Arctic freeze-up period. Geophys Res Lett 39:L05501
42. Mäkynen M et al (2020) Satellite observations for detecting and forecasting sea-ice conditions: a summary of advances made in the SPICES project by the EU's horizon 2020 programme. Remote Sens (Basel) 12:1214
43. Le Vine DM, Dinnat EP, Meissner T, Wentz FJ, Kao HY, Lagerloef G, Lee T (2018) Status of Aquarius and salinity continuity. Remote Sens (Basel) 10:1585
44. Meissner T, Wentz FJ, Le Vine DM (2018) The salinity retrieval algorithms for the NASA Aquarius version 5 and SMAP version 3 releases. Remote Sens (Basel) 10:1121
45. Dinnat EP, Le Vine DM, Boutin J, Meissner T, Lagerloef G (2019) Remote sensing of sea surface salinity: comparison of satellite and in situ observations and impact of retrieval parameters. Remote Sens (Basel) 11:750
46. Cerrone D, Fusco G, Simmonds I, Aulicino G, Budillon G (2017) Dominant covarying climate signals in the southern ocean and antarctic sea ice influence during the last three decades. J Climate 30:3055–3072
47. Wadhams P, Aulicino G, Parmiggiani F, Persson POG, Holt B (2018) Pancake ice thickness mapping in the Beaufort Sea from wave dispersion observed in SAR imagery. J Geophys Res Oceans 123:2213–2237
48. Tateyama K, Enomoto H, Toyota T, Uto S (2002) Sea ice thickness estimated from passive microwave radiometers. Polar Meteorol Glaciol 16:15–31
49. Martin S, Drucker R, Kwok R, Holt B (2004) Estimation of the thin ice thickness and heat fluxes for the Chukchi Sea Alaskan coast polynya from SSM/I data, 1990–2001. J Geophys Res 109:C10012-1–C10012-15
50. Naoki K, Ukita J, Nishio F, Nakayama M, Comiso JC, Gasiewski AJ (2008) Thin sea ice thickness as inferred from passive microwave and in situ observations. J Geophys Res 113:C02S16-1–C02S16-11

51. Aulicino G, Fusco G, Kern S, Budillon G (2014) Estimation of sea-ice thickness in Ross and Weddell seas from SSM/I brightness temperatures. IEEE Trans Geosci Remote Sens 52:4122–4140
52. Richards JA (2009) Remote sensing with imaging radar. Signals and communication technology series. Springer, Berlin
53. Lee JS, Pottier E (2009) Polarimetric radar imaging: from basics to applications. CRC Press, Boca Raton
54. Filippazzo G, Dinand S (2017) The potential impact of small satellite radar constellations on traditional space systems. In: 5th federated and fractionated satellite systems workshop, Toulouse
55. Kramer HJ, Cracknell AP (2008) An overview of small satellites in remote sensing. Int J Remote Sens 29(15):4285–4337
56. Peral E et al (2018) Radar technologies for Earth remote sensing from CubeSat platforms. Proc IEEE 106(3):404–418
57. Paek SW, Balasubramanian S, Kim S, de Weck O (2020) Small-satellite synthetic aperture radar for continuous global Biospheric monitoring: a review. Remote Sens (Basel) 12:2546
58. Deepak RA, Twiggs RJ (2012) Thinking out of the box: space science beyond the CubeSat. J Small Satell 1:3–7
59. Apel JR (1987) Principles of ocean physics, vol 38. Academic, New York
60. Wackerman CC et al (1996) Wind vector retrieval using ERS-1 synthetic aperture radar imagery. IEEE Trans Geosci Remote Sens 34(6):1343–1352
61. Grieco G, Nirchio F, Migliaccio M (2015) Application of state-of-the- art SAR X-band geophysical model functions (GMFs) for sea surface wind (SSW) speed retrieval to a data set of the Italian satellite mission COSMO-SkyMed. Int J Remote Sens 36(9):2296–2312
62. Kerbaol V, Chapron B, Vachon PW (1998) Analysis of ERS-1/2 synthetic aperture radar wave mode images. J Geophys Res Ocean 103(C4):7833–7846
63. Grieco G, Lin W, Migliaccio M, Nirchio F, Portabella M (2016) Dependency of the Sentinel-1 azimuth wavelength cut-off on significant wave height and wind speed. Int J Remote Sens 37(21):5086–5104
64. Corcione V, Grieco G, Portabella M, Nunziata F, Migliaccio M (2019) A novel azimuth cutoff implementation to Retrieve Sea surface wind speed from SAR imagery. IEEE Trans Geosci Remote Sens 57(6):3331–3340
65. Abdallah S et al (2021) Altimetry for the future: building on 25 years of progress. Advances on space research 68(2):319–363.
66. Aulicino G, Cotroneo Y, Ruiz S, Román AS, Pascual A, Fusco G, Tintoré J, Budillon G (2018b) Monitoring the Algerian Basin through glider observations, satellite altimetry and numerical simulations along a SARAL/AltiKa track. J Mar Syst 179:55–71
67. Taburet G, Sanchez-Roman A, Ballarotta M, Pujol M-I, Legeais J-F, Fournier F et al (2019) Duacs dt-2018: 25 years of reprocessed sea level altimeter products. Ocean Sci Discuss 2019:1–30

Chapter 9
Sea Monitoring Networks

Maurizio Ferla, Gabriele Nardone, Arianna Orasi, Marco Picone, Pierpaolo Falco, and Enrico Zambianchi

Contents

Abstract This chapter aims to describe and analyse different types of sea monitoring networks and their potential and characteristics. The life history of operational instruments involves different phases, such as planning according to the recorded parameter, selection and installation of sensors, operation, calibration, maintenance and training activities. These factors are illustrated and discussed. Moreover, the quality of the measurements data is considered of paramount importance because it must guarantee the efficacy of monitoring, design, environmental studies and civil protection activities along the coast. Main procedures of data quality control and dissemination, both in real and delayed time, are summarized, and reference is made to international guidelines.

M. Ferla · G. Nardone (✉) · A. Orasi · M. Picone
Istituto Superiore per la Protezione e la Ricerca Ambientale ISPRA,
Via Vitaliano Brancati, Rome, Italy
e-mail: maurizio.ferla@isprambiente.it; gabriele.nardone@isprambiente.it;
arianna.orasi@isprambiente.it; marco.picone@isprambiente.it

P. Falco
Department of Life and Environmental Sciences, Università Politecnica delle Marche,
Via Brecce Bianche, Ancona, Italy
e-mail: pierpaolo.falco@staff.univpm.it

E. Zambianchi
Department of Science and Technology, University of Naples "Parthenope",
Centro Direzionale, Isola C4, Naples, Italy
e-mail: enrico.zambianchi@uniparthenope.it

P. Daponte et al. (eds.), *Measurement for the Sea*, Springer Series in
Measurement Science and Technology,
https://doi.org/10.1007/978-3-030-82024-4_9

Still today, a series of meteo-marine observations are currently spread in a large number of public and private institutions, making difficult the realistic and updated knowledge of what is available and how to obtain part of those data for climatic studies, numeric model calibration, planning and management of coastal zone.

The need of an integrated national sea state monitoring system is demonstrated as the way to be undertaken to reach a correct management and safety of both coastal and open sea areas; this system must ever take into account a series of technological and scientific progress which has broadened the spectrum of potentially available tools to the scientific community and institutional stakeholders.

9.1 Introduction

9.1.1 Scope and Main Types of Marine Observation Network

The marine environment is an essential component of the planet, and it is why the knowledge and a deep study of this biosphere are a challenge that has increasingly involved modern societies, from the point of view of scientific research but also of economic interests. Sea monitoring consists of recurrent, systematic investigations about the status, the changes and the effects of measures adopted on this environment. For this reason, the oceanographic science and technology industry has developed a multitude of equipment for the automatic monitoring of a multiplicity of parameters that we will try to describe below. This chapter aims to present a brief summary of the challenges for the observation of the marine environment, to describe the state of the art in the field of sea monitoring networks, providing a broad vision of the technology of existing platforms. However, the goal is ambitious as for the same physical phenomenon different parameters can be monitored, and for each type of parameter, there may exist different types of platforms suitable for observation.

For this reason, it was decided to limit the concept of monitoring network to a homogeneous set of fixed or ship-based platforms for physical sea state monitoring and some related atmospheric parameters, excluding other types of observations or instruments which in a broad sense can still be considered as a monitoring network. For example, it will not include drifters, floats, ROVs, gliders and autonomous surface craft.

Furthermore, it will be mainly dealt with the aspect related to surface monitoring networks, in particular buoys and inshore platforms, although many of the considerations developed can be extended to bottom observatories, moored profilers and many others. Very innovative systems will also be treated at the end of the chapter, which could constitute interesting monitoring tools, especially in undersampled regions, even if they are currently still to be considered at the level of scientific research. In the next paragraph, the theme of the integration of observational systems will be addressed, discussing why an integrated monitoring system is not the

simple sum of the various components but must constitute a new infrastructure enhanced by their synergy.

9.1.2 Towards an Integrated Observation System

Generally, the principal sea observation systems are managed by different entities in charge of national environmental monitoring and protection programs. Universities and research centres mainly contribute to sampling and data analysis; there are also networks managed to provide commercial services, sometimes dedicated to very restricted groups of users. A shared and integrated management of existing observation systems would be preferable, in order to obtain a more efficient monitoring system.

The development of such integrated systems, which is crucial for the proper management and safety of both coastal areas and the open sea, must take into account a series of technological and scientific advances that have broadened the spectrum of platforms potentially available to the scientific community and institutional stakeholders. The different methodologies available must not be considered in competition, but they must be thought of as connected in a complementary way so to be able to take full advantage of the strengths of each one. The goal is therefore the integration of all observations in order to monitor the essential parameters needed to a deeper understanding of the marine environment in the short and long term.

On this way goes the work of the JCOMM (www.jcomm.info), WMO-IOC Joint Technical Commission for Oceanography and Marine Meteorology, which is contributing to the coordination, development and recommendation of standards and procedures for a fully integrated marine observing, data management and services system. Inside the JCOMM structure, the Global Ocean Observing System (GOOS: www.goosoceans.org) is a collaborative system of ocean observations, encompassing in situ networks, and satellite systems, sponsored by Governments and UN agencies like World Meteorological Organization (WMO), Intergovernmental Oceanographic Commission (IOC) of UNESCO, United Nations Environment Programme (UNEP), and International Council for Science (ICSU). It is designed to provide observations from the global ocean, and related analysis and modelling of ocean fields in support of operational oceanography and climate change applications.

9.2 Design of a Sea Monitoring Network

The design of a sea monitoring network must take into account the limits and potential of each marine data collection methodologies in relation to the different purposes to which a systematic monitoring activity can be oriented.

There are specific guidelines for the design of a network depending on the purpose of the monitoring, addressed to specialized operators who conduct monitoring activities and own specific training and experience. An excellent example of these documents is the set of WMO guidelines which generally contain basic notions on physical phenomena and some technical details of instrumentation [1].

Other indications may result from documents that meet the urgent environmental, political and economic challenges at a global, regional or local scale. An example is the UN Sustainable Development Goals (SDGs) born during the United Nations Conference on Sustainable Development in Rio de Janeiro in 2012 that in the next decades will provide a framework for a collaborative and participative research on oceans, supporting the integration of different knowledge systems deriving from various scientific disciplines and ocean communities. Another one is the UE Integrated Maritime Policy encompassing Marine Strategy Framework Directive (Directive 2008/56/EC) that specifically aims to the protection of the marine environment and natural resources, creating a framework for the sustainable use of European marine waters.

The basic criteria to design a sea monitoring network may be considered the same established by the WMO observational networks:

1. The identification of the best equipment should take into account the monitored parameters, the location of the station and the purpose of the monitoring activity.
2. The station spacing and interval between observations should correspond with the desired spatial and temporal resolution of the meteorological variables to be measured or observed.
3. The location of each station should be representative of the conditions in space and time.
4. The total number of stations should, for sake of economy, be as small as possible but as large as necessary to meet scientific requirements.

These aspects will be addressed in the next paragraphs.

9.2.1 Identification of the Best Equipment

The first elements to take into account in choosing the best equipment when developing a sea monitoring network are the nature of the parameters to be monitored and the characteristics of the instruments in terms of automation level, maintenance requirements and places of use.

A sea monitoring station is composed of various components, including a power system (e.g. solar cells), a data logger, telemetry equipment, sensors and probes. Customizing the features and functions of a sea monitoring station allows users to design and create the perfect equipment for their specific applications, needs and budgets.

The choice of the best equipment depends on the application, whether it is close to the coast or on the high seas, for short or long deployments, for severe or

moderate marine states and for the concomitance of other factors such as biofouling, chemical corrosion and others.

The WMO Manual on the Global Observing System [2] reports a comprehensive classification of the sea stations.

The study of the main meteorological and oceanographic phenomena is closely related to the knowledge of some fundamental parameters such as sea level, waves, currents and meteorological parameters at the sea–air interface. Interest in these parameters grows as the coast approaches due to the impact of marine phenomena on the coast and on the shore infrastructure.

Instruments capable of detecting these parameters can be fundamentally classified according to where they are used. Those along the coast, in protected marine areas, can be smaller, lighter and easier to manage. Coastal instruments (especially mounted aboard buoys) require strong mooring equipment and reliable and robust components and an adequate data transmission system. They are deployed using ships equipped with cranes and require great survivability due to adverse weather conditions.

Moreover, the choice of the best equipment depends on the application, whether near-shore or deep sea, for short or long deployment, for severe or moderate sea states and for the concurrency of other factors as biofouling, chemical corrosion and others.

A sea monitoring station consists of various components, including a data logger, solar power, sensors and sondes, a temperature string and telemetry equipment on a buoy platform secured by mooring hardware. Customizing the features and functions of a sea monitoring station allows users to design and create the perfect equipment for their specific applications, needs and budget.

9.2.2 Identification of the Optimal Spatial and Temporal Sampling

The WMO Guide on the Global Observing System [3] provides a useful guide on the spatial and temporal accuracy and resolution requirements of observation data from a sea monitoring network.

Fixed marine stations should be sited to provide data representative of a marine area over a long period of time, as long-term stable time series of repeated observations are required for climate applications. As a minimum requirement, observations should be collected during major synoptic times, preferably on hourly time scale for parameters such as waves, currents and sea levels.

A rigorous statistical procedure on the uncertainty of spatial or temporal variations can be used to decide the configuration of a network. However, to do this, a lot of information is needed because the variations in space and time differ for single variables and may depend on the exposure conditions, the maritime traffic of the area or the population density on the coast.

For a wave buoy network, the requirements for horizontal spacing are determined by the validation needs of the numerical models (for the dominant wave period and the significant wave height), and those for the time spacing are driven from the needs of real-time validation and assimilation of both maritime security models and services. These models require ranges from 20 km for regional models to 60 km for global models, with minimum temporal and spatial accuracy of 1 s and 0.25 m, respectively. The equivalent requirement for wave energy frequency spectrum and wave direction energy frequency spectrum ranges from 100 km for regional models to 300 km for global models with a minimum accuracy of 0.2 m^2 Hz-1 and 0.2 m^2 Hz-1 rad-1, respectively. The required observation cycle is 24 h.

The primary reference for a tide gauge networks is the GLOSS (Global Sea Level Observing System) technical standards. These requirements are described in the GLOSS implementation plan and the IOC manuals and, in short, imply that the equipment must measure with centimetre accuracy in all weather conditions for the indicated average time (typically hourly).

9.2.3 The Identification of the Best Location and the Right Number of Stations

High station density may be required for coastal monitoring, due to local situations or to reflect differences in coastal conditions, while lower density is sufficient in open sea. Moreover, a higher station density in the coastal area can fill the limitations of satellite data near the coast.

However, in a practical way, it is not possible to achieve the optimization of such different requirements without having a serious impact on operational and scientific requirements or economic aspects, and, on a global scale, in situ measurements are often currently too sparse in the open sea to be of high scientific value. At least, they can provide accurate observations to complement and correct biases in satellite products and numerical models and are of great value on a local scale.

Moored buoys, providing in situ wave data and SST observations, have a still limited spatial coverage, and most measurements are taken in the Northern hemisphere (mainly off the North American and Western European coasts). The majority of wave data are provided by nonspectral and spectral buoys.

9.3 Management of a Sea Monitoring Network

9.3.1 Logistics and Administrative Aspects

Maintenance requirements can vary greatly depending on the size and the number of the stations, the likelihood of breakage and the damage due to vandalism.

It could be necessary in case of networks with a huge number of stations to have a central unit with subcentres. The location of these subcentres depends on the needs of the organization. Economic considerations should be considered as well as technical and logistical issues, such as personnel, communications and transportation facilities.

The management approach varies on the basis of the specific functions of the stations network, changing if there are weather stations, tide gauge, wave buoy, coastal radar and so on. Each type of network should have its own standards for activities, equipment, means of deployment, instrumentation and operating procedures; these must comply with international regulations.

The necessary supplies should be forwarded as needed for the stations via a reliable and suitable system, bearing in mind that most of the material is fragile. If necessary, special wooden or cardboard packaging must be used to ensure adequate protection of the instrumentation and avoid plastic.

9.3.2 The Fundamental Role of the Maintenance Operations

The proper functioning of a sea monitoring network is guaranteed by regular maintenance activities at the automatic stations and inspections by the network manager. A detailed programme must be drawn up by the network manager and its staff, scheduling maintenance according to international and national guidelines and specific technical requirements. Routine maintenance should be performed at least every 6 months following a checklist, failure notifications from users and, if necessary, special investigations carried out after relevant events. Field check tests on instruments have to be included among the maintenance operations so that faults can be discovered at an early stage. If faults are discovered or suspected, the unit must be notified immediately. Depending on the nature of the fault and the type of station, the operator will decide if the instrument needs to be changed or if a repair can be done on-site. The installation, repair and maintenance of the equipment are the responsibility of the maintenance staff, frequently entrusted to specialized companies. The WMO Manual on the Global Observing System [2] provides guidance on the range and frequency of inspections for a monitoring system.

9.3.3 Possible Expected and Unexpected Events During the Network Life

Failures at the network central processors can paralyze a whole network or large parts of it. For safety reasons, it is recommended that a double central processor system should be provided. Even for failures of a completely double system, procedures should be planned to ensure the continuation of minimal real-time network functions.

Generally, weather and ocean buoy outages and key failures are primarily attributable to mooring failure, mechanical damage to superstructure, physical damage to electrical system components, cables or sensors.

A significant portion of these failures is related to acts of vandalism. Countries participating in the JCOMM Data Buoy Cooperation Panel (DBCP), and other buoy operators have recognized the vandalism problem for a long time, and they attributed the major causes of vandalism for the buoys to:

- vessels colliding with buoys;
- fishing vessel nets or lines entanglement;
- fish operations using the buoys as fish aggregating devices (FADs);
- theft of the buoy system or its equipment.

9.3.4 The Principal Costs of a Sea Monitoring Network

Marine and ocean observation systems are managed by governments for strategic purposes and often funded by research funding of limited duration. This causes gaps in maintenance operations, or in the worst cases, the out of action of instruments unless continued funding is assured to sustain the proper operation of a monitoring network.

Due to the financial implications, the cost-effectiveness of any new type of equipment will be an important factor to consider.

For example, the communication system represents a major cost because it must be designed to allow the transmission of messages and information, with more than one type of communication if possible. The costs of data transmission could be reduced in the coming years, thanks to the developments of satellite communication systems. For these reasons, financial planning should consider a short-term (1 or 2 years) and medium-term and long-term (5 years or more) scheduling, previewing system changes and improvements, and development with new technologies.

9.4 Data Management and Dissemination

Observation of the sea involves several working phases. The first consists on the measurement of the phenomenon. The second phase, complementary to the first, consists in the methodological reordering, organization, revision of the collected data to disseminate reliable and good quality data to the public. It is not easy to give an exhaustive definition of quality; according to an old EN ISO standard, quality is "the totality of features and characteristics of a product or a service that bear on its ability to satisfy stated or implies needs". So, it is clear that a good observation capability of the phenomenon is necessary but not sufficient to guarantee the quality of the information.

At the beginning of 1970s, with the conversion from mechanical to digital instruments, data were collected in particular storage directly located inside the instruments or in closer cabins collecting any electronic device and linked to the measurement sensors through simple communication bridge (i.e. radio signal). Dedicated operators were designed to download these data at fixed time intervals that depend on the complexity of this operation (daily if the storages were easily reachable, every 6 months or at the end of instrument life if data were collected onboard in open seas), and transmit them to the final destination. This is called observation in delayed time. As a result, data collection was discontinuous and irregular, with a large amount of information to elaborate every time step. Usually, data were processed, and no importance was given to any other activity that now are known as data engineering, such as validation, collection, classification, modelling, dissemination and protection of the data.

The technological advances, mainly in informatic and telecommunication engineering, allow to own data just few seconds (or less) after the observation continuously. This is what is known as observation in real time. These observations can nowadays simply be treated to apply all the necessary operations to transform data into information, starting from the validation to the correct dissemination.

On the other hand, due to the continuous transmission of the observations, these activities must be automatic and fast. In many cases, it is useful to apply further non-automatic mechanisms (i.e. expert judgements validation) to entire sets of data. In these cases, the real-time observation is coupled with a delayed time one.

9.4.1 Validation

There are many factors affecting data quality. Neglecting any issue related to the instrument installation (in many cases, this operation is complicated due to particular manufacturing in complex situation, especially in open sea) or accidental instances, three main events generate wrong or missing observations:

– Lack of maintenance of the monitoring station: marine environment facilitates the biofouling expansion, sediment coverup, instrument block or drift and aggression of corrosive agents;
– Extreme events: sea or wind storms transfer large energy on monitoring structure. If the stations or moorings are not correctly dimensioned, the risk of unmoorings, damages, failures and sinks is high. It is often recommended to use elements to avoid damages due to lightning.
– Vandalism.

Data quality control (QC), or data validation, is a stage in data management which is essential whenever data are used by any individual or group other than the originators of the data. It is distinct from the instrument calibration, sensor checks, field deployment checks and quality control of laboratory analysis. In fact, it consists in a set of operations, from verification to correction and validation of data to ensure scientific validity. In particular, "Data quality control information tells users of the data in a brief way how it was gathered, how it was checked, processed, what algorithms have been used, what errors were found, and how the errors have been corrected or flagged" [4]. It is not possible to provide rigid standards of QC for all data types which are applicable in all oceanographic and climatic conditions and for all purposes. Some checks depend upon presumed average climatic conditions, upon presumed accuracy of instruments, or acceptable levels of noise, or desired accuracy of the final output. As an example, a typical QC is the application of an allowable range within which the observations can exist. In some cases, it is simple to write this interval (i.e. the wave direction must be a value between 0° and 360°); in other cases, it is possible to define surely only one extreme (i.e. salinity must be greater than 0 ppm). But in many cases, the observation is theoretically not bounded, so the experts estimate a suitable range to consider all reasonable cases (i.e. water temperature between −10 °C and 50 °C). This kind of interval could be useless because it includes also a great number of anomalous values that must be deleted or corrected. In this case, a narrower range should be defined by taking into account the physical conditions of the monitored basins (i.e. maximum wave height in a gulf of the Mediterranean Sea is lower than the corresponding values in the middle of Atlantic Sea) or statistical inferences on sufficient long time series (percentiles, multiples of the standard deviation, etc), taking into account that real values outside this range are possible in specific situation such as extreme events.

It is possible to assign some common quality levels to all observed data, and for each level, several QC procedures can be applied [5, 6]:

– Level 0 includes the raw data as recorded by the monitoring station, generally not corrected according to the periodic settings of the instrument. This type of measure can be made available to the public by the organization responsible for the collection and processing of data to provide information in real time.
– Level 1 includes data that have passed a basic quality control. Usually, these QC are applied automatically, so the data set is disseminated in real time. The main controls involved the presence of the data, the format coherence and the value

coherence (compared to minimum and maximum thresholds and anomalous distances with previous values).
– Level 2 includes data that has been subjected to a complete quality control, also comparing data from comparable stations or validate through expert judgement. In some cases, data could also be manipulated through removal, corrections, imputations, etc. This level is rarely published in real time.
– Level 3 includes data that have undergone further corrections from level 2, made, for example, following statistical and deterministic models, specific analysis and comparison with data observed with different technologies; as in the previous level, data could be manipulated. This level is published in delayed time.

This classification is highly hierarchical. It is not possible to skip one or more levels. It is important to start analysing raw data, and it is also fundamental to save data from level zero without overwriting them with data from subsequent levels.

All quality control procedures of a data set must be adequately documented and always accompany the respective data. Appling a QC means provide observed values with a specific quality code (e.g. missing value, suspect value and interpolated data). There are many lists of codes, developed by several organizations or projects (BODC, NOAA, SeaDataNet, etc.) for different datasets and procedures.

9.4.2 Data Dissemination and Open Data

Data dissemination, when implemented, was and is realized in various shapes. Historically, observations were collected on appropriate ship diaries, and data collected in mechanical way were periodically published through annals.

Digital data are disseminated though the Web in different formats, from the simple text files to the specific formats widely used for oceanographic observations (i.e. NetCDF and GRIB). Several informatic protocols are used to spread information: the most popular are those who allow the transfer of computer files between a client and server on a computer network, such as emails, ftp, http, ssh and similar.

Nowadays, an increasing numbers of Web applications provide a means of accessing data for a simple visualization or with sophisticated interactive tools. Scientific, and also oceanographic, data are increasingly published on the Web from many national, regional and local governments.

The Data on the Web Best Practices ("https://www.w3.org/TR/dwbp/") provide a set of recommendations that are applicable to the publication of all types of data on the Web. Those best practices cover aspects including data formats, data access, data identifiers, metadata, licensing and provenance. In fact, data expressed as list of values are not sufficient. It is fundamental to join these data to a set of metadata useful for the correct use of the information by all users (except the data providers).

Metadata consist in a set of information strictly related to the observation. Typical metadata for marine observation regard the type of measured parameters, the field of interest, the measurement period, the used instruments, the quality level, the

geographical area investigated and the type of investigation points (regular grid, single point, multiple points, surface observation, water column observation, etc.). Any kind of operation such as data comparison or augmentation, model acquisition and statistical analysis cannot be separated by the knowledge of the metadata. The use of data with different metadata (i.e. different time or space resolution) must be carried out very carefully. So, the correct information about metadata can avoid several problems in terms of data interpretation. In this framework, correct and reliable data from rigorous monitoring plans and campaigns play a very important role not only for scientists and technicians, but also for stakeholders and citizens if they are actively involved in the dissemination, sharing, uptake and use of the collected information and knowledge.

Even if data are often viewable, it is not so obvious that is also open and free for any use.

Several international guidelines are encouraging data providers to open the information to meet the needs of society.

The Aarhus Convention (2001) established the right of public to have free access to environmental data held by public bodies and the right of citizens to participate in decision-making focused on environmental issues. Many initiatives, best practices and new governance approaches have been promoted in the last decade on societal challenges including marine relevant topics to improve the communication among stakeholders and make policies more effective.

During the last years, the European Commission has encouraged the development of open data portals to share knowledge among all possible interested subjects by publishing guidelines and issues new legislation, such as the INSPIRE directive (2007) aiming at ensuring that spatial data infrastructures in the EU member states are compatible and usable in the European community.

At the same time, several national and regional institutions have implemented open data systems, following the rules and the processes established by their national competent authorities.

Even if there is not a legally binding regulation for sharing knowledge, it is widely accepted among the Open Government Data Community [7] that to be fully open, data must be:

- complete: public data are not private, without privilege limitation.
- primary: data are as collected at the source.
- timely: data are open as quickly as possible.
- accessible: data are available to the widest range of users and for the widest range of purposes.
- machine-readable: data can be processed in an automated way.
- non-discriminatory: data are available to anyone, no registration requirement.
- non-proprietary: data are available in an open format.
- license-free: data are not subject to Intellectual Property Rights.
- permanent: data are findable over time.

A rating system for open data was proposed by Tim Berners-Lee, founder of the World Wide Web: open data are classified according to their possible benefits from one (simply readable data) to five stars [8].

One of the main interesting projects (https://www.go-fair.org/) identifies four principals to give values to data and make them "FAIR". FAIR data are as follows:

- Findable: metadata and data should be easy to find for both humans and computers.
- Accessible: the access point to the data is known, the protocol is open, free and universally implementable, and metadata are always accessible.
- Interoperable: data can be simply integrated with other data, applications or workflows for analysis, storage and processing.
- Reusable: well-described metadata and open data are fundamental to optimize the reuse of data.

9.5 Some Examples of Operative Sea Monitoring Network

To observe the marine environment, many options are nowadays available: FerryBoxes, Poles in shallow waters, Gliders, regular ship cruises for vertical resolution of parameters, wave rider buoys, coastal radars like HF and XF, and remote sensing from satellites. A combination of different approaches enables coverage on different time and spatial scales.

The need of an integrated national sea state monitoring system is the way to be undertaken to reach a correct management and safety of both coastal and open sea areas; this system must take into account a series of technological and scientific progress which has broadened the spectrum of potentially available tools to the scientific community and institutional stakeholders.

9.5.1 The In Situ Buoys Network

At international level, the JCOMM is primarily responsible for the development, coordination and maintenance of moored buoys and related telecommunication facilities. The Data Buoys Cooperation Panel (DBCP) is an official joint body of the World Meteorological Organization (WMO) and the Intergovernmental Oceanographic Commission (IOC). It consists of the data buoy component of the Joint WMO-IOC technical Commission for Oceanography and Marine Meteorology (JCOMM) and the Global Ocean Observing System (GOOS). DBCP considers the expressed needs of the international meteorological and oceanographic communities for real-time or archival data from ocean data buoys on the high seas, supports and organizes appropriate actions that may be necessary to implement the

deployment of data gathering buoys to meet the expressed needs of oceanographic and meteorological programs.

Data buoy networks offer many benefits for their versatility for monitoring different environmental parameters, including weather, water quality, waves and currents and air quality. They are projected to resist rough seas, high winds and severe storms. Moreover, they are reliable, simple to use, perform well and provide highly accurate data, and furthermore, they are easily relocatable.

Both policy makers and scientists could take advantages from these instruments to understand important wave effects beyond the well-known wave application. For example, waves can affect the rate at which sea and air gases are exchanged, which in turn affects surface water and coastal currents and can alter water quality, as sediments are resuspended. Measurement of surface gravity waves is accomplished by buoys, sensing the vertical acceleration caused by incoming waves.

Buoys data have many applications and integrate remote sensing and numerical model information on sea state.

These data are fundamental when buoys are deployed where no other valuable data sources are available. Data buoys provide some of the observational data that is used in the meteo-marine model, alongside data from floats, land stations, satellites, ships and weather balloons. They improve forecasts of extreme weather such as cyclones and hurricanes because buoys can resist into the "hotspots" where the storms originate. Wave, current and surface wind parameters from data buoys can help to ensure the safety at sea of travellers and workers, as search and rescue operations. Furthermore, sea surface temperature data can improve fisheries control activity and prevent losses.

Weather data from monitoring buoys can help researcher in calibrating and validating satellite measurements; it can also improve seasonal forecasting techniques, climate change prediction and oceanographic/meteorological research, allowing better predictions of regional and global events.

The measurements by buoys are made usually trough an accelerometer that returns an electrical signal that is an analogue of the acceleration. Further processing of the signal, using both analogue and digital methods, allows to compute statistical parameters that characterize the sea state.

Data buoys typically measure all or many of the following parameters:

- wave height, period and spectra;
- wind direction and speed;
- air pressure;
- air temperature;
- currents from buoys;
- downwelling radiation and relative humidity;
- rainfall;
- sea surface and subsurface salinity and temperature;
- other biogeochemistry such as fluorescence, O_2 and CO_2.

As an example, the list of measurements and requirements for data buoy payload drawn up by the National Data Buoy Center (NDBC) for the NOAA is listed in Lessing et al. [9].

Telecommunications or telemetry systems allow to return data in real time. The best situation is when stations make data available immediately after acquisition and processing, via a communication system such as via radio modem or satellite links using systems such as Iridium, Inmarsat and GPRS. In a few cases, near-shore platforms are hard-cabled to an ocean observatory or a station onshore.

In any case, it is important to ensure minimum energy consumption by peripheral devices, often powered by solar panel and buffer battery.

The communication must be bidirectional to support both the download of data and system statuses from the periphery to the centre and to send programming commands or information updates from the centre to the sea.

The International Association of Marine Aids to Navigation and Lighthouse Authorities (IALA) has assigned the colour yellow to the buoy-type oceanic data acquisition system (ODAS). For the buoy hull, the best choice is a multipurpose buoy designed for a variety of applications. High performance and low maintenance buoys are recommended, allowing for a variety of applications (including shallow water with strong currents). They are generally made with a seamless hull that can withstand bumps and knocks in a robust material (metal alloy or polyethylene) that is abrasion-resistant and reduces marine growth (biofouling) and eliminates the need for expensive sandblasting and painting, with stainless steel parts (e.g. the mooring and lifting eye). To ensure long-term durability, foam-filled hull buoys are preferred to prevent water ingress in the event of a puncture and good mooring.

Traditional mooring systems typically consist of a chain or a rubber chord and heavy anchor or a concrete block. The arrangement of the moorings is of fundamental importance for the measurement, so it is important to design it for all wave and current conditions.

9.5.2 The In Situ Tide Gauges Network

Tide gauge represents the oldest fixed instrument used to monitor continuously a marine physical parameter, because it allows to observe the sea surface from a stable support along the coast. The first sea-level observations were published by the geodesists and astronomers Jean Picard and Philippe de la Hire in 1680 [10], measuring the high and low waters at Brest (France) over a period of 10 days [11]. Systematic sea-level observations have been performed and recorded since the seventeenth century, in particular in Amsterdam, (since 1682), in Liverpool (since 1768) and in Stockholm (since 1774) [12].

The first used devices were simple graduated rods, called ‘tide poles’, fixed at locations where the instantaneous sea level could be easily read off at any time by an observer. Data were reported on special diaries reporting only high and low water levels, as well as the time of their occurrences [11].

Automatic recording devices appeared only during the nineteenth century, in 1831, in Sheerness (UK) and in 1842 in Toulon (France). These were mechanical gauges, equipped with a float, wires, counterweights, a timepiece, a pen, a paper-chart recorder and a stilling well [12].

For about 150 years, these kinds of instruments were widely used. In 1983, the UNESCO Intergovernmental Oceanographic Commission (IOC) showed that 94% of the tide gauges were mechanical [13]. The floating gauges have been progressively replaced by new technologies. Modern types of gauges are mainly based either on the subsurface pressure measurements or on the measurement of the time of a pulse flight (acoustic or radar) [14].

Networks of tide gauges have been gradually developed according to the purposes of the sea-level observation. Since the only relevant information was the highest and the lowest level, only few fixed points per nation were monitored. Starting from the ninetieth century, sea level data from tide gauges have been used to establish the vertical reference systems on land and on sea in order to define the height and depth data [11]. In this sense, networks of tide gauges were used to collect both terrestrial and marine information and these instruments were periodically linked to a set of closed geodetic control networks through high precision levelling.

The new role assumed by these instruments needed a particular design of the manufacture hosting the gauge, built in solid materials (i.e. concrete), located in a stable area easily reachable, close enough to the water surface, linked to the sea through a stilling well and protected from extreme events. The manufacture assumed the shape of a cabin or a small house containing all the necessary equipment. Except few cases, most of the "tide houses" were located in harbours or gulfs.

Tide gauges are now used also to capture a variety of local and regional phenomena related to decadal climate variability, tides, storm surges, tsunamis, swells, evolution of climate change and other coastal processes. The collected data are used to validate ocean models and to detect errors and drifts in satellite altimetry. In this sense, a single tide house assumes the shape of a small concentrate network that integrates a large number of instruments that contribute to the sea level to describe the meteo-marine state. More and more frequently, the cabin hosts anemometers, barometers, thermometers, multiparametric instruments for the biogeochemical observation, GPS, and also transmission equipment, solar panels and other devices.

Nevertheless, very small instruments are not uncommon, overall, when it is not possible to build extensive structures. In these cases, pressure hydrometers or radar gauges are often used directly into the sea area (on the bottom) or over the sea.

Networks of tide gauges represent now the most evident example of complex marine network, because they combine the well-known needs of a network system (robust connection between elements, good spatial coverage, the choose of the correct locations, etc.), the use of device for the observation of terrestrial and marine components, the levelling operations, the integration and diffusion of different kinds of data.

9.5.3 The Coastal HF Radars Oceanographic Network

HF coastal radar technology represents to some extent a fortuitous outcome of the military use of radars for aircraft and ship detection. As of World War II, a strong backscattering of radar signals from the sea surface was often observed in installations close to the sea and considered as noise [15]. The mechanism underlying this effect was first understood by Crombie [16], whose observations were followed, after more than a decade, by a number of theoretical investigations which laid the ground to the development of actual measuring systems (for a review of earlier developments of this technique see [17]; for the current state of knowledge [18]).

The functioning principle of HF coastal radar relies on the Bragg scattering of an electromagnetic signal by the "lattice" represented by surface gravity waves whose wavelength is half the wavelength of the signal itself.

In case of standing surface gravity waves, the backscattered signal would show a peak at the same wavelength of the emitted one. In reality, waves are never stationary, but they propagate approaching or moving away from the transceiver apparatus. This will induce a Doppler shift in the frequency of the received signal. If furthermore gravity waves are superimposed on a surface velocity field, the frequency of the return signal will undergo a further Doppler shift induced by the radial component of the current moving towards or away from the receiving station (a typical Doppler spectrum measured by a coastal HF radar is shown in Fig. 8 of Chap. 7 of this same volume: [19]). This effect is relatively simple to quantify, and if at least two two-way transceiving systems are available, it is possible to combine the radial information in order to obtain the vector components of the velocity field [20].

The spectrum of gravity waves that develop in coastal basins has characteristics of a certain universality, and the working frequencies of coastal radars are generally enclosed in a range that optimizes the probability of reflection by the waves themselves. Within this range, the choice of working frequency is dictated by considerations on the desired range and resolution, which are a function of the frequency itself (see, e.g., Table 1 in [21]).

The unrivalled peculiarity of such systems is that they provide in real-time synoptic observations of the surface current field at high resolution in time and space [22]. Therefore, they prove to be best suited to studying circulation and surface dynamics (for a review, see [18]), including ocean model validation and data assimilation [23–26] and to operational applications such as search and rescue ([27, 28], and references therein), hazard detection and mitigation ([29, 30] and refs), environmental management ([31]; see other references in [32]) including fishery studies [33, 34], tsunami warning ([35], and references therein), maritime security and safety at sea [36, 37].

Since signal composition is possible only in the superposition area of the radial fields of at least two systems [38], the necessity to broaden coverage and to limit geometric dilution of precision [39] issues has led to the creation of local micronetworks of a few transceiving stations [40, 41]. This has represented the core of much

broader networks, which have been developed to harmonize, optimize and integrate operations, applications and results.

At a global level, a Global High Frequency Radar Network was founded in 2012 in the framework of the Group on Earth Observations, 2012–2015 Work Plan. In 2017, it was recognized by the Joint Technical Commission for Oceanography and Marine Meteorology (JCOMM) as an observing network of the Global Ocean Observing System (GOOS) [32].

At a continental or national level, at present the broadest network is the U.S. High Frequency Radar Network (HFRNet), which hosts observations also from Canada and Mexico, totalling more than 150 contributor systems. As can be seen from Fig. 9.1, the entire west coast of the continental USA is covered by neighbouring or overlapping systems; this is also true for the main portion of the east coast. Additional systems are installed along the coasts of the Gulf of Mexico, Alaska, Hawaii and Puerto Rico [32].

In Europe, HF radar installations are presently more than 60; several coordination activities and projects exist, for data management and standardization as well as for dissemination. As of 2014, coordination and integration into the Global Network have been carried out through the EuroGOOS HFR Task Team [21].

In Australia, the Integrated Marine Observing System (IMOS) coordinates HF radar facilities in eight different locations distributed around the country coastline [42]; in this case, coordination is much simpler than in the USA or in Europe, as systems are all managed under the very same umbrella.

In many other countries, in particular Asian ones, a quite high number of limited clusters of systems exist, typically organized at a country level, still lacking coordination in structured international networks [43].

In order for a network to work properly and to be able to integrate and disseminate observations and higher level products to public or stakeholders in real or near real time, a number of procedures need to be agreed upon among contributing institutions/observation sites. For this reason, it is advisable to establish best practices,

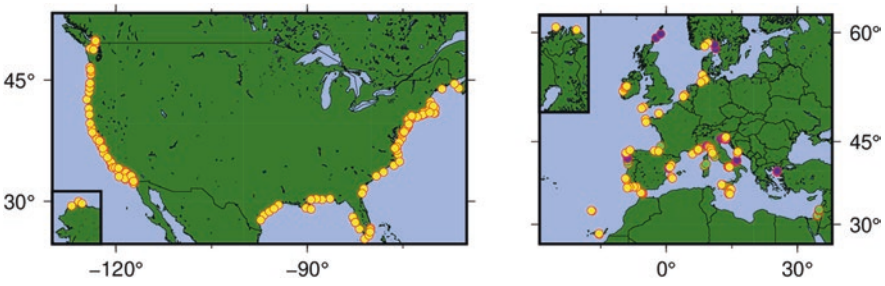

Fig. 9.1 Left panel: Map of HFR sites in the Continental USA (Alaska in the inset). Data provided by the U.S. National Oceanic and Atmospheric Administration (NOAA) Integrated Ocean Observing System (IOOS) and High Frequency Radar Network (HFRNet). Right panel: Map of locations of the HF radars included in the current EuroGOOS Task Team inventory as of March 2020 (Northern Norway in the inset). The currently working sites are plotted in yellow, future installations in green, earlier installations and/or currently inactive stations in purple

procedures and standards to be shared among the network members [44]. Throughout operations, close communications within the community are also of the highest importance.

The first issues to tackle are deployment and maintenance of observing systems: a number of aspects regarding different logistic matters can be of common interest, even though installation and upkeep might differ from site to site. This is particularly true for the case of HF radars, which are often installed in remote sites, not easy to reach and therefore to be accessed remotely. A forum, a wiki (as developed by the U.S. IOOS), a tutorial repository can result very helpful to this aim. This has been done in the USA through the Radiowave Operators Working Group (ROWG) and for the European networks through the EuroGOOS HF Radar Task Team [32].

If setup and maintenance exhibit site-specific needs, quality assurance and quality control must be definitely standardized within a network, as well as data formats. Defining quality issues implies a cooperation among manufacturers, operators and data recipients. This has been accomplished as of 2012 in the USA through the IOOS Quality Assurance/Quality Control of Real-Time Oceanographic Data (QARTOD) Project Plan [45], while in Europe this has been promoted in prevision of the distribution of HF radar data through the Copernicus Marine Environment Monitoring Service (CMEMS) and is a matter of discussion and exchange in the regular meetings of the European HF radar operators community ([21]; for the Australian, IMOS quality control procedures have also been established: [46, 47]).

Calibration and validation (as well as intercalibration and intervalidation) exercises can be organized, in order to make sure that standards are met by all network members. A good example of this is represented by the European MED project Tracking Oil Spill and Coastal Awareness (TOSCA), in whose framework a number of common activities were carried out in close cooperation among different research groups and institutions [48, 49].

Data and metadata formats need to be agreed upon, so as to facilitate procedures for the development of standardized higher level products. In this respect, input from stakeholders can be very beneficial both to data producers and to data exploiters. This has been done, e.g. in Europe, in particular in view of the dissemination of HF radar data through CMEMS.

Different levels of access and visualization for data at different processing levels and for data-derived products need also to be determined. This is best done on a common platform.

Finally, within a functioning network it can be very helpful to set up repositories for hardware and software. In particular, members of real-time observation networks might sometimes find themselves in need of spare parts that have to be purchased in near real time as well. This is not easy to accomplish for certain types of organizations, who might have to go through some bureaucracy in order to be able to purchase. For this reason, establishing exchange protocols for spare parts can be extremely helpful in order to expedite part replacement. This was organized for HF radars in Italy, e.g. in the framework of the RITMare project (action SP6_WP1_AZ3): namely, a support unit for HF coastal radar infrastructure was created, a map

of necessities in terms of hardware was drafted, and one technician was designated to follow this activity [50].

As to software, data standardization and quality assurance can be accomplished by singular network members or can be otherwise centralized. In the former case, necessary software is best shared by network members. At any rate, it can be advisable to promote software exchange for additional data processing that may be ameliorated through open-source exchanges, implementation and application.

9.5.4 The Seismic Signal Network as a Challenging Way to Measure the Sea State

Among the many other measurements that contain a signature of sea states, an increasing attention is given to the microseisms, small- and long-continuing seismic signals unrelated to earthquakes but caused by natural events. The first references to microseism can be found in Bertelli's studies since the nineteenth century [51].

It is possible distinguish between primary and secondary microseisms.

The primary microseisms are generated, in shallow water, by direct ocean wave pressure fluctuations at the ocean bottom and have the same frequency as the generating ocean waves [52]. Its frequency spans from 0.05 to 0.1 Hz.

The secondary microseisms are generated when groups of ocean waves of the same frequency travel in opposing directions [53] and are observed at twice the frequency of the ocean waves and are indicated as double-frequency microseisms. The interaction of two opposing ocean waves, with nearly the same wavelength, travelling in opposite direction generates second-order pressure fluctuations on the ocean floor with double frequency. These waves propagate with very low attenuation and then turn into microseismic energy. The frequency content of secondary microseism ranges from 0.1 to 0.5 Hz.

It is distinguished also between microseisms generated by swell from distant storms and those generated by waves induced by local winds.

Consequently, the secondary microseism, in some areas, can be further divided into long period microseism (0.085–0.2 Hz), due to far away sources (e.g. swell from distant storms), and short period microseism (0.2–0.5 Hz), due to sources located near the coast (e.g. waves induce by local wind) [54, 55].

The generation of seismic waves is in the form of seismic Rayleigh waves, and its spectrum is strongly related to ocean wave energy coupling into the vertical ground of a few micrometers motion. The sea state that is most effective for generating microseisms can be classified into three broad classes and includes, in order of magnitude, the generally broad directional spectrum at high frequency, the effect of coastal reflection and the collision of two wave systems from different storm [56].

Analysis of the relationship between microseisms and ocean waves has a long story. Already in the late 1930s, Lee [57] studied large microseisms caused by storms and the pressure system variations in weather maps.

Later, in the 1950s, Longuet-Higgins [53] related the large-amplitude secondary peak microseisms (5–7 s) with the dominant period of ocean waves (10–14 s for ocean and 8 s for enclosed seas).

More recently, for the sea state description, the study of microseism has been focused on the relationship between microseism and wave climate changing, analysis of climate change and planning shore protection measures [55, 58, 59].

Recently, Ardhuin et al. [56] presented the first comprehensive numerical modelling of microseism, valid for global ocean and based on random ocean waves generation furthermore taking into account coastal reflections.

Seismic stations located near the coast could be very useful in retrieving information about sea state ([60, 61]) covering many regions of the world where ocean buoys or satellite are not available and there was no measurement of wind sea spectra. Moreover, one of the greatest interests in microseisms arises from the long-term time series that can be obtained to reconstruct sea state.

9.5.5 Ship-Based Observation

Forecasting and hindcast meteo-marine numerical models as analysis and reanalysis are becoming more and more reliable and very useful to address sea state studies. However, measured data keep on to be in any case essential for the elaboration of statistics, for verification and validation studies, for the calibration of the numerical models themselves, and in some cases for their assimilation in the weather reconstruction models. Voluntary Observing Ships, named VOS, are merchant ships, ferries, fishing vessels and sailing yachts that around the world observe the weather. Volunteer crew members on nearly 1000 ships around the world observe the weather at their location, collect each observation in a standard format and send these data to the many national meteorological services that have responsibility for marine weather forecasts.

The origins of the VOS Scheme date back to the 1850 and became more established at the start of the twentieth century when wireless telegraphy was introduced. The fleet of the international VOS scheme peaked in the 1980s and 1990s, but thereafter the number of ships recruited has declined. However, the number of observations acquired did not have the same trend. This is in part due to the increased number of about 250 Automatic Weather Stations (AWS) on observing ships which typically provide hourly data.

The Ship of Opportunity, named SOO, is a network of different kinds of ships providing upper ocean data for data assimilation in models and for various other ocean analysis scopes. Usually, SOO mounts FerryBox an automated measuring system used for the measurement of physical and biogeochemical parameters in surface waters. Parameters measured are among others: water temperature, conductivity, turbidity, oxygen, pH and chlorophyll-a-fluorescence. Water samples for

further laboratory analysis are taken. On some routes, measured additionally are as follows: algal classes and nutrients (ammonia, nitrite/nitrate, o-phosphate, silicate). In the near future sensors for pCO_2, alkalinity, a flow-cytometer and an instrument to measure gene probes to detect specific species can be installed.

This network in itself supports many other operational needs (such as for fisheries, shipping and defence). One of the continuing challenges is to optimally combine upper ocean thermal data collected by XBTs from the SOO with data collected from other sources.

Applying such measuring systems on ferry boats or ships-of-opportunity has several advantages:

- protection from harsh environment,
- easier biofouling prevention,
- no energy restrictions,
- easier maintenance,
- lower costs,
  transects instead of point measurements.

9.5.6 Animal-Borne Instruments

Marine mammals, travelling up to the harshest places on the planet and diving to great depths, with miniaturized ocean sensors on their fur, help gather useful information. Antarctic and Arctic seals and turtles have been fitted with a new generation of Argos tags.

Pushing the efforts on sensors calibration, animal tagging allowed to obtain reliable oceanographic data in polar regions, that are chronically undersampled regions, and in many coastal areas.

The newly endorsed Animal Borne Ocean Sensors (AniBOS) network provides a cost-effective and complementary observing capability to the GOOS. AniBOS monitors several essential ocean and biodiversity variables, yielding data to estimate global ocean indicators and contributing to the quantification of the upper ocean variability.

These data include temperature and salinity profiles, but also fluorescence, oxygen or surface wave and wind activity.

In the last decade, about five hundred thousand temperature–salinity–depth profiles were obtained in high latitudes, coastal shelves and tropical areas, exploiting the marine mammals' movements. The areas where these animals can reach are currently poorly covered by traditional observing platforms. This particular 'network' greatly improves studies of climate variability and the delivery of information to perform climate prediction estimates at global and regional scales.

References

1. WMO-No. 8 (2014) WMO guide to meteorological instruments and methods of observation—the CIMO guide. (2014 edition, Updated in 2017)
2. WMO-No. 544 (2010) Manual on the global observing system (WMO, 2010, 2011a)
3. WMO-No. 488 (2010) Guide to the Global Observing System. (2010 edition, Updated in 2017)
4. IOC (1993) Manual of quality control procedures for validation of oceanographic data", IOC Manuals and guides
5. ESEAS (2002) Quality control of sea level observations—version 1.0, European Sea level service— research infrastructure, p. 22
6. Raicich F (2002) Review of current quality control applied to tide gauge data. CNR, Istituto Sperimentale Talassografico, Trieste, p 5
7. Ubaldi B (2013) Open government data: towards empirical analysis of open government data initiatives. OECD Working Papers on Public Governance
8. Open Knowledge Foundation (2010) The open data handbook. http://opendatahandbook.org/
9. Lessing P, Cambre R, Landry B (2005) System specifications and requirements for design of national data buoy advanced modular payload system specifications and requirements for design of national data buoy advanced modular payload system. https://doi.org/10.13140/RG.2.2.24604.49287
10. Cartwright DE (1999) Tides – a scientific history. Cambridge University Press, Cambridge
11. Woppelmann G, Zerbini S, Marcos M (2006) Tide gauges and geodesy: a secular synergy illustrated by three present-day case studies. C R Geosci 338(14–15):80–991
12. Woppelmann G, Pirazzoli PA (2005) Tide Gauges. In: Schwartz ML (ed) Encyclopedia of coastal science, Encyclopedia of earth science series. Springer, Dordrecht
13. IOC (1983) Stations marégraphiques opérationnelles, Commission océanographique intergouvernementale de l'UNESCO, série technique n. 23
14. IOC (2006) Manual on sea level measurement and interpretation, Inter-governmental Oceanographic Commission of UNESCO, manuals and guides No. 14
15. Teague CC, Vesecky JF, Fernandez DM (1997) HF radar instruments, past to present. Oceanography 10(2):40–44
16. Crombie DD (1955) Doppler spectrum of sea echo at 13.56 mc./s. Nature 175(4459):681–682
17. Barrick DE (1978) HF radio oceanography — a review. Boundary-Layer Meteorol 13:23–43
18. Paduan JD, Washburn L (2013) High-frequency radar observations of ocean surface currents. Ann Rev Mar Sci 5:115–136
19. Piscopo V, Rossi GB, Crenna F, Gaglione S, Scamardella A, Uttieri M, Zambianchi E (2021) Measurement of sea waves. This volume
20. Paduan JD, Graber HC (1997) Introduction to high-frequency radar: reality and myth. Oceanography 10(2):36–39
21. Rubio A, Mader J, Corgnati L, Mantovani C, Griffa A, Novellino A et al (2017) HF radar activity in European coastal seas: next steps toward a pan-European HF radar network. Front Mar Sci 4:8
22. Haus BK, Graber HC, Shay LK (1997) Synoptic measurement of dynamic oceanic features. Oceanography 10(2):45–49
23. Barth A, Alvera-Azcárate A, Weisberg RH (2008) Assimilation of high frequency radar currents in a nested model of the West Florida shelf. J Geophys Res 113:C08033. https://doi.org/10.1029/2007JC004585
24. Iermano I, Moore AM, Zambianchi E (2016) Impacts of a 4-dimensional variational data assimilation in a coastal ocean model of southern Tyrrhenian Sea. J Mar Syst 154:157–171
25. Marmain J, Molcard A, Forget P, Barth A (2014) Assimilation of HF radar surface currents to optimize forcing in the North Western Mediterranean Sea, nonlinear process. Geophysics 21:659–675. https://doi.org/10.5194/npg-21-659-2014
26. Paduan JD, Shulman I (2004) HF radar data assimilation in the Monterey Bay area. J Geophys Res Oceans 109:7

27. Futch VC, Allen A (2019) Search and rescue applications: on the need to improve ocean observing data systems in offshore or remote locations. Front Mar Sci 6:301
28. Harlan J, Terrill E, Hazard L, Keen C, Barrick D, Whelan C et al (2010) The integrated ocean observing system high-frequency radar network: status and local, regional, and national applications. Mar Technol Soc J 44:122–132. https://doi.org/10.4031/MTSJ.44.6.6
29. Abascal AJ, Castanedo S, Medina R, Losada IJ, Alvarez-Fanjul E (2009) Application of HF radar currents to oil spill modelling. Mar Pollut Bull 58(2):238–248
30. Abascal AJ, Sanchez J, Chiri H, Ferrer MI, Cárdenas M, Gallego A et al (2017) Operational oil spill trajectory modelling using HF radar currents: a northwest European continental shelf case study. Mar Pollut Bull 119(1):336–350
31. Cianelli D, D'Alelio D, Uttieri M, Sarno D, Zingone A, Zambianchi E, d'Alcalà MR (2017) Disentangling physical and biological drivers of phytoplankton dynamics in a coastal system. Sci Rep 7(1):1–15
32. Roarty H, Cook T, Hazard L, George D, Harlan J, Cosoli S et al (2019) The global high frequency radar network. Front Mar Sci 6:164
33. Emery BM, Washburn L, Love MS, Nishimoto MM, Ohlmann JC (2004) Do oil and gas paltforms off California reduce recruitment of boccaccio (Sebastes Paucispinis) to natural habitat an analysis based on trajectories derived from high-frequency radar. Fish Bull 104:391–400
34. Sciascia R, Berta M, Carlson DF, Griffa A, Panfili M, La Mesa M et al (2018) Linking sardine recruitment in coastal areas to ocean currents using surface drifters and HF radar: a case study in the Gulf of Manfredonia, Adriatic Sea. Ocean Sci 14(6):1461
35. Lipa B, Barrick D, Isaacson J (2016) Coastal tsunami warning with deployed HF radar systems. Tsunami, p. 73
36. Roarty H, Glenn S, Kohut J, Gong D, Handel E, Rivera E et al (2010) Operation and application of a regional high-frequency radar network in the mid-Atlantic bight. Mar Technol Soc J 44(6):133–145
37. Roarty HJ, Rivera Lemus E, Handel E, Glenn SM, Barrick DE, Isaacson J (2011) Performance evaluation of SeaSonde high-frequency radar for vessel detection. Mar Technol Soc J 45(3):14–24
38. Ranalli M, Lagona F, Picone M, Zambianchi E (2018) Segmentation of sea current fields by cylindrical hidden Markov models: a composite likelihood approach. J Roy Stat Soc Ser 67(3):575–598
39. Lipa B (2003) Uncertainties in SeaSonde current velocities. In: Proceedings of the IEEE/OES seventh working conference on current measurement technology, pp. 95–100
40. Falco P, Buonocore B, Cianelli D, De Luca L, Giordano A, Iermano I et al (2016) Dynamics and sea state in the Gulf of Naples: potential use of high-frequency radar data in an operational oceanographic context. J Operation Oceanogr 9(sup1):s33–s45
41. Wan B, Wu X, Zhang L, Yue X, Wang L, Yi X (2020) A study of a novel high frequency radar network for ocean dynamics surveillance. In: 2020 IEEE international conference on computational electromagnetics (ICCEM) IEEE, pp. 110–112
42. Hetzel Y, Cosoli S, Pattiaratchi C, De Vos S (2019) Monitoring Australia's coastal currents with the IMOS HF radar network. In: Australasian coasts and ports 2019 conference: future directions from 40 [degrees] S and beyond, Hobart, 10–13 September 2019. Engineers Australia, p. 560
43. Fujii S, Heron ML, Kim K, Lai JW, Lee SH, Wu X et al (2013) An overview of developments and applications of oceanographic radar networks in Asia and Oceania countries. Ocean Sci J 48(1):69–97
44. Mantovani C, Corgnati L, Horstmann J, Rubio A, Reyes E, Quentin C et al (2020) Best practices on high frequency radar deployment and operation for ocean current measurement. Front Mar Sci 7:210
45. U.S. Integrated Ocean Observing System [IOOS] (2017) QARTOD project plan accomplishments for 2012–2016 and update for 2017–2021. U.S. IOOS, Silver Spring

46. Cosoli S, Grcic B (2019) Quality control procedures for IMOS Ocean radar manual version 2.1. Integrated marine observing system. https://doi.org/10.26198/5c89b59a931cb
47. Cosoli S, Grcic B, De Vos S, Hetzel Y (2018) Improving data quality for the Australian high frequency ocean radar network through real-time and delayed-mode quality-control procedures. Remote Sens (Basel) 10(9):1476
48. Bellomo L, Griffa A, Cosoli S, Falco P, Gerin R, Iermano I et al (2015) Toward an integrated HF radar network in the Mediterranean Sea to improve search and rescue and oil spill response: the TOSCA project experience. J Operation Oceanogr 8(2):95–107
49. Kalampokis A, Uttieri M, Poulain PM, Zambianchi E (2016) Validation of HF radar-derived currents in the Gulf of Naples with Lagrangian data. IEEE Geosci Remote Sens Lett 13(10):1452–1456
50. Corgnati L, Mantovani C, Griffa A, Forneris V, Tronconi C, Santoleri R, Kalampokis A (2014) The "RITMARE Italian coastal radar network: operational system and data interoperability framework. In: Proceedings of the 7th EuroGOOS conference, pp. 28–30
51. Bertelli T (1873) Appunti storici intorno alle ricerche sui piccoli e spontanei moti dei pendoli fatte dal secolo XVII, In: Bullettino di Bibliografia e di Storia delle Scienze Matematiche e Fisiche di B. Boncompagni, t.VI, gennaio
52. Hasselmann K (1963) A statistical analysis of the generation of microseisms. Rev Geophys 1(2):170–210
53. Longuet-Higgins MS (1950) A theory of the origin of microseisms source. Philos Trans Roy Soc Lond 243(857):1–35
54. Dorman LM, Schreiner AE, Bibee LD, Hildebrand JA (1993) Deep-water seafloor array observations of seismo-acoustic noise in the eastern Pacific and comparisons with wind and swell, natural physical sources of underwater sound. Springer, New York, pp 165–174
55. Bromirski PD, Duennebier FK, Stephen R (2005) Mid-ocean microseisms. Geochem Geophys Geosyst 6:4
56. Ardhuin F, Stutzmann E, Schimmel M, Mangeney A (2011) Ocean wave sources of seismic noise. J Geophys Res Oceans 116:C9
57. Lee AW (1935) On the direction of approach of microseismic waves. Proc Roy Soc Lond A 149:183–199
58. Grevemeyer I, Herber R, Essen H-H (2000) Microseismological evidence for a changing wave climate in the Northeast Atlantic Ocean. Nature 408:349–352
59. Stutzmann E, Schimmel M, Patau G (2009) Global climate imprint on seismic noise. Geochem Geophys Geosyst 10:11
60. Ferretti G, Zunino A, Scafidi D, Barani S, Spallarossa D (2013) On microseisms recorded near the Ligurian coast (Italy) and their relationship with sea wave height. Geophys J Int 194:524–533
61. Andrea, Cannata Flavio, Cannavò Salvatore, Moschella Giuseppe, Di Grazia Gabriele, Nardone Arianna, Orasi Marco, Picone Maurizio, Ferla Stefano, Gresta (2020) Unravelling the Relationship Between Microseisms and Spatial Distribution of Sea Wave Height by Statistical and Machine Learning Approaches. Remote Sensing 12(5):761. https://doi.org/10.3390/rs12050761

Chapter 10
Sea Level Measurement

Gwenaële Jan, Begoña Pérez Gómez, Corinne Salaün, Didier Rouxel, Nicolas Pouvreau, Yann Ferret, and Alexa Latapy

Contents

Abstract A sea height for whom, for what? This question finds several answers in wide multidisciplinary scientific domains varying from in situ measurements to spatial altimetry and fields of studies linked mainly via oceanology and metrology. A water height is first an instantaneous measurement that feeds into the knowledge and calculation of sea level change, mean, lowest and highest, sea levels, tide amplitude and phase. These are all water level definitions that do not figure the same physical content. The definition of these levels can vary substantially depending on the purpose of the study. For this reason, several international organizations (IHO, GLOSS, and SONEL) aim to provide recommendations on some key definitions related to water levels. From former measurements to current observations, tech-

Gwenaële Jan*(§10.1, 10.3, 10.4, 10.5, 10.6), Begoña Pérez Gómez (§10.3, 10.4, 10.5), Corinne Salaün (10.§2), Didier Rouxel (§10.2), Nicolas Pouvreau (§10.5, 10.6), Yann Ferret (§ 10.5,10.6), Alexa Latapy (§10.6).

G. Jan (✉) · C. Salaün · D. Rouxel · N. Pouvreau · Y. Ferret · A. Latapy
Shom, Brest, France
e-mail: gjan@shom.fr; corinne.salun@shom.fr; didier.rouxel@shom.fr; nicolas.pouvreau@shom.fr; yann.ferret@shom.fr; alexa.latapy@shom.fr

B. P. Gómez
Puertos del Estado, Madrid, Spain
e-mail: bego@puerto.es

P. Daponte et al. (eds.), *Measurement for the Sea*, Springer Series in Measurement Science and Technology,
https://doi.org/10.1007/978-3-030-82024-4_10

niques evolved and constantly question the quality and the continuity of data. The large family of sensors measuring water level is populated by tide gauges, GNSS and radar altimeters onboard a satellite that provide a global geographical coverage and complement fixed-point observation.

Seawater height measurement structures the profile of important issues for the knowledge of marine environment. It is one of the essential ocean variables impacting and driving studies in ocean currents, climate change, engineering for the design of coastal installations and a large community engaged in operational oceanography. Its measurement and surface signature are a keystone in the calibration and validation of altimeters, coastal marine environment and ocean dynamic forecast and hindcast systems. Even further downstream in the field of applications, this ocean variable is a part of sustainable coastal economic activities, including applications in marine renewable energy. In this challenging frame, collected sea level data needed to be referenced in time and space (x, y, z, t), so that it is crucial to control the measurement and ensure the consistency of its monitoring.

Acronyms

IOC	Intergovernmental Oceanographic Commission (UNESCO)
GLOSS	Global Sea Level Observing System
GNSS	Global Navigation Satellite System
MSL	Mean sea level
SLA	Sea level anomaly
SSH	Sea surface height
Rms	Root mean square
LAT	Lowest astronomical tide
HAT	Highest astronomical tide

10.1 Measurements of Sea Height

Water height is measured by multiple sensors using different physics and techniques. It can be obtained from thermodynamic seawater properties, based on the principle of the equation of state which links pressure, density and depth Eqs. (10.1) and (10.2). Considering sea surface height (SSH) measurement from bottom pressure gauge, the principle operates using pressure (P) and temperature (T), completed by conductivity (χ) when possible. Pressure sensor tide gauge (e.g. quartz crystal) is placed on the ocean floor which is characteristic of depth, surrounding pressure and atmospheric pressure at sea surface. The knowledge of atmospheric pressure and water density is then essential to compute the water heights knowing the thermodynamic properties linking these parameters. These are defined in the international thermodynamic equation of seawater (UNESCO guide 2010 [8]).

$$p = -\rho g dz \tag{10.1}$$

$$\rho = f\left(S,T,P\right) \tag{10.2}$$

with P ambient pressure (kg. m^{-1}.s^{-2}); ρ water volumic mass (kg. m^{-3}); g local gravity acceleration (9.80665 m.s^{-2}); dz water height (m) and; S salinity (ppm) a function of conductivity χ (S/m).

Consider a homogeneous ocean where density is constant in the water column; a bottom pressure tide gauge measurement is directly proportional to water height column and so representative of the water surface fluctuation (Fig. 10.6). The subject becomes more complex in an inhomogeneous ocean in which thermocline, halocline and internal tides structure internal layers of the ocean (i.e. isopycnal). The equation of the free surface elevation (Eq. 10.1) is thus modified by the thermodynamic content of the water column and is then written in Eq. (10.4). In this equation, the velocity is set as a function of total height and g (Eq. 10.3). This conversion between bottom pressure and equivalent sea surface height can impact by several centimetres of the total water height and acts as a compression factor [44]. Today, thanks to sensors precision, this signature on the SSH is detectable in the measurement.

$$c = \left(gH\right)^{0.5} \tag{10.3}$$

$$\eta = \delta p_b \left(1 - gH / 2c^2\right) / \left(g\varrho_{\text{mean}}\right) \tag{10.4}$$

with η free sea surface level (m); p_b bottom pressure (kg. m^{-1}.s^{-2}); H total water height (m); c celerity (m.s^{-1}); and g and ϱ as in Eqs. (10.1) and (10.2).

In such a configuration, this type of water level sensor does not need to be materially connected to a land point and there is no technical imperative for near real-time data transmission. If this is particularly useful in deep ocean, the control of the sensor can only be done during the tide gauge recovery steps. Therefore, from the first to last time step of record, a potential drift can affect the sensor without any possible control during the measure time period. The issue can come from an internal sensor drift or bias (e.g. on time clock), or it can result from a vertical position shift of the gauge. A pitch or roll disturbs the local sea level measurement adding a non-dynamic signal, only due to the change in position of the instrument. Some corrections can sometimes be applied but, when possible, levelling the sensor allows increasing the power of a water level measurement tenfold. Indeed, it allows to calculate the height measurement on a fixed reference which is moreover common to various observations. Indeed, it allows to calculate the height measurement on a fixed reference which is moreover common to various observations (e.g. ellipsoid).

The water level can also be measured by radar, thanks to the physical properties of the radar wave's propagation into ambient air environment. A radar gauge works totally differently and is deployed in open-air configuration offering an easy practical access for installation and maintenance. The two main types of radar sensors for

sea level measurements are frequency-modulated continuous-wave radars (FMCW, Fig. 10.7) and pulse radars; this latter emitting pulses in K band (26 GHz). A radar wave propagates in the air is reflected at the sea surface and then goes back to the transmitter on tide gauge (Figs. 10.1, left; 10.8). Half of the wave transmission time between emission and signal reception gives access to the height between the sensor reference point and water surface. The water height is then deduced removing the air draught to absolute water height expressed on a vertical reference level as an ellipsoid (Figs. 10.10, 10.11). In a moving ocean, the radar return echo frequency follows multidirectional paths and is affected by the Doppler effect (Fig. 10.1, right), so that, for a consistent measurement of water height, these interferences with multidirectional beams have to be reduced as much as possible. This is typically the case with sea roughness or air temperature gradient between the sensor and the water surface, particularly if a tranquilization tube is installed around the sensor. This impact on the water height measurement can be centimetric, which is precisely the expected precision on the observation. One the other hand, the onshore installation offers a capacity of real-time data transmission and so a possible near real-time control of the measurement. It should be noted that the radar technique has a low uncertainty budget on SSH and meets performance among the most accurate which today is of ~O[10^{-2} m] and several millimetres at the best.

It should be noted the roughness of sea surface may disturb the individual measurements in the radar gauges. A description of the method is proposed with radar altimeter which is based on a similar principle; below, in the history of sea level measurement technology, a major milestone took place in the years 1970s and in a more meaningful way in the 1990s. Indeed, the SSH sensors have undergone a small revolution with the rise of altimetry complementing in situ observation. The radar altimeter on-board satellite is characterized by several features that provide a new type of sea level data. In orbit from 800 km to 1366 km altitude, the technique is, first of all, designed from emitted radar waves bands defined to fit the frequencies corresponding to the water observation capacity and depend also upon regulations (Fig. 10.2). The water height under the satellite's Nadir measurement is computed from the propagation time between the transmitting radar and the ocean surface.

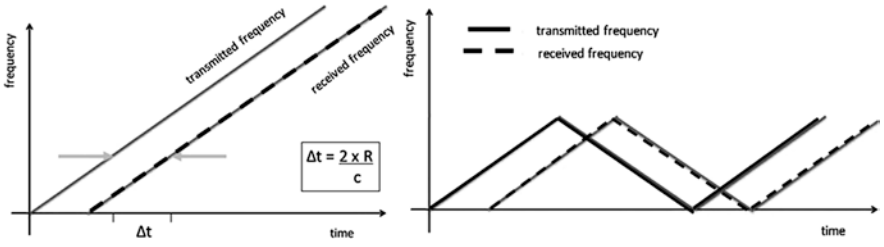

Fig. 10.1 Principle of FMCW measurement: Δt (s) is time between the same frequency transmitted and received and is proportional to the distance to the target R (m); c is the speed of light in air (ms^{-1}) (left); Triangular modulation of frequency used in an FMCW radar gauge (right) (Vanicek et al. [9])

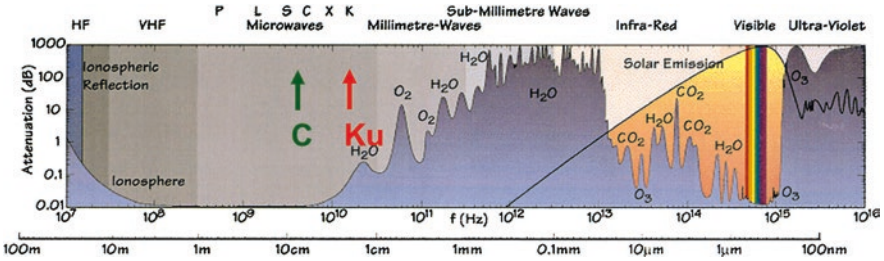

Fig. 10.2 Electromagnetic spectrum with different bands indicated. (Credits ESA) Ku, C, bands for altimetry dedicated to water observation. Ku band 13.6 GHz (12.5–18 GHz), C band 3.2 GHz (4–8 GHz) and Ka band 35 GHz (26.5–40 GHz

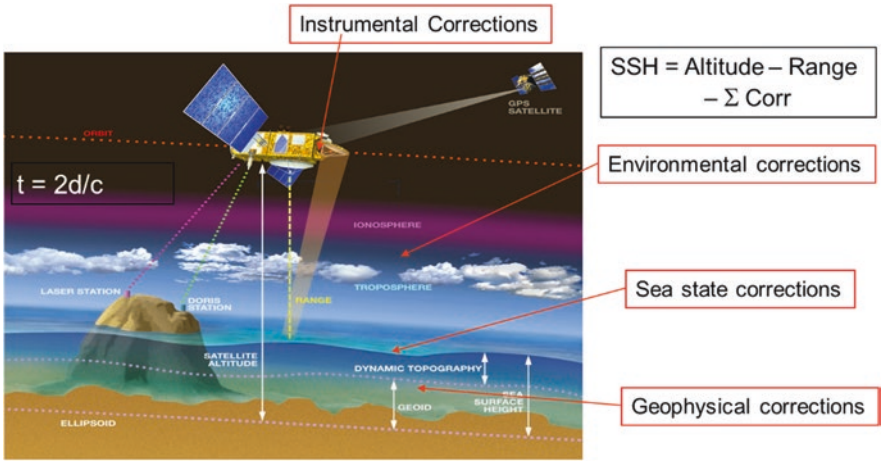

Fig. 10.3 Altimetry principle: *t* time for return radar wave (s); *d* range (m); c celerity of wave propagation between altimeter and a surface of reference, e.g. ellipsoid (ms^{-1}) (© CNES/ill./ DUCROS David, 1998)

The waves' velocity varies as they travel through the different layers of the atmosphere (Fig. 10.3). From radar pulse and its waveforms, the epoch at mid-distance is the time delay of the expected return of the radar pulse, estimated by the tracker algorithm. Thus, it provides the range (i.e. height) derived from the time for the radar pulse to go through space, from satellite orbit, atmosphere and ocean surface where it is reflected and sent back to the signal receiver on-board satellite radar. The sea surface height is calculated from the residual height between altitude and range and a sum of corrections (Corr): ionosphere, troposphere; sea state (electromagnetic bias) and instrumental correction (Fig. 10.3).

The key radar equation expresses the power of radiation received (Pr), which varies with wavelength of the pulse (λ_0); antenna gain (G); power emitted (Pe); two-way atmospheric transmittance (T^2); range from the target surface (R); backscatter

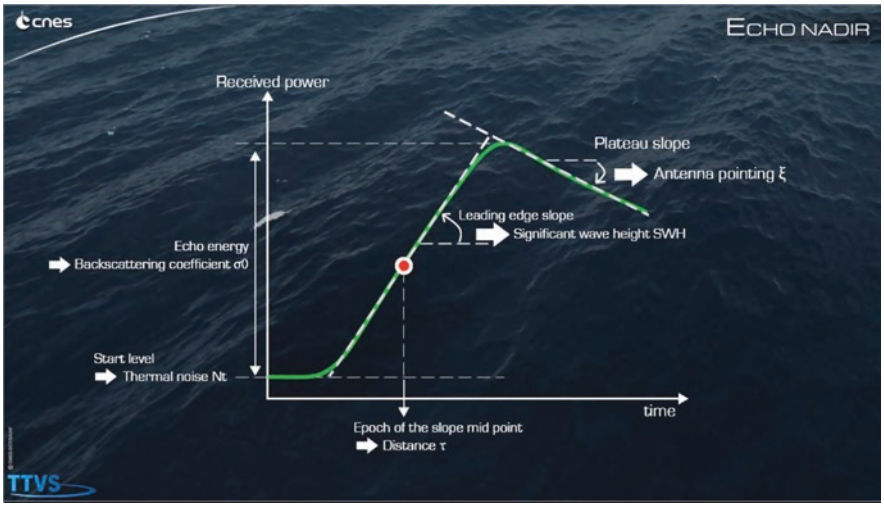

Fig. 10.4 Estimation of altimetry parameters, using Browns' model: sea surface height (SSH) derived from epoch at mid height and skewness. Abscissa for time, ordinate axis for power signal (src: CNES)

coefficient (σ) (Eq. 10.5). The principle of measurement is shown on Fig. 10.4, where from the radar altimeter waveform, the time (t) is derived from altimetry parameters estimation using Browns' model (e.g. the epoch at mid height). Note that for rough sea surface, the backscatter is calculated over the surface (S) illuminated by the antenna.

$$P_r = T^2 P_e \frac{\lambda_0^2}{(4\pi)^3 R^4} G^2 \sigma; \sigma = \int_{\text{Surface}} \sigma_0 dS\left(m^2\right) \tag{10.5}$$

Satellite's exact position needs to be accurately determined at less than O [10^{-2}] m (Sect. 10.3). To face this challenge, satellite tracking is made using complementary systems with for GNSS system: (1) satellite laser ranging (SLR), (2) a network of laser ground stations measuring directly and precisely the distance between the satellite and the ground station, (3) on-board GPS receiver providing precise and continuous tracking of the satellite by monitoring range and timing signals, (4) a network of DORIS beacons[1] which determine the Doppler effect from the distance between the satellite and the ground beacon.

Orbit precision is crucial for SSH measurements; 25 years ago, the mean orbit error was estimated to 3.10^{-2} m and SSH precision of the order of 10^{-1} m [21]. Precise orbit improvement is now contributing to a SSH result up to centimetre.

[1] DORIS beacons emit 2 frequencies. An on-board captor measures the Doppler shift between the signals to determine the distance between the satellite and the ground beacon.

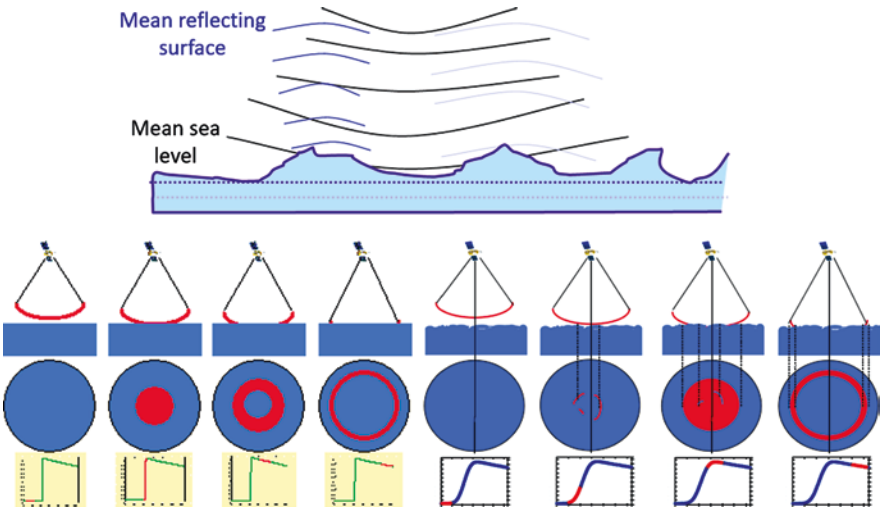

Fig. 10.5 Schematic view of electromagnetic bias (sea state bias) (left upper panel); reflexion of the altimeter radar pulse as a function of sea state: ideally calm sea (upper right panel) and rough sea state (low panel) (upper right and lower panel: source CNES)

In addition to orbit topic, the wavelength beam is not reflected in the same incident angle direction, depending on the roughness of the sea (Fig. 10.5). In particular, the altimeter pulse is more widely reflected by a concave wave than by a wave crest. Then, under windy conditions, the mean reflecting surface is shifted away from mean sea level. The difference leads to a skewness bias, called electromagnetic bias whose fluctuation with wind speed and wave height is non-linear. The electromagnetic bias is estimated using empirical formulas. Furthermore, if the on-board algorithms are fitted for water measurement, they are disturbed in the vicinity of land points and cause errors on the SSH estimate of the order of several centimetres (Sect. 10.3).

We can consider that a required centimetre precision from altitude of 800–1350 km has to go with an accurate satellite position, an excellent quality control of sensors and the best geophysical errors estimation. After what, the resulting sea surface topography is a combination of ocean dynamic topography and the marine geoid (Fig. 10.11). Ultimately, radar altimeter meets a centimetric sea surface height measurement uncertainty and equals the ones carried by several other types of in situ tide gauges. In this context, we could define the radar altimeter onboard as a tide gauge in space (Figs. 10.6, 10.7, 10.8).

A part from radar, the water height sensors are also made up of different types of gauges: the GPS-GNSS buoy and antennas are one of them and measure water level over geoid or ellipsoid, levelled with geo-positioning system satellites constellations. The GNSS constellation precision is improved by a strong density of precise positioning satellites and DORIS beacons, which give access to the position in x, y

Fig. 10.6 (Left) Bottom pressure sensor and stilling well of Kerguelen tide gauge (ROSAME network); (right) immersed operational bottom pressure (CalVal activities CNES, NASA, OST-ST meeting; photograph, courtesy of C. Gaillemin). Requirement and admitted total error for water level are of the order of 1.10^{-2} m

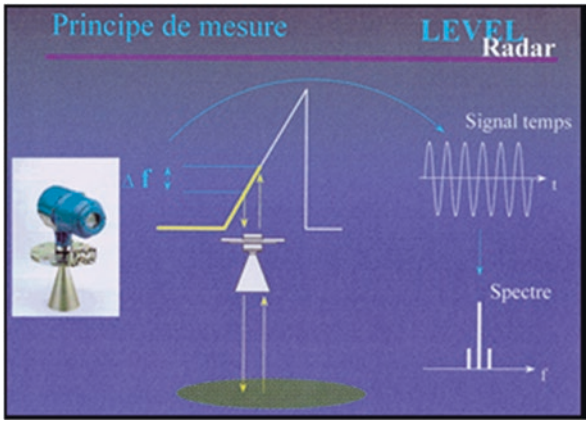

Fig. 10.7 Radar gauge FMCW measurement (src: Shom)

and z. Z component value is accurate to within few millimetres in optimal geometric configuration but can be degraded to several centimetres, depending on latitude and configuration of the measured location. In optimal configuration, the high accuracy of this measurement is undoubtedly one of its advantages. CNES and Space Agencies promoted this type of SSH measurement and are developed in the 1990's GPS buoys to complete the calibration and validation of Topex–Poseidon satellite with in situ experiences; today, GPS buoys become GPS-GNSS buoys (Figs. 10.9, 10.10). LEGOS, IRD, OCA, INSU, Shom and other research centres developed this type of in situ system and are continuously improving them. GNSS buoy is deployed at sea surface, and data transmission can be operated at near real-time data acquisition and transmission. One of the issues of GNSS sea surface height measurement consists in maintaining the stability at ocean surface that may be difficult to ensure

Fig. 10.8 Current tide gauge observatory with a radar sensor measuring sea level associated with a tide staff (10^{-2} m high square graduations) for monitoring the measurements. (Aix Island, France, 2019. Shom credits—IES team)

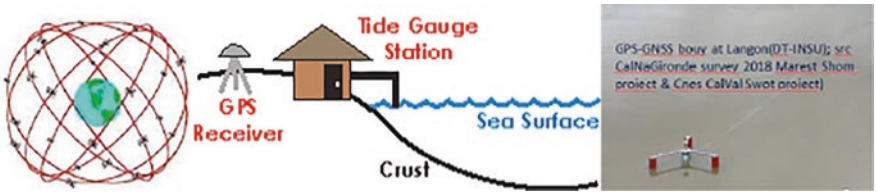

Fig. 10.9 (Left) Schematic view of GNSS constellation for precise positioning; (middle) gauge installation (src: PSMSL); (right) GPS-GNSS buoy (src: Insu) deployed during CalNaGironde-Marest survey, CNES Swot and Shom project [1]

over a long deployment. Most often, the use of the buoy is a relatively short-term deployment (several days with subdaily control).

A dense literature exists on this topic (e.g. CNES, NASA websites and OST-ST meetings [2, 3, 5, 29]. It is now established that a mean difference in height between a GPS-GNSS buoy and a tide gauge is below or of the order of 10^{-2} m (rms 10^{-2} m) which makes it possible to consider this type of buoy as a water level gauge or a very good complement to a long time series of measurements. For about 10 years, similar experiments have been carried but with the particularity of being installed on a towed floating structure [1, 4]. Linked to GPS-GNSS, another aspect of the measurements concerns the reflectometry which is a field of study under development

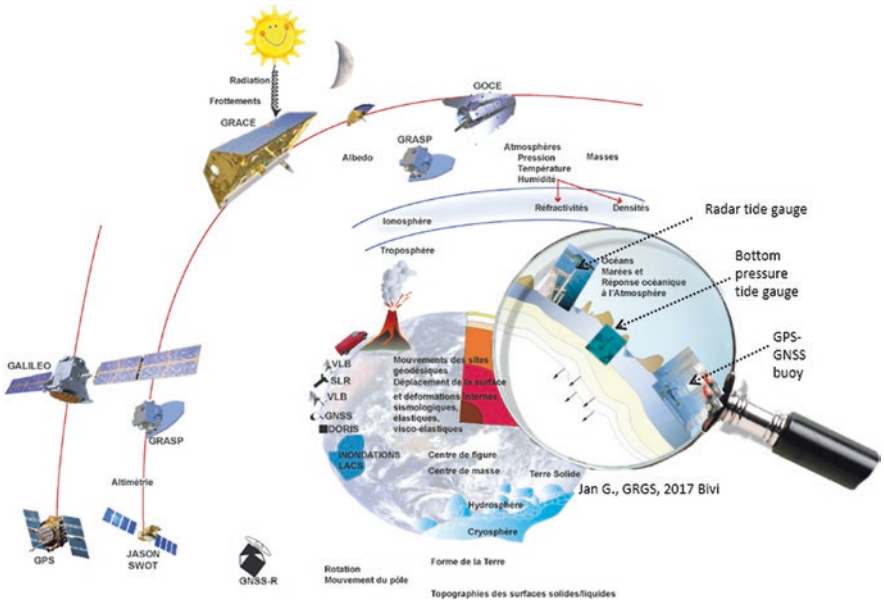

Fig. 10.10 Schematic view of observation network (GRGS [20])

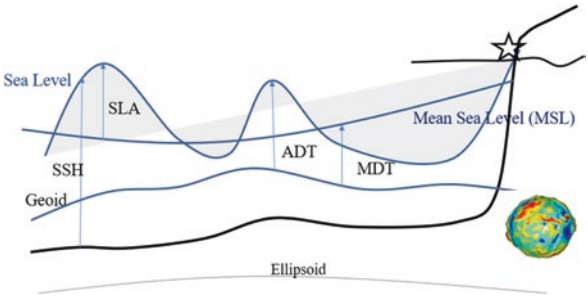

Fig. 10.11 Schematic view of sea surface height: sea surface height (SSH), sea level anomaly (SLA), mean dynamic topography (MDT), mean sea surface (MSS), absolute dynamic topography (ADT) and geoid on Earth (right), one of the key point

involving dedicated antennas receivers and the Interference Pattern Technique (IPT). The latter uses the same standard antenna receivers than for geodetic networks. In the context of ocean observation by a dense and perennial sensors network, all techniques and sensors measuring SSH are challenging. The density of the precise positioning network, the accuracy of its geometric resolution and the complementary nature of the measurements have thus advanced hydrography by giving relief to the calculation of reference heights for hydrography (Figs. 10.10, 10.11).

In complement, other types of sensors exist or have existed throughout a history written for more than 100 years. Thus, among the tide gauges, there are tide staff (Fig. 10.8) or, floating tide gauges. The latter is installed in a tranquilization tube and is equipped with a stylus connected to the float which allows to trace the evolution of the water height on a paper support. In this case, digitizing is required if the

objective is to use these data in a numerical model or shared it with data centres. Among all the different sensors measuring sea surface height, some are less used or are not meeting the centimetre requirement for the water heights' uncertainty (e.g. tide staff). But always, the recurring question about choice of techniques to record water level comes from a consensus between the science to be measured and the way to do so, taking into account the geodynamics of the measurement location. In this frame, the deployment of the tide gauges provides a punctual spot view, the spatial altimetry provides a view of a large areas including offshore domain and between open sea and coastal areas, and the GPS-GNSS network fills a gap in measurement. A geoid product can also fill the lack of data at wavelength larger than 200 km (e.g. geoid from space agencies mission GOCE, GRACE launched in 2002 and GRACE Follow-on launched in 2017[2]).

Measuring sea level requires a stable and accessible height value on a stable device. Ideally, a levelling over a common and fix reference level is required allowing a cross-comparison with different sensors on a common vertical height reference. Ellipsoids GRS80 and WGS84 are two references, commonly used, and a key to transpose a relative water level to an absolute water height over ellipsoid or geoid, as geodetic reference (Fig. 10.11). Water level geodetically levelled is an essential ocean variable (EOV) for many sciences merging it with coastline height values, projected on a reference frame of terrestrial height.

10.2 Relative and Absolute Height

Geoid height models over the oceans can be obtained by different methods, including those which consist in exploiting direct measurements of the gravity field to deduce the free-air gravity anomaly (FAA). The free-air anomaly corresponds to the difference between the actual gravity field measured on the geoid and a theoretical field on the reference ellipsoid modelling homogeneous and uniform Earth.

Over the oceans, those measurements are made aboard oceanographic ship using marine gravimeters, during dedicated campaigns. The technology of conventional relative gravimeters enables the measurement of the gravity field variations between two points. Considering that the measure is relative, these systems must be regularly calibrated during stopovers on land to determine the absolute gravity value at each acquisition point. In the few past years, the emergence of cold atomic technologies has enabled the development of on-board absolute cold atoms gravimeters [11], which allows avoiding the calibration steps at ports and thus improving productivity. These acquisition systems enable to reach variable precision, depending on the sea state (up to 0.5 mGal), and resolutions around a few kilometres [14].

[2] GRACE mission measures the distance between the two satellites and allows estimation of Earth masses distribution, every month at 300 km wavelength resolution.

The quality of marine gravity measurements has a direct impact on the accuracy of the computed geoid heights. They still remain the more qualitative data source to compute an accurate high-resolution geoid height model. However, the use of these data raises two main issues:

– The accuracy of marine gravity surveys is extremely variable, depending on the used acquisition system, the sea state, the data processing or the considered references. Thus, the merger of these surveys requires an important work of homogenization.
– Marine gravity surveys are carried out locally in order to characterize the gravity field over specific and relatively small areas of interest. These surveys are very sparse, and their concatenation hardly ever eliminates all data gaps. To solve this problem, the solution consists in filling the gaps by merging marine gravity measurements with a free-air anomaly model derived from satellite altimetry [16, 17, 10].

The computation of an accurate geoid model can thus be obtained from a merged free-air anomaly model. Indeed, the different gravimetric data types of the gravity field are linked by mathematical relationship, which enable to determine one by knowing the second (Fig. 10.12).

The collocation method is a statistical estimation method which takes into account the observations errors and their correlation [15]. It allows producing models from the merger of heterogeneous data by weighting the accuracy of the determined value according to the quality of the input data.

Thus, the collocation method enables the direct determination of the geoid height (free-air anomaly > geoid height) through the use of a cross-covariance model allowing the passage between the two components of the gravity field. The Stokes method [13] can be implemented as well. Solving the Stokes equation allows the direct determination of the geoid height from the free-air anomaly according to the following formula (Eq. 10.6):

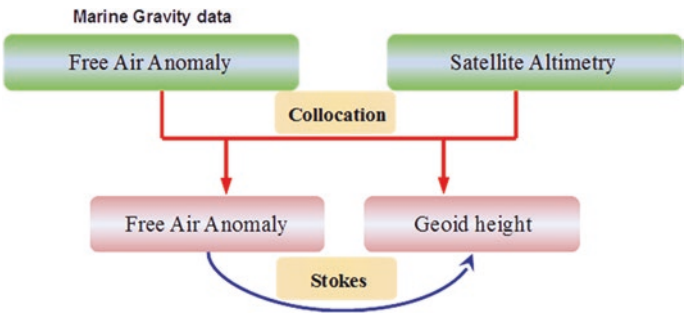

Fig. 10.12 Methodology to compute geoid height from marine gravity data merged with satellite altimetric models

$$N = N_{GM} + R/4\pi\gamma \int_0^{2\pi}\int_0^{\pi} \left[\Delta g(\varphi,\lambda) - \Delta g_{GM}(\varphi,\lambda)\right] S(\psi)\, d\psi\, d\alpha \tag{10.6}$$

with N geoid height (m); R Earth radius (m); φ et λ latitudes and longitudes (°); ψ spherical distance (m); α azimuth (degree); Δg_{GM} et N_{GM} global models (EGM08, EIGEN6, etc.); Δg measured free-air anomaly (mGal); and S Stokes spherical kernel function.

In such a case, the collocation method can be used first, to merge the marine gravity data with a model derived from altimetry. The improvement of the free-air anomaly models derived from altimetry is constant, thanks to the multiplication of satellite missions and the improvement of processing methods [18]. Moreover, the continuation of the acquisition surveys at sea and the instrumental improvement will provide access to more and more in situ data with increasing accuracy.

The effort focused on coastal areas will also enables to solve the problem of gravimetric knowledge in the 0–30 km fringe and on the land–ocean transition. Finally, the improvement of data homogenization and merging methods will allow the integration of quality data from different sources [12].

10.3 Sea Level Uncertainty and Total Error Budget

A reference of measurement in space and time can be introduced echoing the following point of view "The validity of a measurement only makes sense if the measurand is well defined and a poor definition of the measurand leads at least to an increase in measurement uncertainty" (Barbier P., Edito 2010[3]; [20]). This is why, thinking measurement is also thinking temporal and spatial reference. A benchmark must be stable and its vertical position controlled in time. The control of the uncertainty and the error balance on the measurement also requires the control of its temporal sampling parameters.

By the principle of the measuring technique, a tide gauge reconstitutes the sea level by averaging records following two temporal parameters: the time sampling and the integration time. The latter averages the records between two measurements within the time sampling interval. Both parameters are defined depending on the dynamics to be observed and the depth of water level gauge (e.g. SSH filtered from swell). Temporal sampling can be set by a rate with usual range from 1 min up to 1 h, noting that 1 min becoming a more standard temporal sampling justified for high-frequency dynamics studies such as infragravity waves, storm surge or resonance effects in bays and harbours. This is particularly important during extreme events, where these processes contribute to the sea level and coastal flooding in combination with tide and lower frequency processes (Pérez B. et al. 2013 [24]). Consequently, recommended standards, handling the different sampling rates on data processing, are provided with

[3] Barbier P., Edito 2010 August, Afnor Bivi Metrology

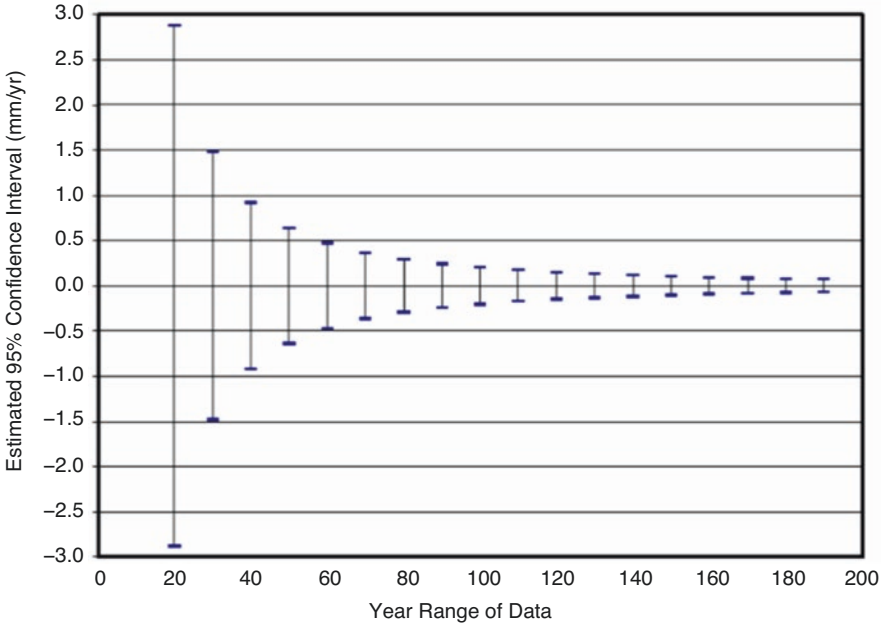

Fig. 10.13 Comparison of 95% confidence intervals versus series length for linear mean sea level trends (units: cm) (Src: NOAA). X-axis: year range of data, Y-axis: estimated 95% confidence interval (mm/yr)

criteria for quality control of high-frequency sea level data, including the data filtering [6]. According to GLOSS recommendations, the nominal accuracy of each of these individual SSH measurement should be less or equal to 10^{-2} m and the long-term mean sea level trend studies, derived from measurements, should meet a 10^{-3} m per year accuracy [7, 41]. This latter requirement is difficult to achieve and has to deal with a combination of instrumental issues and external factors such as drifts in pressure sensors, fooling plugging sensors, incorrect datum assignment, datum changes over time and movements of sensor or station. Figure 10.13 provides an illustration of the recommendations for measuring and combining SSH data with characterized errors and uncertainties. Sea level uncertainty decrease is particularly highlighted when using validated records of several years long. The 95% confidence interval of the mean sea level trend is reduced by half from 20–40 years SSH time series (Fig. 10.13).

In addition to temporal topic, attention should be paid to 3D position of the tide gauge [25], CalVal OST-ST CNES, NASA activities [3]. A sensor that has been tilted during the measurement session measures a water height which is made of sea dynamics but also instrument shift, impacting the observed water height. To control the 3D position of gauge, GPS-GNSS data can be used with a relevant SSH accuracy below centimetre in coastal areas. Furthermore, a tide gauge combined with GPS-GNSS measures and the knowledge of the geodetic levelling between the observation stations provides a strong validation of a Worldwide Vertical Datum. In

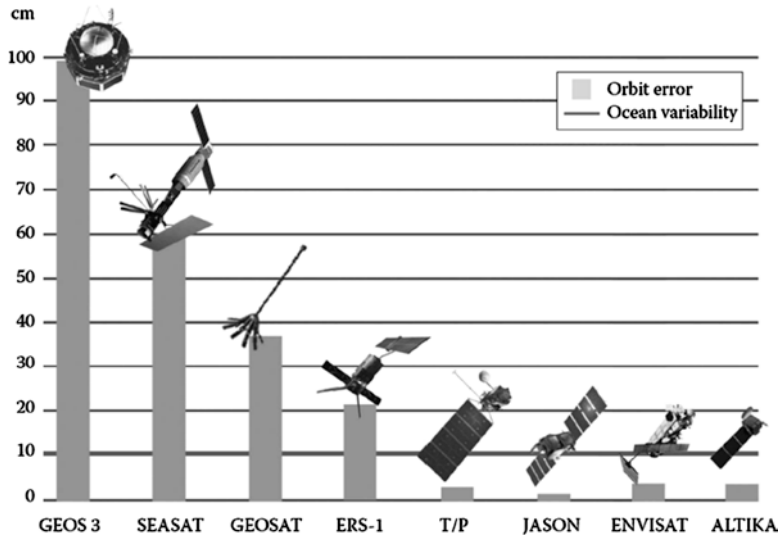

Fig. 10.14 Radial orbit error and ocean variability (cm) [21]

this framework, SONEL[7] is one of the international organisms that expertises, assembles, archives and distributes GNSS data.

The uncertainty on SSH takes also into account a set of signal corrections, uncertainties and filtering of the raw data, so that all techniques open up areas of research aimed at approaching, quantifying and controlling uncertainties like instrumental biases, data processing strategies, noise signal estimation, geodynamic factors and method used to propagate these errors in algorithms. A global centimetre uncertainty is a current order of magnitude for the measurement of water height (IHO (Sect. 10.4.3) and IOC-GLOSS recommendations).

In altimetry, the technique must calibrate and control additional source of uncertainty related to the fact that the altimeter navigates from space (Sect. 10.1). Indeed, an error in satellite's along-track position, multiplied by the orbit slope, gives an error in SSH. On this topic, precise orbit determination is made by specialist teams and tracking data expertises lead to a millimetre uncertainty (Fig. 10.14) [21, 23]. But crossing the atmosphere imposes the control of uncertainties and errors related to the route in space, in the atmosphere, at ocean surface and the reverse path. Raw data sets are impacted by various sources of geographically correlated error patterns ranging from instrument and processing error residuals to orbit standards.[4]

Taking into account these items of uncertainty, altimeter errors impacting global mean sea level have strongly decreased from 2002 to 2012 (Jason-1 and Jason-2

[4] Radar altimeter delay and disturbances due to ionosphere (range error O [10^{-2}]); dry and wet troposphere (respectively, with an average error budget of 7 10^{-2} m; 10^{-2} to 10^{-1} m); internal drift in the oscillator frequency (range error O [10^{-2}]); land points perturbation with recent improvements in data post-treatments giving now access to SSH up to 3 km from the coast [23].

Table 10.1 Total SSH error budget for satellite Jason-2 [21]

Parameters		Altimetry uncertainties (cm)
Parameters and correction for sea surface height	Altimeter range	1.7 (noise)
	Filtered-out altimeter ionosphere correction	0.2
	Sea state bias	0.2
Radiometer wet troposphere	Dry troposphere and dynamical atmospheric corrections	0.7
	Radiometer wet troposphere	0.2
	Ocean tide	1.0
	Orbit (radial component)	1.5
Sea surface height	Corrected with all corrections	<3.5

missions) and are now reaching a millimetre precision on annual trend SSH error budget [19, 26]. This estimate of uncertainty on sea level trend faced with an overview of Jason-2 satellite error budget on SSH raises two points: on one hand; since 2013, the uncertainties on sea level have continued to decrease from 3.5 cm (Table 10.1) to 1 cm (Fig. 10.14) with a trend of mm per year, cited previously. On the other hand, thanks to the error budgets' improvement on SSH measure, the estimation of the sea level trend reaches a remarkable accuracy.

Considering that the error budget of sea surface height is very precise for more than a decade, new challenges appear and some are turned towards interferometry and densification of the satellite constellation. The challenge is now towards satellites constellations and their cross-calibration to give a huge access to valuable measurement for oceanography and hydrography. Current developing systems aim to maximize the altimetry data Earth coverage and archive, using GPS-GNSS constellation with several altimeters onboard operating simultaneously; interferometer will cover a larger data measurements compared to a Nadir Altimeter onboard (Fig. 10.15).

"The future international Surface Water and Ocean Topography (SWOT) Mission, planned for launch in 2021, will make high-resolution 2D observations of sea surface height using SAR radar interferometric techniques. SWOT will map the global and coastal oceans up to 77.6°N latitude every 21 days over a swath of 120 km (20 km nadir gap). Today's 2D mapped altimeter data can resolve ocean scales of 150 km wavelength, whereas the SWOT measurement will extend our 2D observations down to 15–30 km, depending on sea state. SWOT will offer new opportunities to observe the oceanic dynamic processes at these scales" [23]. This future will offer opportunities to rely on continental water level, like estuaries to ocean SSH.

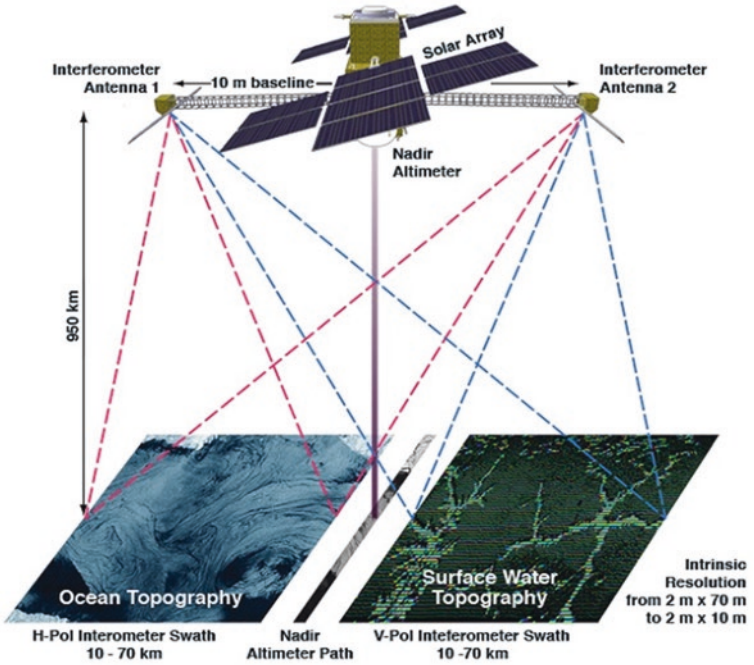

Fig. 10.15 Schematic of SWOT measurements over oceans and terrestrial surface waters, NASA/CNES mission (courtesy of NASA/K. Wiedman)

10.4 Uses of Water Level for Marine Dynamics Environment

10.4.1 Ocean Tide and Sea Level Measurement

Tide prediction is a major product of sea level measurements. With Terra watts of energy transported over ocean, tide rhythms global ocean dynamics up to estuaries areas. It impacts marine environment from ecosystems to human infrastructure and economy. Tide is predicted from Moon, Sun and Earth celestial mechanics and analysed based on harmonic formulation and equations (e.g. Laplace, Doodson and Schureman). Its calculus required a tidal potential derived for astronomical mechanics and a geographic reference to compute the tide phase from a starting point (Greenwich meridian). Tide is a combination of several waves forced by Moon, Sun and Earth astronomical mechanics for which each of these movements has to be to characterized (Earth trajectory relative to solar ecliptic plane, mean Moon trajectory, etc.). These are tidal components expressed by equations and called harmonic constant (Eq. 10.7). Tidal theory and sea level observations form a duo mainly working in two modes. Mode 1 is the harmonic way from observation and theory to predict tide dynamics, and mode 2 corresponds to calibration and validation studies, using observation to evaluate the

consistency of tidal numerical model output or a derived tidal product for validation purpose.

In the first mode of use, SSH value is injected into the tidal equations to compute harmonic components. This is a keystone since a tide prediction can be operated from the set of harmonic constants. Harmonic constant is characterized by amplitude (height) and phase (degree). Phase indicates the direction and speed of the tide wave with reference to Greenwich O° longitude. Let h(t) be the tide amplitude at time t and reduced to its components i: i is considered as a serial number ($i \in N*$ in complex space with N, the Nyquist frequency).

$$h(t) = \sum_{i,n\max} h_i \cos\left(V_{0i} + q_i t - G_i\right) \tag{10.7}$$

with h_i the tide harmonic amplitude (m); V_{0i} astronomic argument at initial time t_0, computed, thanks to Legendre polynomial development [45]; q_i ith angular speed ($°.s^{-1}$); nmax maximum number of tidal harmonic selected; and G_i ith harmonic situation (phase lag between the ith harmonic and the corresponding tidal potential derived from V_{0i}). h_i and G_i characterize tide harmonic constants at one site (e.g. harbour).

The amplitude ai, the frequency_i (≥ 0) and the phase_i at the origin instant t = 0. h(t) can be written in first approximation, setting mean level at zero and involving cosine arguments with phases (Eq. 10.8). The tidal equation is also written as a sum of exponentials (Eq. 10.8). The Fourier transform is the fundamental rule that allows computation from the real space to the frequency space (i.e. from height and time to harmonic amplitude and frequency. Each harmonic corresponds to the ocean feedback, forced by the tidal generator potential and combination of waves characterized by frequencies covering large spectra from few seconds and 10^{-3} m to more than 19 years and 100 km. From Eqs. (10.8) and (10.9), the Fourier transform of hi(t) is a sum of two distributions of Dirac at opposite frequencies (*j* and *-j*) and weighted by amplitudes conjugated complexes. Then, the discrete sum of harmonics is equivalent to the total tide amplitude.

$$h(t) = \sum_i h_i(t) = \sum_i a_i \cos\left(2\pi\nu_i - \varphi_i\right) \tag{10.8}$$

$$h_i(t) = \eta_i e^{j2\pi\nu_i t} \tag{10.9}$$

Directly due to Fourier Transform property, this method is particularly fitted for continuous time series and less powerful in case of discontinuous sea level measurement (lack of data and data transfer issue). Consequently, the observability of tide signal has to meet the Nyquist criterion. Thus, if the absolute value of frequency (νi) is greater than the Nyquist frequency, the problem cannot be solved due to the non-respect of Shannon's theorem.

Moreover, tide can be considered as a specific dynamics, in the sense that, although it is perceived as a regular movement, the tide is not totally periodic. This

is due to the multiple frequencies combinations of tidal components of which the sum and its Fourier transform are themselves a sum of Dirac distributions, weighted by the amplitudes of the corresponding waves. At first approach, it should be noted that a minimum of 25 days is required to be able to separate diurnal and semidiurnal tidal components, signing respectively, one and two high and low tides per day. Only a qualified longer time series of measurements can solve tidal signal containing non-linear component that occurs by tidal waves combinations. Each harmonic is, then, better defined including slow tidal variations. A 19 years' time series is thus recommended for interannual tide evolution study allowing to take into account several "slow" variations of the celestial mechanics of Earth, Moon and Sun, involved in the tidal phenomenon and having an impact of several centimetres on the SSH (e.g. evolution at 18.6 years with the Saros phenomena). Considering the tidal interannual variation, this slow component acts as a modulation of the tidal signal, called nodal factors.

Studying tide from observation raises the question of temporal sampling and the tide signal that can be observed and analysed. But up to what extent is the tide observable across the SSH?

The past use has often relied on the hourly dynamics of the tide for reasons justified among others by data storage capacity limit, computing power, and techniques. From temporal sampling introduced previously, a time series longer than 1 year is thus necessary to solve the large tidal spectra of harmonics. Most of tide gauges are now recording at a 5 min sampling or 1 min.

A second mode using SSH observation is focusing on numerical modelling which offers a tide predictions' capacity over a gridded area and can provide a water level time series, including the parametrization and the calculation of friction and tidal energy dissipation. The objective is to model the tide as realistic as possible and analyses it with respect to the observation containing tidal signal but also local dynamics like swell, wind, atmospheric pressure, gravity wave and thermal front. Consequently, the models' output needs to be validated with independent observation which plays the role of in situ "truth". In addition, SSH observation can be assimilated in a numerical model and constrains the predicted water level towards observation. This type of assimilated system is highly dependent on in situ data (e.g. SSH, topic Sect. 10.1).

The tide study from satellite SSH altimetry has an additional feature from other in situ observations that relates to the repeatability period of a satellite which requires SSH temporal sampling of several days. Due to a specific designed orbit, the revolution time period and repeatability, the time to return to the same geographical point, are ranged from 9.9 days to 35 days and more, not omitting the stationary satellites. The data time sampling can be reduced to a 3 days repeatability taking advantage of all the satellites tracks crossing them all around the ocean. For tide, it means that radar altimeter observations catch a tidal signal of 12 days period. This point introduces the notion of aliasing the measurement and how to reconstruct the water height taking into account this sampling set by the orbit of the altimeter satellite. It comes down to the fact that altimeter measurement subsamples high-frequency signals and folds the high-frequency spectrum on to low-frequency spectrum. But due to the high variance

of the tidal signal, its dynamics can be partly deduced from the altimeter observation, using the repeatability of the measurement combined with a long time series.

Another peculiarity needs to be solved and can be summarized by the physics content of SSH in altimetry data that is not equivalent to the one measured with in situ tide gauge which is in solidarity with the movement of the earth. Indeed, the on-board SSH "tide gauge" is not impacted by vertical movement of Earth, contrary to in situ tide gauge where solid and polar tides occur. Solid tide results from the gravitational attraction fluctuation exerted on earths' crust and polar tide has for origin the variation in the position of the 2 earth poles. The vertical movement is a several centimetres at latitudes close to 35, 45 °N near the European coasts and is due to tidal load effect that weighs on the earth's crust as the tide moves in. Both types of data sets have to be processed before comparing each other. SSH between satellite footprints at sea surface and single position of tide gauge is propagated using ocean numerical model to fill the gap in between. In this case, dedicated filters are applied on water level data in order to collocate the different SSH measurements and to remove the short or long wavelengths, depending on the studied dynamics.

Using several SSH sets from distinct altimeters densify the observation network, but it is crucial to cross-calibrate potential water heights bias from multimission sources and ensure its consistency. An example of SSH use for tidal prediction is illustrated on Fig. 10.16 and comes from tide gauges, altimeter and tidal model. A result is proposed for semidiurnal (M2, the dominant harmonic in Atlantic Ocean) tidal harmonic wave (Fig. 10.16, left panel). This result was computed from SSH observations assimilation combined in T-ugom tidal model (F. Lyard et al. (FES2012 and recently FES2014 [40]). One of its characteristics is a low error budget. Low error is characterized by both amplitude with a range from 0 to 3.10^{-2} m (Fig. 10.16, upper right panel) and relative error, highlighted by alias in M2 signal (Fig. 10.16, lower right panel). Relative error is lower than 5% of signal, except for particular coastal areas where it can increase up to 75% error. These areas are in constant improvement adding in situ SSH observation on seas with continental shelf and improving the performance of on-board satellite measurement and its post-processing.

A part from tidal scales, a specific attention should be paid to the ocean dynamic induced by the atmosphere at a scale close to the gravitational astronomical tide. This process is radiational, and its source is the solar radiation partly responsible for the air masses' formation and their movements with the wind regime and atmospheric pressure. It may contribute significantly to sea level measured for several centimetres which is not negligible, knowing that mean amplitude of ocean tide is 10^{-2} m to 2.5 m in the open ocean with larger amplitudes in coastal regions (15 m Saint-Malo (France), 18 m Bay of Fundy (Canada)). The radiational waves act mechanically and thermodynamically on water surface and require to be solved as much as possible in order to deconvolve the part of the atmospheric tide from the total sea level signal. For high-frequency barotropic motions, wind and pressure forcing creates a high-frequency barotropic response at periods less than 20 days which is not resolved by 10 days altimeter sampling but can be corrected by ocean models. Sea surface height is therefore a key factor in estimating tidal accuracy

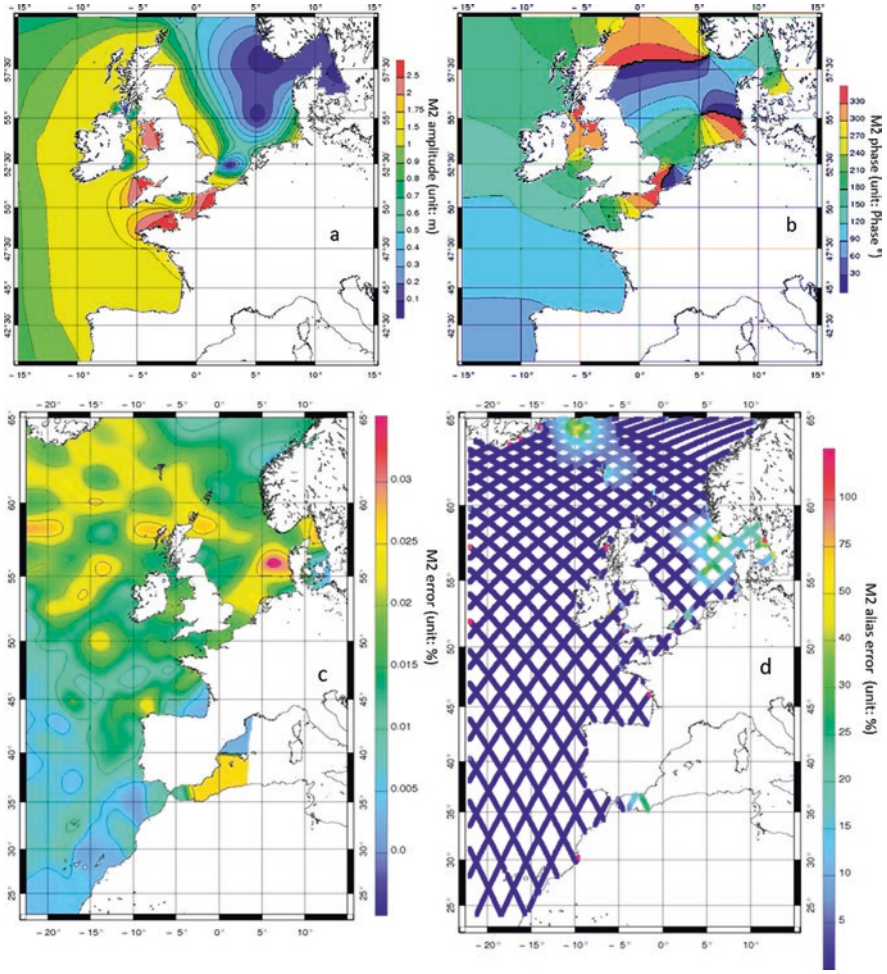

Fig. 10.16 Fes2012 Tide atlas: semi diurnal harmonic M2 amplitude (m) panel a; M2 phase (°) panel b; error on M2 harmonic (m) panel c; M2 alias error (% of amplitude) panel d; courtesy of F. Lyard, CNRS

through its implication in the tidal theory equations and through its direct measurement in situ and its derivation from satellite SSH [47].

From this key, the mean sea level (MSL), several different water heights can be computed and compared with other set of SSH observations as the lowest astronomical tide, the highest spring tide, the zero hydrographic and values over ellipsoid or over marine geoid (Fig. 10.17). The mean sea level allows calculation of SSH anomalies defined as SSH instantaneous subtracted from the SSH average. This average level is a high point that evaluates an SSH in relation to a reference in space and time (place and period studied). Some of the important levels for tide are presented in Fig. 10.17.

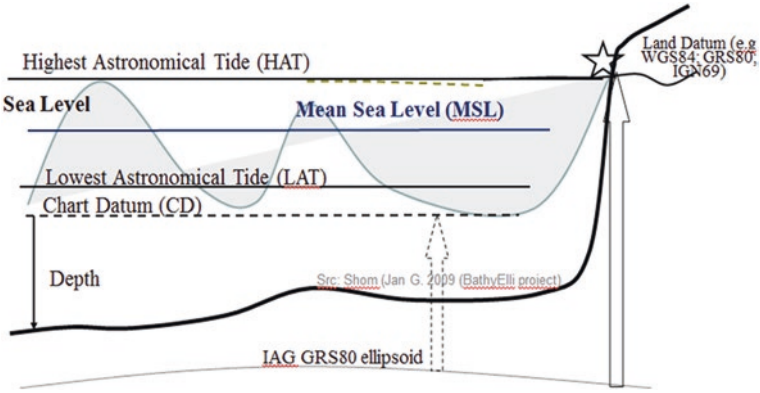

Fig. 10.17 Levels of reference: MSL is a key point from which lowest astronomical tide (LAT), highest astronomical tide (HAT) and SSH anomaly (departure from MSL) can be computed

10.4.2 Ocean Dynamics, Climate and Water Level Data

The sustainable development objectives for 2030 adopted by the United Nations countries place climate change at the heart of international thinking and action. Intrinsically to these goals, the ocean measurement is essential to the Earth system in order to quantify trends and is a keystone for the implementation of operational services. Many applications draw the plurality of sea level uses. These include climate change, tide science, CalVal activities, marine navigation and hydrography, environment monitoring, marine conservation and policies, natural resources and energy. Indeed, the SSH measurement is an estimator of the quality of sea level and complete the SSH map of the ocean. Knowing that, at large spatial scales, ocean dynamics is characterized by height anomaly variations of the order of a few tens of centimetres, with slopes of about 1 metre over a geographical extension of hundred kilometres, the SSH observations, known to the nearest centimetre, are essential to achieve water height forecasting system and are a keystone of the physical reality of the ocean for these systems (Fig. 10.18 and Sect. 10.3).

The SSH measurement as quality estimator for hindcast and forecast systems lies in taking advantage of the accuracy of this measurement and the use of sea level anomaly (SLA) analysis method to detect fluctuations like water level gradient. SLA can be computed from repetitive satellites' track data, corrected by cross-track geoid gradient, from which the average sea level is removed. The along-track SLA is useful to build co-located distinct sea level data series and to complete the knowledge of small scales of the geoid (Fig. 10.11). After what, a cross-validation of the SLA content allows mapping SSH and SLA from multimissions and diversity of SSH measures. The method requires a priori knowledge of the covariance of sea level and measurement errors.

Researches and activities using SSH have a major goal which is to compare data to other independent in situ sea levels, allowing detecting processes and parameters

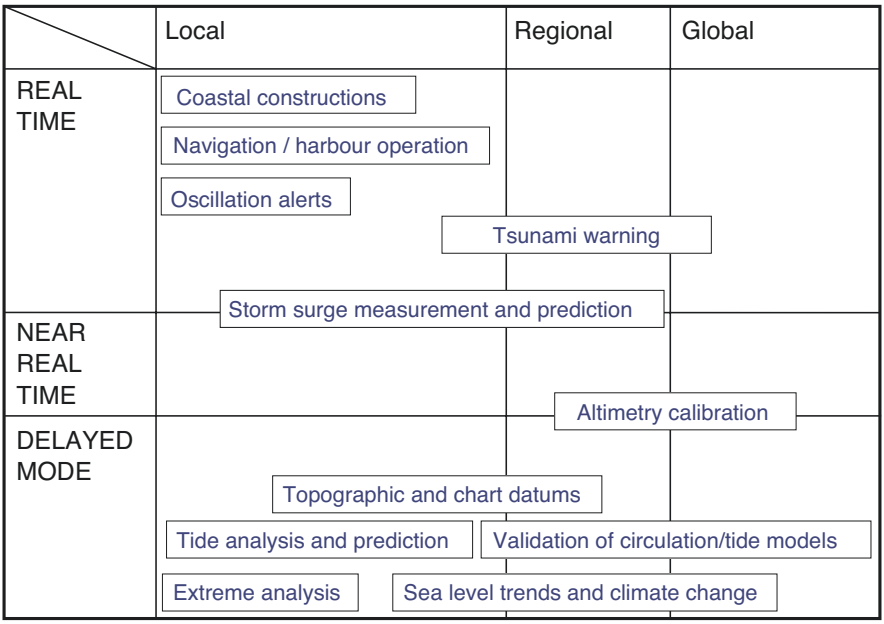

Fig. 10.18 Different applications of an ideal multipurpose station, in relation to the latency of data transmission and the spatial scale of interest [24]

that are integrated into the measurement and not directly visible. The sea level to be qualified is compared to a set of SSH measurements from independent observations that serve as a kind of tuning fork (Fig. 10.18). For altimetry, this calibration and validation topic involves distinct environments of measures, space, atmosphere and in situ sea state (Sect. 10.1). This type of analysis is routinely performed for multiple altimeter data sets (CalVal OST-ST, [3], FOAM: From Ocean to inland Altimeter Monitoring project [31, 5, 51, 38].

Once the calibration and validation processed, the SSH data give access to the knowledge of the sea level trend which is one of the most telling parameters of climate change [46]. Immediately afterwards, it is easy to conceive the consequences of the sea level evolution on the ecosystems and the coastal human infrastructures. We can consider the measure of SSH as the slow component of climate, the atmosphere being the rapid component. A large literature exists on these topics, with among them, the GIEC report providing a global interconnected understanding on ocean climate couple [36]. Recent studies estimate a sea level acceleration of +15 10^{-2} m between 1900 and 1990. Moreover, from 1993/01 to 2020/10, sea level change is estimated to +3.3 (+ − 0.3) 10^{-3} m per year (Fig. 10.19) [30].

SSH, when used in operational systems, is also a criterion for estimating the risk like marine submersion, combining in situ data, flood and tide models to provide alerts in advance [28, 32]. In this context, over an extended period of time, water level measurement must be able to demonstrate whether the overall average

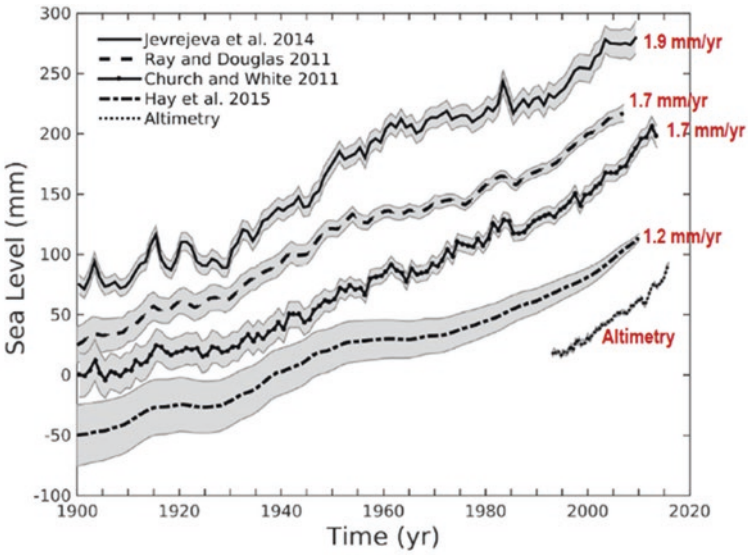

Fig. 10.19 Historical sea level rise since 1900 from tide gauge-based reconstructions (Courtesy of A. Cazenave [30])

elevation applies to a particular location. Moreover, SSH data can be assimilated into numerical ocean models designed for different targets because it provides information on ecosystems, water quality and dynamics of the ocean. The capacity encompasses the description of the current ocean state, the variability at different spatial and temporal scales, the prediction of the ocean state forecast (e.g. 10 days ahead) and the provision of consistent retrospective data records for recent years (reprocessing and reanalysis [41]. The clear and achievable objective of the operational ocean dynamics systems is the realistic representation of the ocean circulation in offshore areas and partially at coast (e.g. Copernicus Marine Environment Monitoring Service, CMEMS). The distribution of observations points gathering various observations and models can also be considered as an application supporting operations and climate studies (Fig. 10.20).

Among the physical links between SSH and ocean dynamics, the sea level reflects the variation in the ocean's heat content and its Halin content. Other essential variables like SST, subsurface variables from Argo and sea ice concentration impact SSH variation and result from it, via thermodynamics laws and principles of conservation of mass and momentum. Among it, the sea level slope variation induces dynamics and therefore a current characterizing the ocean circulation (e.g. Fig. 10.21). The numerical simulations, the reanalyses experiments, are built to be as close as possible to the observations and in agreement with the model physics (e.g. CMEMS products).

There are as many sea current structures as there are distinct physical origins of the SSH slope. A thermodynamic current derives from a circulation involving

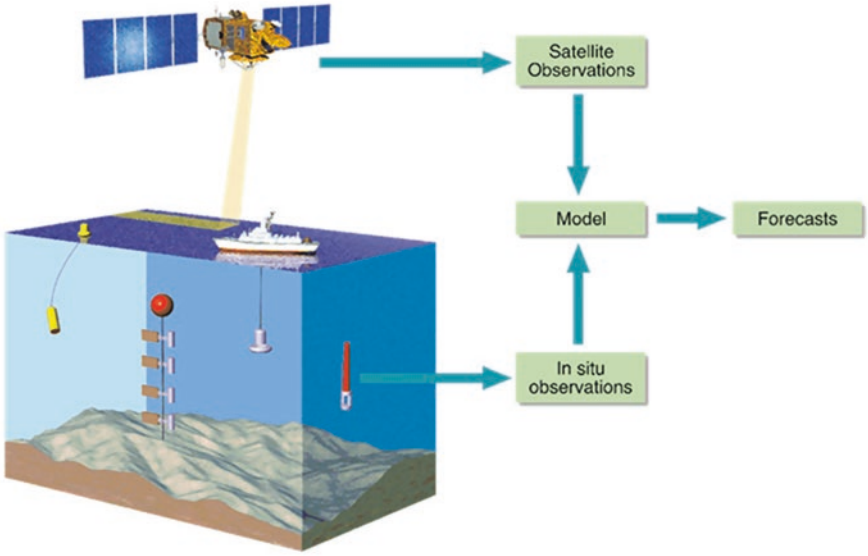

Fig. 10.20 Ocean dynamics observation (courtesy of Mercator Océan and ARGO program)

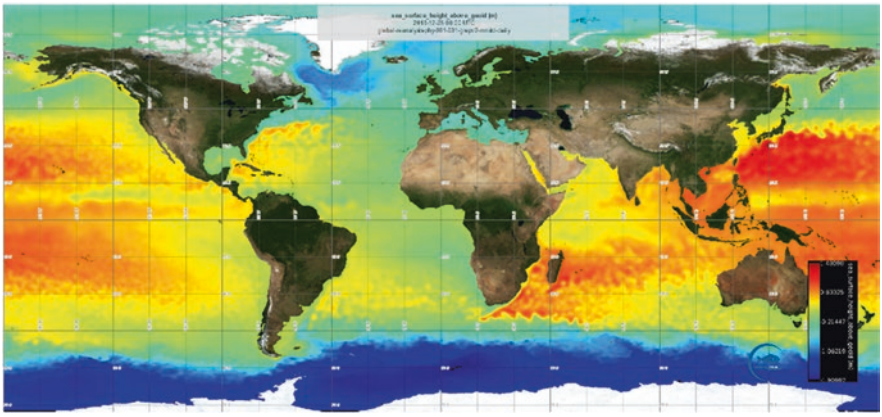

Fig. 10.21 Sea surface height above geoid (m) Copernicus Marine Service Global Ocean Ensemble Reanalysis product at ¼ degree resolution, produced with a numerical ocean model constrained with data assimilation of satellite and in situ observations (1993/01–2020/01) using GLORYS2V4 from Mercator Ocean (Fr); ORAS5 from ECMWF; GloSea5 from Met Office (UK); and C-GLORS05 from CMCC (It) [37]. Credits: Copernicus Marine Service (marine.copernicus.eu, Product Ref GLOBAL_REANALYSIS_PHY_001_03)

different contents of heat, temperature and salinity. A slope current is also a SSH slope which is constrained by the bathymetry. This SSH slope is a first-level approximation of the shape of the bathymetry. In this area of study, ocean geostrophic equilibrium implies that the ocean current velocity is proportional to the sea surface slope. Starting from the development of the primitive equations, this approximation provides the part of the ocean dynamic that is balanced between the Coriolis acceleration and the force due to the horizontal pressure gradient. The geostrophic approximation is expressed by Eqs. (10.11), (10.12), (10.13), (10.14).

$$2\Omega \sin\theta v = \frac{1}{\rho}\frac{\delta p}{\delta x} \tag{10.11}$$

$$2\Omega \sin\Theta u = -\frac{1}{\rho}\frac{\delta p}{\delta y} \tag{10.12}$$

$$V_g = u\overrightarrow{g_i} + v\overrightarrow{g_j} \tag{10.13}$$

$$V_g = \vec{k} \bullet \frac{1}{\rho f}\nabla P \tag{10.14}$$

with Ω Earth angular rotation speed in rad.s^{-1}; Θ latitude in °; P pressure in Pa; ρ volumic mass in kg.m^{-3}; u and v velocity in m.s^{-1}; V_g geostrophic velocity module in m.s^{-1}; $f = 2\Omega\sin\Theta$ Coriolis factor in s$^{-1,}$ function of latitude; and $\vec{k}$ vertical component radial dimension vector.

By Eqs. (10.11) and (10.12), we conceive that the geostrophic equilibrium is no longer verified around the equator, close to 0° of latitude. Surface current circulation, under geostrophic balance, is related to sea surface slope (i.e. pressure gradient) at Coriolis acceleration-sensitive scales, so at planetary scale. This explains how sea level gradient estimates a surface geostrophic transport, which is used to monitor ocean circulation at geographic key points. The ocean heat content impacts, in turn, the total water height by the steric contribution. For some parts of the ocean, it can contribute significantly to the annual sea level variation [43, 33].

In addition, the wind-driven velocity and ocean heat content are other important ocean variables intrinsically linked to sea level and dynamic topography above geoid. The SSH variability is also associated with ocean dynamics studies at climate scale, e.g. El Niño Southern Oscillation (ENSO) [39], upwelling dynamics and ocean eddies ([42], DYNED atlas [34, 35]). Ongoing research in ocean circulation and upper ocean processes require very frequently the SSH knowledge and a global measurements network (Sect. 10.5). Conceiving different applications with different requirements on SSH measurement is one objective of an international reference proposing indicators and prerequisites for the observed SSH data quality (GLOSS tide gauge requirements (Table 10.2) and in complement the IHO recommendations (http://ioh.int)). A temporal prerequisite of 1 or 5 min for tidal observation and 1 min, for the storm surge tracking, could complete these recommendations (Table 10.2), as well as a requirement for interferometry SSH observation (Sect. 10.3).

Table 10.2 Tide gauge requirements for different scientific applications (Src: Global Sea Level Observing System GLOSS [6])

	A. Sample interval	B. Reporting interval	C. Spatial coverage	D. Datum stability
1. Sea-level rise, decadal	1 month	1 year	Global, polar	High
2. Surface currents, heat	1 day	1 month	Global, choke points, tropics	High
3. Tidal processes	15 min	1 year	Global	Medium
4. Storm surge	15 min	1 h	Storm regions	Low
5. Tsunamis	1 min	1–15 min	Global, fault zones	Low
6. Altimeter	1 day	1 month	Global	High

10.4.3 Hydrography and Navigation

In the maritime domain, water height is a critical value that conditions many activities, from navigation to renewable marine energies. The height of water is useful for navigation route planning and navigation on the approach to ports where real-time water height measurement supersedes forecasts. Moreover, this key height is noted on nautical charts and navigation products, under values representing the minimum height under keel. It is an integral part of the systems that work for the safety of navigation, and it is one of the core missions of national hydrographic offices and international hydrographic organizations (IHO).

Water level is dealt with in many hydrographic specialties, from measurements to navigation warnings as well as maritime delimitations, nautical books and services portrayal. Among these specialties, the IHO is in the process of defining a future international standard for surface e-navigation products (the S-104 for water level and S-111 for surface ocean current product specification). In the field of water height for future e-navigation products, the interoperability between all navigation products and systems is a major challenge on the horizon of the next 3 years. In addition, if a chart carries fixed information with lowest water level guaranteed under keel value gridded on chart, the future navigation products will carry the data temporality by proposing time series of water heights that are observed, modelled and predicted. De facto, it is essential to access to the uncertainty on the water height as well as its trend, its definition, calculation method and critical values depending on the local dynamics. Even the definition of high and low tide time, which can be thought of as an easy step, has its importance in some cases such as areas where several maximum of water heights occur during the high tide. These maximums have little height differences between them and can be considered as high tide disturbances or the result from non-linear interactions between tidal harmonic components or the effect of wind at the ocean surface. This is why, before thinking about navigation services and products, hydrography sets standards and recommendations on measures essential to the maritime fact.

Among these, regular surveys provide recommendations on water height measurements, on marine geoids and on tidal harmonic analyses. It is the IHO framework in particular that abounds with rich subjects of studies at the same time

scientific and technical. All the derivatives applications are essential to maritime navigation, and this fact remains very much alive with the advent of drones and autonomous vessels. The IHO is organized in several working groups under the authority of Hydrographic Services and Standards Committee (HSSC). One IHO-working group is focusing on water level and tide with among its work programme:

- To monitor developments related to tidal, water level and current observation, analysis, prediction, vertical and horizontal data;
- To develop and maintain the relevant IHO standards, specifications and publications for which it is responsible in liaison with the relevant IHO bodies and non-IHO entities;
- To develop standards for the delivery and presentation of navigationally relevant surface current/water level information;
- To provide technical advice and coordination on matters related to tides, water levels, currents and vertical data.

10.5 Sea Level Networks

Until the beginning of the nineteenth century, the notion of a sea level observatory network did not exist. The only tide observations were attributable to few people who were concerned by the understanding of this phenomenon. Water level was directly measured by reading the value on a graduated tidal staff. Observers had to be permanently at the seaside to be able to read the sea level on the staff, and it was also challenging to get a precise time to be associated with each sea level measurement. Whewell was the first to propose a large-scale measurement campaign to the countries bordering the Atlantic Ocean [57]. These water level observations were conducted simultaneously on both sides of the ocean in order to be able to carry out the first global study of the tide propagation. Thus, during June 1835, 666 tide staffs were deployed.[5] The first global network had just been created, at least temporarily. This network required extensive human resources to continuously measure water levels at such large geographic cover. During the second half of the nineteenth century, tide gauge network started to become widespread at national scales, thanks to the invention of mechanical tide gauges by Palmer in 1831. The use of this instrument allowed performing continuous measurements.

The first international service concerned with mean sea levels has appeared in 1933: Permanent Service for Mean Sea Level (PSMSL, National Oceanography Centre (NOC)).[6] This service has been responsible for the collection, publication, analysis and interpretation of sea level data from the global network of tide gauges.

[5] 1835: a first demonstration of a tide gauges network, deployed on the coasts of the USA, Spain, Portugal, Belgium, the Netherlands, Denmark, Norway, England, Scotland, Ireland and France.

[6] https://www.psmsl.org/; https://www.gloss-sealevel.org/; http://www.ioc-sealevelmonitoring.org/; http://uhslc.soest.hawaii.edu/; https://www.bodc.ac.uk/; https://www.sonel.org

Since 1985, the tide gauges networks are worldwide coordinated through the Global Sea Level Observing System (GLOSS), which is an international sea level monitoring programme designed to produce high-quality in situ sea level observations to support a broad research and operational user base. GLOSS was established by the UNESCO Intergovernmental Oceanographic Commission (IOC-GLOSS provides oversight and coordination sea level networks and relies on feedback and direction from local tide gauge operators to maintain the creation of high-quality sea level observations). The backbone of the global tide gauge network is the GLOSS Core Network, a global set of 290 tide gauge stations that provide optimal sampling of the global ocean for a range of oceanographic applications.

GLOSS Core Network gauges are allocated to each island or group of islands at intervals not closer than 500 km and along continental coasts at intervals generally not less than 1000 km. Preference has been given to islands in order to maximize exposure to the open ocean. GLOSS is a global endeavour requiring the coordinated participation of an international group of agencies. It provides sea level data through five data centres depending on the type of data:

- Real-time data delivery (The Flanders Marine Institute, VLIZ) provides a Web-based global sea level station monitoring service for viewing sea level data received in real time from different network operators (e.g. information about operational status of GLOSS stations through quick inspection of the raw data stream [11].
- Fast mode data delivery (UHSLC, GLOSS sources) distributing a sea level data after a preliminary quality control by Member Nations. Data are delivered at 1–2 months delay after measurements.
- Delayed mode (GLOSS) providing data post-quality control. The Delayed Mode Centre handles hourly (or subhourly) sea level measurements, together with ancillary variables (e.g. atmospheric pressure) where these are available, from the GLOSS sites.
- Mean sea level data delivery (PSMSL) provides publication, analysis and interpretation of sea level data from the global network of tide gauges, including the GLOSS Core Network. Monthly and annual sea level means are provided on a common international datum allowance.
- Coordinates and land motion (SONEL) is the dedicated centre for Global Navigation Satellite System (GNSS) data at tide gauge stations. It provides GNSS data.

These sea level data are used for a wide variety of scientific, economic, social and political purposes (climate/oceanography studies, coastal management, tsunami and flood warning, e.g. SSH applications provided in Copernicus Marine Environment Monitoring Service (Sect. 10.4.2)).

10.6 Data Archaeology: Long-Term Time Series

For centuries, the sea level has been widely observed in order to address specific needs. A large number of studies focused on tide mainly motivated by the understanding of the tidal phenomenon in order to be able to predict it and to ensure the navigational safety. Then, these measurements have satisfied multiple needs and have been used by a wide variety of users and on different time scales. Sea level data are crucial to provide relevant information regarding sea level trend and tide (Abstract of this chapter).

Over historical times, observation of sea level has considerably been improved, thanks to continuous technical progress and because of the variety. An example of this historical evolution will be illustrated through the French experience where sea level observations were already made at the end of the seventeenth century. Within a major project aiming at updating the map of France, the astronomers de La Hire and Picard carried out the first systematic sea level measurements at Brest and Nantes in order precisely determine the limits of the kingdom [54]. Encouraged by the Royal Academy of Sciences, the measurements became widespread in the eighteenth century. Measurements of water level were still made by a direct reading on a graduated tide staff (Sect. 10.2). Until the middle of the nineteenth century, measurements of sea level were commissioned by astronomers in order to understand the laws of universal attraction, enunciated by Isaac Newton (1687) and to develop a method for predicting the tide. Under the impetus of the creation of a tide service at the end of the 1830s, the Dépôt des cartes et plans de la Marine, the forerunner of Shom, industrialized water height measurements by deploying the first tide gauge network on the French coasts and later to extra-marine territories. The objectives of this network were to meet hydrographic needs (datum definition) and to rely on sea level measurements in order to calculate the tidal prediction published in tide directories. The installation of float tide gauges was a major technological upgrading in water level measurements by process automation. In the twentieth century, after some decades during which the interest in sea level observations experienced declined, a growing interest emerged since the end of the 1980s due to new societal challenges, indeed such as meteo-ocean and climatic studies [53].

Measurements also contribute to the marine risk management for multirisk warning networks. For these reasons, tide gauge networks are being modernized with the replacement of float tide gauges by digital sensors (Sect. 10.1) enabling water level measurements to be accessed, transmitted and disseminated as quickly as possible and directly usable with the help of computer tools. If water level observations have been made for centuries, the corresponding data are not necessarily available. Regularly, an important effort has to be undertaken to recover these data. Individual projects (single station efforts) and some concerted national campaigns have been carried out to rescue sea level data [55, 48, 56, 50]. This is time demanding work, including research, scanning, digitizing and quality control of analogue tide gauge charts. Long-term time series of sea level are essential and rare. These data sets contribute to improve our knowledge in the research into sea level change and ocean

Fig. 10.22 Evolution of the average sea level in Brest (France) since 1711 (N. Pouvreau; Credits Shom-SONEL)

circulation or help at understanding changes in tidal properties due to non-astronomical factors [51]. Brest (France) is an example of outcome from data archaeology work. Sea level since 1711 shows an increase in the average sea level of between 30 and 35 cm. This evolution does not appear to be linear with significant interannual fluctuations (Fig. 10.22). The sea level data archaeology is encouraged by the GLOSS programme of the Intergovernmental Oceanographic Commission of UNESCO [49], meeting Paris 2020 [49].

Acknowledgments Acknowledgments to R. Morrow (Legos) for SWOT mission description, M. Drevillon (Mercator Océan) for introducing Copernicus Marine Environment Monitoring Service (CMEMS).

References

1. Ayoub N, Barbot S, Benoit L, Bonnefond P, Brachet C, Calzas M, Conessa C, Drezen C, Fichen L, Froideval L, Garcia J, Giry C, Guillot A, Jan G, Lyard F, Magot L, Ternon P, Valladeau G (2018) Gironde campaign. CalVal OST-ST meeting, 2019
2. Bonnefond P, Exertier P, Laurain O, Jan G (2010) Absolute calibration of Jason-1 and Jason-2 altimeters in corsica during the formation flight phase. Mar Geod 33(S1):80–90
3. Bonnefond P, Haines B, Watson C (2011) situ calibration and validation: a link from coastal to open-ocean altimetry. In: Vignudelli S, Kostianoy A, Cipollini P, Benveniste J (eds) Coastal altimetry. Springer, Berlin
4. Chupin C, Ballu V, Testut L, Tranchant Y-T, Calzas M et al (2020) Map-ping Sea surface height using new concepts of kinematic GNSS instruments. Rem Sens 12(16):2656. https://doi.org/10.3390/rs12162656.hal-02941779
5. Jan G, Menard Y, Faillot M, Lyard F, Jeansou E, Bonnefond P (2004) Offshore absolute calibration of space borne radar altimeters. Mar Geod 27(3–4):615–629
6. IOC The Global Sea-Level Observing System (GLOSS): implementation plan Merrifield M., Holgate S., Mitchum, G., Pérez B. Begoña, Rickards L., Schöne T., Woodworth P.L., Wöppelmann, G., 2012; IOC, Paris
7. Martin MB, Testut L, Wöppelman G (2012) Performance of modern tide gauges: towards mm-level accuracy. In: Advances in Spanish physical oceanography. Scientia Marina, Consejo Superior de Investigaciones Científicas, Barcelona, pp 221–228. https://doi.org/10.3989/scimar.03618.18A

8. OC, SCOR and IAPSO (2010) The international thermodynamic equation of seawater – 2010: Calculation and use of thermodynamic properties'. In: Intergovernmental oceanographic commission, manuals and guides no. 56. UNESCO, Paris, p 196
9. Vanicek P, Featherstone WE (1998) Performance of three types of stokes's kernel in the combined solution for the geoid. J Geodyn 72(12):684–697. https://doi.org/10.1007/s001900050209
10. Andersen OB, Knudsen P, Kenyon S, Holmes S, Factor JK (2019) Evaluation of the global Altimetric marine gravity field DTU15: using marine gravity and GOCE satellite gravity. In: International association of geodesy symposia. Springer, Berlin. https://doi.org/10.1007/1345_2018_52
11. Bidel Y, Zahzam N, Blanchard C, Bonnin A, Cadoret M, Bresson A, Rouxel D, Lequentrec-Lalancette M-F (2018) Absolute marine gravimetry with matter-wave interferometry. Nat Commun 9:627
12. Barzaghi (2018) The Geomed2 project: estimating the geoid and the DOT in the Mediterranean area. Geophys Res Abs 20:13841. https://doi.org/10.1007/1345_2018_33
13. Featherstone WE, Evans JD, Olliver JG (1998) A Meissl-modified Vanicek and Kleusberg kernel to reduce the truncation error in gravimetric geoid computations. J Geodesy 72(3):145–160
14. Lequentrec-Lalancette M-F, Salaun C, Bonvalot S, Rouxel R, Bruinsma S (2016) Exploitation of marine gravity. Measurements of the Mediterranean in the validation of global gravity field model. In: International association of geodesy symposia. Springer, Berlin Heidelberg, pp 1–5. https://doi.org/10.1007/1345_2016_258
15. Moritz H (1980) Advanced physical geodesy. H. Wichmann Verlag, Karlsruhe, p 500
16. Sandwell DT, Smith WHF (2009) Global marine gravity from retracked Geosat and ERS-1 altimetry: ridge segmentation versus spreading rate. J Geophys Res 114:81. https://doi.org/10.1029/2008JB006008
17. Sandwell DT, Harper H, Tozer B, Smith WHF (2019) Gravity field recovery from geodetic altimeter missions. Adv Space Res 68:1059. https://doi.org/10.1016/J.asr.2019.09.011
18. Zhang SJ, Sandwell DT (2017) Retracking of SARAL/AltiKa radar altimetry waveforms for optimal gravity field recovery. Mar Geod 40:40–56. https://doi.org/10.1080/01490419.2016.1265032
19. Ablain M, Cazenave A, Larnicol G (2015) Improved sea level record over the satellite altimetry era (1993–2010) from the climate change initiative project. Ocean Sci 11(1):67–82. https://doi.org/10.5194/os-11-67-2015
20. Jan G Au fil de l'eau: mesure de la hauteur de mer; Edito 2017 décembre, ©Copyright Afnor Bivi Metrology
21. Escudier P, Couhert A, Mercier F et al (2018) In: Stammer DL, Cazenave A (eds) Satellite radar altimetry: principle, accuracy and precision, in 'Satellite altimetry over oceans and land surfaces. CRC Press, Taylor and Francis Group, Boca Raton, New York, London, p 617
22. IOC (2020) Quality control of in situ sea level observations: a review and progress towards automated quality control, volume 1; 2020/MG/83Vol.1; https://unesdoc.unesco.org/ark:/48223/pf0000373566
23. Morrow R, Fu L-L, Ardhuin F, Benkiran M, Chapron B, Cosme E, d'Ovidio F, Farrar JT, Gille ST, Lapeyre G, Le Traon P-Y, Pascual A, Ponte A, Qiu B, Rascle N, Ubelmann C, Wang J, Zaron ED (2019) Global observations of fine-Scale Ocean surface topography with the surface water and ocean topography (SWOT) Mission. Front Mar Sci 6:5. https://doi.org/10.3389/fmars.2019.00232
24. Pérez B, Fanjul EÁ, Pérez S, de Alfonso M, Vela J (2013) Use of tide gauge data in operational oceanography and sea level hazard warning systems. J Operation Oceanogr 6:1–18. https://doi.org/10.1080/1755876X.2013.11020147
25. Santamaría-Gómez A, Gravelle M, Dangendorf S, Marcos M, Spada G, Wöppelmann G (2017) Uncertainty of the 20th century sea-level rise due to vertical land motion errors. Earth Planet Sci Lett 473:24–32

26. Zawadzki L, Ablain M et al (2016) Error characterization report: altimetry measurements errors at climate scales. CLS-DOS-NT-13-100
27. Altamimi Z, Collilieux X, Legrand J, Garayt B, Boucher C (2007) ITRF2005: a new release of the Inter; national terrestrial reference frame based on time series of station positions and Earth orientation parameters. J Geophys Res: Solid Earth 112:1–19
28. Bertin X, Li K, Roland et Bidlot JR (2015) The contribution of short waves in storm surges: two recent examples in the central part of the Bay of Biscay. Cont Shelf Res 96:1–15
29. Bouin M-N, Ballu V, Calmant S, Boré J-M, Folcher E, Ammann J (2009) A kinematic GPS methodology for sea surface mapping, Vanuatu. J Geodyn 83(12):1203–1217. https://doi.org/10.1007/S00190-009-0338-x
30. Cazenave A (2018) LEGOS-CNES, Toulouse & ISSI. Earth Observation Summer School, ESA, Bern
31. Cazenave A, Nerem RS (2004) Present-day sea level change: observations and causes. Rev Geophys 42:RG3001
32. Chaumillon E, Bertin X, Fortunato A, Bajo M, Schneider J-L, Dezileau L, Walsh J-P, Michelot A, Chauveau E, Créach A, Hénaff A, Sauzeau T, Waeles B, Gervais B, Jan G, Baumann J, Breilh J-F, Pedreros R (2016) Storm-induced marine flooding: lessons from a multidisciplinary approach. Earth Sci Rev 165:151. https://doi.org/10.1016/j.earscirev.2016.12.005
33. Cotroneo Y et al (2016) Glider and satellite high resolution monitoring of a mesoscale eddy in the Algerian basin: effects on the mixed layer depth and biochemistry. J Mar Syst 162:73–88
34. DYNED-Atlas is a unique database of surface intensified eddies for a 18 year period (2000–2018) in two specific areas: the Mediterranean Sea and the Arabian Sea. Six partners: 3 research laboratories (LMD, LPO and LEGOS), a company (CLS), an SME (ECTIA) and the Shom. Support: ANR- Astrid, Cnes, Shom)
35. Garreau P, Dumas F, Louazel S, Stegner A, Le Vu B (2018) High-resolution observations and tracking of a dual-core anticyclonic eddy in the Algerian Basin. J Geophys Res Oceans 2018:123. https://doi.org/10.1029/2017JC013667
36. GIEC; IPCC (2019) In: Pörtner H-O, Roberts DC, Masson-Delmotte V, Zhai P, Tignor M, Poloczanska E, Mintenbeck K, Alegría A, Nicolai M, Okem A, Petzold J, Rama B, Weyer NM (eds) IPCC special report on the ocean and cryosphere in a changing climate. IPCC, Geneva
37. Storto A, Masina S, Simoncelli S, Iovino D, Cipollone A, Drévillon M, Drillet Y, von Schuckman K, Parent L, Garric G, Greiner E, Desportes C, Zuo H, Balmaseda MA, Peterson KA (2019) The added value of the multi-system spread information for ocean heat content and steric sea level investigations in the CMEMS GREP ensemble reanalysis product. Climate Dynam 53:287. https://doi.org/10.1007/s00382-018-4585-5
38. Leuliette EW, Nerem R, Mitchum G (2004) Calibration of TOPEX/poseidon and Jason altimeter data to construct a continuous record of mean sea level change. Mar Geod 27:79–94
39. Lin J, Qian T (2019) A new picture of the global impacts of El Nino-southern oscillation. Sci Rep 9:17543. https://doi.org/10.1038/s41598-019-54090-5
40. Lyard F et al FES2014 global ocean tides atlas: design and performances. Ocean science special issue: developments in the science and history of tides (OS/ACP/HGSS/NPG/SE interjournal SI), MS Nos-2020-96
41. Le Traon P-Y, Reppucci A, Alvarez Fanjul E et al (2019) From observation to information and users: the Copernicus marine service perspective. Front Mar Sci 6:234. https://doi.org/10.3389/fmars.2019.00234
42. Mason E, Pascual A, McWilliams JC (2014) A new sea surface height–based code for oceanic mesoscale Eddy tracking. J Atmos Oceanic Tech 31(5):1181–1188. https://doi.org/10.1175/JTECH-D-14-00019.1
43. Picco P, Vignudelli S, Repetti L (2020) A comparison between coastal altimetry data and tidal gauge measurements in the Gulf of Genoa (NW Mediterranean Sea). J Mar Sci Eng 8:862
44. Ray RD (2013) Precise comparisons of bottom-pressure and altimetric ocean tides. J Geophys Res Oceans 118:4570–4584. https://doi.org/10.1002/jgrc.20336

45. Simon B (2007) Coastal tide, Institut océanographique, Fondation Albert I prince de Monaco, Janvier. (cooperation with Shom and IHO)
46. Wöppelmann G, Martin-miguez B, Bouin M, Altamimi Z (2007) Geocentric Sea-level trend estimates from GPS analyses at relevant tide gauges world-wide. Global Planet Change 57:396–406
47. Zawadzki L, Ablain M, Carrere L, Ray RD, Zelensky NP, Lyard F, Picot N (2016) Reduction of the 59 -day error sign al in the Mean Sea Level derived from TOPEX/Poseidon, Jason-1 and Jason-2 data with the latest FES and GOT ocean tide models. Ocean Sci Discuss 2016:5. https://doi.org/10.5194/os-2016-19
48. Araújo IB, Bos MS, Bastos LC, Cardoso MM (2013) Analysing the 100 year sea level record of Leixões. Portugal J Hydrol 481:76–84. https://doi.org/10.1016/j.jhydrol.2012.12.019
49. Bradshaw E, Woodworth PL, Hibbert A, Bradley LJ, Pugh DT, Fane C, Bingley RM (2016) A century of sea level measurements at Newlyn. Southwest England Marine Geodesy 39:115–140. https://doi.org/10.1080/01490419.2015.1121175
50. Goutx D, Baraer F, Roche A, Jan G (2014) Ces tempêtes extrêmes que l'histoire ne nous a pas encore dévoilées. La Houille Blanche 2:27–33. https://doi.org/10.1051/lhb/2014013
51. Haigh ID, Pickering MD, Green JAM, Arbic BK, Arns A, Dangendorf S, Hill D, Horsburgh K, Howard T, Idier D, Jay DA, Jänicke L, Lee SB, Müller M, Schindelegger M, Talke SA, Wilmes S-B, Woodworth PL (2020) The tides they are a-changin': a comprehensive review of past and future non-astronomical changes in tides, their driving mechanisms and future implications. Rev Geophys 58:1. https://doi.org/10.1029/2018RG000636
52. Intergovernmental Oceanographic Commission of UNESCO (2020) In: IOC-UNESCO workshop on sea level data archaeology, Paris, 10–12 March 2020. Paris, p. 48
53. Latapy A (2020) Influence des modifications morphologiques de l'avant-côte sur l'hydrodynamisme et l'évolution du littoral des Hauts-de-France depuis le XIXe siècle (Thèse de doctorat). Littoral
54. Picard J, de La Hire P (1729) Observations faites à Brest et à Nantes pendant l'année 1679. Mémoire de l'Académie Royale des Sciences, rédigé entre 1666 et 1698 7:379–390
55. Pouvreau N (2008) Trois cents ans de mesures marégraphiques en France: outils, méthodes et tendances des composantes du niveau de la mer au port de Brest, PhD thesis, Université de La Rochelle
56. Wahl T, Haigh ID, Woodworth PL, Albrecht F, Dillingh D, Jensen J, Nicholls RJ, Weisse R, Wöppelmann G (2013) Observed mean sea level changes around the North Sea coastline from 1800 to present. Earth Sci Rev 124:51–67
57. Whewell W (1836) Tide observations made on the coasts of Europe and America in june 1835. Philos Trans R Soc Lond A 126:289–341

Chapter 11
Measurements in Marine Geology: An Example in the Gulf of Taranto (Northern Ionian Sea)

Maria Rosaria Senatore, Agostino Meo, and Francesca Budillon

Contents

Abstract This chapter reports a synthesis of the presentations at the past International Workshops on Metrology for the Sea that points out some applications of measurements in marine geomorphology, stratigraphy and sedimentology on sediment samples. The research has been carried out on the continental margin of the Puglia region in the Gulf of Taranto (Ionian Sea). In this area, multibeam echosounders data and Chirp seismic profiles have been acquired, offshore of the Taranto harbour to investigate the impressive Taranto Landslide, which has an estimated volume of about 0.30 km^3. Based on morphometric measurements and empirical calculations, the kinematics and the tsunamigenic potential of the landslide were evaluated. The outcomes of these analysis revealed that the sediment mass displacement was almost fast, with an inferred peak velocity exceeding 42 m/s, and possibly generated a wave up to 2–3 m high.

The stratigraphic and sedimentological analyses were performed in an adjacent area to the landslide, on a 150 cm long section of marine sediments, retrieved by a

M. R. Senatore (✉) · A. Meo
DST, University of Sannio, Benevento, Italy
e-mail: senatore@unisannio.it

F. Budillon
ISMAR, CNR, Naples, Italy
e-mail: francesca.budillon@cnr.it

P. Daponte et al. (eds.), *Measurement for the Sea*, Springer Series in Measurement Science and Technology,
https://doi.org/10.1007/978-3-030-82024-4_11

gravity corer at 268 m of depth. The measurements regarded the sediment particles grain size, carbonate content, biogenic and terrigenous content and the Fe/Ti, K/Ti, Ca/Ti ratios by X-ray fluorescence analysis. The multivariate analysis has allowed the recognition of a local morphoclimatic signal recorded in the stratigraphic succession that spans back the last thousand years.

11.1 Introduction

Since 2017, with the beginning of the International Workshops on Metrology for the Sea, efforts have been made to emphasize the importance of measures in marine geology and several special sessions have been organized on this issue since then. In this chapter the authors make a synthesis of their presentations at the last Imeko workshop that points out some application of measurements in marine geomorphology, stratigraphy and sedimentology, with outcomes that may contribute to the geohazard evaluation of the Ionian Sea and to the definition of the late Holocene morphoclimatic variability in the region. The researches were carried out on the continental margin of the Puglia region, facing the Gulf of Taranto (Southern Italy, Ionian Sea) (Fig. 11.1), a foredeep basin of the Apennine chain and Calabrian Arc since Plio-Pleistocene [1–3].

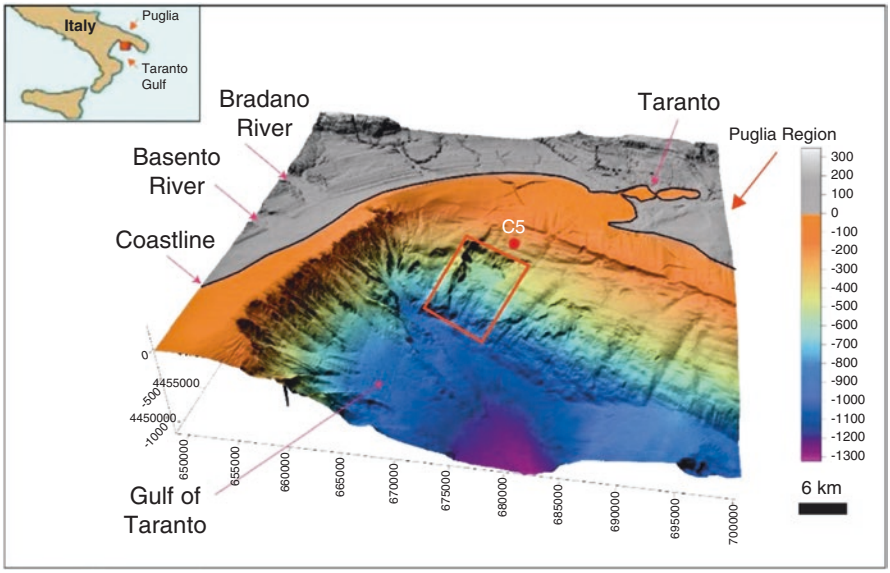

Fig. 11.1 Digital Elevation Model (DEM) of the Gulf of Taranto (northern Ionian Sea) and location of the Taranto Landslide (red box) and core C5 (red dot) along the Puglia continental slope. Modified from Falco et al. [4]

11.2 Geomorphology

The geomorphological analyses were performed mainly using bathymetric data from multibeam echo sounder, acquired by a *Reson Seabat 8160* (60 kHz) and focused on a wide landslide occurring on the continental slope. Although the landslide failed some thousand years ago [5–7], a hypothetical reactivation might be potentially dangerous for the coastal strip. The dataset was based on a total of 670 nautical miles and adjacent routes overlapping by 10–20% of the swath; the software used for the data acquisition was the *PDS2000*. The processing of data, performed with the *Caris Hips & Sips*® software, had led to the production of a high resolution Digital Elevation Model (DEM) with cell dimensions of 20 m × 20 m.

11.2.1 The Taranto Landslide

The Taranto Landslide develops along the Apulian continental slope bounding the Taranto Canyon, where the gravitational instabilities are very common; the DEM shows that it sets up on a former mass-transport deposit zone (Figs. 11.1 and 11.2).

The Taranto Landslide is located about 12 km far from the coastline and develops between 380 and 1000 m depths. The landslide has well-distinct morphological features and consists of a headwall laterally passing into two sub-parallel sidewalls, an evacuation zone and an accumulation zone, almost lobe-shaped (Fig. 11.2). The headwall is identified by an abrupt change in slope at a depth of about 380 m

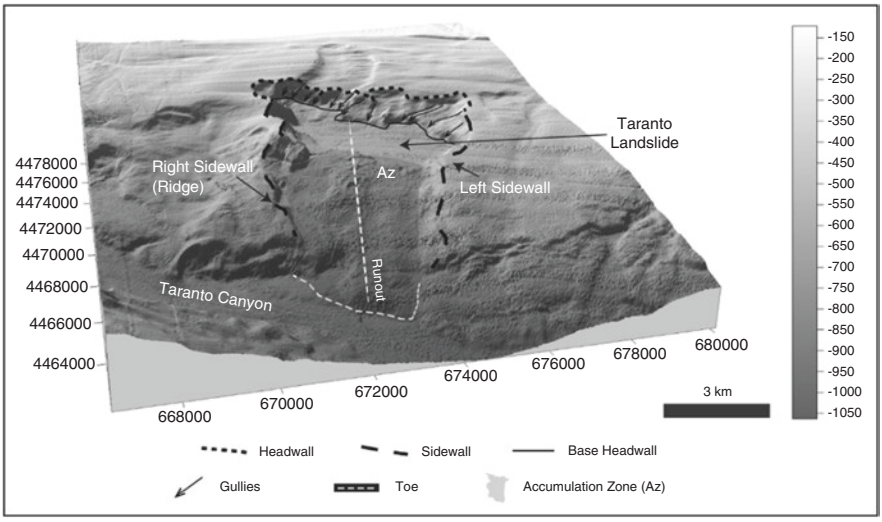

Fig. 11.2 3D view showing the morphological features of the Taranto Landslide. Modified from Meo et al. [9]

extending about 7 km in the NW-SE direction. The average gradient of the exposed scarp is about 20°, but locally exceeds 32°. The exposed scarp is furrowed by gullies, which extend perpendicularly to the headwall, for about 600 m.

The scar is laterally bounded by two sub-parallel scarps almost 70 m high. The left sidewall shows a good spatial continuity, whereas the right one is carved by minor landslide scars that give raised to detached tilted blocks, forming an intra-scar ridge.

The evacuation zone develops from the headwall, down to 470 m deep.

The accumulation zone (A_z) of the Taranto Landslide develops from 570 m to 1000 m deep, over an area of 26 km^2 (7.5 km long × 3.5 km wide) and presents a rough morphology (Fig. 11.2).

The volume involved in the failure, about 0.29 km^3, was calculated by using the empirical equation developed by McAdoo et al. [8], which considers the wedge-shaped thickness of the displaced sediments and the wideness of the evacuation area:

$$V_{\text{slide}} = \frac{1}{2}(As)(h\cos\alpha) \tag{11.1}$$

where As is the area of the scar, h and α are, respectively, the height and the angle of the slope.

The observed runout for the Taranto Landslide is about 10,000 m, however, this is an underestimated value, because the Taranto Canyon might have eroded and transported a part of the sediments involved in the slide movement.

On the basis of the available data and empirical relationships, the kinematics of this massive landslide has been calculated, according to Meo et al. [9]. The kinematics of a landslide is defined by the position (differential depth), velocity and thickness of the material as it moves downslope [10]. The parameters to define the kinematic are duration (T_c); mean velocity (V); peak of velocity (V_{peak}):

$$T_c = \left[\frac{8L_c}{g\sin\beta}\right]^{1/2} \tag{11.2}$$

$$V = \left[\frac{L_c g\sin\beta}{8}\right]^{1/2} \tag{11.3}$$

$$V_{\text{peak}} = \left[\frac{8\sqrt{3}}{9}\right]V \tag{11.4}$$

where L_c is the length of the runout, β is the initial slope angle and g represents the acceleration of gravity. In the Taranto Landslide L_c is 10,000 m and β is 3.8°. By using these empirical formulas, it turns out that the failure process duration was 6.13 min and the mean velocity reached 27.37 m/s, with a peak of 42.12 m/s. Furthermore, a mathematical model has been determined, calculating the

acceleration (*At*), velocity (*Vt*) and distance (*Dt*) of the slide front versus time (Fig. 11.3). It must be considered that these values are largely conservative and

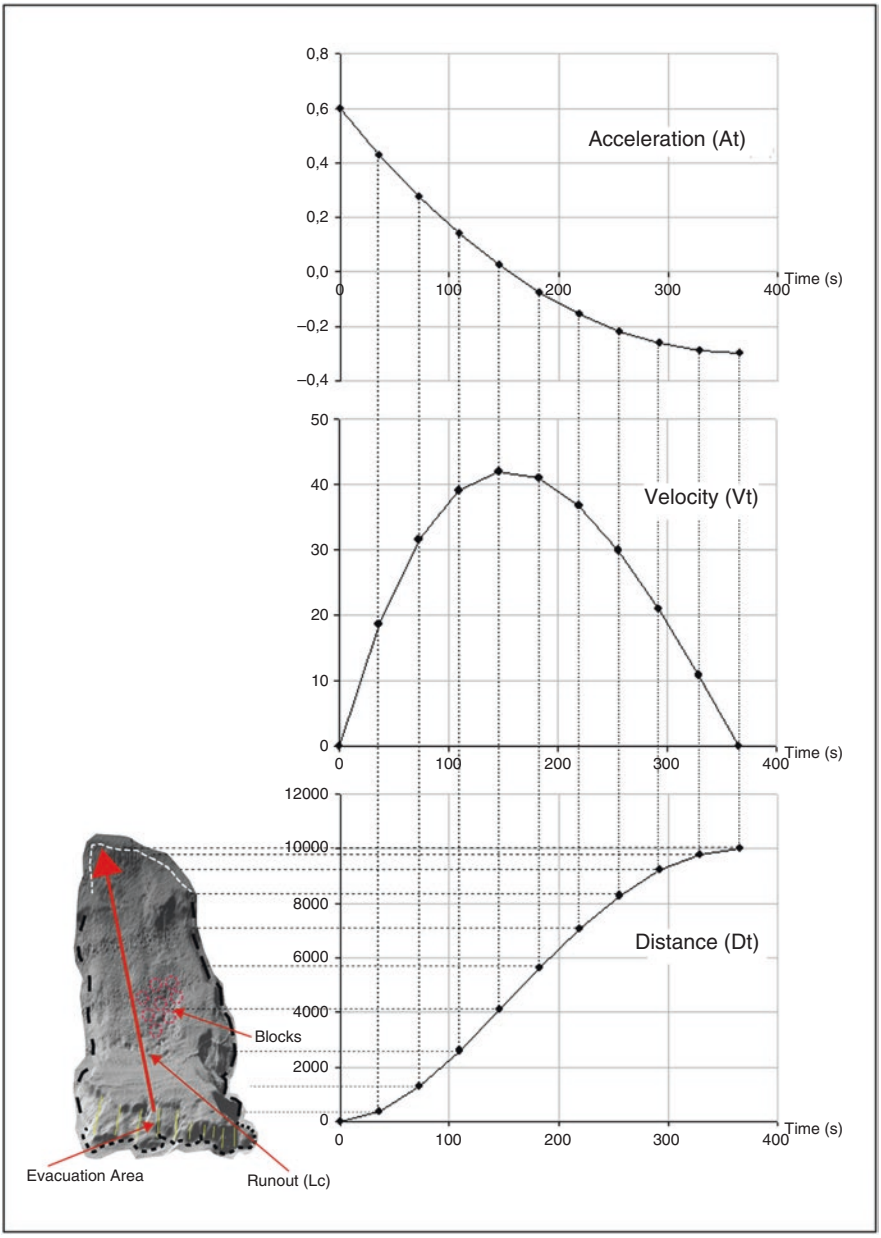

Fig. 11.3 Diagram describing the numerical empirical model of the acceleration (*At*), velocity (*Vt*) and distance (*Dt*) of the slide versus time [11]. Modified from Meo et al. [9]

could be underestimated, as the real runout L_c might be greater than the one considered.

According to Varnes [11], this slide was extremely rapid and the sediment accumulation underwent a rapid emplacement. The diagram in Fig. 11.3 shows the trend of velocity, acceleration and distance travelled by the displaced mass as a function of time, from the evacuation area towards the landslide foot. By analysing the diagram, it can be observed that the peak velocity is reached after about 2.5 min starting from the landslide trigger in the evacuation area. From that moment, the moving mass begun to decelerate and the velocity to decrease. The projection of the flex in the velocity curve on the distance curve corresponds to a distance of about 6 km far from the headwall. Actually, the DEM of the landslide shows within the scar, at about 6 km from the headwall, an area characterized by the presence of blocks up to 35 m high, involved in the landslide (Fig. 11.3). Downwards, the sediment mass debris are gradually smaller down to the foot of the landslide. This distribution of the deposits, as emerged from the morphological analysis of the DEM, allows the schematization of a sedimentological model (Fig. 11.4), which can be considered a validation of the landslide kinematics (Fig. 11.3).

A main issue regarding the submarine landslides and their possible mobilization or remobilization is the assessment of their tsunamigenic potential. Understanding and evaluating whether and how a mass failure may form a tsunami is not an easy task, considering also that the analytical and quantitative study of a submarine landslide is a very complex assessment and a huge literature has been produced so far. Nowadays, there is a general agreement, that by using the morphometric parameters of the landslide, it is possible to infer approximately the tsunamigenic potential associated with landslide events in the marine environment by relatively simple assumptions [9, 12, 13].

The evaluation of the tsunamigenic potential requires to estimate the possible run-up of the wave, through the definition of the maximum amplitude of a tsunami wave generated by a submarine landslide [12]. It has to be stressed that this evaluation is a remarkable simplification compared to what really happens in the process of a tsunami formation; in fact, it is evident that a wave can have significant modifications during its propagation, especially when it approximates to the coastline. Therefore, it is considered more correct to estimate the relative measure of the potential tsunamigenic as related to events of instability [14]. The wave amplitude has been calculated by using some empirical relationships, derived from simulations for fluid dynamics made in a laboratory and mathematical models [12, 15, 16]. The assumptions behind such a modelling are (1) the geometry of the landslide is assimilated to a semi-ellipse sliding on an inclined plane; (2) the centre of mass of the landslide body is identified through an analytical solution of the equation of motion; (3) deformation inside the landslide body was not considered because it seems to have a limited influence on the magnitude of the tsunami [12]. The estimation of the wave amplitude was made considering a model of translational slide affected by the resistance exerted by the fluid above it during sliding [15, 16].

The following relations are used in the calculation (characterized by uncertainty on the intrinsic estimation of ±2.1%, [17, 18]):

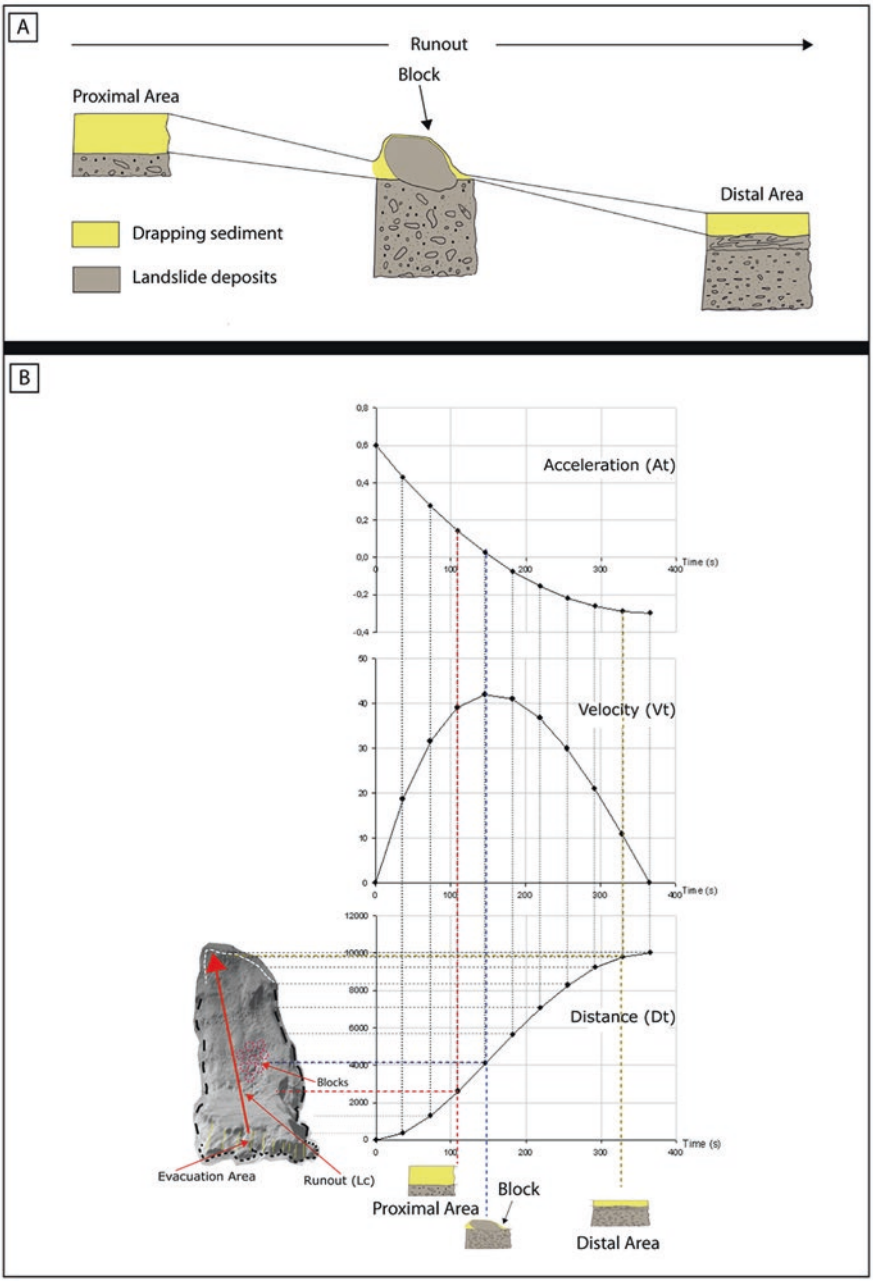

Fig. 11.4 Sedimentological model of Taranto Landslide deposits [not to scale]; (**a**) the thickness of the sediments increases in the central part of the accumulation zone, which corresponds to the point where the velocity peak is achieved by the moving mass and where the larger blocks are observed; (**b**) shows the correlation between the sedimentological and the kinematic models

$$\Lambda = 3.87\left(bd / \sin\theta\right) \tag{11.5}$$

$$H = 0.224T\left[\frac{w}{w+\lambda}\right]\left[\left(\sin\theta\right)^{1.29} - 0.746\left(\sin\theta\right)^{2.29} + 0.170\left(\sin\theta\right)^{3.29}\right]\left(\frac{b}{d}\right)^{1.25} \tag{11.6}$$

where λ is the wave length, H is the height of the wave, b-d-θ depend on the morphology of the submerged slope, respectively, the length, the water depth in the median part and the average slope of the landslide, and w represents the width of the headwall. The depth at the central part of the landslide (d) was obtained through the analysis of several bathymetric sections, which allowed the reconstruction of the original seafloor surface, while the thickness of the landslide (T) was obtained by multiplying the height of the headwall (h) by the cosine of the slope angle of the landslide ($\cos\alpha$), thus representing a hypothetical estimate [8]. The values obtained for the Taranto Landslide indicate a potential wave height of about 2.89 m. This value, however, is a hypothetical estimate, assuming that the landslide body can reactivate all at once. Besides, the value of the run out could be underestimated, because the sediment involved in the mass movement might have been eroded by the bottom currents flowing in the Taranto Canyon.

In the study area, during two oceanographic cruises (CONISMA 11/10 and SAND_16), Chirp profiles were acquired in the landslide body, one dip-oriented (Figs. 11.5 and 11.6) and several strike-oriented.

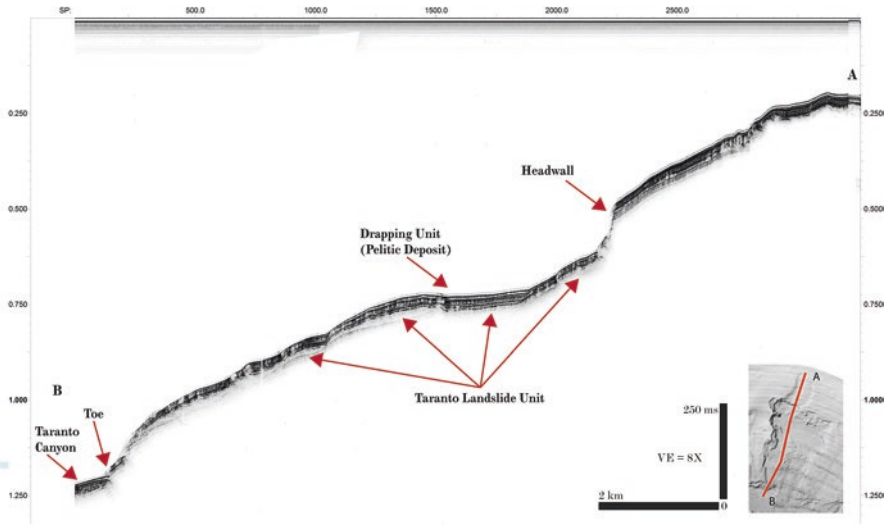

Fig. 11.5 The Chirp profile along the Taranto Landslide shows the mass-transport deposits (Taranto Landslide Unit) seaward of the headwall, whose thickness exceeds 27 m in the central sector of the depositional area, and is drapped by the post slide unit (Pelitic Deposit)

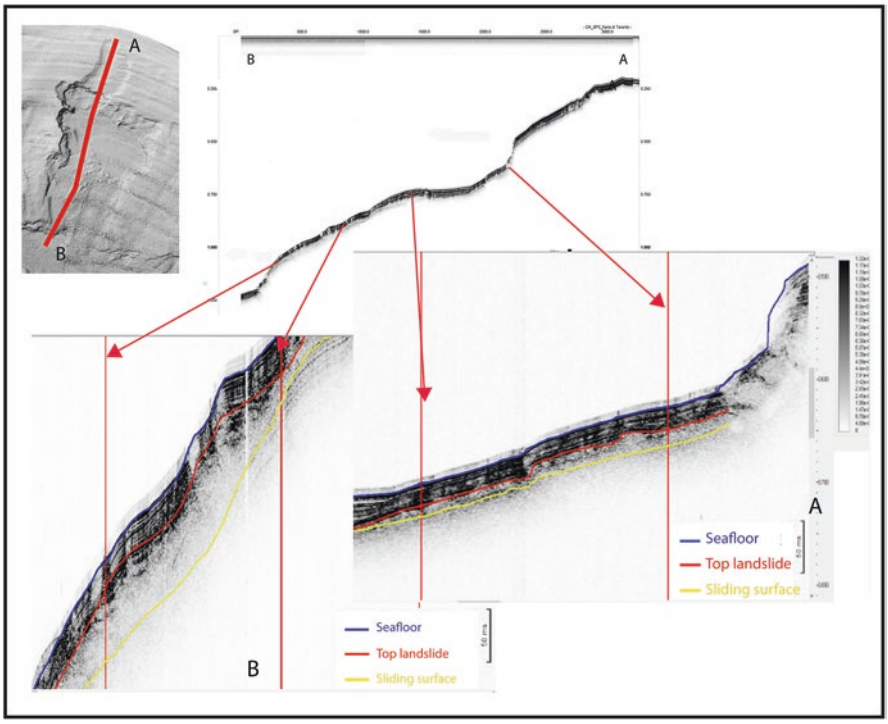

Fig. 11.6 Zoom view of the Chirp seismic profile along the Taranto Landslide. Spot A: from the headwall to the onset of the accumulation zone. Spot B: accumulation zone

Based on the analysis of the ecofacies of gravitational movements, the stratigraphic framework of the area affected by the Taranto Landslide has been defined and the thickness of the sediments involved in the gravitational instability has been estimated. The thickness ranges from about 11 m in the upslope sector of the landslide at about 420 m depth, to 33 m at about 980 m, with an average thickness of 27 m, therefore an estimated volume of the landslide deposit of about 0.29 km^3 was inferred.

11.3 Stratigraphy and Sedimentology

In this section we report the sedimentological analysis carried out on of the sediment samples taken from the C5 core and collected on the continental slope of the Puglia region (Lat.:40°24′,3 –long.:17°05′), in the Gulf of Taranto. It retrieved 150 cm of upper Holocene deposits at a depth of 268 m (Fig. 11.1). The

sedimentological analyses include the sediment particles grain size, the carbonate content, the biogenic and terrigenous content and the *Ca/Ti, Fe/Ti, K/Ti* content, by using an X-ray fluorescence analysis [4, 19]. In particular, the working half section of the core was sampled at a 5 cm step, obtaining a total of 28 samples for the sedimentological and elemental analysis.

11.3.1 The Laser Granulometer

The quantitative assessment of the sediment particles grain size has been determined on the basis of the laser indirect method. The laser granulometer uses the principle of optical diffraction of a beam of coherent light when meeting a particle. The diffraction granulometer *Horiba LA-950,* owned by the Department De Geociències Marines De L'institut De Ciències Del Mar (ICM- CSIC), Barcelona, was used to perform the grain-size analysis of the sediment samples taken from C5 core (Fig. 11.7). The *Horiba LA-950* consists of two light sources, a management system of the sample to control the interaction of the particles with the incident light, and a matrix of photodiodes at high quality to detect the scattered light with a

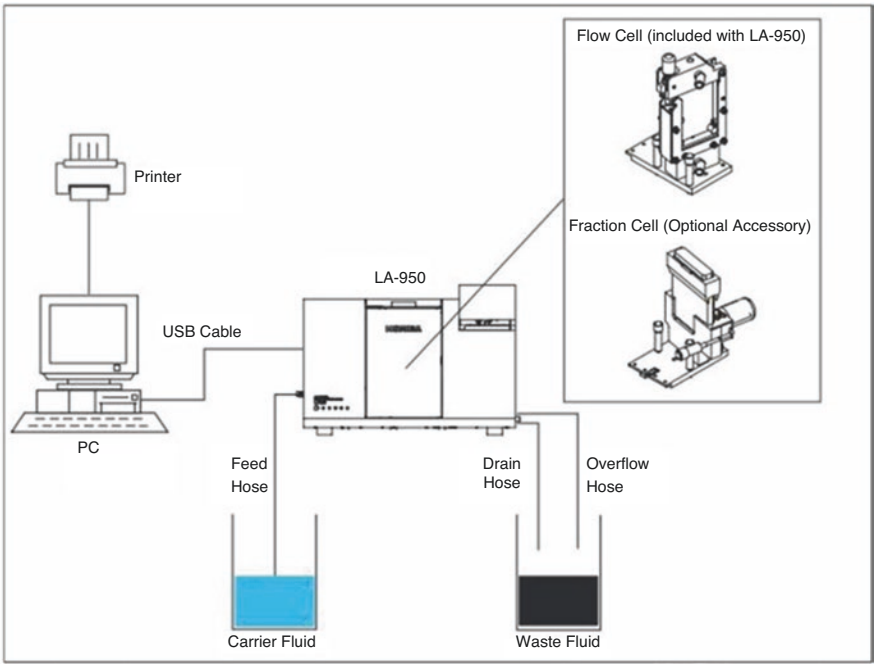

Fig. 11.7 The Horiba LA-950 configuration (from Meo et al. [19])

wide range angle. The analyser does not measure the particle size but it measures the angle and intensity of the light diffused by the particles in the sample. The scattered light collected on the detectors is used to calculate the distribution of the particle size of the sample analysed, using the Mie Theory (a Fraunhofer model). This information is then passed to an algorithm designed to use the Mie Scattering Theory that transforms data of the light spread in information on particle size. Before each analysis group, the laser source is put on axis, the focal length comes into focus manually or with an autofocus system, and then it is made a reference measurement with the cell filled with distilled water. During the analysis, the duration may be established by the operator (average 1 min), the detector records signals in response and transmits them to the computer that processes them in numerical and graphical form [20].

On the basis of the laser *Horiba LA-950* granulometer results, the particle size fractions were grouped into size classes to define the particle size distribution of the sediment and to calculate the value of the mean grain size (Table 11.1). The statistical parameters for each sample were also calculated (Table 11.1). The grain size values (Table 11.1) were plotted in the Shepard diagram [21] (Fig. 11.8), showing that all the samples fall into the clayey silt field.

11.3.2 Content of Carbonate

The content of carbonate in each sample has been determined through the chemical reaction between the known amount of prepared sediment and hydrochloric acid. The analysis has been performed with the *Bernard Calcimeter* of laboratory of sedimentology at ICM of Barcelona (Fig. 11.9). The carbonate content varies between about 18% and 30% and the higher values are recorded between 45 cm below seafloor and 120 cm below seafloor.

11.3.3 Content of Biogenic and Terrigenous Clasts

The content in percentage of biogenic and terrigenous clasts was performed by means of the binocular microscope *Leica MZ12.5* of the ICM laboratory. The fraction larger than 50 microns was collected from all samples by wet sieving after removal of the organic matter with hydrogen peroxide. The relative frequencies were determined by counting 300–400 grains per sample. The grain counts were made by unit area measurements as opposed to point counting. The observed biogenic clasts have been the following: planktonic foraminifera, benthonic foraminifera, planktonic fragments, benthonic fragments, Ostracods, Bryozoa, Echinoderms, spicules, serpulids, Pteropods, Gastropods, other. The terrigenous clasts have been

Table 11.1 Grain-size classes and statistical parameters for each sample of the core C5

ID-**N**	%Sand	%Silt	%Clay	Mean(Ø)	Skewness(Ø)	Kurtosis(Ø)
C5_0-1 - **1**	5.67	61.59	32.74	7.24	0.34	3.20
C5_5-6 - **2**	2.95	61.44	35.61	7.60	0.44	3.79
C5_10-11 - **3**	2.87	60.88	36.25	7.63	0.44	4.15
C5_20-21 - **4**	1.02	63.45	35.53	7.69	0.75	4.12
C5_25-26 - **5**	2.01	60.85	37.14	7.66	0.57	3.63
C5_30-31 - **6**	4.41	56.64	38.95	7.65	0.27	3.63
C5_35-36 - **7**	3.73	56.37	36.9	7.64	0.36	3.93
C5_40-41 - **8**	1.55	57.81	40.64	7.87	0.59	3.72
C5_45-46 - **9**	1.11	63.89	35.00	7.65	0.78	4.05
C5_50-51-**10**	4.36	62.84	32.8	7.32	0.38	3.50
C5_55-56 - **11**	5.35	59.24	35.41	7.48	0.19	3.64
C5_60-61-**12**	2.16	61.44	36.4	7.66	0.58	3.99
C5_65-66- **13**	1.5	57.64	40.86	7.86	0.61	3.66
C5_72-73 -**14**	2.77	59.73	37.5	7.68	0.44	3.76
C5_80-81 -**15**	1.52	56.89	41.6	7.96	0.67	3.52
C5_85-86 - **16**	1.89	58.07	40.04	7.77	0.53	3.43
C5_90-91-**17**	1.59	54.84	43.58	7.92	0.50	3.23
C5_95-96 -**18**	4.00	61.54	34.46	7.46	0.30	3.79
C5_100-101-**19**	3.1	59.06	37.83	7.66	0.42	3.77
C5_105-106-**20**	2.06	61.88	36.06	7.57	0.55	3.66
C5_110-111-**21**	2.24	61.87	35.9	7.61	0.51	3.95
C5_115-116-**22**	0.45	62.49	37.06	7.78	0.85	3.93
C5_120-121-**23**	1.72	63.85	34.43	7.56	0.61	3.90
C5_125-126-**24**	2.25	62.14	35.61	7.61	0.54	4.08
C5_130-131-**25**	2.43	66.66.	30.91	7.33	0.54	3.86
C5_135-136-**26**	0.88	65.00	34.12	7.63	0.84	4.12
C5_141-142-**27**	1.03	61.45	37.53	7.74	0.71	3.79
C5_145-146-**28**	1.59	65.36	33.05	7.51	0.65	4.01

determined as: quartz, mica, light minerals, rocks fragments, pyrite, glauconite, other. The analysis results show a constant increase of the terrigenous fraction from the bottom to the top core with both negative and positive peaks at a higher frequency (Fig. 11.10).

11.3.4 X-Ray Fluorescence Analysis

The X-ray fluorescence (XRF) analysis was also performed to know the chemical composition of the elements contained in the samples. The method is fast, accurate and non-destructive, and requires a minimum of sample preparation. In XRF, X-rays

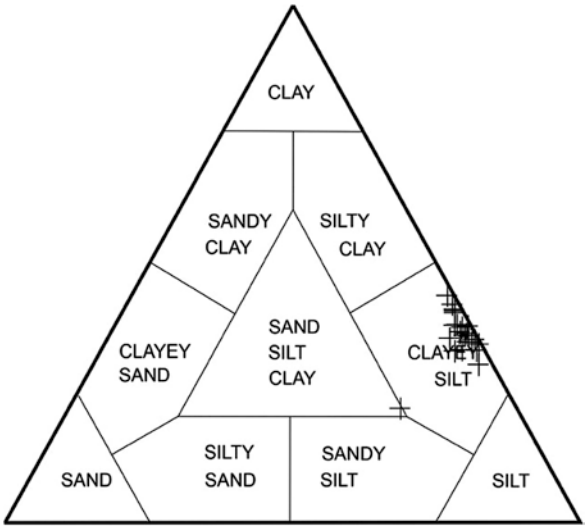

Fig. 11.8 Shepard diagram showing that almost all samples fall in the field of the clayey silt. Modified from Meo et al. [19]

Fig. 11.9 The *Bernard Calcimeter* at ICM of Barcelona (from Meo et al. [19])

produced by a source, an X-ray tube, irradiate the sample. The source could be alternatively a synchrotron or a radioactive material. The elements present in the sample will emit their characteristic fluorescent X-ray radiation with discrete energies. The qualitative analysis is achieved by measuring the energies of the radiation emitted by the sample which allows to determine the type of elements contained in

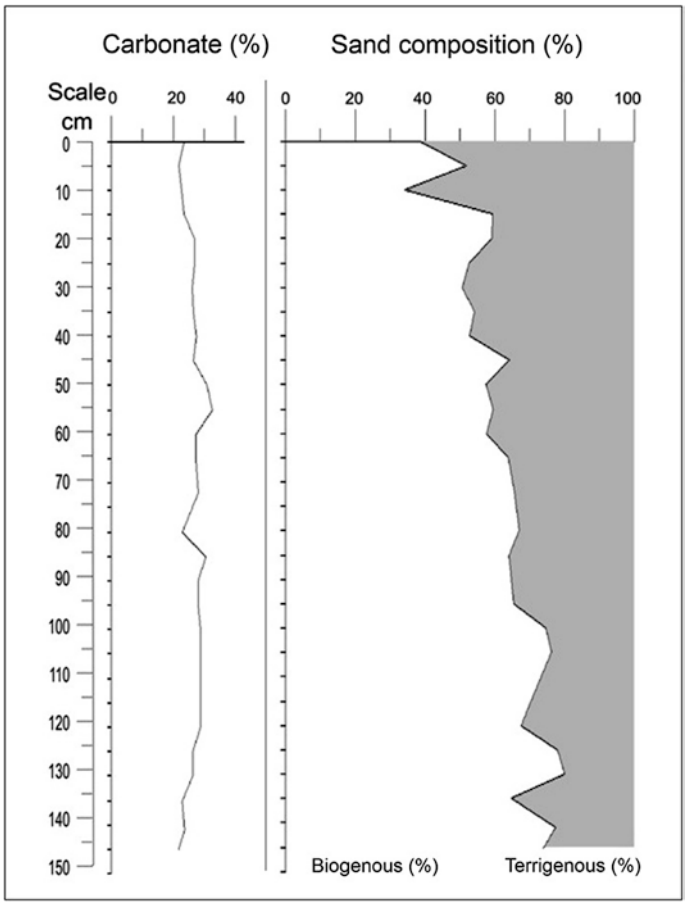

Fig. 11.10 The carbonate content and sand composition in % through the core sediment. Modified from Meo et al. [19]

it. The quantitative analysis is achieved by measuring the intensities of the emitted energies which allows to determine how much of each element is present in the sample.

The core C5 was scanned at 10 mm resolution with the *Avaatech XRF Scanner* (Fig. 11.11) at the Laboratory of University of Barcelona. The elements Al, Si, S, K, Ca, Ti, Mn, Fe were measured every 10 mm using a Rh X-ray tube at 10 kV. The analysis gives back element abundances in counts per area per 30 s (cts) or expressed as element-to-element ratio. According to Rothwell and Croudace [22]: high Fe/Ti proxy reflects an enhanced fluvial terrigenous input and weathering and varies positively with hydrological changes; high K/Ti proxy emphasizes the yield of detrital material and illite-rich material, which is transported in greater abundance during

Fig. 11.11 The *Avaatech XRF Scanner* at the Laboratory of University of Barcelona (from Meo et al. [19])

wet periods [23]; low K/Ti proxy points out to dryer environmental conditions; high Ca/Ti proxy marks coarser than clayey sediment particles possibly linked to increased content of forams; therefore Ca/Ti proxy is useful for assessing relative changes in biogenic versus lithogenic sedimentation and recording carbonate content (e.g. Piva et al. [24]), it represents the biogenic/detrital ratio and an indicator of biogenic carbonate (thus authigenic) versus terrestrial (thus allogenic) input [25]. The Ca/Ti ratios of C5 core were then compared to those of the DP30 core, a well-dated core retrieved at the same depth (−270 m) some 80 km south-eastwards in the Taranto Gulf [26–28], to identify similar trends.

11.3.5 Outcomes of Sedimentological and Stratigraphic Measurements on C5 Core

The multivariate analysis on the C5 core, i.e., the integration of all the measured proxies downcore, allowed the identification of four well-distinct sedimentological patterns, assimilable to local morphoclimatic trends (unit 2–5 in Fig. 11.12a; [29]), from −10 cm down to 150 cm. These trends were compared to those identified in the last 1500 years in the Gulf of Taranto by Grauel et al. [26, 27]. In particular, the climatic trend found in the C5 core was correlated to the one reconstructed in the Gulf of Taranto by [26, 27], based on δ18O and δ13C of *Globigerinoides ruber* and on Ca/Ti ratio in the first 2 m below the seabed. Five units have been defined from the bottom to the top core, timewise (Fig. 11.12):

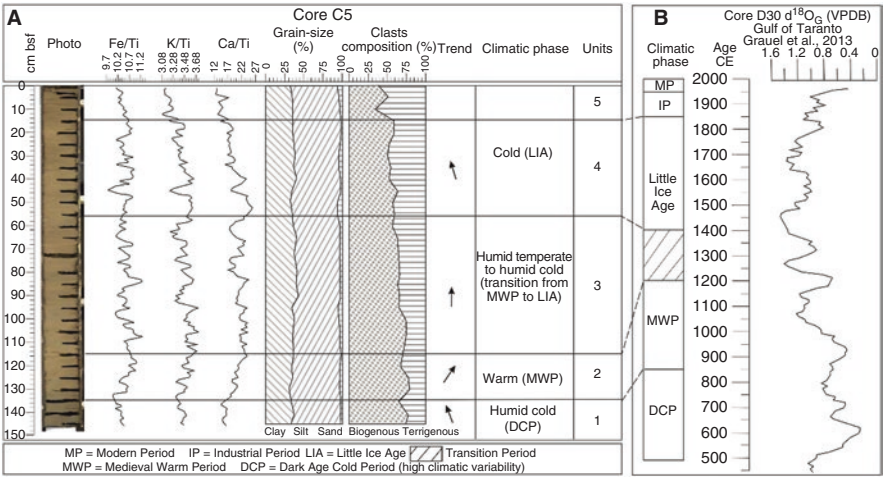

Fig. 11.12 (**a**) Morphoclimatic trends in C5 core are depicted on the basis of the integration of different proxies downcore, then compared to the (**b**) chronologically tuned record of Grauel [26, 27] and Lirer et al. [28]

Unit 1—from 150 cm to 135 cm: this interval, characterized by an increase in Fe content and relatively low Ca/Ti ratio, probably records an increasing fluvial input, linked to humid cold climate conditions; according to Grauel [27]. During this interval, cold and wet climate conditions relative to a larger-scale climate events (Dark Age Cold Period) were recorded in the Gulf of Taranto.

Unit 2—from 135 to 115 cm: this interval is characterized by a marked increase in the Ca content due to a greater intake of nutrients and organism productivity, and almost unstable Fe/Ti and K/Ti proxies: biogenic content also is relatively high during all the whole phase. According to Lirer et al. [28] this sediment interval records a warm period (the MWP) that begun around 800 AD and ended around 1200 AD.

Unit 3—from 115 to 58 cm: this interval is defined by a fast-oscillating trend of all the three proxies, around high ratios and points to varying cool-humid and humid-temperate environmental conditions. According to Grauel [27] this unit has been correlated to a transition phase ranging between 1400 (AD) and 1200 (AD).

Unit 4—from 58 to −15 cm: in this unit to a fast-oscillating signal of the Fe/Ti proxy, corresponds a net decrease of the Ca/Ti and K/Ti ratios, probably due to the onset of a cold–dry period. According to Grauel [24] this phase is recorded in the Gulf of Taranto between 1400 (AD) and 1850 (AD).

Unit 5—from −15 cm to the seabed: this unit consists mainly of reworked sediment with an unclear trend of the geochemical signal but with a marked increase of the terrigenous content; it may correspond to the record of the most recent Industrial Period (IP) of Lirer et al. [28].

In conclusion, grain size, chemical and sediment composition of the sediment core are linked to fluvial input and palaeo-productivity variations. Moreover, the

alternation between units characterized by prevalent fluvial input and units characterized by increased palaeo-productivity in the stratigraphic record of C5 core highlights centennial-scale morphoclimatic variations. The sediment of C5, from top core, sea bottom, to base core, could span from the Present to about 800 AD, if the correlation to the climatic phase record of Fig. 11.12b is correct. Given the inferred age at the base of the core and no erosional events at this site, the averaged local sediment aggradation rate could approximate 0,1 cm/y on the upper slope. This value is in good agreement with the outcomes of Grauel [27], which estimated the sedimentation rate, in a site much distant than the C5 core site, with respect to the fluvial mouths (Fig. 11.1), in 0.07 cm/y.

Absolute dating analyses are needed to provide the validation of the chronostratigraphic correlations between C5 and DP30 core and to define the age-model of the C5 core.

References

1. Pescatore TS, Senatore MR (1986) A comparison between a present-day (Taranto Gulf) and a Miocene (Irpinian Basin) foredeep of the southern Apennines, Foreland basins. pp. 69–182. Blackwell Scientific; Special Publication—International Association of Sedimentologists, 8, Allen P.A., Homewood P. (eds), DOI: https://doi.org/10.1002/9781444303810.ch8
2. Senatore MR, Meo A, Bosman A, Chiocci FL (2020) Progetto Magic, Foglio 43 Taranto. http://www.protezionecivile.gov.it/media-comunicazione/news/dettaglio/-/asset_publisher/default/content/progetto-magic-pubblicati-i-risultati-dello-studio-sui-fondali-marini-italiani
3. Senatore MR, Meo A, Bosman A, Chiocci FL (2020) Progetto Magic, Note a Compendio del Foglio N. 43 –Taranto. http://www.protezionecivile.gov.it/media-comunicazione/news/dettaglio/-/asset_publisher/default/content/progetto-magic-pubblicati-i-risultati-dello-studio-sui-fondali-marini-italiani
4. Falco M, Meo A, Ercilla G, Alonso B, Senatore MR (2016) Centennial-scale climatic variability in the Gulf of Taranto during the Late Holecene. Rend. Online Soc. Geol. It., La geologia marina in Italia Primo convegno dei geologi marini italiani, 41, (1), 38–38, https://doi.org/10.3301/ROL.2016.167
5. Ceramicola S, Senatore MR, Coste M, Meo A, Boscaino M, Cova A (2012) Seabed mapping for geohazard in the Gulf of Taranto, Ionian Sea (Southern Italy). Rend Online Soc Geol It 21:951–952. ISSN:2035-8008
6. Senatore MR, Meo A, Chiocci FL (2013) Geohazard marino nello Ionio settentrionale: evoluzione della testata della Valle di Taranto attraverso l'analisi ipsometrica. Miscellanea Ingv, Riassunti del Congresso AIQUA, L'ambiente Marino Costiero del Mediterraneo Oggi e nel Recente Passato Geologico. Conoscere Per Comprendere, Napoli 19–21 Giugno 2013, vol. 19, ISBN:2039–6651
7. Meo A, Falco M, Chiocci FL, Senatore MR (2016) The Taranto Landslide (northeastern Ionian Sea): stratigraphic framework and geological model. Rend. Online Soc. Geol. It., Geosciences on a changing planet: learning from the past, exploring the future, 40, (1), 612–612, https://doi.org/10.3301/ROL2016.79
8. McAdoo BG, Pratson LF, Orange DL (2000) Submarine landslide geomorphology, US continental slope. Mar Geol 169(1–2):103–136
9. Meo A, Falco M, Chiocci FL, Senatore MR (2016) Kinematics and the tsunamigenic potential of Taranto landslide (north-eastern Ionian Sea): morphological analysis and modelling.

Landslides and engineered slopes. Experience Theory Pract 173:1409–1416. https://doi.org/10.1201/b21520
10. Ward SN, Day S (2002) Suboceanic landslides. Yearbook of Science and Technology, McGraw-Hill, V1.2
11. Varnes DJ (1978) Slope movement type and processes. In: Schuster RL, Krizek RJ (eds) Landslide-analysis and control. Transp. Res. Board, Natl. Res. Counc, Washington, D.Cspec. Rep. 176,12-33
12. Watts P, Grilli ST, Kirby JT, Fryer GJ, Tappin DR (2003) Landslide tsunami case studies using a Boussinesq model and a fully nonlinear tsunami generation model. Nat Hazards Earth Syst Sci 3:391–402
13. Alberico I, Budillon F, Casalbore D, Di Fiore V, Iavarone R (2018) A critical review of potential tsunamigenic sources as first step towards the tsunami hazard assessment for the Napoli Gulf (Southern Italy) highly populated area. Nat Hazards 92:43–76. https://doi.org/10.1007/s11069-018-3191-5
14. Casalbore D, Romagnoli C, Bosman A, Chiocci FL (2011) Potential tsunamigenic landslides at Stromboli Volcano (Italy): insight from marine DEM analysis. Geomorphology 126(1):42–50
15. Grilli ST, Watts P (1999) Modeling of waves generated by a moving submerged body. Applications to underwater landslides. Eng Anal Bound Elem 23(8):645–656
16. Watts P (2000) Tsunami features of solid block underwater landslides. J Waterw Port Coast Ocean Eng 126(3):144–152
17. McAdoo BG, Watts P (2004) Tsunami hazard from submarine landslides on the Oregon continental slope. Mar Geol 203(3):235–245
18. Rahiman TI, Pettinga JR (2006) The offshore morpho- structure and tsunami sources of the VitiLevu seismic zone, southeast VitiLevu. Fiji Mar Geol 232(3–4):203–225
19. Meo A, Falco M, Ercilla G, Alonso B, Senatore MR (2018) Sedimentological analyses to identify Centennial-scale climatic variability during the Late Holocene: a gravity core collected on the Apulia continental slope in the Gulf of Taranto. IEEE International Workshop on Metrology for the Sea (MetroSea 2018), Proceedings, IEEE Catalog. Num. CFP18P82-ART., 273–277, https://doi.org/10.1109/MetroSea.2018.8657826
20. Allen T (1997) Particle size measurement, V.2: powder sampling and particle size measurement. Springer, ISBN 978–0–412-75350-3
21. Shepard FP (1954) Nomenclature based on sand–silt–clay ratios. J Sediment Petrol 24:151–158
22. Rothweel RG, Croudace IW (2015) Chapter 2. Twenty years of XRF core scanning marine sediments: what do geochemical proxies tell us? In: Croudace IW, Rothwell RG (eds) Micro-XRF studies of sediment cores, developments in paleoenvironmental research, vol 17. Springer Book, pp 25–102. https://doi.org/10.1007/978-94-017-9849-5_2
23. Yarincik KM, Murray RW, Peterson LC (2000) Climatically sensitive eolian and hemipelagic deposition in the Cariaco Basin Venezuela, over the past 578,000 years: results from Al/Ti and K/Al. Paleoceanography 15(2):210–228
24. Piva A, Asioli A, Schneider RR, Trincardi F, Andersen N, Colmenero-Hidalgo E, Dennielou B, Flores J-A, Vigliotti L (2008) Climatic cycles as expressed in sediments of the PROMESS1 borehole PRAD1-2, central Adriatic, for the last 370 ka: 1. Integrated stratigraphy. Geochem Geophys Geosyst 9:Q01R01. https://doi.org/10.1029/2007GC001713
25. Richter TO, Van der Gaast S, Koster B, Vaars A, Gieles R, De Stigter HC, De Haas H, Van Weering TCE (2006) The Avaatech XRF Core Scanner: technical description and applications to NE Atlantic sediments. Geol Soc Lond, Spec Publ 267(1):39–50
26. Grauel AL, Goudeau MLS, de Lange GJ, Bernasconi SM (2013) Climate of the past 2500 years in the Gulf of Taranto, Central Mediterranean Sea: a high-resolution climate reconstruction based on δ18O and δ13C of Globigerinoides ruber (white). TheHolocene 23(10):1440–1446
27. Grauel AL (2012) Calibration of the clumped isotope thermometer to Foraminifera and its application to high-resolution climate reconstruction of the past 2500yr in the Gulf of Taranto (Eastern Mediterranean Sea). Dissertation No. 20360 ETH Zurich, Switzerland

28. Lirer F, Margaritelli G, Alberico I, Bonomo S, Capotondi L, Cascella A, Di Rita F, Ferraro L, Insinga DD, Magri D, Pelosi N, Petrosino P, Vallefuoco M (2019) Climatic variability over the last two millennia in the Mediterranean area: a review from marine paleoarchives. Geogr Fis Dinam Quat 42:215–224
29. Budillon F, Senatore MR, Insinga DD, Iorio M, Lubritto C, Roca M, Rumolo P (2012) Late Holocene sedimentary changes in shallow water settings: the case of the Sele river offshore in the Salerno gulf (South-Eastern Tyrrhenian Sea, Italy) rend. Fis Acc Lincei 23:25–43. https://doi.org/10.1007/s12210-01

Chapter 12
Computer Vision and Deep Learning Applied to the Photo-identification of Cetaceans

Vito Renò, Giovanni Dimauro, Carmelo Fanizza, Roberto Carlucci, and Rosalia Maglietta

Contents

Abstract Photo-identification is the non-invasive process of uniquely identifying an individual among a set of individuals, based on the analysis of one or more photos. This is a specific task in cetaceans' abundance and distribution studies, which can be effectively automated using computer vision and deep learning algorithms in large-scale studies. In this chapter, recent advances in the photo-identification of Risso's dolphins are presented, covering the process from manual approaches to modern deep learning techniques. This manuscript highlights the strong

V. Renò · R. Maglietta
Institute of Intelligent Industrial Technologies and Systems for Advanced Manufacturing, National Research Council of Italy (CNR STIIMA), Bari, Italy
e-mail: vito.reno@cnr.it; rosalia.maglietta@cnr.it

G. Dimauro
Department of Computer Science, University of Bari, Bari, Italy
e-mail: giovanni.dimauro@uniba.it

C. Fanizza
Jonian Dolphin Conservation, Taranto, Italy
e-mail: carmelo@joniandolphin.it

R. Carlucci (✉)
Department of Biology, University of Bari, Bari, Italy
e-mail: roberto.carlucci@uniba.it

P. Daponte et al. (eds.), *Measurement for the Sea*, Springer Series in Measurement Science and Technology,
https://doi.org/10.1007/978-3-030-82024-4_12

multidisciplinary approach that is mandatory to accelerate and bring innovations working in multiple domains (marine biology and computer science in this case study). Particular attention is also given to the importance of data sharing, especially because it can be seen as a mandatory step that enables the proficient use of modern deep learning approaches to photo-identify a specimen. In the first part of the chapter, we present the state-of-the-art methods currently applied to the photo-identification task; the second part is devoted to describing the Smart Photo-Identification of Risso's dolphins (SPIR) methods developed by our research team. Finally, future perspectives and directions of this research are discussed.

12.1 Introduction

The photo-identification is an extremely useful technique that finds application in the field of population ecology and conservation biology, resulting in wide applicability for study on marine mammals [1] and useful to infer knowledge about the health status of marine ecosystems and their changes over time. To achieve this goal, studies on the spatial distribution, habitat use, site fidelity of cetacean species occurring in a specific study area, and their abundance, behavior patterns, and genetic structures need to be done in order to investigate their population structure and dynamics [2–14]. To this regard, photo-identification can become the key for enabling these studies, even on a large scale, if high data availability is guaranteed as well as cutting-edge automatic techniques and algorithms to process such data. Briefly, with photo-identification, it is possible to univocally and efficiently determine if a specimen has been seen repeatedly over time in a noninvasive way, basing the assumption on the results of image analysis. This means that there must be some physical distinctive features that make an individual unique within a species, thus enabling its precise identification if multiple images are compared with one another.

However, in the last few years, domain experts are facing the problem of processing huge amounts of data that can be easily made available thanks to the diffusion of relatively low-cost electronic devices able to capture a large number of high-quality photos, such as reflex or mirrorless digital cameras or last generation smartphones. Moreover, marine mammals' observers tend to take a large number of photos during surveys in order to avoid the unlikely event of losing valuable information, thus accumulating a high number of images that make the manual photo-identification approach increasingly impractical. This is the main reason why domain experts need to be assisted in the photo-identification task by automated or semi-automated algorithms. In fact, manual photo-identification studies show two undoubted drawbacks that make the process incompatible on a large scale:

1. manual procedures, even state-of-the-art ones, independent of the species being studied, are time consuming and subject to a bias introduced by the human operator that performs photo-identification [15–17];

2. it is practically impossible to manually photo identify specimens on large datasets, thus making this approach unfeasible for large-scale studies. In many cases, large standardized datasets (or catalogues) are unavailable [18–20].

It is therefore evident the increasing need for algorithms and procedures that can help domain experts in the analysis of huge image datasets over time, keeping track of previous analyses in appropriate digital catalog. The need is consequently followed by a large demand for automatic procedures that involve multidisciplinary approaches mixing up marine biology, computer vision, and artificial intelligence (AI) expertise. In particular, focusing on AI, deep learning models recently spread among multiple disciplines becoming powerful resources able to solve both classification and regression problems if properly trained feeding the model with a high number of samples. Deep learning architectures can learn complex patterns directly from data, even directly from images or multidimensional signals, with applications also in the marine biology area [21–23].

In this paper, a multidisciplinary activity devoted to the automatic photo-identification of cetaceans is described focusing on the case study of the Risso's dolphin Grampus griseus, one of the least known mid-sized odontocetes in the Mediterranean Sea and on global scale [5, 24–26] to be ranked as Data Deficient by IUCN Red List [27]. The Risso's dolphin is known for typical patterns on the body and dorsal fin [28–30] that can be considered effectively distinctive and useful to discriminate single individuals relying on image data (observations).

We aim to highlight the impact of using automatic approaches for bringing innovations over multiple domains, specifically marine biology and computer science, performing automatic photo-identification using computer vision and deep learning. The chapter is divided into two main parts: the first to give details about DARWIN, the pioneering photo-identification system based on fin contour extraction and matching; the second is devoted to describing the comprehensive software pipeline built around the Smart Photo-Identification of Risso's dolphins (SPIR) [31] algorithm and the DolFin catalog [32], developed by our research team during the last few years and enriched by deep learning classifiers specifically designed to solve some known problems in photo-identification studies [33, 34].

12.2 Contour-Based Photo-identification

One of the most widely used methods to perform cetaceans' photo-identification, either manual or at least semiautomatic, is based on contour matching. In fact, it is known that the shape of dolphin's dorsal fins can be effectively exploited to recognize an individual due to the presence of particular outlines, notches, or generally speaking points of interest that made the fin contour almost unique. Another benefit of relying on the contour is that the approach can be considered species independent because of its formulation. In the last few years, the state of the art for cetaceans' photo-identification based on contour analysis was DARWIN [35]. DARWIN is a

system whose development started at Eckerd College in 1995 and continued since 2008. Its aim was to automate the photo-identification process of dolphins by using photos of their dorsal fins. In particular, DARWIN approach is based on the research of a fin in a database of previously captured and cataloged fins, thus allowing the researcher to find the most similar dorsal fins after a comparison with a generic image that depicts the dorsal fin of a new, previously unidentified dolphin. DARWIN output is represented by an ordered list of fins from its database that most closely match the one to be identified. In this way, the tool assists the researcher in analyzing the images by giving priority to the fins that may correspond to the one to be identified.

DARWIN is made of several submodules:

- The first one extracts the contour extraction in order to make it comparable with the others;
- The second one manages database reading and writing operations;
- The third one is devoted to contour matching and returns the ranked list of matches described beforehand.

These modules are accessible through a graphical user interface (GUI).

Contour extraction is performed in two steps: first, the chain of points that describe the edge of the dorsal fin is extracted and then the extraction of specific keypoints of the resulting chain is computed.

DARWIN lets the user choose between two different algorithms to achieve this goal and perform fine tuning, because the extracted contour can be noisy in a certain number of cases. Both algorithms are semiautomatic because they require user interaction: the first one needs the starting and ending points of the dorsal fin to be clicked by the user using the mouse and the second one needs the whole edge to be drawn manually with the mouse pointer.

The chain of points consists of a sequence of points, each connected to the previous one and the next through two segments (excluding the first and the last); in this way, they form a segmented line that describes the edge of the fin. The chain of points can also be adjusted manually using the tools within the graphical interface, giving the user the possibility to add new points, move the existing ones, or delete one or more points. Figure 12.1 shows an example of chain of points computed on a Risso's dolphin image. It is worth specifying that this result can be achieved with user intervention as specified beforehand.

The chain of points obtained from the previous step is then analyzed to obtain key points that are used to compare two fins. In particular, the fin tip, the beginning of the fin, and the most prominent notch on the back of the fin are extracted. Figure 12.2 shows the position of the key points that lie on the fin contour: (b) refers to the beginning of the contour, (e) represents its ending, (t) stands for the fin tip, and (n) points to the notch.

To automatically identify the starting point of the outline at the beginning of the dorsal fin, absolute angles between subsequent points in the chain are examined with a threshold-based procedure, with the aim of excluding any point belonging to the dolphin's body instead of the dorsal fin. A similar procedure is applied to

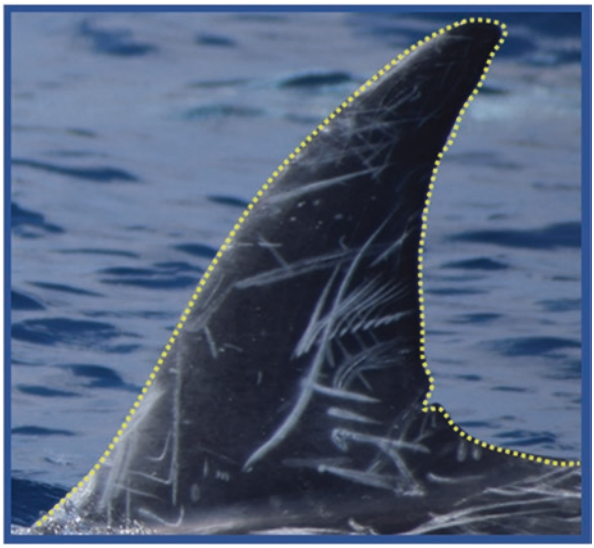

Fig. 12.1 Example of chain of points extracted on the contour of a dorsal fin

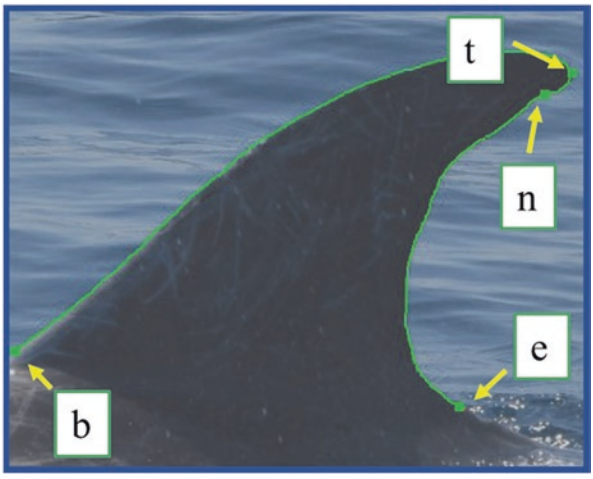

Fig. 12.2 Another example of fin contour with explicit indication of the four keypoints *b* beginning, *t* tip, *n* notch, and *e* ending

determine the ending point. The fin tip is identified by analyzing the wavelet decomposition of the signal represented by the sequence of angles with a coarse-to-fine approach. Finally, the notch is extracted from the same signal starting from the position of the fin tip.

The comparison between two fins, i.e., the contour matching, takes place after the alignment of the fin and consists of a distance calculation. To perform this step,

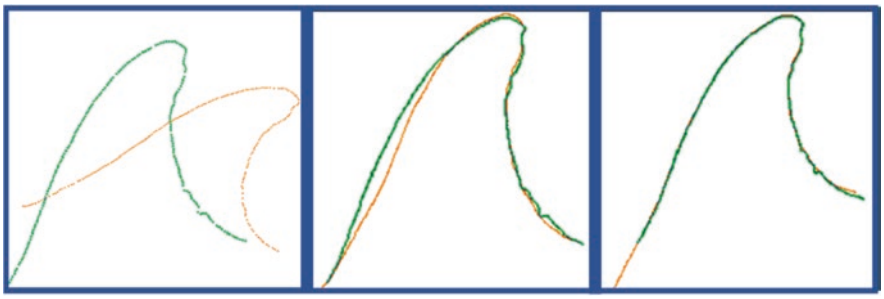

Fig. 12.3 Example of fin contour alignment in DARWIN

fin alignment is carried out on the basis of the key points as shown in Fig. 12.3. Newton-Raphson optimization is iteratively used to adjust the position of the beginning and end of the contour of each pair of contours to be analyzed.

The fin contour of a new unknown dolphin is analyzed with all the contours stored in the local database, returning a ranked list of fins in descending order of similarity.

Although this pioneering approach has undoubtedly brought benefits thanks to the use of software for the photo-identification of cetaceans, there are some aspects of its functioning that make it impractical especially for large-scale studies for three main reasons:

- using DARWIN is time consuming;
- it requires great manual effort;
- the approach is based only on contour matching.

In fact, the main drawback of contour-based procedures is that no other relevant information (for example, color, shape, appearance, relevant features, and so on) is considered, but can actually be exploited in a certain number of cases. Furthermore, DARWIN approach requires a lot of user interaction to import and process the data, making the approach unfeasible when very large amounts of data need to be analyzed.

12.3 Smart Photo-Identification of Risso's Dolphins

The aim of this paper is to show the complete pipeline for the photo-identification of Risso's dolphins developed and currently maintained by our research team. This pipeline has been designed and developed for the analysis of Risso's dolphins in order to exploit the distinctive marks that these kinds of dolphins show on their dorsal fins, thus overcoming the limitations of contour-based approaches that do not consider at any step the information embedded by the scarring pattern of such dolphins. Before going on through the analysis of all the steps involved in the pipeline,

it is worth mentioning the work [32] in which an innovative digital platform (DolFin) for cetaceans' analyses has been presented, along with a standardized catalog that can be easily extended and adopted for large scale studies. In fact, shared and open catalogs with heterogeneous kind of data (ranging from images to GPS coordinates and so on) are essential for effectively studying cetaceans. The importance of such catalogs increases more, and it becomes necessary to train new algorithms or develop innovative methodologies for data analysis, even in the field of artificial intelligence, where huge amounts of data are required to develop models at the frontier of research. Our software pipeline is basically built around the DolFin platform and the SPIR algorithm [31], in which a new photo-identification paradigm for Risso's dolphins identification over time has been presented. SPIR is deeply based on computer vision and works very efficiently for the analysis of Risso's dolphin images. The software pipeline is enriched by two deep learning models – namely convolutional neural networks – specifically designed to be integrated as shown in Fig. 12.4. It is based on three main parts:

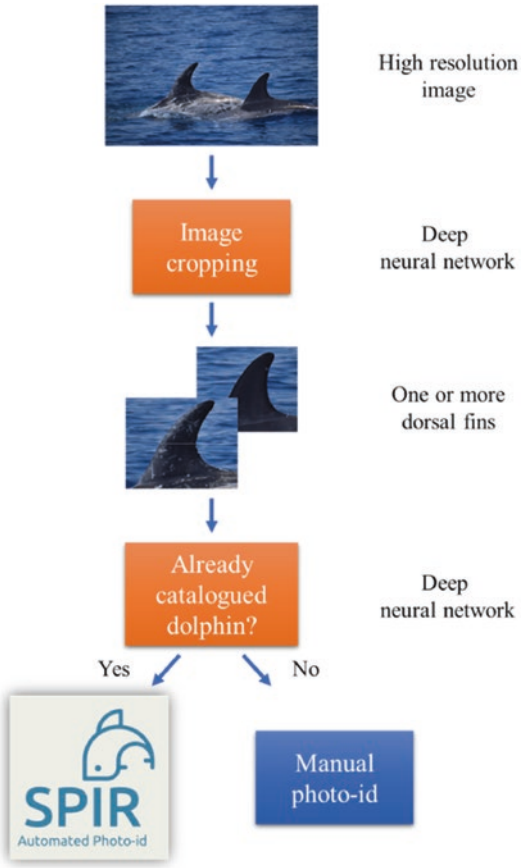

Fig. 12.4 Block diagram of the processing pipeline

1. Image Cropping—performed by a convolutional neural network.
2. Recognition of an already cataloged dolphin, i.e., determine whether a specimen is new or not—performed by another convolutional neural network.
3. SPIR algorithm.

Each one of the building blocks will be described in detail in the following subsections. However, before going on through the software pipeline description, a summary of the deep learning model used is briefly presented.

12.3.1 Convolutional Neural Networks

Convolutional neural networks (CNNs) are deep learning models that can be used to enable machines to view the world as humans do. CNNs were first introduced in LeCun et al. [36], but their effective use in computer vision application spread out in the last few years due to the large availability of computational power at a relatively low cost. In fact, these complex architectures are costly in terms of computational resources needed to train the model, due to the fact that they need to process complex signals such as images or even multidimensional tensors, but the main drawback is that thousands of images could be needed to learn a specific task. Today CNNs are successfully used to perform handwriting recognition (one of the first applications), image segmentation, object recognition, or generally speaking high level image analysis, but a CNN can be potentially trained to implement a custom classifier or regressor based on specific inputs as it will be shown later in the manuscript.

To give an overview of a convolutional neural network architecture, these networks are made up of artificial neurons that are connected to one another trying to emulate the human brain connectivity pattern [37]. Each neuron is solicitated by specific stimuli coming from restricted regions of the visual field (the so-called receptive fields), and neurons are arranged and stacked in subsequent layers as will be detailed later. CNNs are powerful models because they automatically learn the weights of the kernels used to perform convolutions with the backpropagation algorithm. Convolutions are the core operations used to extract high-level features from the input (i.e., edges, notches, col-our gradients or deviations, and so on). For this reason, whenever a specific kernel is learned, it is.

used as the operand of a convolution operation in order to cover the entire visual field (represented for example by the input image).

A CNN can be made of a high number of layers (hundreds in modern complex models) that are useful thanks to their ability of automatically learning how to process the input to detect and extract its relevant features. Similar to what happens in common artificial neural networks, a classical CNN architecture is generally composed of an input layer, and then one or more hidden layers are placed in the middle until an output layer is reached. Each time an input is given to a layer, a specific operation takes place with respect to the finality of each layer, altering the data and

manipulating them as they are simultaneously processed by a bank of filters. The aim of this filter is to compute and use specific data features specific to produce the correct output. The most common layers that can be used in CNNs for classification problems are

- Convolutional layer, used to pass its input through one or more convolutional filters, each one responsible for the analysis of a specific feature on images;
- Rectified linear unit or ReLU, used to introduce a nonlinearity in the learning process due to its formulation; in fact, ReLU maps all the negative values to zero, while positive values remain unaltered.
- Max Pooling layer, used to reduce the dimensionality of its input performing a down sampling operation. In the case of Max Pooling, for each portion of the input (it can be, for example, a 2×2 region), only the maximum value is kept, while the other are thrown away. It has the dual effect of significantly reducing the number of parameters to be learned by the CNN and making the subsequent layers operate on larger portions with respect to the input signal.
- Fully Connected layer, in which all the neurons are connected to one another (as in classical artificial neural network). A fully connected layer is generally used immediately after one or more repetitions of convolutional layers followed by ReLu and pooling, before returning the output value. It acts as a classifier that works on the features extracted by the convolutional part of the network.
- SoftMax layer that maps the set of values produced by a fully connected layer to class probabilities using a normalized exponential function.
- Classification layer, used to compute the cross entropy loss when the CNN solves classification problems with mutually exclusive classes.

The alternation of these layers according to a predetermined pattern constitutes the architecture of the convolutional neural network. A typical example we used in our automatic photo-identification pipeline for Risso's dolphins is given in Fig. 12.5. As reported in the block diagram (Fig. 12.4), our photo-identification pipeline relies on two different CNNs that share a similar architecture but are trained to solve two distinct problems: the image cropping and the recognition of already cataloged specimens. With reference to the architecture of the CNN in Fig. 12.5, the different parts of the network are depicted with different colors. The input is represented by an RGB image that feds a Convolutional layer followed by ReLU and Max Pooling. These three layers represented in orange are a repeated structure in many CNN architectures. They are stacked subsequently with the goal of learning the best kernels that will be used to process the input and perform the classification task. Then, the blue boxes refer to the final layers of the CNN where the classification takes place. The output depends on the specific problem that the network was designed to solve.

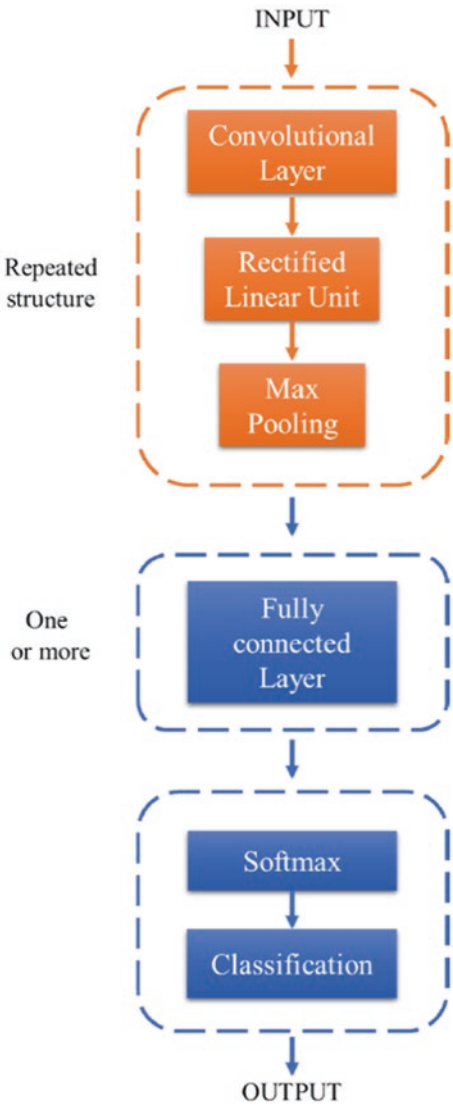

Fig. 12.5 Example of typical CNN architecture used for the photo-identification of Risso's dolphins

12.3.2 Image Cropping

With reference to Fig. 12.4, automatic image cropping is the first block called in our photo-identification pipeline. Starting from a full frame image of any spatial resolution (for example a 1920 × 1080 full-hd image or higher resolution), the aim is to extract one or more dorsal fin crops that will be subsequently analyzed by other software modules. We have developed a deep neural network to perform this task,

using the original photo as input and producing as many outputs as the number of dorsal fins present in the photo.

The software is built in MATLAB language and can perform batch image cropping on one or multiple folders, i.e., it looks for images in a specific input folder and produces all the cropped images of fins in a few minutes, depending on the number of original photos to be processed and the computer performance.

The output is organized in folders with respect to the result of the CNN classification: Fins or Not fins. The first folder contains cropped images of fins from original photos, while the second one contains discarded cropped images that actually do not represent fins.

The problem of image cropping is known in literature, especially when a massive amount of data (for example, gigabytes of photos) must be processed for photo-identification purposes [38]. Our deep learning-based approach has been formulated as a binary classification problem (fin vs. no fin) solved by a convolutional neural network in Reno et al. [34] that has been successfully used to crop real images coming from specific acquisition campaigns demonstrating its viability on large-scale studies. In this paper, we propose a CNN built directly from scratch, basing the assumption on the fact that a similar structure in a different domain was proved to be effective in the resolution of a binary classification problem [39], trying to minimize the number of layers involved to solve the problem, so minimizing the number of parameters required for the network to reach the convergence and become ready to identify and crop the fins. The architecture is simple but effective and clearly reflects the one depicted in Fig. 12.5, being composed of a Convolutional layer (dimensioned to learn 3×3 kernels) followed by a nonlinearity (ReLU) and a Max pooling down sampling, repeated three times. Then, three Fully connected layers, Softmax, and classification directly follow. If compared to state-of-the-art architectures such as GoogleNet or ResNet, our architecture is extremely simplified. This is mainly due to the fact that we specifically decided to design and train this CNN to solve a specific problem, while the previously cited models are designed to discriminate among a higher number of classes.

The following figures show the performance of the algorithm in different situations. The capability of cropping a dolphin dorsal fin from a full-frame image is shown both in the case of single individual (Fig. 12.6) or if images with more than one fin are fed to the neural network (Fig. 12.7). Finally, the robustness of the proposed approach is demonstrated by the capability of discarding cropped images that do not represent a dorsal fin (Fig. 12.8).

12.3.3 Recognition of an Already Cataloged Dolphin

The second block to be described consists of identifying known dolphins, i.e., understanding if a cropped fin belongs to one of the individuals that have been already photo-identified in the past and collected in the catalog. A second deep neural network has been designed and developed to solve this task [33]. In this case, the

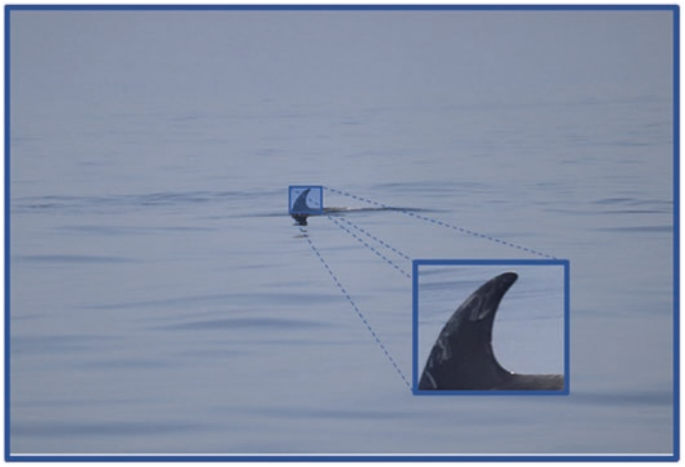

Fig. 12.6 Image cropping with a single fin

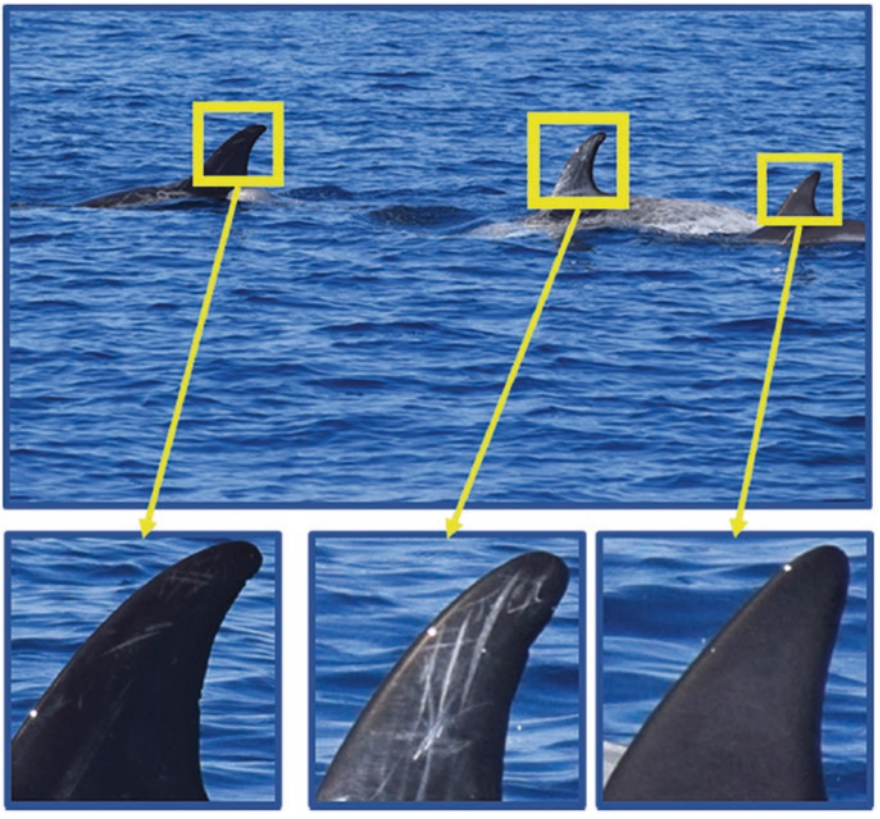

Fig. 12.7 Image cropping in the case of multiple fins

Fig. 12.8 Discarded cropped images that do not represent a dorsal fin usable in the automatic photo-identification pipeline

classification problem is formulated to recognize known dolphins (i.e., previously identified ones) versus unknown dolphins. The motivation behind this choice is strictly connected to the behavior of SPIR, which shows an extremely high performance if at least one image of the dolphin being photo-identified is already cataloged. However, details about SPIR will be given in the next paragraph. As far as this task is concerned, the methodology proposed in Maglietta et al. [33], namely, Neural Network pool (NNpool), has been successfully used to recognize unknown individuals in large dataset without any user interaction, consequently solving the problem of requiring a high user interaction, thus avoiding the manual observation of all the pictures stored in a dataset. The impact of using NNpool applied to our software pipeline is also reported in Maglietta et al. [40], showing that the combination of the convolutional neural network with the SPIR algorithm is useful to reinforce the strengths of the two approaches, minimizing the intrinsic weaknesses of one or the other algorithm. With reference to Fig. 12.4, running NNpool immediately after the image cropping step is useful to divide the processing in two distinct branches:

- if the image depicts an already cataloged dolphin, then SPIR analysis can take place to identify the specimen among the ones of the catalog;
- otherwise, a manual photo-identification procedure needs to be performed, only the first time, to add the new specimen in the catalog.

From an architectural point of view, the CNN built for NNpool follows the same structure of the previously defined one: for the first structure made of Convolutional layer, ReLU and Max pooling is repeated three times, setting the network for learning respectively 8, 16, and 32 filters. Then, a pair of Fully connected layers follows, ending with Softmax and classification.

12.4 SPIR

SPIR stands for Smart Photo Identification of Risso's dolphins and is the core algorithm developed by our research team aimed to this task. SPIR is based on a computer vision technique known as feature extraction and matching. The core idea of this approach is that the inner part of a dorsal fin contains an extremely useful visual information that cannot be thrown away in automatic photo-identification algorithms. In fact, for the case study of Risso's dolphins, domain experts perform photo-identification not only relying on the fin contour but also basing their judgment on white scarring patterns. This assumption suggested the investigation of a new paradigm for the photo-identification of this species, first described in Maglietta et al. [32] and then detailed in Renò et al. [31]. The way SPIR works is simple but effective: it analyses each cropped fin image representing the inner part in terms of relevant image portions—namely the key points—so that each cataloged image has a sort of distinctive signature. This signature is built computing relevant image features, in our work the SIFT ones [41], enabling the subsequent matching of these signatures. This means that if an image of a known specimen can be represented in terms of relevant keypoints, it is sufficient to compute the same SIFT features of an "unknown" image to find the best matching dolphin in the catalog. The comparison is made evaluating the distance between the SIFT features: closer distance suggests a high probability of seeing the same individual. However, since the captured dolphins can assume different poses and appearance in the images, due to the absence of orientation and light constraints when photos are captured, there is the need of extracting scale and rotation invariant keypoints. This means that the algorithm needs to know if the fin depicted in the image being processed has a particular orientation or is generally speaking affected by a noise. SIFT features can describe an image in terms of small regions (the keypoints) that are modeled along with the surroundings with an appropriate descriptor. In fact, an SIFT key point is basically a circular region of interest of an image with a specific orientation, described by its center, orientation, and radius. Each key point is then described with a certain number of points that make it recognizable in other images, independent of the scaling, the position, the translation, and rotation. The aim of using SIFT features is to extract the informative content of an image (in this case, the dorsal fin) in order to recognize the same specimen if comparing different images. An example of SIFT feature descriptors computed on a dorsal fin is given in Fig. 12.9, where a high number of keypoints is depicted in yellow. The information about the surroundings of each keypoint is graphically represented in purple. It is immediate to notice that the whole dorsal fin is represented by distinctive keypoints. Since the image can be described in terms of SIFT features, then it is possible to find the best matching dolphin in the catalog, performing photo-identification rapidly with high accuracy. An example of matched dolphin is reported in Fig. 12.10.

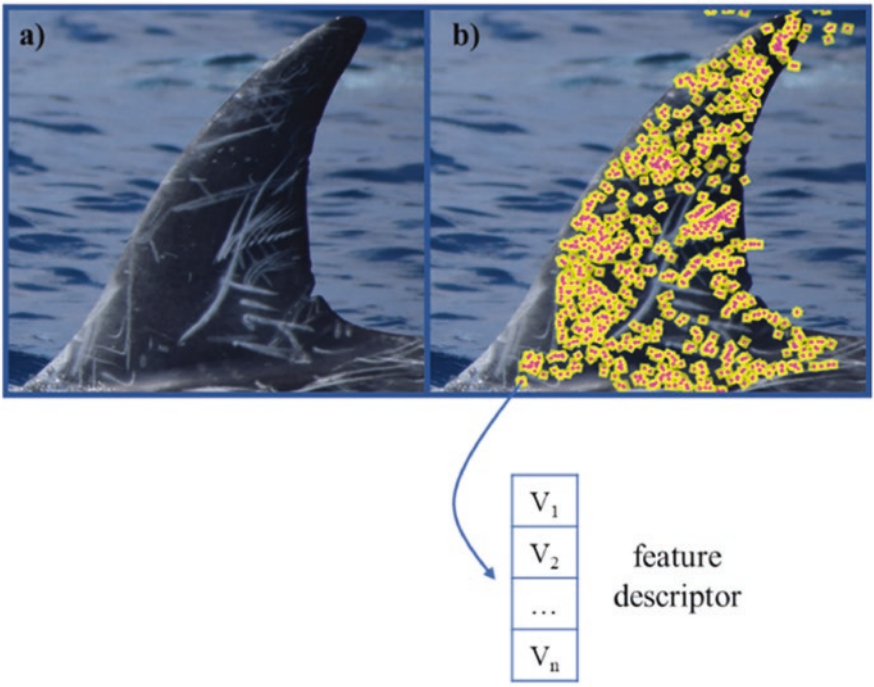

Fig. 12.9 Example of SIFT features computed and extracted on a Risso's dolphin dorsal fin

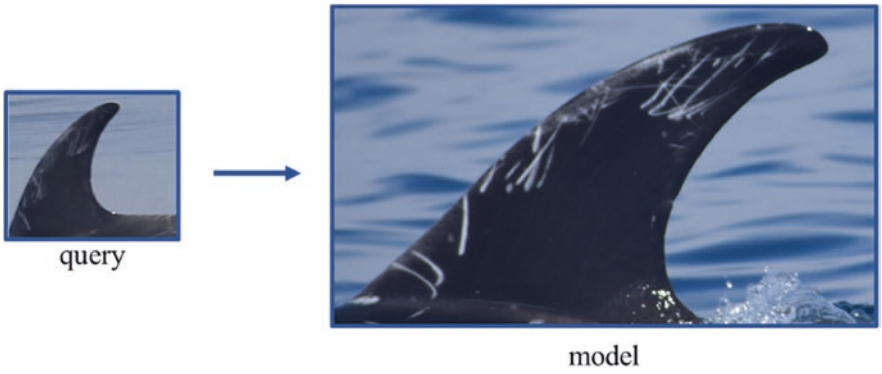

Fig. 12.10 Example of matching. On the left, a new image is fed to the photo-identification pipeline. On the right, the best matching model is shown

12.5 Conclusions

In this paper, the case study of the automatic photo-identification of Risso's dolphin G. griseus relying on computer vision and deep learning has been described. First, currently used contour-based photo-identification methodologies are reported, along with their benefits and intrinsic limits. Then, the software pipeline developed and currently used by our research team is reported, highlighting the fact that this pipeline uses both classical computer vision approaches (SPIR) assisted by specific deep learning modules aimed to overcome the limitation of classical approaches. All the software has been built around the innovative digital platform DolFin, in which standardized data about the species being investigated are collected. The results achieved in terms of automatic photo-identification have been made possible with the multidisciplinary approach that mixed up expertise coming from the marine biology area and the computer science one. This approach enabled us to effectively perform photo-identification of large datasets, opening the way for conducting large-scale habitat use, site fidelity, or spatial distribution studies of the species being investigated. Our efforts in the future will be devoted to the extension of these software modules and also to the photo-identification of other species, finding relevant image features that can be studied as well as developing new deep learning models that can solve specific problems in the photo-identification task.

References

1. Hammond PS, Mizroch SA, Donovan GP, (eds.). (1990) Individual recognition of cetaceans: use of photo-identification and other techniques to estimate population parameters. Rep Int Whal Commission 12:1–440
2. Akkaya A, Awbery T, Lyne P, et al (2020) Comparison of acoustic pattern recorded for the sperm whale (Physeter macrocephalus) in the Northen Ionian Sea (Central Mediterranean Sea) and in the north-western Levantine Sea (eastern Mediterranean Sea). In: Proceedings IMEKO metrology for the sea, Napoli, Italy, 5-7 October 2020, pp. 123–128
3. Azzolin M, Arcangeli A, Cipriano G et al (2020) Spatial distribution modelling of striped dolphin (*Stenella coeruleoalba*) at different geographical scales within the EU Adriatic and Ionian Sea region, central-eastern Mediterranean Sea. Aquat Conserv Mar Freshwat Ecosyst 30:1194–1207
4. Bellomo S, Santacesaria F.C, Fanizza C, et al (2019a) Photo-identification of Physeter macrocephalus in the Gulf of Taranto (northern Ionian Sea, Central-Eastern Mediterranean Sea). In: Proceedings IMEKO metrology for the sea, Genova, Italy, 3–5 October 2019, pp. 33–37
5. Carlucci R, Baş AA, Liebig P et al (2020b) Residency patterns and site fidelity of *Grampus griseus* (Cuvier, 1812) in the Gulf of Taranto (northern Ionian Sea, central-eastern Mediterranean Sea). Mammal Res 65:445–455
6. Carlucci R, Akkaya Bas A, Maglietta R, et al (2018d) Site fidelity, residency and habitat use of Risso's dolphin Grampus griseus in the Gulf of Taranto (northern Ionian Sea, Central-Eastern Mediterranean Sea) by photo-identification. In: Proceedings IEEE metrology for the sea, Bari, Italy, 8-10 October 2018, pp. 173–177

7. Carlucci R, Cipriano G, Paoli C et al (2018b) Random Forest population modelling of striped and common-bottlenose dolphins in the Gulf of Taranto (northern Ionian Sea, Central-Eastern Mediterranean Sea). Estuar Coast Shelf Sci 204:177–192
8. Carlucci R, Fanizza C, Cipriano G et al (2016) Modeling the spatial distribution of the striped dolphin (*Stenella coeruleoalba*) and common bottlenose dolphin (*Tursiops truncatus*) in the Gulf of Taranto (northern Ionian Sea, Central-Eastern Mediterranean Sea). Ecol Indic 69:707–721
9. Carlucci R, Ricci P, Cipriano G, Fanizza C (2018c) Abundance, activity and critical habitat of the striped dolphin *Stenella coeruleoalba* in the Gulf of Taranto (northern Ionian Sea, Central Mediterranean Sea). Aquat Conserv Mar Freshwat Ecosyst 28:324–336
10. Carlucci R, Manea E, Ricci P, Cipriano G, Fanizza C, Maglietta R, Gissi E (2021) Managing multiple pressures for cetaceans' conservation with an ecosystem-based marine spatial planning approach. J Environ Manage 287:112240. https://doi.org/10.1016/j.jenvman.2021.112240
11. Ciccarese S, Carlucci R, Ciani E et al (2019) Cytochrome b marker reveals an independent lineage of *Stenella coeruleoalba* in the Gulf of Taranto. PLoS One 14:5
12. Marangi M, Carlino P, Fanizza C (2020) Occurrence of zoonotic parasites in free-ranging dolphins and sea turtles in the Gulf of Taranto (northern Ionian Sea, Central-Eastern Mediterranean Sea). In: Proceedings IMEKO metrology for the sea, Napoli, Italy, 5–7 October 2020, pp. 93–98
13. Papale E, Fanizza C, Buscaino et al (2020) The social role of vocal complexity in striped dolphins. Front Mar Sci 2020:7. https://doi.org/10.3389/fmars.2020.584301
14. Santacesaria F.C, Bellomo S, Fanizza C, et al (2019b) Long-term residency of Tursiops truncatus in the Gulf of Taranto (Northern Ionian Sea, Central-Eastern Mediterranean Sea). In: Proceedings IMEKO metrology for the sea, Genova, Italy, 3–5 October 2019, pp. 28–32
15. Abdeldaim AM, Houssein EH, Hassanien AE (2018) Color image segmentation of fishes with complex background in water. In: International conference on advanced machine learning technologies and applications. Springer, New York, pp 634–643
16. Arzoumanian Z, Holmberg J, Norman B (2005) An astronomical pattern-matching algorithm for computer-aided identification of whale sharks Rhincodon typus. J Appl Ecol 42:999–1011
17. Van Tienhoven A, Den Hartog J, Reijns R, Peddemors V (2007) A computer-aided program for pattern-matching of natural marks on the spotted raggedtooth shark Carcharias taurus. J Appl Ecol 44:273–280
18. Carvajal-Gámez BE, Trejo-Salazar DB, Gendron D, Gallegos-Funes FJ (2017) Photo-id of blue whale by means of the dorsal fin using clustering algorithms and color local complexity estimation for mobile devices. EURASIP J Image Video Process 2017:6
19. Coleman T, Moon J (2019) A biometric for shark dorsal fins based on boundary descriptor matching. In: Proceedings of 32nd international conference. pp. 63–71
20. Gilman A, Hupman K, Stockin KA, Pawley MD (2016) Computer-assisted recognition of dolphin individuals using dorsal fin pigmentations. In: 2016 international conference on image and vision computing New Zealand (IVCNZ). IEEE, pp. 1–6
21. Losapio G, Maglietta R, Politi T, et al (2020) Lightweight and efficient convolutional neural networks for recognition of dolphin dorsal fins. In: 2020 Imeko TC-19 international workshop on metrology for the sea (MetroSea 2020). IEEE, Napoli
22. Mahmood A, Bennamoun M, An S et al (2017) Deep learning for coral classification. In: Handbook of neural computation. Elsevier, Amsterdam, pp 383–401
23. Pollicelli D, Coscarella M, Delrieux C (2020) RoI detection and segmentation algorithms for marine mammals photo-identification. Eco Inform 56:101038
24. Carlucci R, Bandelj V, Ricci P et al (2018a) Exploring spatio-temporal changes in the demersal and benthopelagic assemblages of the north-western Ionian Sea (Central Mediterranean Sea). Mar Ecol Prog Ser 598:1–19
25. Carlucci R, Capezzuto F, Cipriano G et al (2020a) Assessment of cetacean–fishery interactions in the marine food web of the Gulf of Taranto (northern Ionian Sea, Central Mediterranean Sea). Rev Fish Biol Fisher 31:135. https://doi.org/10.1007/s11160-020-09623-x

26. Carlucci R, Cipriano G, Santacesaria FC et al (2020c) Exploring data from an individual stranding of a Cuvier's beaked whale in the Gulf of Taranto (northern Ionian Sea, Central-Eastern Mediterranean Sea). J Exp Mar Biol Ecol 533:151473
27. Gaspari S, Natoli A (2012) *Grampus griseus* (Mediterranean subpopulation). IUCN, Gland
28. Bearzi G, Reeves RR, Remonato E et al (2011) Risso's dolphin *Grampus griseus* in the Mediterranean Sea. Mamm Biol 76:385–400
29. de Boer MN, Clark J, Leopold MF et al (2013) Photo-identification methods reveal seasonal and long-term site-Fidelity of Risso's dolphins (*Grampus griseus*) in shallow waters (Cardigan Bay, Wales). Open J Marine Sci 3:66. https://doi.org/10.4236/ojms.2013.32A007
30. Mariani M, Miragliuolo A, Mussi B et al (2016) Analysis of the natural markings of Risso's dolphins (*Grampus griseus*) in the Central Mediterranean Sea. J Mammal 97:1512–1524
31. Renò V, Dimauro G, Labate G et al (2019) A SIFT-based software system for the photo-identification of the Risso's dolphin. Eco Inform 50:95–101
32. Maglietta R, Renò V, Cipriano G et al (2018) DolFin: an innovative digital platform for studying Risso's dolphins in the northern Ionian Sea (north-eastern Central Mediterranean). Sci Rep 8:1–11
33. Maglietta R, Renò V, Caccioppoli R et al (2020a) Convolutional neural networks for Risso's dolphins identification. IEEE Access 8:80195–80206. https://doi.org/10.1109/ACCESS.2020.2990427
34. Renò V, Losapio G, Forenza F et al (2020) Combined color semantics and deep learning for the automatic detection of dolphin dorsal fins. Electronics 9:758. https://doi.org/10.3390/electronics9050758
35. Stanley R (1995) DARWIN: identifying dolphins from dorsal fin images. Senior thesis, Eckerd College
36. LeCun Y, Boser BE, Denker JS et al (1990) Handwritten digit recognition with a back-propagation network. In: Advances in neural information processing systems. MIT Press, Cambridge, pp 396–404
37. Goodfellow I, Bengio Y, Courville A (2016) Deep learning. MIT Press, Cambridge
38. Buehler P, Carroll B, Bhatia A et al (2019) An automated program to find animals and crop photographs for individual recognition. Eco Inform 50:191–196
39. Renò V, Mosca N, Marani R, et al (2018) Convolutional neural networks based ball detection in tennis games. In: Proceedings of the IEEE conference on computer vision and pattern recognition workshops, pp 1758–1764
40. Maglietta R, Renò V, Caccioppoli R, et al (2020b) NNPool in SPIR pipeline for Risso's dolphins identification. In: 2020 Imeko TC-19 international workshop on metrology for the sea (MetroSea 2020). IEEE, Napoli
41. Lowe DG (2004) Distinctive image features from scale-invariant Keypoints. Int J Comput Vis 60:91–110. https://doi.org/10.1023/B:VISI.0000029664.99615.94
42. Ricci P, Libralato S, Capezzuto F et al (2019) Ecosystem functioning of two marine food webs in the North-Western Ionian Sea (Central Mediterranean Sea). Ecol Evol 9:10198–10212
43. Ricci P, Ingrosso M, Cipriano G, et al (2020a) Top-down cascading effects driven by the odontocetes in the Gulf of Taranto (northern Ionian Sea, Central Mediterranean Sea). In: Proceedings IMEKO metrology for the sea, Napoli, Italy, 5-7 October 2020, pp. 75-80
44. Ricci P, Ingrosso M, Carlucci R, et al (2020b) Quantifying the dolphin-fishery competition in the Gulf of Taranto (northern Ionian Sea, Central Mediterranean Sea). In: Proceedings IMEKO metrology for the sea, Napoli, Italy, 5–7 October 2020, pp. 135–140

Chapter 13
Economic and Legal Implications of Setting Standards: The Case of ISO Containers

Monica Brignardello and Claudio Ferrari

Contents

Abstract Network industries rely on the definition of standards. Standards in fact have several implications in reducing the lock-in effect for consumers and in shaping the market and the network of users as well as in defining the formation of scope economies (and positive feedbacks). The present chapter focuses on the ISO freight container as the most striking example of standard in the shipping sector. After a historical description of the standardization process of containers and the benefits gained by the transport industry, the paper discusses the juridical nature of ISO standards and the connected legal issues as well as the economic relevance of standards for the liner shipping industry and for the paramount of backward and forward industries forming the supply chain.

M. Brignardello (✉) · C. Ferrari
Department of Economics, University of Genoa, Genoa, Italy
e-mail: monica.brignardello@economia.unige.it; claudio.ferrari@economia.unige.it

P. Daponte et al. (eds.), *Measurement for the Sea*, Springer Series in Measurement Science and Technology,
https://doi.org/10.1007/978-3-030-82024-4_13

13.1 A Brief History of Shipping Containers' Standardization

It is well known that containers were introduced in the shipping industry in the middle of the last century. The father of containerization was an American trucking entrepreneur, Malcolm McLean. Having to transport a cargo by sea, he realized that, instead of using truck trailers with goods inside, it would be easier and quicker to stow the cargo in a container in order to lift it from a vehicle into another without unloading its content. Therefore, in April 1956, he accommodated a container on a tanker ship, which made her maiden journey, and in 1957, he launched the first maritime regular container service between New York and Texas.

Thanks to the invention of containers, Malcolm McLean, as highlighted by [1], "makes his mark in history". As a matter of fact, the practice of transporting goods in containers has revolutionized international trade [2]. Not only it has reduced the time of loading and unloading process of the cargo and the risk of theft and shortened the transit time, but also it has determined a significant decrease in the cost of freight transportation.

These advantages soon became apparent to competitors so that in the following years other shipping entrepreneurs began to employ containers of different lengths (8, 10, 20, 25, 35, 40 ft). On the contrary, from the beginning the height and width of the containers were standard, corresponding to 8 ft [3–5].

In this scenario, it immediately became evident that the lack of containers' standardization would have slowed down the development of intermodal containerized transport due to the difficulty to transfer containers of different sizes from one vehicle to another. In fact, as noted by [6], to obtain the maximum benefits, containers must be able to travel by all modes and anywhere in the world. Standard lengths were therefore necessary.

As we will see in Sect. 13.3, in order to solve this problem, in the end of the 1950s the International Organization for Standardization (ISO), in collaboration with the American Standards Association (ASA), began to work in order to standardize the length of the containers. However, several years passed before coming to an international consensus, which is because, if the need for standardization was peaceful, it was not possible to reach immediately an agreement on the containers' standard lengths.

An agreement was reached in the second half of the sixties of the last century. In 1968, the first ISO standard rules relating to container sizes were adopted in order to regulate internal and external dimensions of containers. The principle of these standard rules was to maintain height (calibrated on the height of railway tunnels) and width equal to 8 feet (ft) and to vary only the length of the containers on the basis of a measuring unit divisible by 10. The ISO therefore initially proposed 10-, 20-, 30- and 40-ft containers.

Despite this agreement, in the early years, a significant minority of containers of different sizes (the so-called non-ISO containers) continued to circulate [7] and this represented an obstacle to the possibilities of developing effective intermodal

transport services. Over time, the shipping operators increasingly moved towards the use of containers according to ISO standards, although nowadays non-standardized containers are still in circulation, albeit to a limited extent [8].

In these times, the two most commonly used containers are 20- and 40-ft. The unit of volume of the 20-ft container is known as twenty-foot equivalent unit (TEU) and this abbreviation is used to indicate the capacity of ships and terminals, as well as the statistical unit of measurement of the number of containers that pass through a port. Therefore, TEU represents now the standard measure for containerized traffic. The 40 ft containers are the so-called forty-foot equivalent unit (FEU).

13.2 Benefits of Containers' Standardization

The containers' standardization has undoubtedly brought numerous advantages; the most evident is the fact that containers can quickly, easily and efficiently be moved between ships, trucks and trains without being opened, simplifying the whole logistical process.

For example, in the case of an intermodal transport combining road and sea transport mode, once the truck arrives at the port, today, unlike in the past, it is no longer necessary to unload the goods from the truck and then load them on the ship, but it is sufficient to move the container, where the goods are stowed inside, with special cranes. The same applies, of course, for the containers travelling by train.

Through the years, the means of transport have adapted to move containers of different lengths as defined by ISO. Let us think about container ships built with increasingly larger dimensions and capacities. Not only the means of transport but also sea and land terminals have equipped with special cranes for the loading and unloading of standard containers and their transfer on trains, trucks and ships. The container terminals have therefore been equipped to handle ISO standardized containers, while containers with different sizes are usually managed in general cargo terminals. As time went on, the creation of automated or semi-automated container terminals has made container handling operations increasingly efficient.

The containers' stowage plan on board of ships and in the port and inland terminals has to consider different variables including the container's size. Therefore, the complexity of rules and procedures for loading, unloading and moving containers has aroused the interest of academics in order to optimize them (in recent years, see, among many others authors, [9–13] also taking in consideration the potential benefits of containers' standardization) [14].

All this has made possible the development of intermodal transport whose success is largely due to the introduction of containers and their standardization. Therefore, the standard containers have become the dominant intermodal transport unit. After all, the resulting advantages are evident in terms of economies of scale, optimization in ship scheduling, reduction in time for carrying out loading and unloading operations, lower costs of containers' design, construction and

inspection, and decrease in freight and terminal costs and, finally, of price for the sale of goods with obvious advantage for the end consumer.

13.3 ISO Standards Regarding Freight Containers: The ISO 668:2020 Series 1

It is not possible to talk about containers' sizes without considering the fundamental role played by the International Organization for Standardization (see [7]). ISO is an independent, non-governmental international organization, created in 1946. ISO members are the national standard bodies (today 166), each representing their own country (one member per state). The Italian member body of ISO is UNI (*Italian National Unification*), a nonprofit association established in 1921 with the initials UNIM. ISO works in close cooperation with other international organizations such as the International Maritime Organization (IMO) and the World Trade Organization (WTO).

The main purpose of ISO is to elaborate international standards usually prepared by technical committees and subcommittees made up of experts from relevant industry, consumer associations, academia, government, etc., from all over the world and working in a specific field. The process leading to the creation or updating of ISO standards is quite lengthy [15, 16] and passes through several stages: (1) confirmation of the need for a new standard (proposal stage), (2) preparation of a working draft (preparatory stage), (3) distribution of the first draft to all ISO member bodies for comments and, if required, for voting (committee stage), (4) approval of a final draft international standard (enquire stage), (5) if the draft international standard is approved with technical changes, circulation of the final draft for a final vote (approval stage), and (6) publication of the final test of the international standard (publication stage). As it has been noted by [16], this process is governed by four key principles: first of all, ISO standards respond to needs arising in the market; secondly, they are founded on expert opinions from all over the world; thirdly, they are originated from a multi-stakeholder process; and finally, they are based on a general agreement.

In response to the containers' standardization, in 1961 the so-called ISO/TC 104 Freight containers have been created with the scope of standardizing the freight containers as regards not only to their classification and dimensions but also to many other aspects such as corner and intermediate fittings, specification and testing, handling and securing, coding, identification and marking, automatic identification, container tracking and monitoring systems.

In 1968, as above mentioned, ISO published the first edition of the ISO 668 Series 1, prepared by the Subcommittee SC 1 General purpose containers of ISO/TC 104. This series, titled "Freight containers - Classification, dimensions and ratings", classifies shipping containers and standardizes their size and weight specifications, regulates external dimensions and specifies the associated gross weight

ratings and some of the minimum internal and door opening dimensions for certain types of containers. Conversely, ISO 1496 Series establishes the internal dimensions for each type of container and ISO 1161 Series deals with the specification of corner fittings for series 1 freight containers [14].

ISO 668:2020 is the seventh (and last) edition, which replaces the ISO 668:2013 as amended in 2016. This document refers to freight containers used in intercontinental traffic (art. 1) except for vehicles or conventional packing (note 1). It provides the definition of ISO container such as "freight container complying with all relevant ISO container standards in existence at the time of its manufacture" (art. 3.2). Regarding the dimensions and referring exclusively to the metric system, the ISO containers have an internal volume of 1 m^3 (35,3-ft^3) or more (art. 3.1) and an uniform width of 2.438 mm (8-f) (art. 4). Conversely, the length and height are variable. ISO containers are classified by different letters from A to D preceded by the number 1 (art. 5.4, Table 2). The largest container is known as 45-ft-high cube, designated as 1EEE. It is characterized by a length of 13.716 mm (45-ft) and a height of 2.896 mm (9-ft., 6 in), while the smallest box is the 10-ft container, designated as 1DX having a length of 2.991 mm (approximately 10-ft) and a height of less than 2.438 mm (<8 ft).

As already observed, nowadays the most common containers are 20- and 40-ft.

The 20-ft containers have the same length (6.058 mm corresponding approximately to 20-ft), while, based on height, we can distinguish different containers: 1CCC (2.896 mm, 9-ft., 6-in), 1CC (2.591 mm, 8-ft., 6-in), 1C (2.438 mm., 8-ft) and 1CX (less than 2.438 mm., 8-ft).

The 40-ft containers, long 12.192 mm, are the following: 1AAA with a height of 2.896 mm (9-ft., 6-in), 1AA with a height of 2.591 mm (8-ft., 6-in), 1A with a height of 2.438 mm (8-ft) and finally 1AX with a height of less than 2.438 mm (<8ft).

It is worth noticing that a Draft Amendment, ISO 688:2020/DAMD 1, is right now circulating for comment and approval (third stage). The voting process has just closed, but, as seen above, further steps are required before final approval and publication. At that point, this eighth edition will cancel and replace the current one. However, in this moment the changes, which affect this new version, do not concern containers' length, width and height, which will remain the same as well as the freight containers' designation. The life cycle of ISO 668 can be traced on the website https://www.iso.org/standard/81611.html.

.

13.4 Juridical Nature and Legal Issues of ISO Standards for Freight Containers

The ISO standards relating to container dimensions, as well as all other standards developed by the International Organization for Standardization, are not mandatory [7]. Therefore, they cannot be considered as an international convention, which

shall necessarily be respected by the contracting states. ISO standards are voluntary guidelines, which, as we have already seen, owe their success to the fact that they are widely used all over the world, thanks to the advantages described above. In order to become legally binding, ISO standards shall be incorporated in international or national law [15].

Restricting attention to ISO 668:2020 Series 1 freight containers "classification, dimensions and rating" and taking a quick look at the international shipping conventions, it can be observed that these conventions, while referring to containers, do not provide their definition and do not care about their size. Think about the Hague–Visby Rules, the international convention on the liability of the sea carriers in the international transportation of goods documented by the bill of lading, which applies also, but not only, to containerized cargo.

Conversely, a definition of container and a reference to its size are found in the IMO Convention of Safe Containers (CSC) 1972, entered into force in 1977 [7, 17]. Unlike the Hague–Visby Rules, which regulate the carrier's liability for damage to cargo, whether or not the goods are transported in containers and, in the latter case, whether or not such containers are stowed in a special container ship, CSC is exclusively dedicated to containers and their safety standards. The 1972 Convention for Safe Containers aims to achieve two main goals: the first one is to ensure a high level of safety of human life in the transport and handling of containers and the second one is to create uniform international safety regulations in order to facilitate the international transportation of containers. Art. 2 contains a list of definitions of the most commonly used terms in the text of the convention including the definition of the container. According to this article, "Container means an article of transport equipment" characterized by various requirements, including a condition relating to container size. In this regard, the letter d) of article 2 states that containers, governed by the convention, have "a size such that the area enclosed by the four outer bottom corners is either: (1) at least 14 sq.m. (150 sq.ft.); or (2) at least 7 sq.m. (75 sq.ft.) if it is fitted with top corner fittings". As noted by [7], the CSC, unlike the ISO 668:2020, does not specify the internal and external measurements of containers, but is intended only to exclude from its scope containers smaller than a specific minimum size. It follows that all new and existing containers used in international shipping greater than the dimensions indicated above (except for those specially designed for air transport) are subject to the convention (article III, paragraph 1, CSC), regardless of whether they comply or not with the ISO standards referred to in Series 668:2020.

The fact that the main international conventions in force do not provide specific distinct rules for ISO containers with respect to containers of nonstandard dimensions seems to demonstrate that the standardization of containers arouses interest above all at technical and economic levels, but it does not raise particular problems on the legal point of view.

Actually, looking at the extensive literature about juridical issues related to maritime container transport (see, among others, [18–22]), we can immediately realize that it does not concern the container dimension. In particular, some of the main legal questions refer to (a) the nature of the container as a transport mean (and

therefore as part of a ship) or as a package handed over for cargo transportation and the consequential distinct liability of the carrier for the damage to the container; (b) the lawfulness of the containers' loading on deck without the consent of the shipper; (c) the carrier's duty of due diligence for seaworthiness in case of containers' stowage on or under the deck; (d) the legal nature of the supply of containers according to whether they are provided by the carrier rather than by the shipper; (e) the burden of proof of the carrier in claims for damage to the cargo in case of transport under conditions "Full Container Load" (FCL/FCL) or "Less Container Load" (LCL/LCL); and (f) the carrier's limitation of liability whether the number of packages stowed in a container has been or not clearly reported in the bill of lading.

These very complex issues cannot be examined here. However, it is interesting to note that they are based on elements (position of the containers on the ship, cargo stowage methods, etc.), which never call into question the container standard dimensions. In reality, the circumstance that the juridical issues generally concern ISO containers is based on the simple reason that these containers are more widely used in the world than non-standardized containers.

Returning to the question of the non-binding nature of ISO standards, it should finally be noted that such standards could be made binding not only, as illustrated above, by their transposition into an international convention, but also by referring to them in the contract. In this case, the parties undertake, in a private relationship, to respect them. In this regard, the reference made to these standards in some important forms drawn up by BIMCO is symptomatic. Think about the latest version of BIMCO Standard Container Interchange Agreement—BOXCHANGE 2016. This standard agreement expressly refers to freight containers as defined by ISO (article 1) and states that the supplier shall deliver containers designed, manufactured, tested and maintained in compliance with the regulations and standards detailed by ISO Specifications and Classification Series 1 (article 3, letter a). Similar provisions are included in the BIMCO Standard Container Lease Agreement—BOXLEASE 2006. Therefore, in the event that the supplier in the first agreement and the lessor in the second one deliver containers that do not comply with ISO standard dimensions, they act in breach of contract with a consequential obligation to pay compensation for damages.

13.5 Economic Implications of Standards for Network Industries

13.5.1 Transport as a Network Industry

Transportation is a network industry [23], although for some time economic analysis neglected to consider it under this perspective, until the rapid development of the telecommunications industry made clear the role that the production of network

goods plays in explaining the dynamics of these industries and the way in which competition takes place in markets that exchange network goods.

The product realized by this industry is in fact determined by the way in which the various elements that compose the network are combined and interact with each other: the infrastructure—terminals and transport routes—but also the services that are carried out on them. Different combinations of these elements result in different outputs (i.e. transport services) and serve different demands.

In network industries, the value of each unit of outputs depends also (while in pure network industries, it depends only) on the size of the network [24]. Referring to transportation, this means that the value of the transport service will increase with the compatibility of the different modal transport networks. In the transport sector, the ability to switch easily from one network to another is usually known as intermodality. In fact, according to the definition proposed by the OECD in its website, intermodality refers to the movement of goods (in one and the same loading unit or a vehicle) by successive modes of transport without handling of the goods themselves when changing modes. Containers, together with pallets, trailers and semitrailers, are the loading unit that makes possible a smooth passage from a network to another.

13.5.2 The Role of Standards in Network Industries

In network industries, as above mentioned, the value of the service is given by the size of the network [25]. Therefore, this characteristic represents a clear advantage for the incumbent in order to maintain a leading position in the market and for the same reason newcomers are forced to serve market niches, especially in case the output realized by the industry is not completely compatible.

The benefits to be gained from participating in a larger network made up of networks belonging to different actors but all compatible with each other far outweigh the network economies resulting from the incompatibility of individual networks. Therefore, as seen in Sect. 13.3 the process towards the definition of standard containers began as soon as the huge benefits that the introduction of the container would have on the liner shipping industry were understood.

From a theoretical viewpoint, the definition of standards in network industries changes the nature of competition replacing the competition for the market (in order to be the leader in a market made of several noncompatible network goods) with the competition in the market, mostly based on a price competition (since the service is standardized). Moreover, it benefits the industries supplying the components of the production processes, since they are not forced to choose for a specific network not compatible with all the other ones. Lastly, standards support a quick penetration of the standardized goods (or services) in the market.

In addition to many favourable features, the definition of a standard can also have some negative consequences, the main one being the tendency to crystallize production processes.

In the case of ISO container, for instance, the greatest limitation is due to its internal loading dimensions, which do not allow two pallets to be loaded side by side on its largest side. Overcoming this limitation would mean redefining the standard by having to adapt the entire existing fleet of containers—and all the equipment currently used for handling containers—to a new standard, thus incurring such high costs that it is not economical to revise the standard.

13.6 The Impact of Containers on the Shipping Industry

The idea of moving cargo through a box revolutionized the liner shipping industry. The wide and quick adoption of containers as transport means is illustrated by Fig. 13.1 that shows the development of containerized trade in the world measured by the number of TEU moved by the world seaports as monitored by Containerisation International and the World Bank.

The picture clearly shows how the process of container standardization and the simultaneous construction of the first ships specifically designed for container transport—both occurred in the '1960s—facilitated the progressive adoption of the container as the most popular way for the maritime transport of general cargo.

Since the seventies, the annual number of containers moved in the world seaports has grown year on year, with the sole exception of 2008, which coincided with the economic crisis.

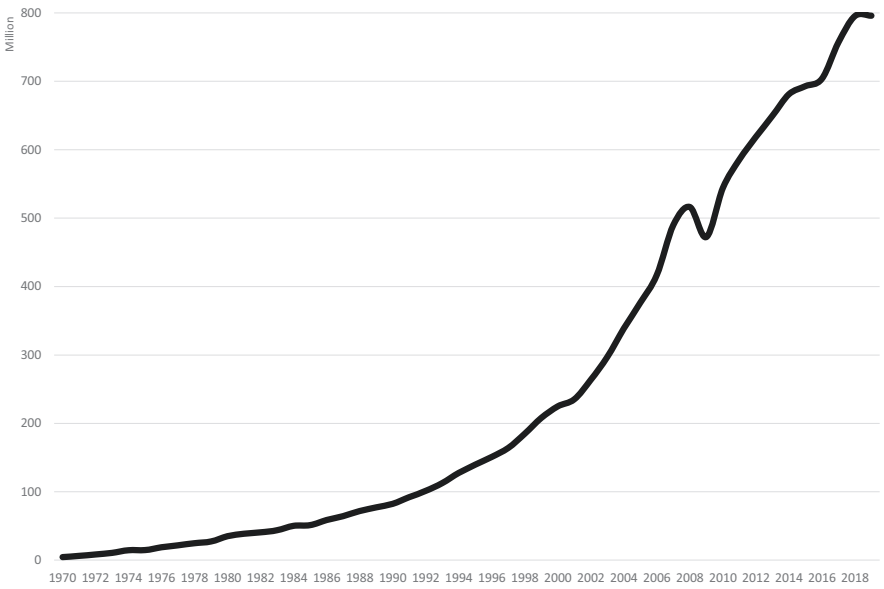

Fig. 13.1 World Container Port Throughput 1970–2019 (million TEU). Source: Containerisation International and World Bank

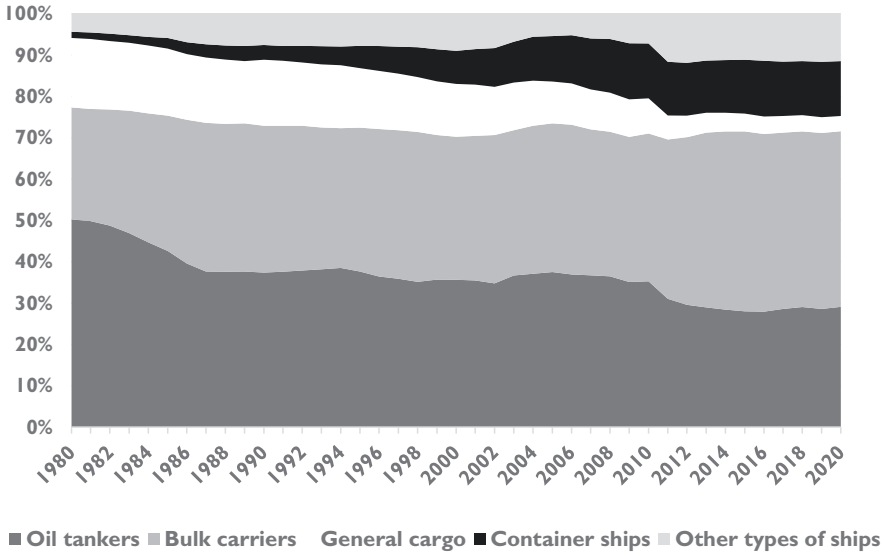

Fig. 13.2 World cargo fleet 1980–2020 (% of deadweight tons). Source: UNCTAD

Figure 13.2 shows the composition of the world cargo fleet in the period 1980–2020.

The figure highlights the quick and constant increase in the fleet dedicated to containers and also the replacement process of general cargo ships (the white area in the picture) with full-container ships (the black area in the same picture) looks quite evident. The latter is a consequence of the increasing number of ships deployed in the market and the trend towards an increase in the average size (deadweight tonnage) of ships.

13.6.1 The Containerization of Commodities

The cost of transporting containers is so (relatively) convenient that even some commodities that do not normally fall under the definition of general cargo may under certain circumstances find it convenient to move in containers. This is the case, for example, for certain bulk commodities such as grain and coal and also of many foodstuffs, which, thanks to the use of reefer containers (special boxes equipped with an electric device to keep the temperatures inside the box low), have led to the virtual disappearance of refrigerated ships. Also, some liquid types of cargo—as fruit juices, spirits, sweet oils, wine or some chemical products—may be containerized using special boxes as tank containers.

There are several circumstances that are fuelling such process [26]. The most important is the possibility for small and medium exporters of benefiting from lower

freight rates, also due to the possibility of embarking on ships that are on average larger than those used in minor tramp routes, especially during periods of falling demand for container traffic, while in the bulk shipping sector only great exporters can benefit of the economies of scale of larger ships. A second one is the relative stability of freight rates in liner shipping in comparison with the large and quick fluctuations that usually characterize the tramp shipping. In addition, the use of liner shipping is a convenient alternative in routes characterized by high trade imbalances.

13.7 The Effects on Transport-Related Industries

The role of complementarity in network industries implies that increases in the capacity of one element of the network, e.g. the fleet dedicated to container transport, must be followed by similar increases in the other elements of the network—e.g. port terminals and railways trucks—either opting for size economies due to an increase in the network capacity (e.g. adding a railway line) or increasing the network's capacity utilization (e.g. an increase in the number of trains), hence incurring in density economies.

Containers initially travelled on general cargo ships, but the increasing popularity of containers led some companies to invest in a new type of ship specially built to accommodate the boxes, thus asking shipyards to build the first full containerships. Even if it was (at that time) a risky venture, it proved to be successful. According to UNCTAD statistics, full containerships represented 13.3% of the world fleet in 2019 (while they were only 1.5% in 1980).

The increasing adoption of containers and the contextual development of port terminals equipped with cranes and other yard equipment dedicated to the containerized traffic along with the development of international trade favoured the deployment of ever-larger ships. In fact, while in the '70s the first fully cellular ships accommodated about 2,000 TEU, the largest currently operating ship can host more than 21,000 TEU, i.e. about ten times the first full containerships. As the size of ships increases, assuming that the load factor remains stable at 80% (i.e. the ship is considered fully load), the transport cost per container decreases [27]. Thus, favouring carriers (alone or associated in consortia) able to afford the huge investments for largest ships and operating on the shipping routes where the volume of demand is so high to allow the use of such large vessels.

The growth of container traffic and the search for economies on both the supply and demand sides have encouraged the emergence of forms of cooperation between operators. In addition to consortia, as already mentioned, the sector since the '90s has seen the emergence of strategic alliances between carriers [28] aimed at enlarging their own network—through slot charter and vessel sharing agreements—without incurring excessive investments [29].

The impact on port terminals has not only involved the mechanization of ship loading and unloading operations, but has also changed the physical structure of the terminals, which have had to abandon the classic structure (similar to a comb) in

favour of long linear quays capable of accommodating more than one ship at the same time. With the progressive increase in the size of full containerships, it has also become necessary to build new terminals with high water depths and with direct connections to inland infrastructure networks—railways and highways—in order to speed up the passage of containers through the port node. In many cases, especially in Europe, these new container terminals have been created at some distance from the traditional port nodes, resulting in many cases in processes of redevelopment for urban use of the old historic ports [30].

13.8 Conclusion

The present chapter highlighted the role that the introduction of a process innovation, the use of a dry cargo box, has played in revolutionizing the liner shipping industry.

Even if the practice of using wooden crates to move cargo was already in use (especially in the army), only the definition of standards allowed the shipping container to spread on the market very quickly. In fact, in the early '50s there were several different sizes and corner fittings for containers worldwide and only when the ISO developed standards in 1968–1970 the shipping container truly became worldwide.

It is worth noticing that even today there are different types of containers, always consistent with the standards, made necessary by the variety of types of goods that find the use of containers convenient for transport.

The standardization process has interested the whole transport supply chain giving rise to the concept of intermodality and at the same time creating the conditions for a vertical integration of transport and logistics operators.

The effects of containerization are not restricted to the transport industry alone. The reduction in the cost of seaborne transport, due to the strong economies of scale afforded by the use of ever-larger vessels, has led to a significant increase in international (sea) trade and provided favourable transport conditions for the globalization of the world economy.

It cannot be said that all this is the direct and immediate consequence of container standardization alone, but certainly without such standardization process all this would not have happened.

References

1. Thompson D (1967) International carriage by container. I The British background. J World Trade Law 1(2):434–463
2. Levine J (2016) The history of the shipping container. https://www.freightos.com/the-history-of-the-shipping-container/

3. Lewis B (2017) Boxing clever. How standardization built a global economy. ISOfocus Transp Trend 124:40–45
4. Schmeltzer E, Peavy RA (1970) Prospects and problems of the container revolution. J Maritime Law Commerce 1:203–240
5. Seymour S (1974) The law of shipping containers. J Maritime Law Commerce 5(3):507–538
6. Olson RE, Scrogin TW (1974) Containerization and military logistics. J Maritime Law Commerce 6(1):119–146
7. Martin S, Martin J, Lai P (2019) International container design regulations and ISO standards: are they fit for purpose? Marit Policy Manag 46(2):217–236
8. Djadjev I (2017) The obligations of the carrier regarding the cargo. In: The Hague-Visby rules. Springer, Cham
9. Ambrosino D, Sciomachen A (2018) A shipping line stowage planning procedure in the presence of hazardous containers. Maritime Econ Logist 2018:1–22
10. Bilican MS, Evren R, Karatas M (2020) A mathematical model and two-stage heuristic for the container stowage planning problem with stability parameters. IEEE 8:113392–113413
11. Jonker T, Duinkerken M, Yorke-Smith N, de Waal A, Negenborn R (2019) Coordinated optimization of equipment operations in a container terminal. Flexible Servic Manuf J 2019:1–23
12. Poo MC-P, Yip TL (2019) An optimization model for container inventory management. Ann Oper Res 273:433–453
13. Zhao N, Liu Y, Mi W, Shen Y, Xia M (2020) Digital management of container terminal operations. Springer, Singapore
14. Lin Y-H, Meller RD, Ellis KP, Thomas LM, Lombardi BJ (2014) A decomposition based approach for the selection of standardized modular containers. Int J Prod Res 52(15):4660–4672
15. Kumar Songara R, Chouhan P, Singla RK, Tiwari A, Sharma A (2011) Regulatory aspect of International Organization for Standardization (ISO). Indo-Global J Pharm Sci 1(3):258–280
16. Seta M (2019) The contribution of the International Organization for Standardization to ocean governance. Rev Europ Compar Int Environ Law 28:304–313
17. Chacón VH (2017) The due diligence in maritime transportation in the technological era. Springer, Cham
18. Angus W (1968) Legal implications of the container revolution in international carriage of goods. McGill Law J 14(3):395–429
19. Bordahandy P-J (2005) Containers: a conundrum or a concept? J Int Maritime Law 11(5):342–371
20. Mahafzah QA, Naser MA (2019) The inadequacy of the existing international maritime transport regimes for modern container. Transp Modern Appl Sci 13(4):94–103
21. Rath E (1975) Containers: their definition and implications. Transport Law J 7(1):53–82
22. Wiedenbach L (2015) The carrier's liability for deck cargo. In: A comparative study on english and nordic law with general remarks for future legislation. Springer, Heidelberg, New York, Dordrecht, London
23. Ferrari C, Bottasso A, Conti M, Tei A (2019) Economic role of transport infrastructure: theory and models. Elsevier, Amsterdam
24. Economides N (2003) The economics of networks. In: Garud R, Kumaraswamy A, Langlois RN (eds) Managing in a modular age. Blackwell, Malden
25. Katz ML, Shapiro C (1994) Systems competition and network effects. J Econ Perspect 8:93–115
26. Jean-Paul Rodrigue JP (2020) The geography of transport systems. Routledge, New York
27. Merk, O., Busquet, B. and Aronietis, R. (2015). The impact of mega ships. OECD/ITF
28. Midoro R, Pitto A (2000) A critical evaluation of strategic alliances in liner shipping. Marit Policy Manag 27(1):31–40
29. Ferrari C, Parola F, Benacchio M (2008) Network economies in liner shipping: the role of home markets. Marit Policy Manag 35(2):127–143
30. Porfyriou H, Sepe M (2017) Waterfronts revisited. Routledge, New York